Target identification of peptides from *Xenorhabdus* and *Photorhabdus*

Dissertation

zur Erlangung des Doktorgrades

der Naturwissenschaften

vorgelegt beim Fachbereich für Biowissenschaften (15)

der Johann Wolfgang-Goethe-Universität

in Frankfurt am Main

von

Tien Duy Vo

Aus Hanoi

Frankfurt am Main 2020

D30

vom Fachbereich für Biowissenschaften (15) der

Johann Wolfgang-Goethe-Universität als Dissertation angenommen.

Dekan: Prof. Dr. Sven Klimpel

Gutachter: Prof. Dr. Helge B. Bode

Zweitgutachter: Prof. Dr. Eugen Proschak

Datum der Disputation: 17.12.2020

Danksagung

79% der Kinder aus Akademikerfamilien fangen ein Studium an, während nur 27% der Kinder aus Nicht-Akademikerhaushalten studieren. Und von etwa 27 000 Promovierenden in Deutschland (Stand 2019) haben nur etwa 20% einen Migrationshintergrund. In beiden Statistiken gehöre ich zu der Minderheit, ich bin mit 10 Jahren nach Deutschland gekommen und bin bei einer alleinerziehenden Mutter groß geworden. Diese Zahlen machen mir wieder bewusst, wieviel ich meinen Mitmenschen an Zuspruch und Unterstützung für diese Arbeit verdanke.

Zuerst möchte ich mich bei meiner Mutter **Nga, Nguyen Thi Minh** bedanken, meine längste und treuste Mitbestreiterin. Ich danke auch meiner Frau **Giang, Doan Huong**, die für mich während dieser Arbeit sehr viel Verständnis gezeigt hat. Des Weiteren danke ich **Prof. Dr. Helge Bode**, meinem Doktorvater für die Möglichkeit und die Betreuung während meiner Arbeit. **Dr. Frank Wesche** verdanke ich die Einführung in die Peptidsynthese. Ebenfalls danken möchte ich **Dr. Edna Bode** für ihr mikrobiologisches Verständnis. Auch danken möchte ich **Peter Grün** für die Lehrstunden an unseren HPLC-MS Systemen.

Ich bedanke mich ebenfalls bei der **Bode Gruppe** für die erfolgreiche Zusammenarbeit. Insbesondere möchte ich ebenfalls **Dr. Christoph Spahn** für die die tollen Mikroskopiebilder danken und **Lei Zhao** für die Korrektur dieser Arbeit. Schließlich möchte ich mich noch bei **Prof. Dr. Eugen Proschak** für die Übernahme des Zweitgutachtens bedanken.

Table of contents

Table of abbreviations

ABPP	activity based protein profiling
ACN	acetonitrile
AF647	Alexa Fluor 647 dye
AmdU	5-(azidomethyl)-2′-deoxyuridine
AMP	antimicrobial peptides
ATP	adenosine triphosphate
BGC	biosynthetic gene cluster
Boc	tert-Butyloxycarbonyl
C18	octadecyl carbon chain
CFU	colony-forming unit
CH_3I	methyl iodide
CTC	2-chlorotrityl chloride
CuAAC	copper(I)-catalyzed alkyne-azide cycloaddition
$CuSO_4$	copper(II) sulfate
Cy5	cyanin 5
DCC	*N,N′*-dicyclohexylcarbodiimide
DCM	dichloromethane
ddH_2O	bidestilled water
DIC	*N,N′*-diisopropylcarbodiimide
DIPEA	*N,N*-diisopropylethylamine
DMF	dimethylformamide
DMSO	dimethyl sulfoxide
DNA	deoxyribonucleic acid
dStorm	direct stochastic optical reconstruction microscopy
EDC	1-ethyl-3-(3-dimethylaminopropyl)carbodiimide
EdU	5-ethynyl-2'-deoxyuridine
EtO_2	diethyl ether
EtOAc	ethyl acetate
FA	formaldehyde

Fmoc	fluorenylmethyloxycarbonyl
GA	glutaraldehyde
GdmCl	guanidinium chloride
GxpS	GameXPeptide synthetase
H_2O	water
HATU	(1-[bis(dimethylamino)methylene]-1H-1,2,3-triazolo[4,5-b]pyridinium 3-oxide hexafluorophosphate
HCl	hydrochloric acid
HCTU	(2-(6-chlor-1H-benzotriazol-1-yl)-1,1,3,3-tetramethylaminium-hexafluorophosphat)
HF	hydrogen fluoride
HFIP	hexafluoro-2-propanol
HOA	hydroxyoctadecanoic Acid
HOAt	1-hydroxy-7-azabenzotriazole
HOBt	1-hydroxybenzotriazol
HPLC-MS/MS	High-performance liquid chromatography tandem mass spectrometry
iTRAQ	isobaric tag for relative and absolute quantitation
K_2HPO_4	dipotassium phosphate
KCN	potassium cyanide
KEGG	kyoto encyclopedia of genes and genomes
KOH	potassium hydroxide
LB	lysogeny broth
LiOtBu	lithium tert-butoxide
LSCM	laser scanning confocal microscopy
Lys-C	endoproteinase Lys-C
MEA-HCl	2-mercaptoethylamine•HCl
MeI	methyl iodide
MeOH	methanol
$MgSO_4$	magnesium sulfate
mRNA	messenger ribonucleic acid
$Na_2S_2O_3$	sodium thiosulfate
$NaBH_4$	sodium borohydride

NaCl	sodium chloride
NMP	*N*-methyl-2-pyrrolidone
NMR	nuclear magnetic resonance
NRPS	nonribosomal peptide synthetase
OD	optical density
PAX	peptide antimicrobial *xenorhabdus*
Pbf	(2,2‘,4,6,7-Pentamethyldihydro-benzofuran-5-sulfonyl-)
PBS	phosphate buffered saline
PKS	polyketide synthase
PLL	poly-L-lysine
QS	quorum sensing
RPM	revolutions per minute
RXP	rhabdopeptide/xenortide-like peptides
SCX	strong cation exchange
SILAC	stable isotope labeling by amino acids in cell culture
SmI_2	samarium(II) iodide
SMLM	single-molecule localization microscopy
TCEP	tris(2-carboxyethyl)phosphine
TFA	trifluoroacetic acid
THF	tetrahydrofuran
TIS	triisopropylsilane
TMT	tandem mass tag
TPP	thiamine pyrophosphate
Tris	tris(hydroxymethyl)aminomethane
Trt	triphenylmethyl
TX-100	triton X-100
UV/VIS	ultraviolet–visible spectroscopy
WT	wild type
XIC	extracted-ion chromatogram
XU	exchange unit
YPD	yeast extract peptone dextrose

Summary

Xenorhabdus and *Photorhabdus* are bacterial genera that live in symbiosis with entomopathogenic nematodes of the genera *Steinernema* and *Heterorhabditis*, respectively[1,2]. These nematodes infect insect larvae through the trachea[3,4] and then enter the hemocoel. Once inside the hemocoel, the nematodes release the bacteria through their intestine[5]. Thereafter, the bacteria become active and kill the larvae within 48 h[6]. During this process, the immune system of the insect host is compromised by molecules produced and secreted by the bacteria. This illustrates that the bacteria possess not only a large arsenal of biological weaponry such as antibiotics and fungicides but also lipases, proteases, etc[7,8]. Therefore, they are not only able to kill the insect but also protect the cadaver from other food competitors.

During the past decades, a large number of natural products have been identified from *Xenorhabdus* and *Photorhabdus*. However, the targets and functions for many of these biological molecules are still unknown. Therefore, the goal of the doctoral thesis is to elucidate the modes of action of these natural products from *Xenorhabdus* and *Photorhabdus* with the main focus on non-ribosomal peptides (NRPs). The work can be divided into two parts. Initially, it starts with the synthesis of natural compounds and various chemically modified derivatives. Besides that, a number of peptides were synthesized for other projects to either verify their structures or quantify the amount produced by the bacteria. Then, secondary analysis methods are applied and provide additional insight into the modes of action of these compounds.

During the thesis, I carried out peptide synthesis either manually or with an automatic synthesizer system from Biotage. Here, the Fmoc-protecting group strategy was preferred in most cases. Natural products, such as silathride, xenoautoxin, phenylethylamide, tryptamide, rhabdopeptide, 3-hydroxyoctanoic acid, and PAX, were produced during this process. Furthermore, new peptide derivatives derived from synthetic NRPS approaches using the XU concept[9] or SYNZIP[10] were generated as standards.

Most of these natural compounds were experimentally verified by MIC tests (broth microdilution, plate diffusion) to be biologically active. For example, silathride, phenylethylamide, and tryptamide showed quorum quenching effects when tested against *Chromobacterium violaceum*. Initial results from collaborators (PD Dr. Nadja Hellmann/Mainz) showed that tryptamide and phenylethylamide interact with membrane or membrane proteins.

(*R*)-3-hydroxyoctanoic acid was synthesized to verify the molecule structure of phototemtide A, a cyclic lipopeptide with antiprotozoal activity. The rhabdopeptides are another class, which showed remarkable antiprotozoal effects. However, their mode of action was unknown. These compounds are relatively short peptide sequences, which contain hydrophobic residues, such as valine, leucine, or phenylalanine. Moreover, they possess *N*-methylation, resulting in a rod-shaped highly hydrophobic structure. In this work, I synthesized eight new derivatives of rhabdopeptides for photo-affinity labeling (PAL)[11]. These molecules should react covalently under UV-light irradiation with the biological target of the peptides. In addition, these derivatives can be enriched in a pull-down assay using click chemistry. Afterward, analytic methods such as mass detection (proteome analysis[12,13]) can be applied to elucidate the protein targets.

The PAX peptides derivatives are well-known to have anti-microbial activities[14] and believed to be secreted into the environment by the producing bacteria. However, I found that the majority of these peptides are located in the cell pellet fraction and not in the supernatant. This has been shown through quantification using HPLC-MS. New PAX derivatives were synthesized, which carry a moiety suitable for covalent modification using click-chemistry, therefore being functionalizable with a fluorescence dye. In collaboration with Dr. Christoph Spahn (Prof. Dr. Mike Heilemann group), we used confocal, as well as super-resolution microscopy, in particular, single-molecule localization microscopy (SMLM[15]) to investigate the spatial distribution of clickable PAX molecules and revealed that they localize at the bacterial membrane. Furthermore, bioactivity assays revealed that the promotor exchanged *X. doucetiae* PAX mutants, which do not produce PAX molecules without chemical induction (hereby termed as *pax*$^-$), were more susceptible to

several insect AMPs tested. Based on these findings, a new dual mechanism of action for PAX was proposed. Besides the previously shown antimicrobial activity, these molecules with a positive net charge of +5 (pH = 7) would bind to the negatively charged bacterial surface. Hereby, the surface charge (typically negative) would be inversed resulting in a protective effect for *Xenorhabdus* against other positively charged AMPs. Furthermore, PAX was investigated as AMP against *E. coli* to study its antimicrobial mechanism of action. Here, the results show that PAX can disrupt the *E. coli* membrane at higher concentrations (> 30 µg/ml), enter the cytosol, and lead to reorganization of subcellular structures, such as the nucleoid during this process.

Another aspect of secondary analysis is the application of proteomic analysis. Therefore, I induced *X. nematophila*, *X. szentirmaii,* and *P. luminescens* with insect lysate. These samples were analyzed using HPLC-MS/MS (Q Exactive) together with a database approach (Maxquant/Andromeda). The results showed that in all strains the lipid degradation and the glyoxylate pathway were induced. This is in line with the given insect lysate diet, which mostly contained lipids. Moreover, several interesting unknown peptides and proteins were also upregulated and might get into the focus of future research.

Zusammenfassung

Xenorhabdus und *Photorhabdus* sind Bakterien, die mit Nematoden der Gattung *Steinernematiade* und *Heterorhabditidae* in Symbiose zusammen leben[16]. In diesem Zusammenspiel dient der Nematode als Träger, der zunächst Insektenlarven infiziert, während *Xenorhabdus* und *Photorhabdus* als Angriffsorganismen den Tod des Insekts herbeiführen. Um das Insekt zu infizieren kann der Nematode das Hämocoel über die Trachea der Larve erreichen[3,4]. Im Insekt werden die Bakterien dann über den Darm aus dem Anus ausgeschieden[5]. Daraufhin werden die Bakterien aktiv, überwinden das Immunsystem des Wirtes und töten die Larve innerhalb von 48 Stunden[6]. Bei diesem Angriff steht den Bakterien ein großes Waffenarsenal zur Verfügung. Sie produzieren dabei Antibiotika, antimykotische Mittel, aber auch Lipasen und Proteasen[7,8]. Dadurch sind diese in der Lage, nicht nur das Insekt zu töten, sondern können den Kadaver zusätzlich vor anderen Fressfeinden schützen.

Das Ziel der Doktorarbeit ist die Identifizierung von Targets und die Aufklärung der Wirkmechanismen von Naturstoffen. Besonders im Mittelpunkt stehen dabei nicht-ribosomale Peptide (NRPs). Dabei kann die Arbeit im Wesentlichen in zwei Teilen aufgespalten werden. Der erste Teil umfasst die Synthese dieser Naturstoffe und neuer Derivate, die chemisch modifizierbar sind, während der zweite Teil sich mit dem damit verbundenen Analysemethoden beschäftigt. Daneben wurde ein großer Teil von Molekülen chemisch synthetisiert, um biosynthetische Produkte strukturell zu bestätigen.

In dieser Arbeit habe ich viele dieser Naturstoffe hergestellt. Dabei wurde manuell und in einigen Fällen halbautomatisch mit einem Peptidsynthesizer von Biotage gearbeitet. Hier wurde in den meisten Fällen die Fmoc-Schutzgruppenstrategie genutzt. Naturstoffe wie Silathrid, Xenoautoxin, Phenylethylamid, Tryptamid, 3-Hydroxyoktansäure, Rhabdopeptid und PAX wurden hergestellt. Daneben wurde weitere Peptide für die Verifizierung und Quantifizierung von NRPS Funktionen synthetisiert. Die so synthetisierten Peptide wurden z.B. zur Untersuchung des XU Ansatz für Peptidaldehyde (Andreas Tietze) und des SYNZIP Ansatz (Jonas Watzel) genutzt.

Die Struktur von Silathrid wurde ebenfalls mittels chemischer Synthese bestätigt. Diese sind Peptide, die nachweislich Quorum Quenching Aktivitäten zeigen und in einer Δ*hfq* Mutante gezeigt, der diesen Naturstoff ausschließlich herstellt.

Xenoautoxin wird von einer NRPS hergestellt, deren Biosynthesegencluster still ist. Mittels einer *X. doucetiae* Mutante, deren natürlicher Promotor durch einen Arabinose-induzierbaren Promotor ausgetauscht wurde, hatte man eine außergewöhnliche Beobachtung gemacht. Die induzierte Mutante zeigte autotoxische Symptome. Jedoch zeigten Tests mit von außen dazu gegebenen Xenoautoxin keine Aktivität. Es könnte daran liegen, dass das Molekül aufgrund seiner Eigenschaften (Größe oder Ladung), nicht über die Membran aufgenommen werden kann. Daraufhin wurde ein neues Derivat mit einer Biotin-Einheit hergestellt, welches durch einen Biotin-Transporter möglicherweise in die Zelle aufgenommen werden kann. Da diese Kupplung von Biotin an dem N-Terminus herausfordern war, wurde ein zusätzlicher C-6 Linker zwischen Biotin und Xenoautoxin gekoppelt. Leider zeigten die Tests mit *E. coli*, dass das neue Derivat immer noch keine antibiotischen Eigenschaften aufweist. Möglicherweise wurde das Peptid in diesem Fall ebenfalls nicht aufgenommen. In der Zukunft wäre es u.U. möglich Xenoautoxin mit Hilfe von Vesikeln in die Zellen zu schleusen. Somit wäre es möglich, sowohl die Aufnahme als auch die Wirkungsweise des Naturstoffes im Wirt nachzuweisen.

Phenylethylamid und Tryptamid sind sehr einfach aufgebaute Moleküle. Diese bestehen aus einer Fettsäure, welches mit einem Phenylethylamin oder Tryptamin gekoppelt ist. Eine HPLC-MS Analyse ergab, dass sich diese Moleküle zu großen Teilen im Zellpellet befinden. Daneben wurden diese Moleküle im Zuge einer Kooperation (PD Dr. Nadja Hellmann/Mainz) weiter untersucht. Die initialen Ergebnisse zeigen, dass diese lipophilen Moleküle höchstwahrscheinlich mit der Membran oder mit Proteinen wechselwirken, die sich auf der Membran befinden. Dies ist sehr interessant, da diese Naturstoffe Quorum Quenching Aktivität bei *Chromobacterium violaceum* zeigen. Möglicherweise wird der Signalweg durch die membraninteragierenden Eigenschaften dieser Naturstoffe gestört.

3-Hydroxyoktansäure wurde für die Strukturbestätigung von Phototemtide A hergestellt. Hierbei wurde festgestellt, dass die (*R*)-3-OH-Fettsäure zu dem Produkt

mit der richtigen Stereochemie führt. Für die stereoselektive Reaktion wurde das chirale Hilfsmittel Oxazolidinone genutzt. Des Weiteren wurde eine durch SmI_2 vermittelte Reformatsky ähnliche Reaktion genutzt. Der daraus hergestellte Naturstoff Phototemtide A ist ein zyklisches Lipopeptid. Ähnliche Moleküle in diese Klasse zeigen tensidische[17], antibakterielle[18], antimykotische[19], antiprotozoaische und cytotoxische[20] Aktivität.

Rhabdopeptide sind relativ kurze Peptide, die aus Aminosäuren mit hydrophoben Reste bestehen. Beispiele für solche Aminosäuren sind Valin, Leucin oder Phenylalanin. Zusätzlich sind die Moleküle teilweise oder ganz *N*-methyliert. Diese Peptide sind daher sehr hydrophob und stäbchenförmig aufgebaut. Sie zeigen gute antiprotozoische Aktivitäten gegen pathogenen Erreger wie *Trypanosoma cruzi* oder *Trypanosoma brucei*. Dennoch ist der Mechanismus noch nicht verstanden. Daher wurden zunächst einige Derivate dieser Peptide hergestellt und auf bioaktive Eigenschaften getestet.

Zudem wurden in der nahen Vergangenheit neuartige Verfahren entwickelt, die eine chemische Target-Identifikation ermöglichen. Besonders interessant ist zum Beispiel die Nutzung der Click-Chemie[21] verknüpft mit activity-based protein profiling (ABPP[22]) und photo-affinity labeling (PAL[11]). Diese Methoden ermöglichen eine orthogonale Markierung von synthetischen Wirkstoffen im biologischen System. In dieser Arbeit wurden acht neue Rhabdopeptidderivate hergestellt, die auf der Basis von PAL funktionieren. Diese tragen eine Diazarin-Gruppe, welches über Lichtinduktion zunächst mit dem biologischen Target reagieren kann. Als nächstes kann über eine Alkin-Gruppe das Molekül samt gebundenem Target-Protein über ein Pull-down Experiment angereichert und analysiert werden. Besonders interessant wäre hier eine Proteomanalyse, um zu zeigen welche Proteine möglicherweise durch die Rhabdopeptide inhibiert werden. In der Zukunft könnte man dazu isotopenmarkierte Rhabdopeptidderivate synthetisieren. Diese lassen sich besonders leicht einführen, indem man Methylierung mittels kostengünstigen ^{13}C- oder ^{2}H-markiertem Iodomethan einsetzt. Dadurch lässt sich theoretisch eine bessere Auflösung für die Massenspektrometrie erreichen ähnlich zum Verfahren wie „Stable isotope labeling by amino acids in cell culture“ (SILAC)

oder „Isobaric tag for relative and absolute quantitation“ (iTRAQ). Jedoch wäre dies fokussiert auf einzelne Zielmoleküle und nicht für die gesamte Proteinprobe.

PAX ist ein zyklisches Lipopeptid, welches durch seine Lysin-reiche Struktur eine Nettoladung von +5 (pH = 7) trägt. Es hat die typischen strukturellen Eigenschaften eines Biotensids, einen lipophilen Schwanz und eine ringförmige, hydrophile positiv geladene Ringstruktur. Dementsprechend wurde es als antimikrobielles Peptid (AMP) beschrieben, welche Aktivität vor allem gegenüber Gram-positiven Bakterien wie *Bacillus subtilis* und *Micrococcus luteus* zeigt. Neben seinen antibakteriellen Eigenschaften wurde es ebenfalls als antimykotischer Wirkstoff beschrieben. Es wurde vermutet, das PAX-Peptide von den produzierenden Bakterien in die Umgebung abgegeben werden und dort ihre Wirkung entfalten. Dennoch zeigten quantitative Untersuchungen mittels HPLC/MS, dass der Hauptteil dieses Peptides nicht im Überstand gefunden wird, sondern im Zellpellet.

Erklärt werden könnte dies durch die negative Ladung der bakteriellen Oberfläche, durch welche positiv geladene PAX Moleküle elektrostatisch angezogen würden. Dies ist ebenfalls ein oft beschriebener Mechanismus, der bei anderen kationischen AMPs, wie beispielsweise Cecropin, Mellitin und Drosocin, beobachtet wird. Zunächst lagern sich diese positivgeladenen Moleküle an der bakteriellen Oberfläche an, angezogen von der negativen Nettoladung. Dies führt voraussichtlich zu einer Depolarisation der Membran. Im nächsten Schritt dockt der hydrophobe Teil des Peptids an der Membran an und formt entweder Poren oder destabilisiert diese nachhaltig. Durch höchstauflösende Fluoreszenzmikroskopie konnte gezeigt werden, dass PAX bei hohen Konzentrationen (> 30 µg/ml) in das Zytosol von *E. coli* Zellen eindringt. Bei weiteren synthetisierten, wahrscheinlich potenteren PAX-Derivaten konnte zudem beobachtet werden, dass sich dabei Versikel an der Membranoberfläche bilden und abschnürren, was zum kompletten Solubilisieren der Zellemembran führen kann.

Da PAX jedoch gegenüber *Xenorhabdus* selbst keine Aktivität zeigt, besteht die Vermutung, dass diese Peptide eine mögliche Doppelrolle besitzen. Durch die Anreicherung von PAX könnte die Nettoladung der Membran verringert werden. Dadurch wäre das Bakterium gegenüber kationischen AMPs wie z.B. Melittin,

Drosocin oder Cecropin, welche von Insekten als erste Immunantwort produziert werden, zusätzlich geschützt.

In den darauffolgenden Experimenten wurden neue PAX Derivate hergestellt, die entweder eine Alkin- oder eine Azid-gruppe tragen. In einem weiteren Schritt wurden dann Fluoreszenzfarbstoffe wie Cy5 oder AF647 per Click-Chemie kovalent an die funktionalisierten PAX-Moleküle gebunden. Dieses Verfahren bietet einen großen Vorteil, da die Ladung und die Gesamtgröße der chemischen Sonde nicht stark verändert wird.

Diese so synthetisierten Derivate wurden zunächst auf ihre Bioaktivität getestet. Die antibakterielle Wirkung (9-40 µg/ml vs. *E. coli, >125* µg/ml vs. *X. doucetiae*) waren dabei vergleichbar zum Naturstoff. In Zusammenarbeit mit Dr. Christoph Spahn (Prof. Dr. Mike Heilemann) wurden mit den neuen Derivaten Experimente mittels konfokaler und höchstauflösender Fluoreszenzmikroskopie, genauer gesagt Einzelmoleküllokalisationsmikroskopie (SMLM[23]) durchgeführt. Für letzteres wurden neben den PAX-Molekülen selbst noch die Membran, sowie das Nukleoid der Bakterien mit einer räumlichen Auflösung von 20–50 nm abgebildet. Bei diesen Experimenten wurden die unterschiedlichen PAX-Derivate gegen *E. coli* und eine *X. doucetiae* PAX Mutante, welche kein PAX produziert, getestet. Die Resultate zeigten, dass PAX bei Zugabe in subinhibitorischen Konzentrationen an der Membran beider Spezies lokalisiert war. Hierbei gab es keinen Unterschied, ob dabei das Alkin oder das Azid Derivat genutzt wurde. Der Membranfarbstoff Nile Red wurde hierbei als Referenz genutzt. Zugabe der Derivate in Konzentrationen über der minimalen inhibitorischen Konzentration (*minimal inhibitory concentration*, MIC) führte bei *E. coli* Zellen zum Eindringen in das Zytosol, das dabei reorganisiert wurde. Besonders deutlich war die Veränderung beim bakterielle Nukleoid zu beobachten, welches nun statt seiner ursprünglichen langgestreckten und stark strukturierten Form deutlich kompaktiert vorlag. Dies deutet darauf hin, dass PAX antibakteriell wirkt, indem es zunächst die Membran schädigt, anschließend mit anionischen Komponenten des Zytosols interagiert und somit zu einer Reorganisation zytosolischer Strukturen führt.

Im Anschluss darauf wurden Mikrodilutionsverfahren mit AMPs aus Insekten durchgeführt. Dabei wurde *X. doucetiae* (WT) mit der *pax*$^{+}$ und *pax*$^{-}$ Mutante getestet. Die Ergebnisse zeigten, dass der Wildtyp und der *pax*$^{+}$ Stamm höhere Resistenzen gegenüber dem *pax*$^{-}$ Stamm zeigen, welcher kein PAX produziert. In weiteren Test konnten wir bei *E. coli* ebenfalls interessante Resultate erzielen. *E. coli* Stämme, die mit einer PAX Konzentration unterhalb der MIC behandelt wurden, sind gegenüber AMPs resistenter als *E. coli* Stämme, die nicht mit PAX behandelt sind.

Diese Ergebnisse zusammengenommen deuten darauf hin, dass die PAX Moleküle eine duale Funktion erfüllen. Auf der einen Seite sind diese sowohl antimikrobiell als auch antimykotisch. Andererseits könnten die gleichen Peptide die Membran der produzierenden Bakterien depolarisieren und dadurch andere vom Wirtsinsekt produzierte AMPs davon abhalten, mit der Membran von *Xenorhabdus* und *Photorhabdus* Zellen zu interagieren.

In den letzten Jahren gab es bedeutende Fortschritte im Bereich der Proteinanalyse. Vor allem die Entwicklung von hochauflösenden und high-performance Detektoren wie qTOF[24] und Orbitrap[25] schafften eine neue Methodik zur Untersuchung von Peptiden. Zusammen mit Datenbankverfahren (*in silico* Generierung von Peptiden aus bekannten Proteinsequenzen) wurde qualitative und quantitative Analysen von hochkomplexen Proteinproben ermöglicht.

Mit Hilfe dieser Methoden sollte das Proteom von *Xenorhabdus* und *Photorhabdus* untersucht werden. Dazu werden die Stämme zunächst kultiviert und dann mit Insektenlysat versetzt. Anhand der Änderungen des Proteoms sollten neue Erkenntnisse über das Verhalten der Bakterien gewonnen werden. Zusätzlich wurden die quantifizierten Proteine mit Hilfe von „Kyoto Encyclopedia of Genes and Genomes“ (KEGG) innerhalb ihrer jeweiligen metabolischen Stoffwechselwege kartiert.

Die Resultate zeigen, dass in allen untersuchten Stämmen der Lipidabbau und der Glyoxylatzyklus hochreguliert wurde. Dies steht im Einklang mit der Erwartung, da das Insektenlysat bzw. das Insekt selbst sehr fettreich ist. Das aus dem Lipidabbau

gewonnene Acetyl-CoA wird im Glyoxylatzyklus weiter umgesetzt, wo es zu Oxalacetat umgewandelt wird. Dieser Metabolit kann anschließend entweder für den Zuckeraufbau oder im Citratzyklus zur Energiegewinnung eingesetzt werden.

Daneben wurden weitere Proteine gefunden, die ebenfalls für einzelne Stämme hochreguliert wurden. Diese könnte in zukünftigen Arbeiten genauer untersucht werden. Zudem könnte man zukünftig diese Proteomanalysen mit ABPP oder PAL Methoden erweitern, um Proteintargets in komplexen Zellmischungen zu untersuchen.

1. Introduction

1.1 *Xenorhabdus* and *Photorhabdus*

The life cycle of *Xenorhabdus*/*Photorhabdus* and entomopathogenic nematodes

Xenorhabdus and *Photorhabdus* are Gram-negative bacteria from the family Enterobacteriaceae[26–28]. They live in symbiosis with the genera *Steinernema* and *Heterorhabditis*, respectively[16].

In the initial phase of the life cycle (Figure 1), *Xenorhabdus* or *Photorhabdus* are carried in the intestine of infective juvenile nematodes[2,16,29]. To infect the insect larva, nematodes have been reported to enter into the hemocoel via the trachea[3,4]. Inside the host, the nematodes release the bacteria through the anus[5]. In the insect, *Xenorhabdus* or *Photorhabdus* rapidly overcome the immune system of the insect and kill the prey within 48 h[29]. Besides producing several antibiotics[7,8], which lead to the extermination of competitive bacteria, proteins like lipase, phospholipase, and proteases are expressed[16]. In this optimal condition, the nematodes develop and reproduce. Finally, the infective juvenile nematodes accommodate the bacteria in their intestinal tract and emerge from the insect cadaver to find a new host[2].

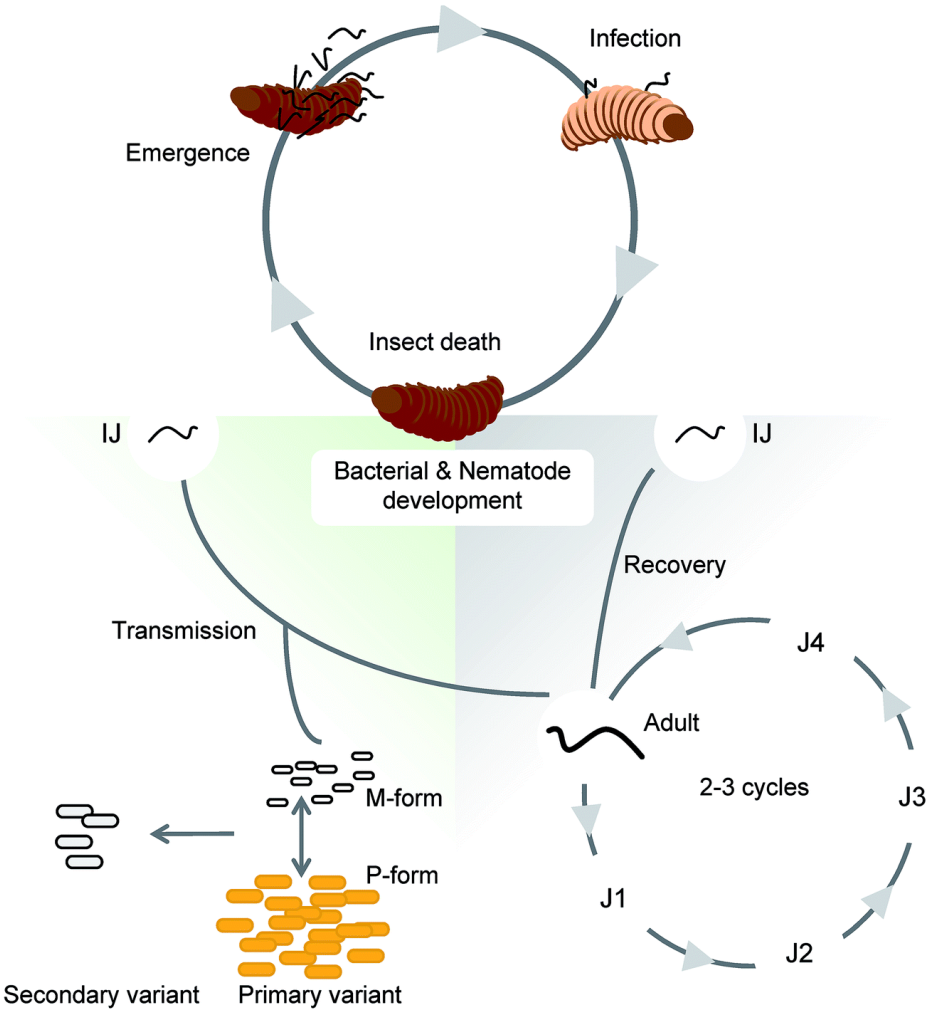

Figure 1: The life stages of *Photorhabdus* in *Heterorhabditis.* Initially, *P. luminescens* lives in *Heterorhabditis's* gut. The nematode in the infected juvenile (IJ) stage enters the insect larvae and releases the bacteria into the hemocoel, where it replicates and kills the insect. Hereby, the nematodes reenter the adult stage, where it takes in food and reproduce. The nematode evolves through four different larval stages (J1-J4), two to three times. The nematodes switch back to the IJ stage when the food source is depleted. Here, the bacteria undergo a unidirectional switch into the secondary variant. An additional promoter switch was found to be responsible for differentiating the primary variant M- from the P-form. In contrast to the M-form, the P-form does not produce natural products and can be transmitted into the nematode[30] (Copyright © Royal Society of Chemistry. Permission/License is granted.).

1.2 Peptides

A peptide is a short chain of amino acids with up to 50 units[31] while larger units are classified as protein (Figure 2). Peptides are essential for life and ubiquitous in all organisms. Bioactive peptides have been described to have modes of action linked to antimicrobial[32], antithrombotic[33], antihypertensive[34], opioid-related[35], immunomodulatory[36], mineral binding[37], and anti-oxidative activities[38].

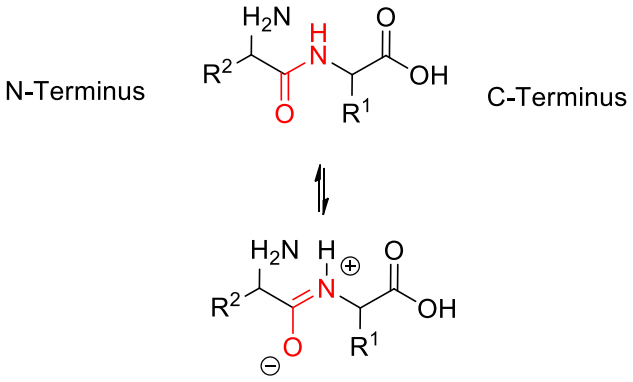

Figure 2: Schematic view of the peptide bond. It is shown as the red marked amide bond between the amine group and the carboxyl group of two consecutive amino acids. This is a stable covalent bond with a partial double bond character.

Moreover, peptide drugs have improved the lives of millions and meanwhile reached blockbuster status (Figure 3). One example is cyclosporine[39]. It is a cyclic peptide derived from a non-ribosomal peptide synthetase (NRPS) from the fungus *Tolypocladium inflatum*. The molecule is described to inhibit highly specific T cell activation[40]. It is marketed as Restasis and used for the treatment of rheumatoid arthritis, psoriasis, Crohn's disease, nephrotic syndrome, keratoconjunctivitis sicca (dry eyes) and in organ transplants to prevent rejection[41]. In 2018, the drug brought in $1.3 billion in revenue[42].

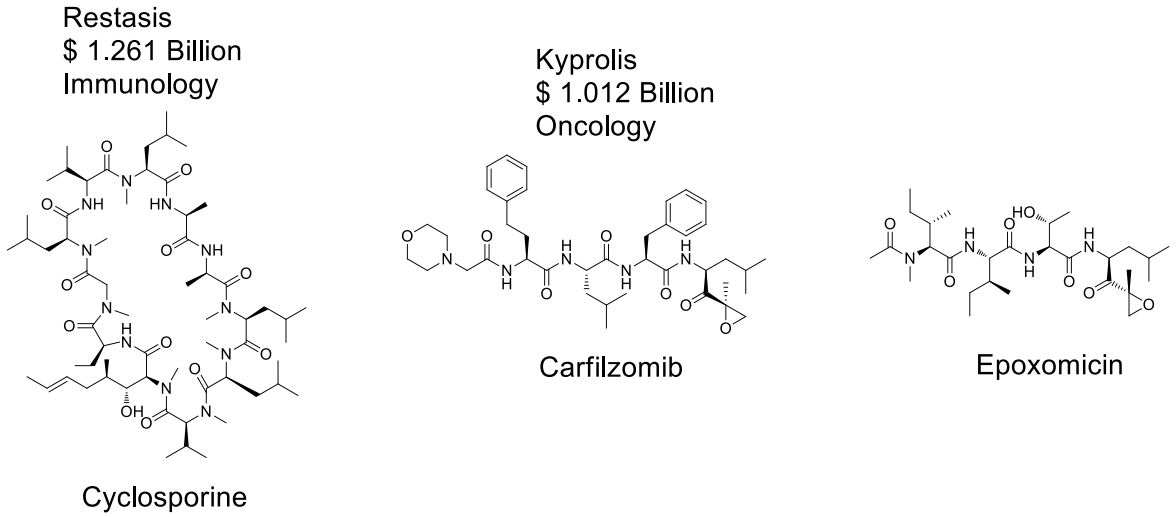

Figure 3: Structures of blockbuster peptide drugs Restasis and Kyprolis. Carfilzomib was originally derived from the NRPS/PKS product epoxomicin.

Photorhabdus and *Xenorhabdus* encode both NRPS and NRPS/PKS-hybrids. Furthermore, they produce a large variety of other natural products[30].

1.3 Non-ribosomal peptide synthetase (NRPS)

NRPSs are large modular-structured multi-enzyme complexes, which can build molecules based on natural and unnatural amino acid building blocks that often have a length of 3-15 amino acids[43]. These non-ribosomal peptides (NRPs) are produced independent of mRNA and the ribosome and they can carry manifold modifications, such as *N*-methylation, *N*-formylation, glycosylation, acylation, halogenation, hydroxylation, etc. Intramolecular cyclization products such as oxazolines and thiazolines can also be catalyzed by these enzymes[44]. Moreover, a broad number of NRPS and polyketide synthase (PKS) hybrids exist in nature[45] and therefore expand the structural range considerably.

NRPs have a wide range of bioactivity, known as toxin[46], surfactant[47], siderophores[48], proteasome inhibitors, etc[49]. This biosynthetic method is called a multi-enzyme thiotemplate mechanism[50]. In this model, the peptide bond formation is produced on a large multi-enzyme complex, which is both template and biosynthetic machinery. Despite their structural diversity, most NRPS have a strict modular architecture[51]. A minimal elongation module consists of three domains: adenylation (A) domain, a peptidyl carrier protein (PCP), or thiolation(T) domain and condensation (C) domain.

In the beginning, the amino acid carboxylic acid group is activated. Here, the A domain is responsible for the recognition and activation of the substrate. ATP hydrolysis is used to create the corresponding aminoacyl-adenylate. The reactive intermediate is transferred to the free thiol group of an enzyme-bound 4'-phosphopantetheinyl cofactor (ppan), resulting in a covalent bond between the substrate and T domain. At this point, the molecule can be modified for example by epimerization or *N*-methylation. In the next step, the substrate is transferred by the T domain to the C domain and elongated with the next building block. Here, the free amine of the next amino acid can attack the carboxy-thioester. The transport of the thioester between catalytically active units is facilitated by the ppan cofactor. After the final coupling step, the C-terminal thioesterase (TE) releases the peptide (Figure 4).

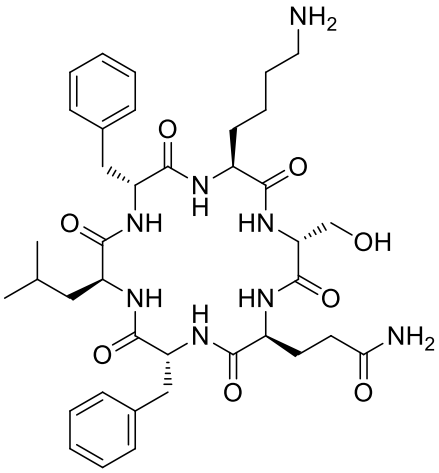

Ambactin

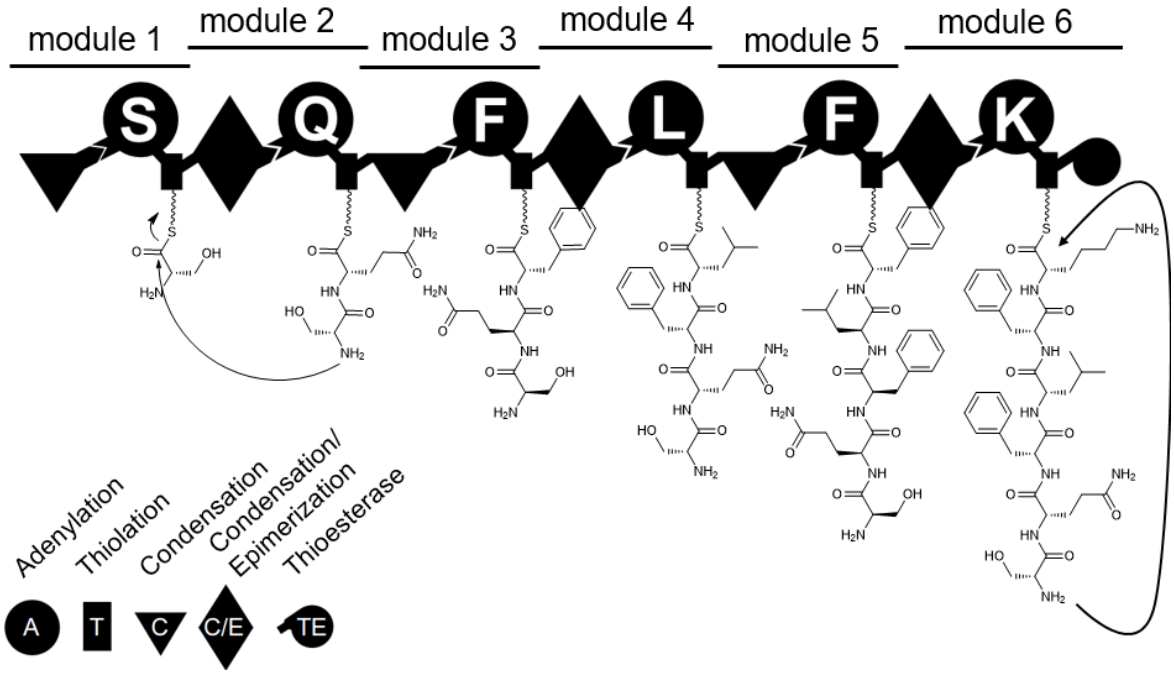

Figure 4: Ambactin structure and biosynthesis[9]. A schematic representation of the NRPS is shown. The NRPS starts with serine and follows with the remaining amino acid subsequently. In the end, the serine side chain cyclizes with the C-Terminus of lysine. The symbols used for domain assignment are **A**, large circle; **T**, rectangle; **C**, triangle; **C/E**, diamond; **TE**, **C**-terminal small circle (Copyright © Springer Nature. Permission/License is granted).

1.4 The art of making peptide bonds

It is possible to force a condensation reaction between an amine and a carboxylic acid by heating the solid mixture over 180°C[52] or with 150°C under microwave irradiation[53]. However, these solvent-free approaches are unsuitable due to unstable residues in amino acids.

The main problem of the reaction is the activation of the unreactive carboxylic acid residue due to resonance stabilization. Over time, many approaches were developed by activating the carboxylic acid via acyl halide, acyl azide, acyl imidazole, anhydride, and ester, etc[54].

However, peptide synthesis is not always straightforward. Racemization can occur (Figure 5) through an intramolecular reaction leading to an oxazolone product. This molecule is deprotonated under mild basic environment and forms a stable achiral anion. Finally, both oxazolone enantiomer can arise from the achiral intermediate.

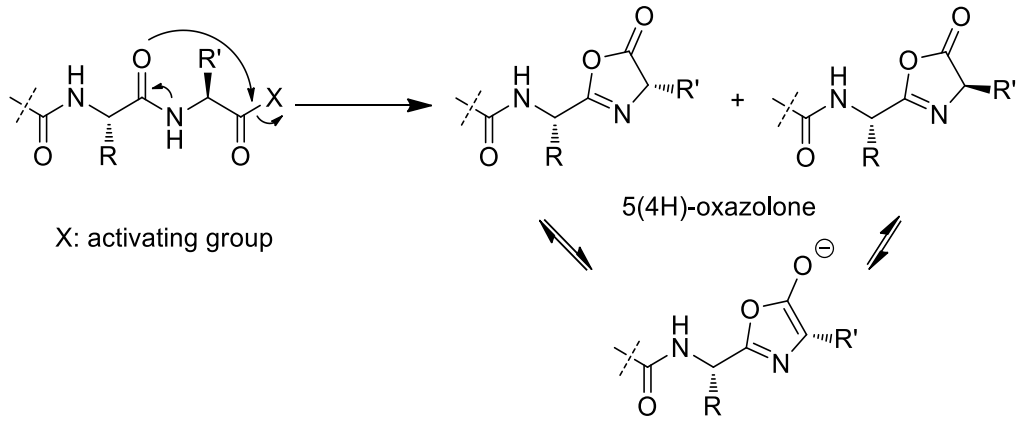

Figure 5: Possible racemization side reaction occurring during peptide synthesis. This can lead to enantiomeric products. The side reaction can be suppressed by adding HOBt or HOAt.

Carbodiimide method

In this method, the amino acid is converted into a mixed anhydride. Therefore, the formation of the urea derivatives is the thermodynamic driver for the reaction. The most often used reagents are dicyclohexylcarbodiimide (DCC), diisopropylcarbodiimide (DIC), and *N*-(3-dimethylaminopropyl)-*N*'-ethylcarbodiimide (EDC). The usage of EDC should be favored due to its low toxicity when compared to DIC and DCC.

A disadvantage of this method is the formation of unreactive *N*-acylurea. However, this can be prevented by cooling the reaction to 0°C or to convert the side product *O*-acylurea with 1-hydroxybenzotrial (HOBt) in a less reactive ester.

Uronium Salt

Uranium salts are another class of popular reagents for peptide bond formation. Similarly, the driving force of the reaction is the formation of urea (Figure 6) when compared with carbodiimide. Popular examples are *O*-(1-H-benzotriazole-1-yl)-*N,N,N',N'*-tetramethyluronium hexafluorophosphate (HBTU) or *O*-(7-azabenzotriazol-1-yl)-*N,N,N',N'*-tetramethyluronium-hexafluorophosphate (HATU). HATU is especially often used in the synthesis of steric demanding amino acid. Another interesting coupling reagent is 2-(6-chloro-1*H*-benzotriazole-1-yl)-1,1,3,3-tetramethylaminium hexafluorophosphate (HCTU). It provides similar coupling efficiency and is more cost-effective[55].

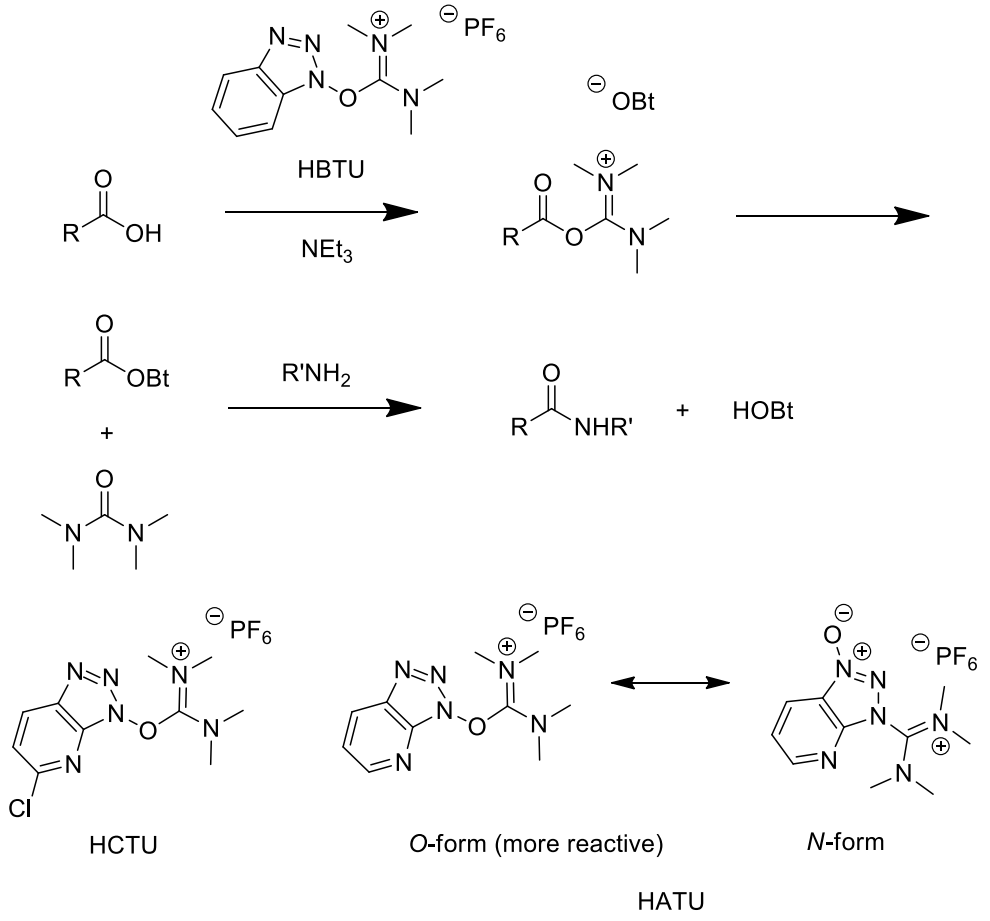

Figure 6: HBTU reacts with the carboxylate ion forming a urea derivative, the driving force of the reaction. The activated amino acid reacts with the free amine group of the next amino acid forming a new peptide bond. Uronium salt, such as HBTU, HCTU, and HATU, can occur in the *O*- or *N*-form. The *N*-form is considered to be more stable, but less reactive[56].

The reaction with uronium salt can lead to a side reaction forming guanidine (Figure 7). This can be prevented by adding HOBt or 1-hydroxy-7-azabenzotriazole (HOAt).

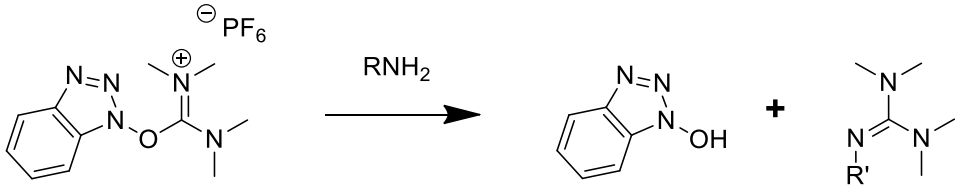

Figure 7: HBTU reacts with free amine leading to an unreactive guanidine side product. This reaction can be suppressed by adding HOBt or HOAt.

1.5 Solid-phase peptide synthesis

Solid-phase peptide synthesis (SPPS, Figure 8) is a widely used method for peptide, DNA, and RNA synthesis. In comparison to solution-phase techniques, it is uncomplicated to automate the tasks using machines[57,58]. Especially for peptide synthesis, the base-labile temporary Fmoc protection strategy is favored due to the absence of corrosive HF usage.

Initially, the synthesis starts with the loading of the first amino acid to the resin. From this point on, the cycle starts with the removal of the protective group and continues with the coupling stage. A wide variety of coupling reagents are available to activate the amino acid[54,59,60]. Especially, Oxyma[61], EDC[62], HOBt[63], HCTU[55], and HATU[64] have gained popularity in recent times.

The amino acid with reactive side chains is protected with base-resistant protective groups to avoid side reactions. The usage of the protective groups with different cleaving conditions is called orthogonal protecting group strategy. It is a common concept in the synthesis to control the synthesis of larger molecules, such as carbohydrates[65] and peptides[66].

After each synthesis cycle, an additional Kaiser-test[67] can be facilitated for turnover control. Besides, a capping[68] step can be added to prevent unreacted side products to be elongated in the next cycles. This simplifies the purification process because the capped side products are smaller in size.

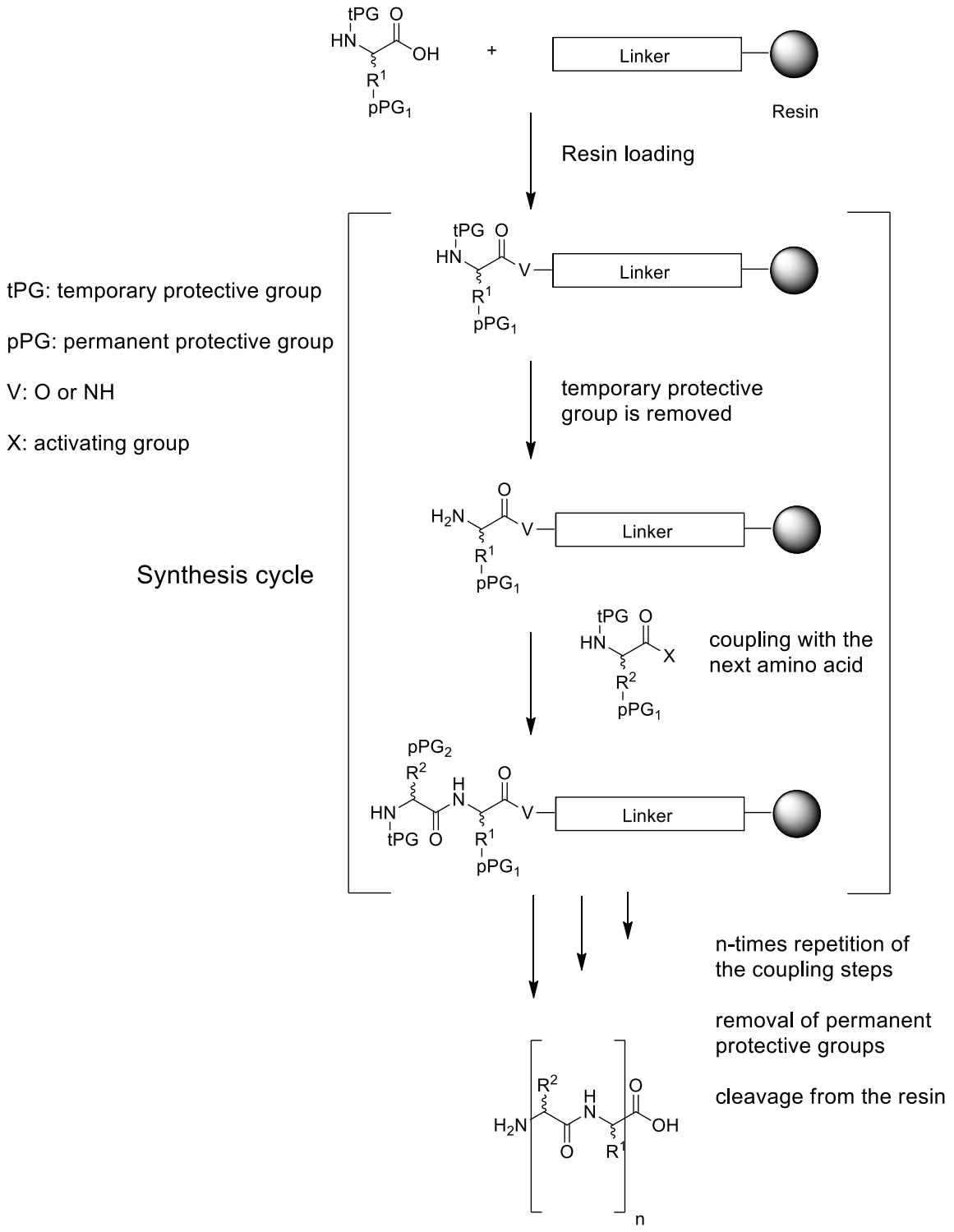

Figure 8: Peptide synthesis coupling cycle. The reaction starts with the loading of the first amino acid on the resin. After that, the temporary protective group (e.g. Fmoc) is removed to couple the free amine group with the next activated amino acid. After the successful coupling, the cycle restarts and proceed until the peptide is finished. Hereafter, the permanent protective groups of the side chains can be removed and the peptide cleaved from the resin.

1.6 Natural products from *Xenorhabdus* and *Photorhabdus*

Xenorhabdus and *Photorhabdus* produce many natural products, which have been found in various strains (Figure 9). Many functions of these peptides are still unknown, and they might become interesting drug candidates in the future.

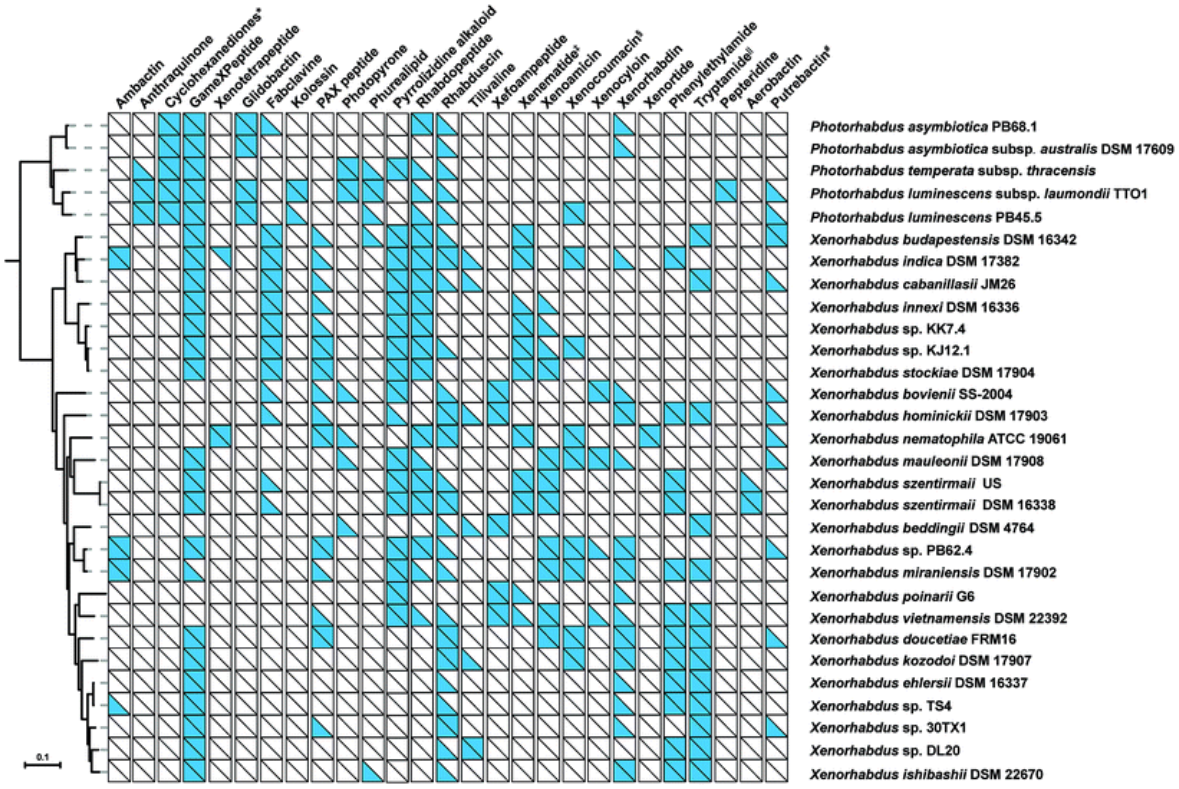

Figure 9: Phylogeny of overall 30 *Photorhabdus* and *Xenorhabdus* strains based on 632 core genes showing the occurrence of known BGCs (lower triangle) and/or the respective natural products (upper triangles)[69] (Copyright © Springer Nature. Permission/License is granted.).

.

Silathride

The peptide silathride **(1)** is a 9-mer peptide (Figure 10), which was initially identified from *P. luminescens* PB45.5[1]. This natural product was recently obtained by promoter activation in Δ*hfq* mutants. Bioactivity tests revealed that the substance had good activities against *Chromobacterium violaceum* (Quorum sensing)*, Candida parapsilosis, Pseudozyma prolifica, and Cryphonectria parasitica*[1] (Figure 11). The peptide has no significant modifications and was not found in any database, such as Pepbank[70], Peptide Atlas[71], or Uniprot[72].

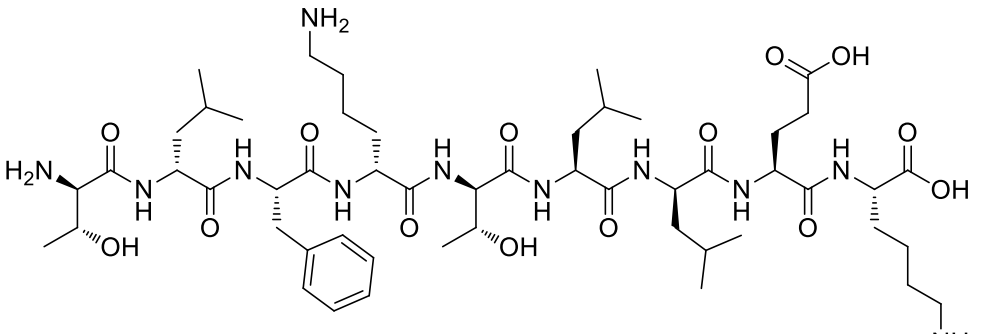

1

Figure 10: Structure of silathride identified in *P. luminescens PB45.5*[1].

In this work, synthetic silathride was produced to verify the structure of the natural compound.

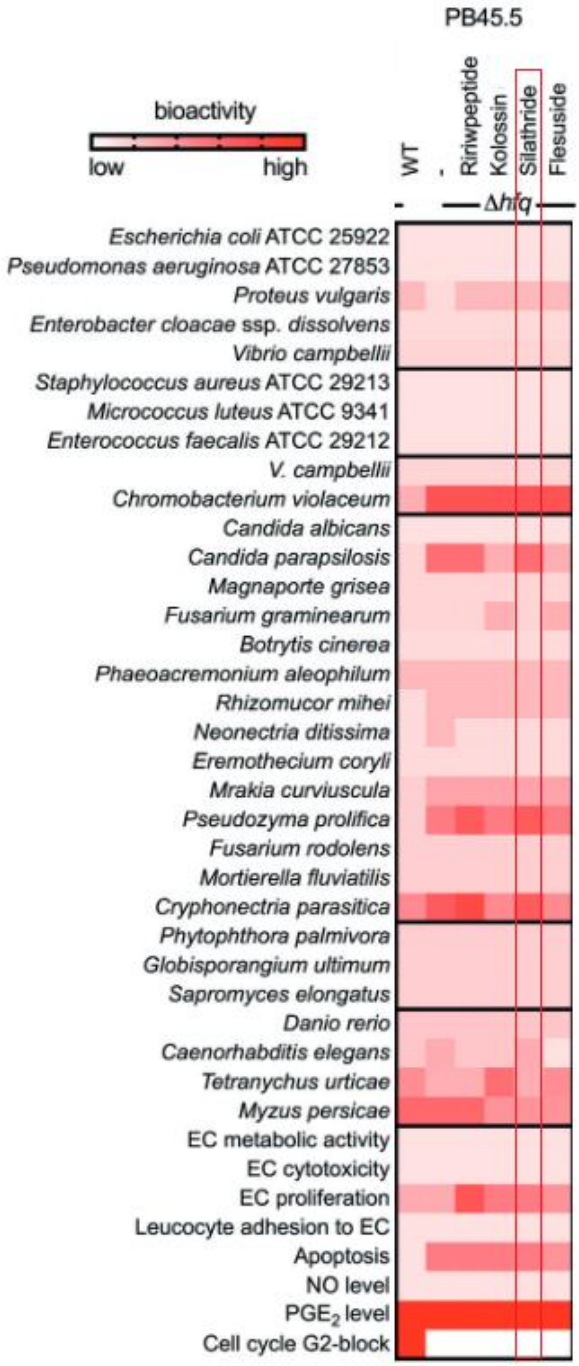

Figure 11: Assays of desired natural products (top) enriched in cell-free culture from *Δhfq*-P_{BAD}-xy mutants against wild type (WT) or *Δhfq* alone against different organisms. Five different levels were determined by different assays: none (white) to the highest activity (red)[1] (This figure is from an open access article under the terms of the http://creativecommons.org/licenses/by/4.0/ License, which permits use, distribution, and reproduction in any medium provided the original work is properly cited).

Xenoautoxin

Xenoautoxin (Figure 12) was discovered in *X. doucetiae* after a promotor exchange using the P_{BAD} promotor in front of the *xaxABC* gene cluster. Under normal laboratory conditions, the cluster was silent resulting in no production of the natural product. However, the cultures of $P_{BAD}xaxA^{+}$ showed surprisingly autotoxic symptoms after induction. Only after a certain time the cultures recovered and were growing at a normal rate[73]. In addition, a biotinylated derivative **(2)** was synthesized to elucidate, whether this peptide can be transported through a biotin transporter into *E. coli* cells and induce toxicity.

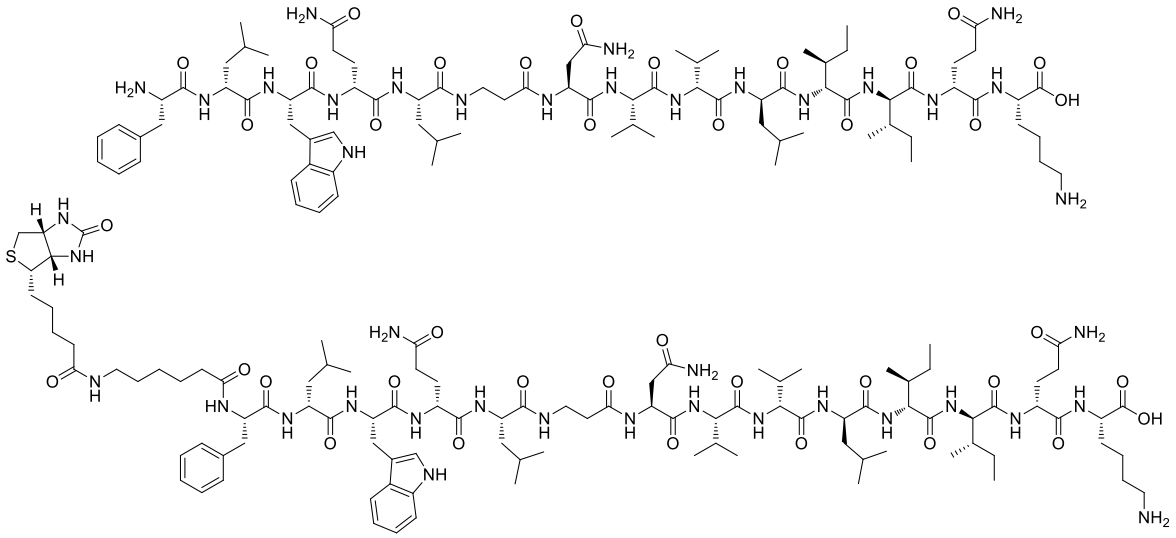

2

Figure 12: Structure of xenoautoxin and biotinylated xenoautoxin (**2**). Xenoautoxin was initially found in *X. doucetiae*, while biotinylated xenoautoxin was synthesized to utilize a biotin transporter for compound uptake into bacteria cells.

Phenylethylamides and tryptamides

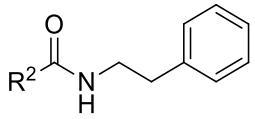

Phenylethylamide

R^2 = methyl **(3)**, nonanyl **(4)**, nonadecanyl **(5)**

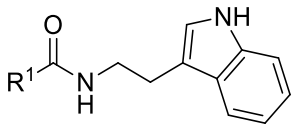

Tryptamide

R^1 = nonyl **(6)**, undecanyl **(7)**, dodecanyl **(8)**, pentadecanyl **(9)**, heptadecanyl **(10)**

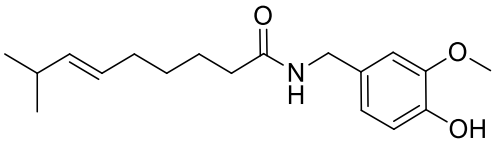

Capsaicin

Figure 13: Structures of phenylethylamides, tryptamides, and capsaicin. Phenylethylamide and tryptamides were extracted from *X. doucetiae*, while capsaicin is an active component found in chili peppers from the family *Solanaceae*[74].

Phenylethylamides and tryptamides are widespread in many organisms, such as bacteria[75–78], sponges[79], plants[80], fungi[81], insects[82], and even octorcorals[83,84]. They are simple fatty acid amide and structurally related to capsaicin, the well-known spicy compound from the *Solanaceae* plant family (Figure 13). Here, instead of phenylethylamine or tryptamine, vanillylamine is coupled to 8-methyl-6-nonenoic acid. These molecules have been linked to quorum sensing activities against Gram-negative bacteria such as *Halobacillus salinus*[85] and *Chromobacterium violaceum*[74] and they are frequently found in *Xenorhabdus* and *Photorhabdus* strains (Figure 9)[30].

In this work, several derivatives were synthesized and tested in a collaboration (PD Dr. Nadja Hellmann/Mainz) in various membrane activity experiments.

Synthesis of various peptide standards (SYNZIP approach)

Peptide standards were synthesized to verify the structures of several biosynthetic products generated as part of the NRPS engineering efforts of the (Jonas Watzel) Bode lab[86]. As a new approach, it was possible to create new NRPS modules using SYNZIPs without impairing domain-domain interface interactions[86] and chemical synthesis was needed to confirm the structures of these new peptides.

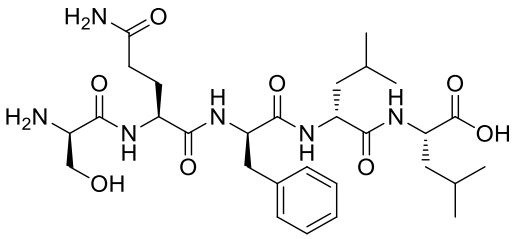

11

SYNZIP peptide 1

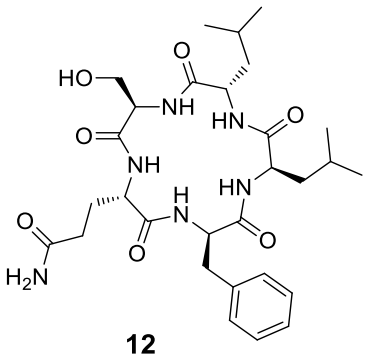

12

SYNZIP peptide 2

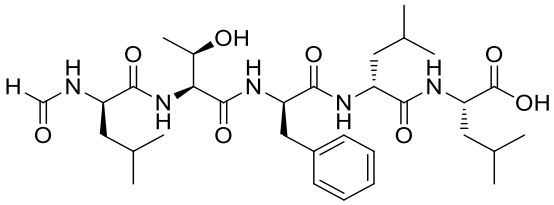

13

SYNZIP peptide 3

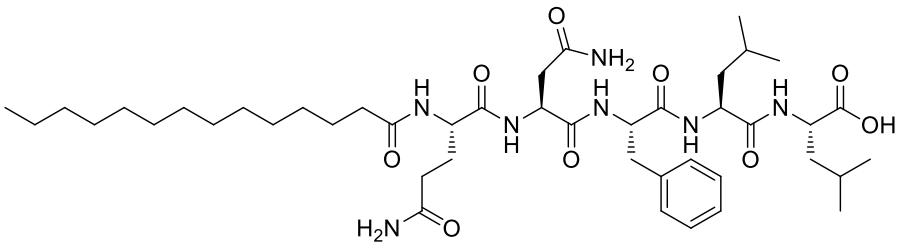

14

SYNZIP peptide 4

Figure 14: NRPs synthesized as standards to allow their quantification of peptides derived from SYNZIP constructs. The new peptides were constructs derived from the assembly of NRPSs involved in szentiamide, GameXPeptides[30], ambactin, and xenolindicins biosynthesis[87].

Synthesis of various peptide standards (Peptide aldehydes)

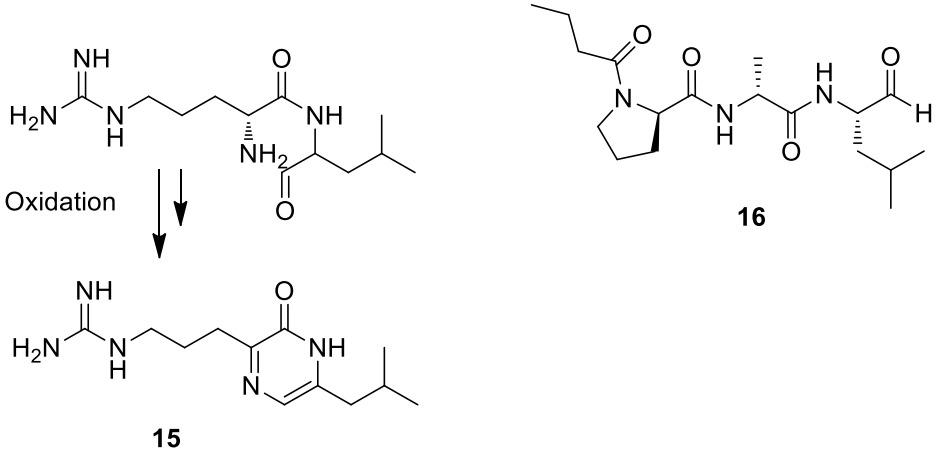

Figure 15: Peptide aldehyde structures synthesized as standards for Andreas Tietze[88] (Bode lab).

These two peptide aldehydes (Figure 15) were constructed by Andreas Tietze using the XU concept[89]. Although they possess different structures, the C-terminus is in both cases an aldehyde. However, the (left) molecule underwent a spontaneous intramolecular reaction to form a six-membered ring.

In general, the two peptide aldehydes are products from NRPS, which contains thioester reductase domain catalyzing two-electron reductions[90] in this case.

Bortezomib[91] has been developed based on these peptide aldehyde products. It is shown that numerous aldehydes demonstrated the ability to inhibit the activity of the proteasome complex[92] forming hemiacetal adducts with a threonine nucleophile of ß-subunits[93]. Therefore, it is very interesting to create new peptide aldehydes to find new possible targets and new applications in the therapeutic area.

Rhabdopeptide, mevalagmapeptide and xenortide derivatives

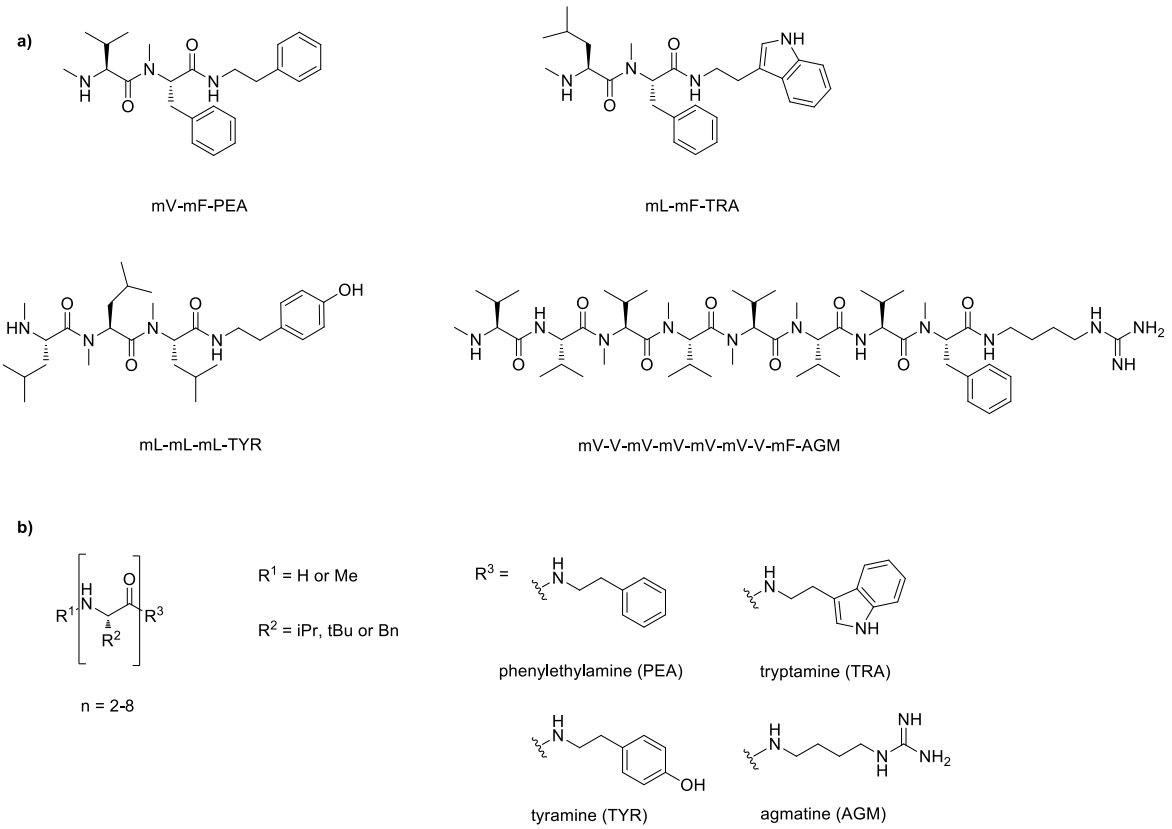

Figure 16: Structures of selected RXP derivatives highlighting the chemical diversity. **a)** Structures of selected RXPs from different *Xenorhabdus* and *Photorhabdus* wild-type strains showing the differences in size, amino acid composition, and terminal amines. **b)** The general formula of RXPs summarizing possible modifications[94].

This class of molecules is produced by entomopathogenic bacteria of the species *Xenorhabdus* and *Photorhabdus*[95] (Figure 9). Examples of rhabdopeptide/xenortide-like peptides (RXPs) namely xenortide[96], rhabdopeptide[95], and mevalagmapeptide[97] are shown (Figure 16).

More than 60 RXP derivatives have been identified in different *Xenorhabdus* and *Photorhabdus* species (Figure 16)[94]. Many of these derivatives showed activity against *Plasmodium falciparum* and several *Trypanosoma* strains, but their mode of action is still unknown[98].

To determine their cellular targets, several derivatives were designed using the PAL approach (Figure 17, Table 1). The main goal is to use them in pull-down experiments with combination with proteome analysis to find putative targets of this compound class.

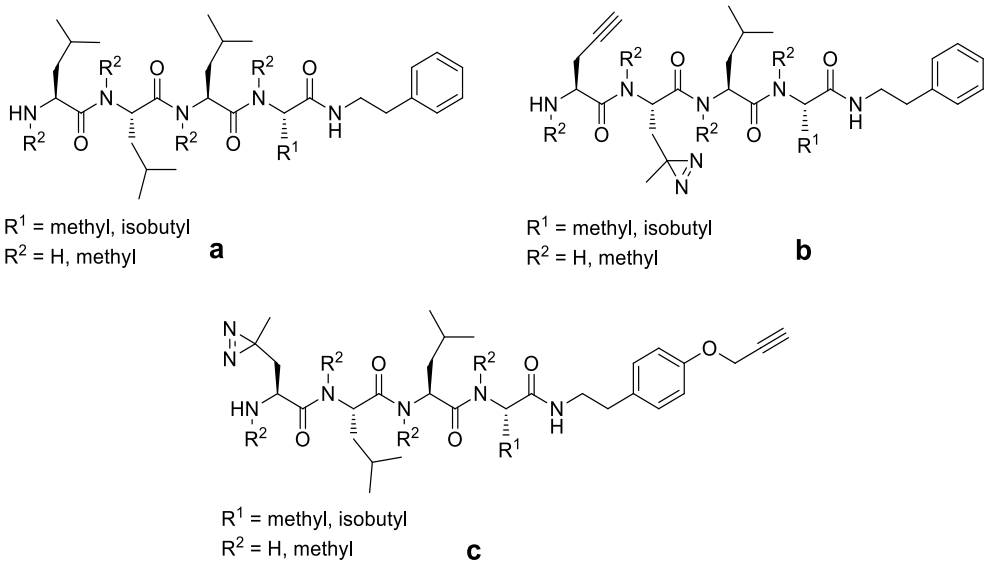

Figure 17: Structures of new synthetic rhabdopeptides. Structure **a)** are natural rhadbopeptides, while **b)** and **c)** are peptides with diazarine (for Photo-affinity labeling PAL) and alkyne moieties (for tandem labeling) (See chapter 1.7 for additional information).

Table 1: Nomenclature of rhabdopeptide derivatives.

Name	Compound	structural class	R^1	R^2
rhabdopeptide 1	**17**	a	methyl	H
rhabdopeptide 2	**18**	a	isobutyl	H
rhabdopeptide 3	**19**	a	methyl	methyl
rhabdopeptide 4	**20**	a	isobutyl	methyl
rhabdopeptide 5	**21**	b	methyl	H
rhabdopeptide 6	**22**	b	isobutyl	H
rhabdopeptide 7	**23**	b	methyl	methyl
rhabdopeptide 8	**24**	b	isobutyl	methyl
rhabdopeptide 9	**25**	c	methyl	H
rhabdopeptide 10	**26**	c	isobutyl	H
rhabdopeptide 11	**27**	c	methyl	methyl
rhabdopeptide 12	**28**	c	isobutyl	methyl

Chiral 3-hydroxyoctanoic acid for phototemtide A

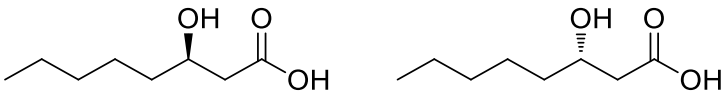

29 **30**

Figure 18: Structures of 3-hydroxy fatty acid synthesized as a building block for the depsipeptide phototemtide A.

3-Hydroxy fatty acids (Figure 18) with 10-18 carbon chain length have been described as constituents of the endotoxin lipopolysaccharide (LPS) of Gram-negative bacteria[99,100]. These fatty acids have been well studied because they were linked to the development of numerous infectious diseases, allergenic responses, and respiratory symptoms[101–104]. 3-hydroxyoctanoic acid is also a building block for the synthesis of phototemtide A.

Phototemtide A was initially found in *Photorhabdus temperata* (Figure 19) and is produced by the biosynthetic gene cluster *pttABC*[105]. It belongs to the family of cyclic lipopeptides, which have been described to show biosurfactant[17], antibacterial[18], antifungal[19], antiprotozoal[106], and cytotoxic activities[20].

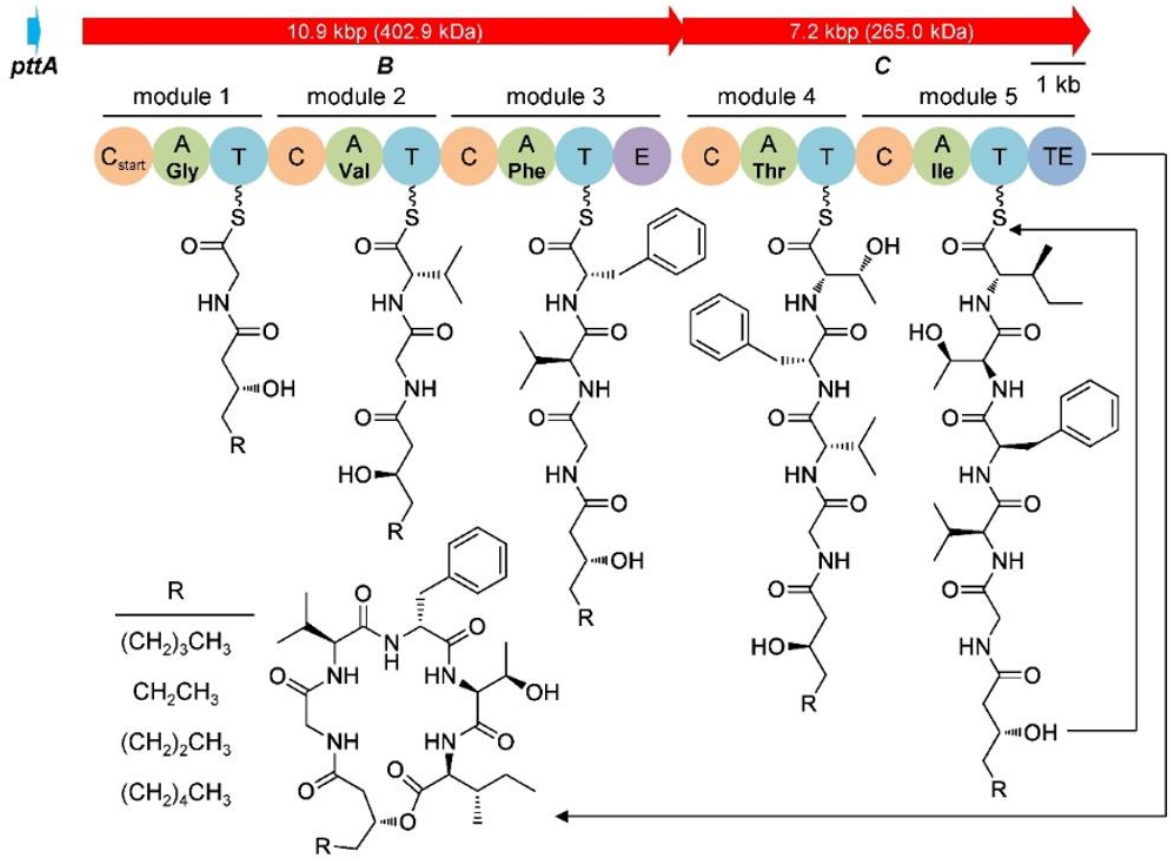

Figure 19: Biosynthetic gene cluster and proposed biosynthesis of phototemtides A–D. Domains: C_{start}: starter condensation, C: condensation, A: adenylation, T: thiolation, E: epimerization, TE: thioesterase[105].

Peptide antimicrobial from *Xenorhabdus* (PAX)

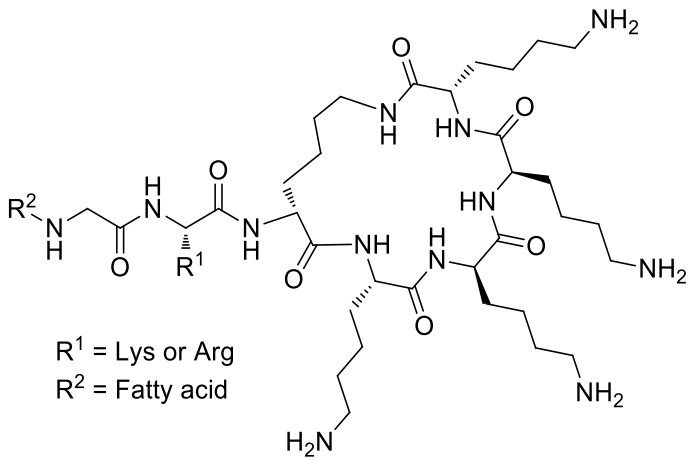

Figure 20: General structure of PAX[107] from *Xenorhabdus nematophila*.

PAX peptides (Figure 20) were initially isolated from an *X. nematophila* F1 strain[14,107]. In general, the PAX biosynthesis cluster is present in many *Xenorhabdus* strains (Figure 9). However, these peptides are not easily detected in the supernatant by HPLC-MS/MS methods without pre-purification using cation exchange chromatography[14,107,108]. It might be the reason, why the biosynthetic gene cluster is present in many strains, but the peptide is only found in a subset of strains. PAX possesses a cationic cyclic structure with a hydrophobic 3-hydroxy fatty acid tail. It can be effortlessly dissolved in water and creates foam when mixed. Therefore, this peptide can be classified as a biosurfactant.

PAX was initially described as anti-microbial peptide and tested against Gram-negative bacteria, Gram-positive bacteria, and fungi. It showed moderate activity against *Micrococcus luteus* CIP 53.45 and *Fusarium oxysporum* H3012[14].

However, producing PAX might have additional benefits for *Xenorhabdus*. The bacterial membrane is negatively charged and therefore a target for AMPs from insects where they are part of the insect immune system. By producing PAX, *Xenorhabdus* might be able to depolarize its membrane charge, therefore avoiding becoming the target for AMPs. Hereby, the peptide might possess a dual offensive and defensive mechanism.

1.7 Chemical targeting and labeling methods

Click reaction

"Click" means to build new molecular bonds of two molecules with ease like joining two pieces of a seat buckle[109]. Moreover, the reactions are tolerant towards various functional groups and occurred under most solvents including aqueous systems and at low temperatures. Furthermore, they have a high thermodynamic driving force, usually greater than 20 kcal mol^{-1}. Therefore, it was possible to develop specific and controllable biorthogonal reactions based on these reactions for complex cell lysates[110,111] and even in live cells[112].

The most well-known type of approach of "click chemistry" is [3+2] cycloaddition, such as huisgen 1,3-dipolar cycloaddition.

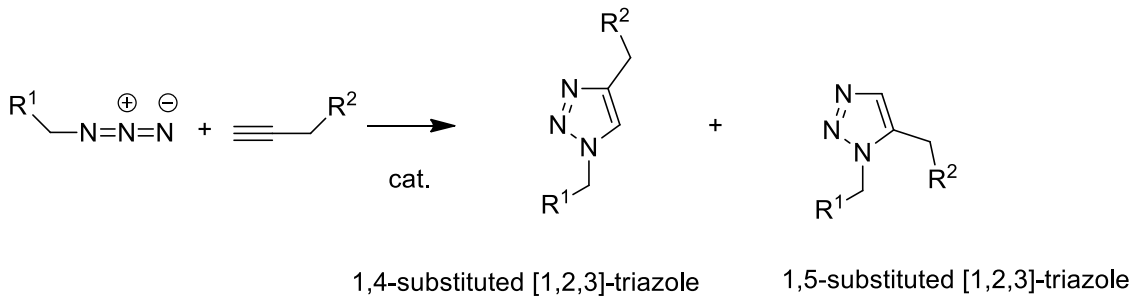

Figure 21: Click reaction between an azide and alkyne resulting in triazole formation.

The stereochemistry of this reaction is highly driven by the functionalities of the 1,3-dipolar species, temperature, and the catalyst. In copper-catalyzed reactions, it was shown, that the 1,4-substituted [1,2,3]-triazole was favored (Figure 21)[113].

Activity-based protein profiling (ABPP)

ABPP probes are generated to interact covalently with specific subsets of enzymes[22]. For example, the probe possesses an electrophilic group as “warhead”. However, these highly reactive moieties might also react with other nucleophilic proteinogenic residues[114,115]. Besides that, the generic ABPP probes contain a linker and a reporter tag, such as rhodamine and fluorescein or an affinity label like biotin, alkyne, and azide (Tandem labeling strategy, Figure 22).

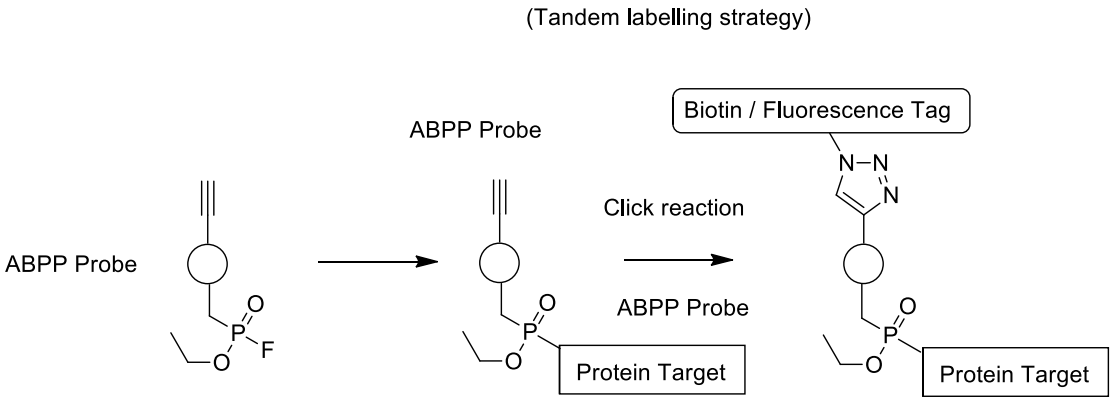

Figure 22: The ABPP approach. First, the probe is incubated with the protein sample leading to specific covalent bonds between probe and protein targets. In addition, the probe can be extended by the tandem labeling strategy allowing its identification based on fluorescence or mass spectrometry.

Photo-affinity labeling (PAL)

PAL is a new method based on ABPP and cross-linking[116]. Here, the probe is designed similarly to the pharmacophore and combined with a reactive cross-linking group, which can form a covalent bond with the protein of interest under light induction[117]. Diazirine is one of the well-known and practical PAL group[118]. Similarly, to the ABPP approach, the molecule can be modified with a reporter tag or an affinity tag to perform tandem labeling (Figure 23).

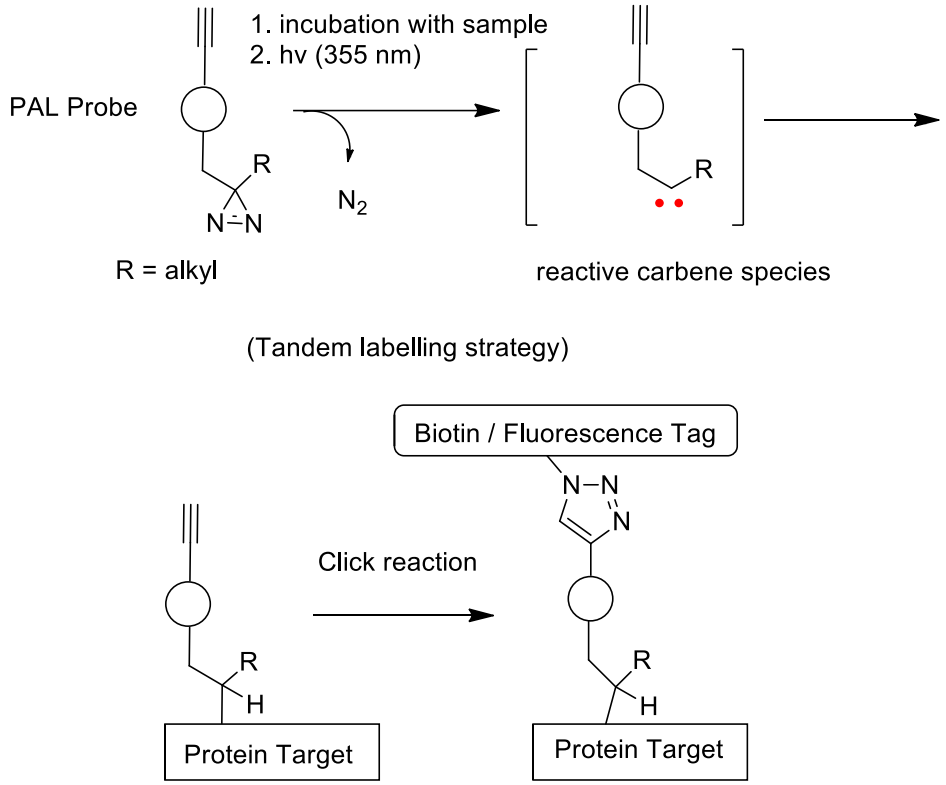

Figure 23: The PAL approach. The PAL probe has an unstable diazirine moiety, which can be activated by light with a wavelength of ~355 nm. During the photoreaction, N_2 and an active carbene species are generated. This carbene can react with the nearby located targeted protein. Moreover, the captured protein can be labelled by a fluorescence Tag for imaging or purified by the addition of a biotin tag.

Tandem labeling strategies

The tandem labeling approach has been developed to prevent interaction between the fluorophore and the desired proteome target[119]. This process uses reactions such as Staudinger reaction[120] and [2+3] cycloaddition[121] ("click chemistry") conducive to minimize the ABPP tag structure. The disadvantages of the method are the utilization of metal catalysts and the yield fluctuation in different systems[119].

1.8 Proteome analysis

There are many existing techniques for the analysis of protein samples. A modern proteome pipeline contains the following steps: proteome purification and peptide preparation, peptide sequencing by tandem mass spectrometry and protein identification by database searching[122].

Proteome purification and peptide preparation

Purification is the crucial step for the proteome analysis as it has a significant impact on the results. It is possible to use a variety of methods, such as gel electrophoreses, column chromatography, or affinity-based procedures to receive the proteins of interest. Besides, contaminations such as keratin, salts, or detergents have to be excluded to achieve the best performance.

The usage of StageTips[123] is, for example, a well-known and robust approach for whole cell lysate samples. Here, the bacteria cell wall was first destroyed by lysis and sonification. Afterward, tryptic digestion was performed to break down the proteins into peptides. Furthermore, a two-layer system with C18 material and SCX is used to pre-fractionate the peptides (Figure 24).

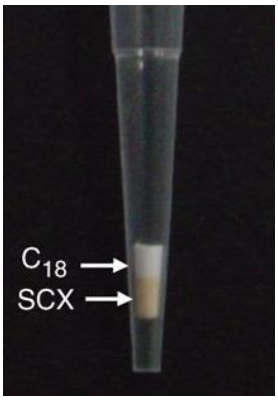

Figure 24: Photo of a StageTips[123], a tool for peptide pre purification. Here, SCX material and C18 material is packed into a 100 µl pipette tip. (Copyright © Springer Nature. Permission granted through the Copyright Clearance Center's RightsLink® service).

.

Besides that, the proteins of interest can be separated by specific affinity-based methods, such as ABPP and photo-affinity labeling (PAL). These are chemical molecules designed after the pharmacophore of interest. Initially, these probes are incubated with the biological samples to react with the target proteins. Later, these probe-labelled proteins are enriched, for example, on (strept)avidin beads and then digested with trypsin. Finally, the tryptic peptide products are analyzed with multidimensional LC-MS[124] (Figure 25).

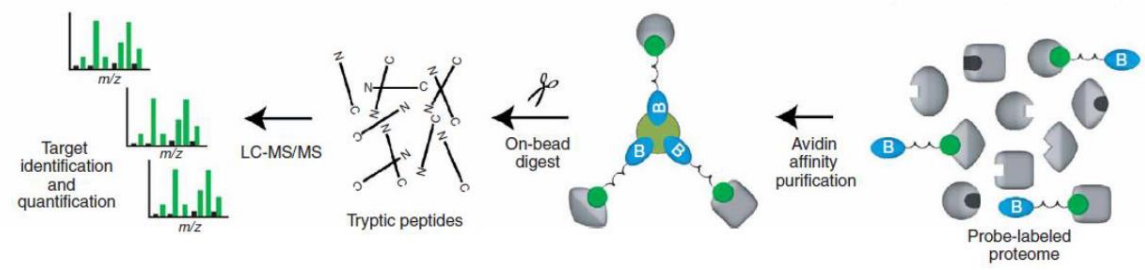

Figure 25: LC-MS/MS approach for ABPP and PAL. Proteome sample is labelled by ABPP or PAL probes and then enriched with avidin-affinity purification. In the next step, tryptic peptides are created by on-bead digestion. Finally, these products are analyzed with LC-MS/MS[124] (Copyright © Springer Nature. Permission granted through the Copyright Clearance Center's RightsLink® service).

.

Liquid chromatography-tandem mass spectrometry (LC-MS/MS)

LC-MS/MS methods have become more and more popular due to the technical advances of mass spectrometry. Especially the development of qTOF[24] and Orbitrap[25] has advanced the field substantially. As a result, it is possible to identify peptides of higher masses with higher mass accuracy. Moreover, new protein identification by database searching algorithms has been successfully developed and significantly improved the results[122].

Protein identification by database searching

The MaxQuant environment is one of the most well-known free licensed software for peptide database searching. It consists of the peptide data search engine Andromeda[125] and the label-free quantification algorithm MaxLFQ[126].

The Andromeda engine uses a probabilistic scoring model to validate whether the matches between the calculated and measured fragments could have occurred by chance (Figure 26).

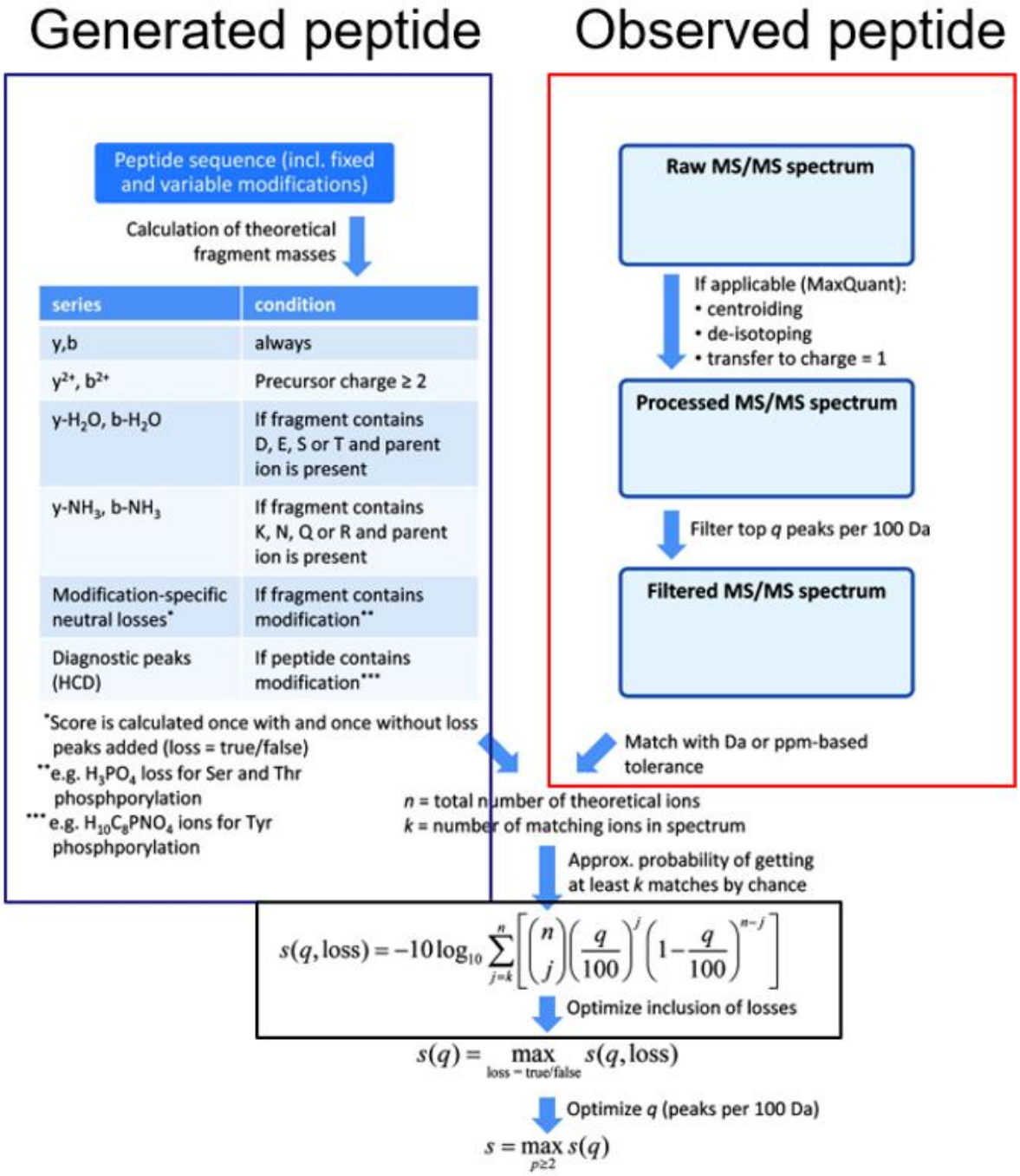

Figure 26: Schematic view of Andromeda's algorithm[125]. The theoretical peptides are derived from user fasta file inputs. The theoretical fragment masses are generated (left). The observed peptides are processed and filtered from the Raw MS/MS spectrum (right). The score is calculated with the given equation (Copyright © ACS publications. Permission requested is granted.).

After identification of the proteome set, it is also possible to quantify these proteins. Here, label-free quantification (LFQ) is the simplest and most economical approach in comparison to other methods such as SILAC[127], Di-methyl[128], TMT[129], and iTRAQ[130]. However, the main disadvantage of LFQ is the loss of accuracy. Therefore, the quantification method such as the MaxLFQ algorithm has become a commonly used tool to improve results[126].

To achieve this goal, the algorithm first normalizes the peptide intensity. This factor is calculated based on the analysis of multiple samples and fractions (Figure 27). In data science, normalization is mainly used to avoid data anomalies in the sample.

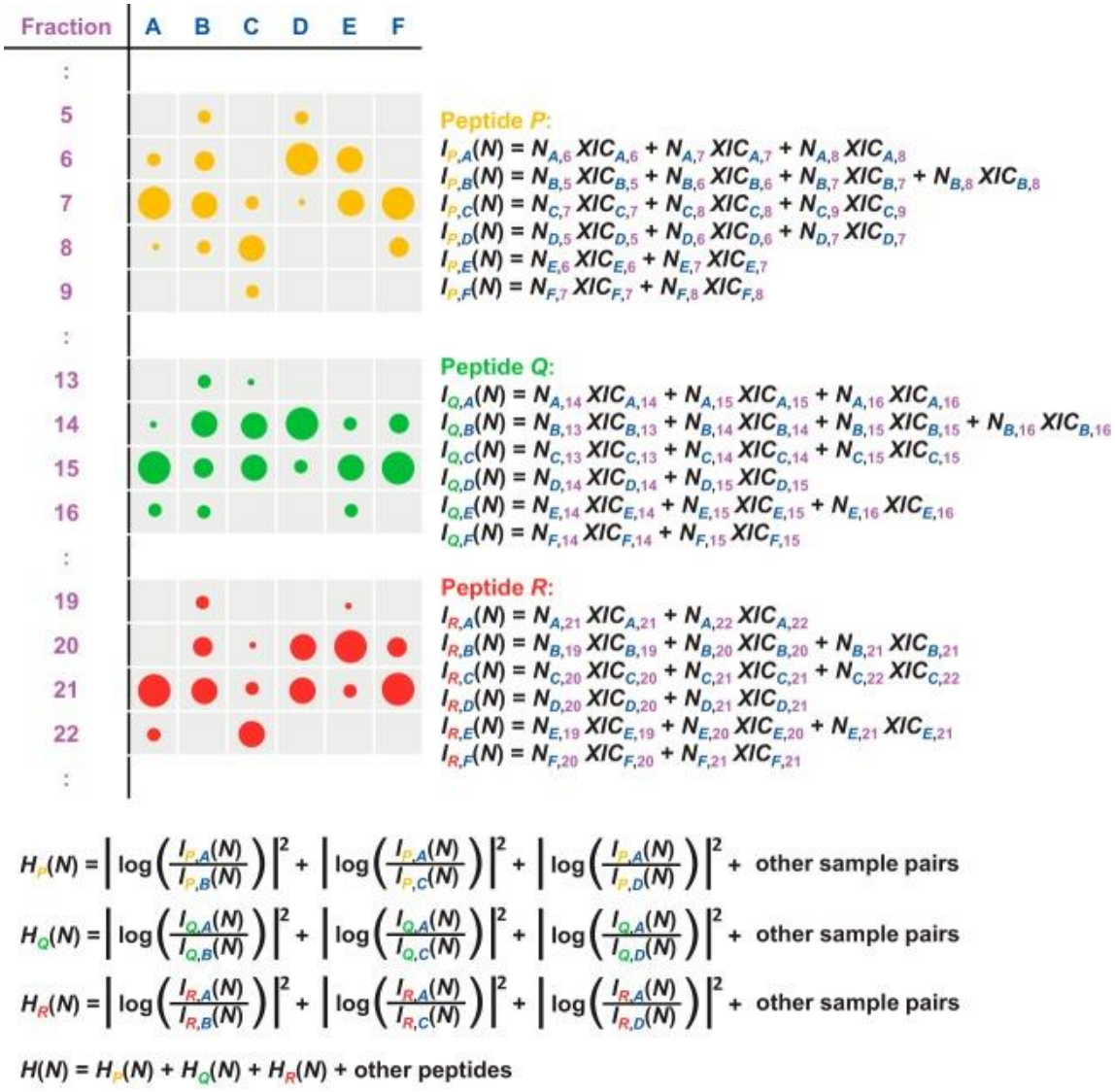

Figure 27: Representation of the normalization process in MaxLFQ[126]. Three different peptides (P: yellow, Q: green and R: red) were identified and quantified in different samples (A, B, C…) and different fractions (1, 2, 3...). The intensity is indicated by the size of the circles. First, the Intensity of each peptide is calculated by adding the extracted ion chromatogram (XIC) of all fractions for each sample. Also, normalization factors (N) are added as a free variable to scale the intensity of peptides from different samples. The normalization factors are then calculated by the defined functions. H(N) is minimized and solved numerically via Levenberg-Marquardt optimization[131] to achieve the least possible amount of differential regulation of the proteome[126] (The figure was distributed under the CC-BY license which automatically grants all commercial and noncommercial use of the article to all, as long as appropriate attribution is given to the original work).

After the normalization, the algorithm uses multiple peptide ratios between samples and a least-squares analysis to determine the protein intensity. This differs from other approaches because it does not use a single extracted ion current (XIC) or counts of identified MS/MS spectra to determine protein abundance in samples (Figure 28).

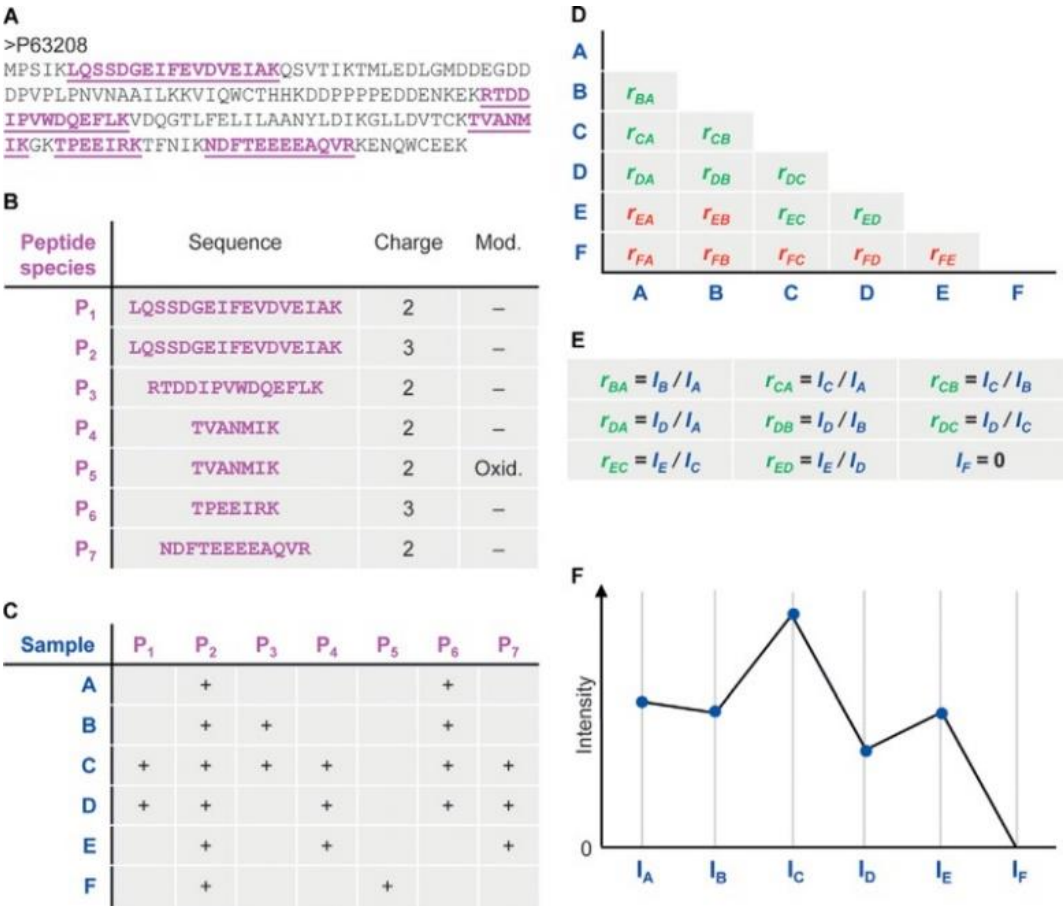

Figure 28: Representation of the LFQ algorithm[126]. Peptide fragments from a specific protein **(A)** are first selected from the database and divided into different peptide species **(B)**. Also, a new table is created which includes samples and detected peptide species **(C)**. Moreover, a triangular matrix with the ratios of proteins between samples is calculated **(D)**. Therefore, only peptide species, that are present in both samples are selected. The minimum number of peptide species is selected by the user. Protein ratios, which are below this set threshold is marked red while valid ratios are marked green. An abundance profile is then constructed to optimally satisfying the protein ratios in the matrix based on the equations **(E)** using a least-squares analysis**.** Finally, the whole profile is rescaled to the summed intensity for all samples resulting in the protein intensity in between samples **(F)** (The figure was distributed under the CC-BY license which automatically grants all commercial and noncommercial use of the article to all, as long as appropriate attribution is given to the original work).

1.9 Overview and aim of the thesis

The main goal of this thesis is the synthesis of natural products from *Xenorhabdus* and *Photorhabdus,* as well as the identification of their targets. Therefore, different techniques such as microscopy[132], chemical labelling[11], and proteomics[22] can be applied to achieve this goal.

Until now most natural products, which were extracted from *Xenorhabdus* or *Photorhabdus* and bacteria in general were primarily tested against other strains for toxicity. In many cases, the lack of experimental methods prevents further mechanistic elucidation of newly discovered compounds. For example, PAX peptides, which is widely covered in this thesis was initially described as an antimicrobial and antifungal peptide[14]. Here, our experimental approach using click chemistry and microscopy (in collaboration with Dr. Christoph Spahn) should reveal a putative new function of this peptide class. Another advantage of this workflow is the ability to label the molecules after adding it to the strains. Therefore, cellular systemic changes can be observed while minimizing interference.

Besides microscopy, proteomic mass spectrometry coupled methods have been developed steadily in the past and could be used as an additional complement method. Here, the usage of chemically labelled derivatives using a PAL or ABBP approach is a common technique to elucidate molecule-target interaction. Therefore, several rhabdopeptide derivatives should be synthesized to elucidate its mechanism. Furthermore, the usage of proteome-wide analysis is a promising approach to observe global changes in a cellular response instead of focusing on certain targets. Here, a robust proteomic workflow should be established to identify and quantify protein changes from different *Xenorhabdus* and *Photorhabdus* strains simulating an insect infection.

Chapter one of the thesis introduces the reader into peptide synthesis, natural products, common techniques for chemical target identification, and proteomics.

Chapter two covers the materials and methods used in this work. Here, the workflow of peptide synthesis is described in detail. In addition, it contains microscopy labelling techniques, which are developed in collaboration with Dr. Christoph Spahn to localize PAX. Furthermore, the proteomic workflow for label-free quantification is explained.

Chapter three contains the results of this work. Several peptides, such as silathride, xenoautoxin, various SYNZIP peptides, peptide aldehydes, and 3-hydroxyoctanoic acid for phototemtide A are synthesized during this thesis as standards required for structure confirmation of NRPS engineering and biosynthetic gene cluster activation – two major methods in the Bode group. Furthermore, several rhabdopeptide derivatives are synthesized, which carry labels that allow covalent binding and enrichment of their target enzymes. PAX peptides as well as derivatives containing an azide or alkyne moieties are synthesized and quantified in bacteria cultures. In this chapter, the analytical results from the synthesis are shown in the form of a compound collection. Furthermore, the microscopy results of PAX localization in collaboration with Dr. Christoph Spahn are described. In the proteome analysis, *X. nematophila*, *X. szentirmaii*, and *P. luminescence* are analyzed with and without the addition of insect broth. The proteome data are processed using statistical analysis, mapped via KEGG/Blastkoala, and compared between different strains resulting in a list of up- and down-regulated proteins during insect infection.

Chapter four covers the discussion of natural product synthesis, investigation of PAX function and antimicrobial activity, the proteome results in a biological context, and an outlook for the projects.

The Ph.D. thesis finishes with the quotation of references, supporting information, a curriculum vitae of the doctoral candidate, the list of publications, and record of conferences as well as the declaration.

2. Material and methods

2.1 Biological Material

During the thesis, the following strains were used (Table 2).

Table 2: Organisms used in this thesis.

Genus	Species	Subspecies/Strain	Source	Reference
Xenorhabdus	*doucetiae*		DSM 17909	132
Xenorhabdus	*doucetiae*	*X. doucetiae*_PBAD-PAX	Edna Bode	
Xenorhabdus	*nematophila*	HGB081		
Xenorhabdus	*szentirmaii*		DSM 16338	133
Photorhabdus	*luminescens*	*namnaoensis* PB 45.5		
Escherichia	*coli*	MG1655		
Bacillus	*subtilis*	B168		
Saccharomyces	*cerevisiae*			
Micrococcus	*luteus*		Matthias Hammelmann	

2.2 The standard protocol for peptide synthesis at the Syro Wave™

The Syro Wave™ has prewritten protocols, which can be utilized for automated SPPS. The loading step is often difficult to automate and is therefore carried out manually. After this step, the resin was transferred into a plastic reaction vessel and placed into the reaction block of the machine. To add one additional amino acid to the peptide, the machine had to undergo one synthesis cycle. One sequence contained three main steps, which were coupling, capping, and deprotection.

Preprotected amino acids were purchased by commercial vendors, such as Sigma Aldrich, Bachem, or Iris Biotech.

The standard coupling protocol for 25 µmol peptides is 6 eq. HCTU (Iris Biotech), 6 eq. amino acid and 10 eq. DIPEA (Iris Biotech). The reaction duration is 50 min at room temperature. During this time, the reaction block is vortexed every 2 min for

15 sec. After the coupling step was carried out, the reaction solution was removed, and the resin was washed four times with NMP (Iris Biotech). It was also possible to do multiple repetitive coupling steps at this point to ensure a complete reaction.

After the coupling step, two capping steps were usually carried out to prevent side reaction. Here, the reaction vessel was filled with the capping mixture of 0.95 ml Ac_2O (Sigma Aldrich) (10 mmol), 0.45 ml DIPEA (250 µmol), and 40 mg HOBt (Sigma Aldrich) (300 µmol) filled up to 20 ml NMP.

The deprotecting step consisted of two reactions, first with 40% piperidine (Carl Roth) in NMP for 3 min at room temperature and then with 20% piperidine in NMP for 10 min at room temperature. After the deprotection step, the resin was washed four times with NMP.

2.3 The standard protocol for peptide synthesis

Loading

For most peptide synthesis, using 2-CTC resin (Iris Biotech) is sufficient to produce efficient yield and avert side reaction. Here, the trityl group minimizes diketopiperazine formation through steric hinderance[135]. However, the 2-CTC resin is often degrading after a certain storage time. To reactivate the resin, it is possible to use thionyl chloride (Sigma Aldrich).

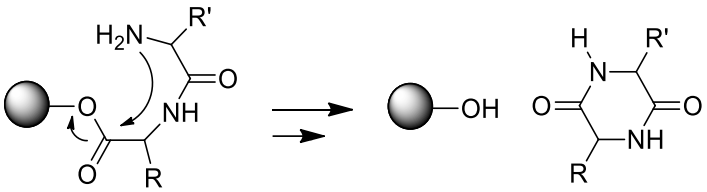

Figure 29: Diketopiperazine side reaction, which can occur during peptide synthesis. CTC-resin can reduce this side reaction by shielding the C-terminus.

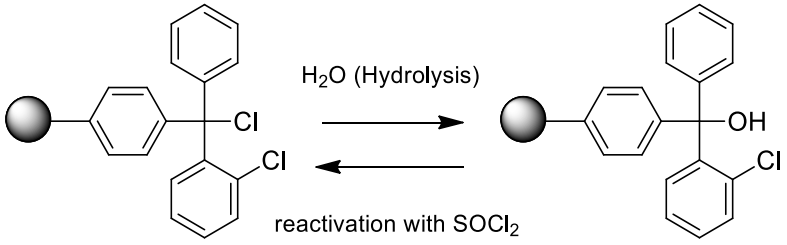

Figure 30: 2-CTC is slowly degrading when exposed to moisture. The resin can be activated using thionyl chloride.

Chain elongation

Using HATU

HATU (Iris Biotech) is one of the most efficient reagents to build up the peptide chain. For the most reaction 6 eq. of the amino acid, 5 eq. of HATU, 5eq. of HOAt, 12 eq. of DIPEA, and the resin were dissolved in 1.5 ml DMF (Carl Roth) or other solvents such as DCM (Merck) or NMP. After adding the reagents, the reaction vessel was incubated for 1h at room temperature.

Using HCTU

For the coupling reaction 6 eq. the amino acid, 5 eq. HCTU and 10 eq. DIPEA was used and dissolved in 1 ml DMF. The reactions were carried out at room temperature for 1 h.

Acylation

1.5 eq. of the acid with 1.5 eq. DCC (Sigma Aldrich) in DMF was initially pre-activated at room temperature. The activation was usually finished after 20 min and could be observed by precipitation of 1,3-dicyclohexylurea. The resin was then incubated with the reaction mixture for 90 min or overnight.

Alternatively, fatty acids were coupled by using 5 eq. of the respective acid, 5 eq. HATU, 5 eq. HOAt (Iris Biotech) and 10 eq. DIPEA. The reaction mixture was dissolved in DMF and at 37°C overnight.

Capping

For capping, a mixture of DCM, MeOH (Merck), and DIPEA was used (v/v 17:2:1). Therefore, the resin was treated with the solution for 45 min at room temperature. Besides that, it is also possible to use a mixture of pyridine (Carl Roth) and acetic acid (Sigma Aldrich) (v/v 9:1) or Ac_2O (Carl Roth) as described above (section 2.2).

Deprotection

Fmoc deprotection

To remove the Fmoc protecting group, 20% piperidine in NMP was used three times for 5 min at room temperature. The liquid was measured by UV/VIS (see p. 64) to determine the product yield.

Boc/TrT/Pbf deprotection

Boc, Trt, and Pbf-groups were deprotected with a TFA (Iris Biotech) /H_2O/TIS (Sigma Aldrich) mixture (v/v 95:2.5:2.5). The deprotection of Boc, Trt, and Pbf was carried out for 2 h (Boc, Trt) and at least 4 h (Pbf).

Cleavage

TFA cleavage

For a full cleavage, 1.5 ml of TFA, H_2O, and TIS (v/v 95:2.5:2.5) was drawn into the syringe with the peptide for one hour at room temperature. After the reaction, the liquid containing the peptide was transferred into a 50 ml flask and the syringe was washed multiple times with DCM. In addition, the vessel was filled with 20 ml DCM and the liquid was removed with a rotary evaporator. The remaining crude product was dissolved in 1.5 ml DMF and purified by HPLC-MS.

HFIP Cleavage

HFIP (Iris Biotech) was used to cleave the peptide from the resin while leaving the protecting groups intact. For this process, a mixture of 1.5 ml of HFIP and DCM was drawn into the syringe and incubated for 30 min at room temperature. The liquid now containing the peptide was transferred into a 50 ml flask and the syringe was washed several times with DCM. The mixture was dried by using the rotary evaporator and the remaining crude product was dissolved in DMF for HPLC-MS based purification.

Analytics

Test cleavage

To verify the product at each step, a very small amount of resin was cleaved in a 5 ml flask (several grains is enough) with one drop of a mixture with TFA, H_2O, and TIS (v/v 95:2.5:2.5). After 10 min at room temperature, the excess solvent was removed by a rotary evaporator at 20 mbar for 3-4 min. The absence of TFA was confirmed by a smell test.

Kaisertest

The Kaisertest is a fast method to detect free amine residues from peptides, which are present in unfinished peptide couplings. For the test, several grains of the resin were taken and transferred into a 1.5 ml Eppendorf tube. 10 µl of each Kaisertest solution 1, 2, and 3 was added into the tube and the vessel was incubated for 5 min at 95°C. The test is positive if the liquid or the resin had a blue color.

Solution 1 (0.5 ml 0.01 M KCN (Sigma Aldrich), 24.5 ml pyridine)

Solution 2 (1 g ninhydrin (Sigma Aldrich), 20 ml n-butanol (Carl Roth)), and

Solution 3 (20 g phenol (Sigma Aldrich), 10 ml n-butanol)

UV/VIS Fmoc determination

If Fmoc is used as a protecting group, it is possible to determine the quantity of the products by observing the dibenzofulvene at 301 nm with the help of Lambert-Beer's law. First, the resin is treated with 20% piperidine in NMP for 20 min. After the reaction, the liquid is transferred into a 100 ml volumetric flask and filled up with DCM. 1 ml of the 100 ml volumetric flask is then transferred into a 10 ml volumetric flask and filled up with DCM. In addition, 2 ml from the 10 ml flask is then added to a glass cuvette and measured with the Genesys 10S UV-Vis spectrometer from Thermo Scientific. The concentration is then calculated by the Lambert-Beer's law: $E_\lambda = \log\left(\frac{I_0}{I_1}\right) = \varepsilon_\lambda * c * d$. The extinction coefficient[136] in DCM is 7.8 $mmol^{-1}cm^{-1}$.

Purification

The purification was carried out by semi-preparative HPLC-MS. In the beginning, test runs with 2 µl injections were performed to develop the best separation method. If the product peak could be separated, additional runs with up to 100 µl were performed. Most of the peptides were purified with a C18 column. In most cases, a gradient of ACN/H_2O (5-95%) was used. The product fractions were then collected. The ACN (Merck)/H_2O mixture was removed by the rotatory evaporator, then the peptides were freeze-dried yielding in a white fluffy powder.

2.4 Synthesis of silathride

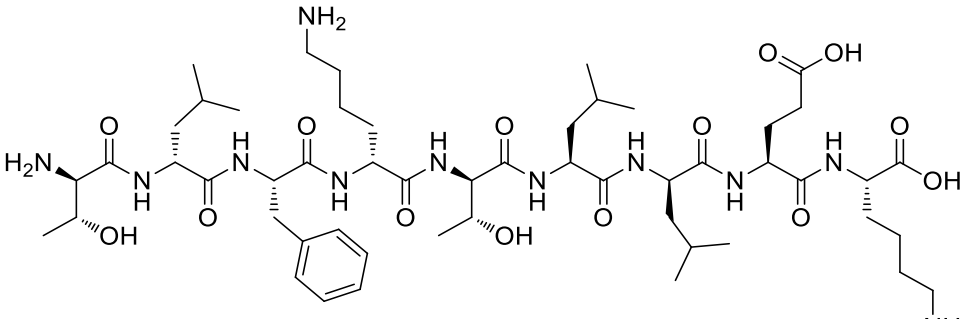

1

The synthesis of the peptide silathride was done by Fmoc SPPS with the Biotage ® Syro Wave™. 2-CTC Resin was used as the solid phase. The procedure is described on page 59 (section 2.2). The final product was verified via HPLC-MS/MS (5-95% ACN/H_2O + 0.1% FA) to be identical to the natural product as deduced from an identical retention time and fragmentation pattern (see chapter 3.1 and 3.2 for additional information).

2.5 Synthesis of xenoautoxin and biotinylated xenoautoxin

Xenoautoxin

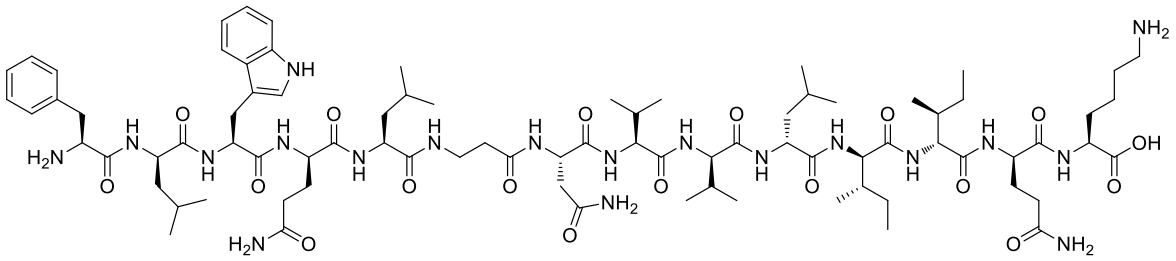

Xenoautoxin was initially produced with Fmoc SPPS utilizing the Syro Wave™ system following the standard procedure on page 59 (section 2.2). The product was purified via semi-preparative HPLC-UV/VIS (5-95% ACN/H_2O + 0.1% FA) to be identical to the natural product as deduced from an identical retention time and fragmentation pattern (see chapter 3.1 and 3.3 for additional information). The product was used as an analytical standard; therefore, the obtained yield was not quantified.

Biotinylated xenoautoxin

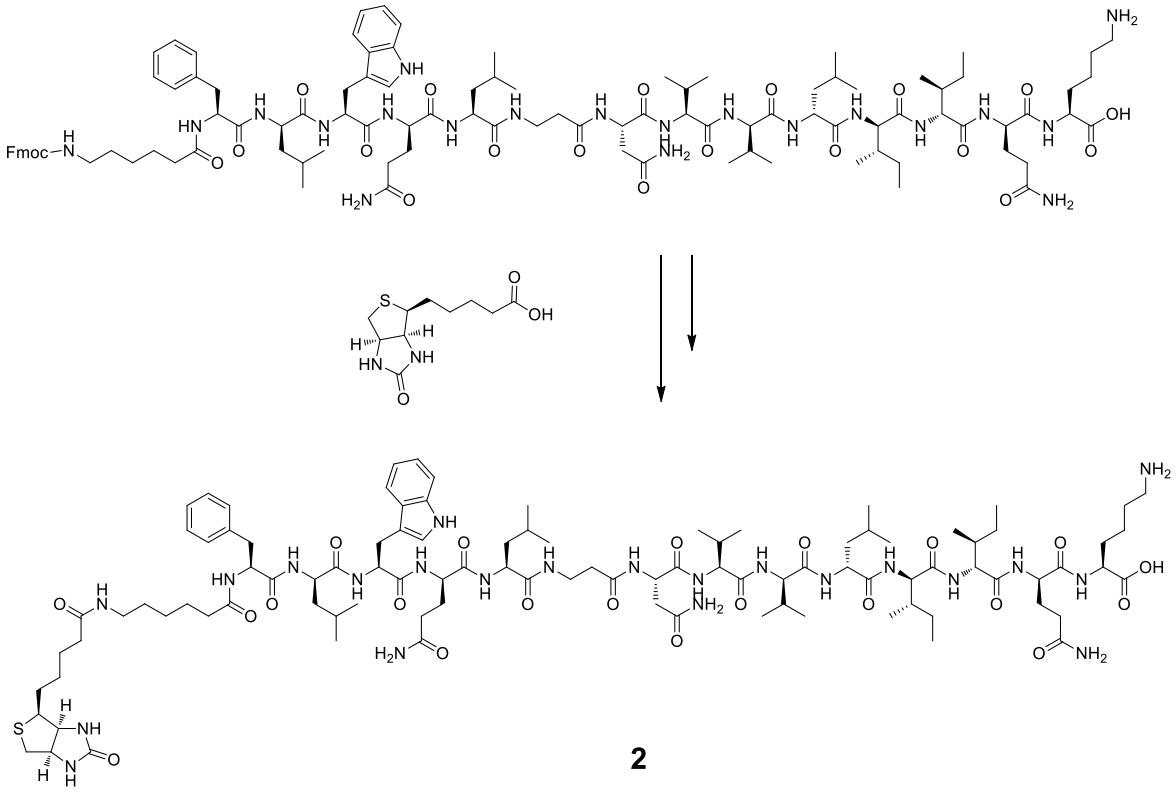

2

For the synthesis of biotinylated xenoautoxin, the same procedure was repeated but the product was not cleaved from the resin. 50 µmol of the xenoautoxin was then coupled with 6 eq. Fmoc-ε-Ahx-OH (Sigma Aldrich) (300 µmol, 106 mg), 5 eq. HCTU (250 µmol, 103 mg), and DIPEA (500 µmol, 84 µl) in 1.5 ml DCM for one hour at room temperature. The Fmoc-group was removed using 40% piperidine for 30 min at room temperature and the product quantity was determined via UV/VIS measurement. 82% (41.15 µmol) of the intermediate product was obtained.

6 eq. of biotin (Sigma Aldrich) (250 µmol, 100 mg), 5 eq. HCTU (200 µmol, 170 mg) and 10 eq. DIPEA (410 µmol, 70 µl) were dissolved in NMP. The reaction was carried out overnight at room temperature. The purification was done via semi-preparative HPLC-MS C18 column (5-95 % ACN/H_2O + 0.1 FA). The product was verified via HR-HLPC-MS analysis (see chapter 3.1 and 3.3 for additional information). The overall yield after purification was ~5%.

2.6 Synthesis of phenylethylamides and tryptamides

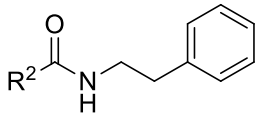

Phenylethylamide

R^2 = methyl **(3)**, nonanyl **(4)**, nonadecanyl **(5)**

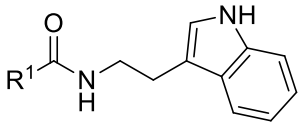

Tryptamide

R^1= nonyl **(6)**, undecanyl **(7)**, dodecanyl **(8)**, pentadecanyl **(9)**, heptadecanyl **(10)**

The standard procedure for the synthesis was to mix 1 eq. of the alkanoic acid and 2 eq. phenylethylamine, 2 eq. EDC*HCl (Iris Biotech), 2 eq. HOBt (Sigma Aldrich) and 4 eq. DIPEA. The reaction was carried out at room temperature overnight. The product was then washed with brine and extracted with EtO_2 (Sigma Aldrich). The crude product was purified via flash silica gel column chromatography (0-50% n-hexane (Merck)/ethylacetate (Sigma Aldrich)). Products were verified via HLPC-MS analysis (see chapter 3.1 for additional information). Yields obtained for the reactions were ~80%.

2.7 Synthesis of various peptide standards (SYNZIP peptides)

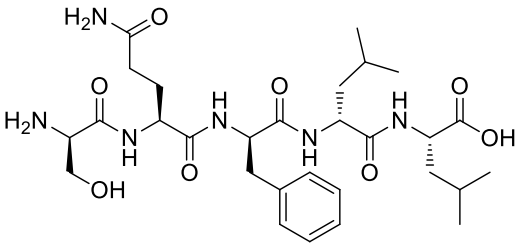

11

SYNZIP peptide 1

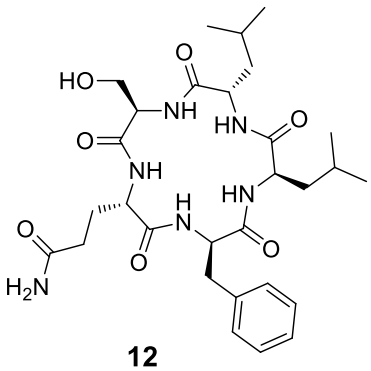

12

SYNZIP peptide 2

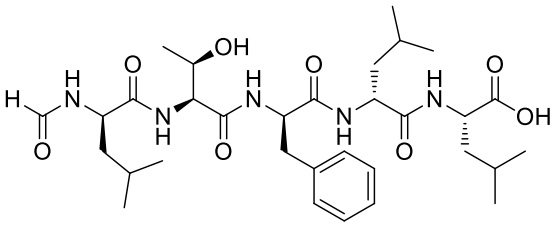

13

SYNZIP peptide 3

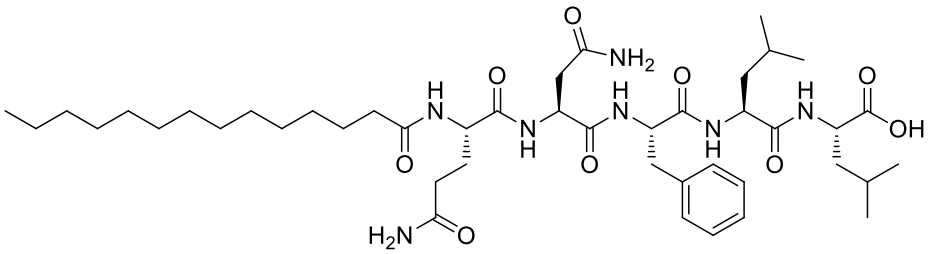

14

SYNZIP peptide 4

The synthesis of the peptides was accomplished utilizing the standard protocol (on page 60) with 2-CTC Resin used as the solid phase. The final products were purified via semi-preparative HPLC-MS (C18 column; 5-95% ACN/H_2O + 0.1% FA). Products were verified via HLPC-MS analysis and compared with natural products. The products were used as analytical standards; therefore, the obtained yield was not quantified (see chapter 3.1 Results for additional information).

2.8 Synthesis of various peptide standards (peptide aldehyde)

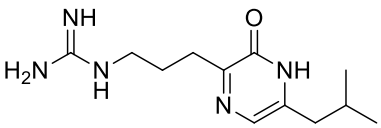

15

peptide aldehyde 1

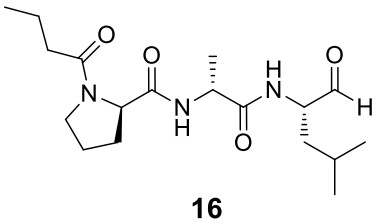

16

peptide aldehyde 2

1 eq. (25 µmol, 50 mg) of H-Leu-H NovaSyn TG resin (Sigma Aldrich) was left to swell in 1 ml ACN for 30 min. 4 eq. of the amino acid, 4 eq. HATU, a catalytic amount of HOBt and 8 eq. NMM (Sigma Aldrich) in 1 ml ACN was added to the resin and incubated under rotation for 1h. After the coupling step, the resin was washed 5 times with 1 ml ACN and DCM. The Fmoc deprotection was accomplished using the standard protocol and cleaved by ACN/H_2O/TFA (79.95:20:0.05 v/v/v). Products were verified via HR-HLPC-MS analysis and compared with natural products. The products were used as analytical standards; therefore, the obtained yield was not quantified (see chapter 3.1 Results for additional information).

2.9 Synthesis of rhabdopeptide derivatives

The synthesis of these new derivatives is based on the previous work of Dr. Frank Wesche[98].

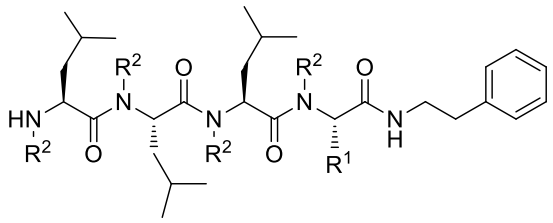

R^1 = methyl, isobutyl
R^2 = H, methyl

a

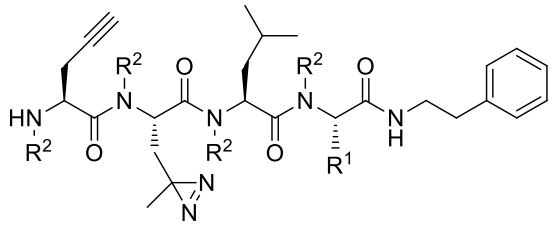

R^1 = methyl, isobutyl
R^2 = H, methyl

b

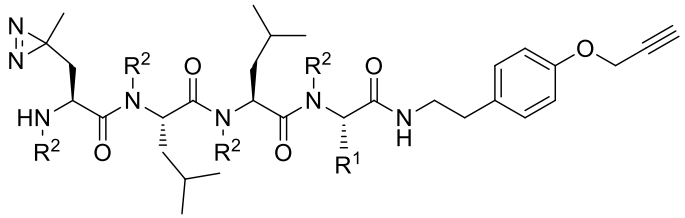

R^1 = methyl, isobutyl
R^2 = H, methyl

c

Synthesis of tert-butyl 4-hydroxyphenethylcarbamate

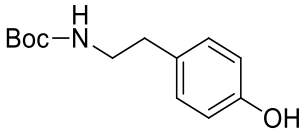

2 eq. (1.28 mmol, 176 mg) tyramine (Sigma Aldrich) and 2 eq. (1.28 mmol, 135 mg) sodium carbonate (ACROS Organics) was dissolved in a 1:1 mixture of H_2O and dioxane (Sigma Aldrich) and cooled to 0°C. In addition, 1 eq. (0.64 mmol, 140 mg) di-tert-butyl dicarbonate (Sigma Aldrich) was slowly added and the mixture was stirred at room temperature overnight. In the next step, the mixture was extracted two times with 10 ml EtOAc (Merck) and the organic phase was dried with $MgSO_4$ (ACROS Organics). The organic phase was dried by a rotary evaporator under reduced pressure. The obtained solid raw product was purified using flash silica gel column chromatography (5-50% n-hexane/Ac_2O). The product was confirmed by HPLC-MS analysis. MS (ESI) m/z: $[M + H]^+$ Calcd for $C_{13}H_{20}NO_3$ 238.14; Found 238.26. (103.1 mg, 68% yield)

Synthesis of 2-(4-(prop-2-yn-1-yloxy)phenyl)ethanamine

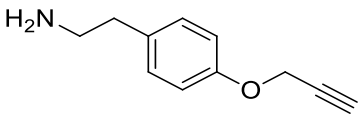

1 eq. (0,64 mmol, 152 mg) tert-butyl-4-hydroxyphenethylcarbamate, 1,2 eq. (0,77 mmol, 106 mg) potassium carbonate (ACROS Organics) and 1,2 eq. (0,77 mmol, 91 mg) propargyl bromide (Sigma Aldrich) were added into a flask and dissolved in 3 ml DMF. The reaction mixture was stirred overnight at room temperature. After the reaction, the mixture was washed twice with 10 ml brine. The solvent was dried under vacuum and the crude product was purified by flash chromatography using silica gel (5-75% n-Hexan/Ac_2O). The purified product was treated with 750 µl TFA for 2 h. In addition, TFA was removed by adding three times 30 ml DCM and removed by the rotatory evaporator until a crystal product was retrieved. The product was confirmed by HPLC-MS analysis. MS (ESI) m/z: $[M + H]^+$ Calcd for $C_{11}H_{14}NO$ 176.11; Found 176.38. (80.3 mg, 71% yield)

Loading

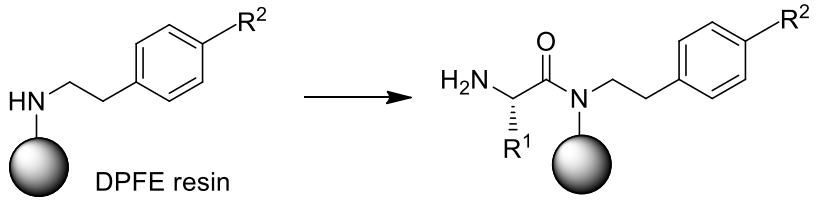

R^1 = isopropyl, methyl
R^2 = H, prop-2-yn-1-oxyl

Four natural rhabdopeptides (**a**) and eight new derivatives were synthesized. These new molecules have two new core structures (**b, c**). The synthesis starts with the loading of phenylethylamine (Sigma Aldrich) or 2-(4-(prop-2-yn-1-yloxy)phenyl)ethanamine, respectively. 1 eq. DFPE resin (Merck) (100 µmol, 125 mg) was poured into a 1.5 ml Eppendorf tube. Then 10 eq. of phenylethylamine (1 mmol, 121.2 mg) or 4.5 eq. 2-(4-(prop-2-yn-1-yloxy)phenyl)ethanamine (0.45 mmol, 80 mg) and 10 eq. sodium cyanoborohydride (Sigma Aldrich) (1 mmol,

62.8 mg) was added. The compounds were dissolved in 800 µl in a mix of DMF, ethanol (Merck), and acetic acid (v/v 80:19:1). The reaction was performed overnight at 60°C in a thermo shaker. The resin was then washed five times with DCM, DMF, NMP in a 5 ml polyethylene syringe with a teflon frit and left to dry at the air. The structures were confirmed by HPLC-MS analysis. The resin was split into different batches and the yield was determined in the consequent step. Here, 6 eq. Fmoc-Alanine (150 µmol, 47 mg) or 6 eq. Fmoc-Leucine (150 µmol, 53 mg) was introduced by activation with 5 eq. HATU (125 µmol, 47 mg), 5 eq. HOAt (125 µmol, 17 mg) and 10 eq. DIPEA (250 µmol, 42 µl) overnight. After Fmoc-quantification by using UV/VIS (Thermo Scientific Genesys 10S UV-VIS) a loading efficiency of 80% was determined.

Chain elongation

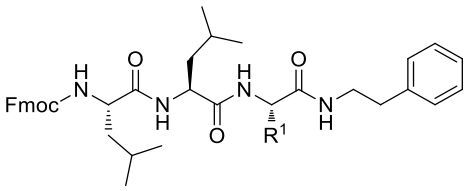

R^1 = H, isopropyl

a

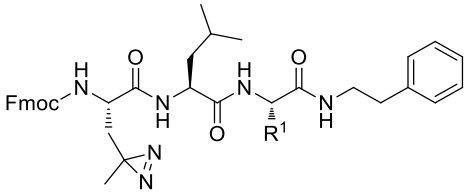

R^1 = H, isopropyl

b

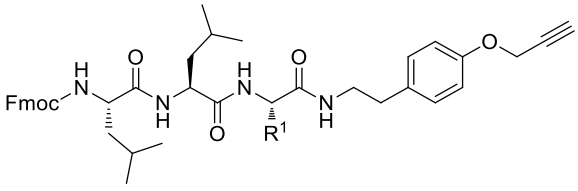

R^1 = H, isopropyl

c

The peptides were synthesized in 25 µmol batches and the reaction vessel was a 5 ml polyethylene syringe with teflon frit. For each step, 6 eq. of the amino acid, 6 eq. HATU, 6 eq. HOAt and 12 eq. DIPEA in 1.5 ml DMF was used. The syringes were shaken at room temperature for 1 h. After each reaction, the resin was washed five times with DCM, DMF, and NMP. After the coupling step, the peptide was deprotected using 20% piperidine in NMP. For the methylated products, either Boc-

propargyl-Gly-OH, Boc-Photo-Leucine, or Boc-Leucine (Sigma Aldrich) was used at the last step of the chain propagation process. The syringes were wrapped in aluminum foil to prevent photo-leucine from decomposition. The structure was confirmed by HPLC-MS analysis resulting in a yield of ~90%.

Methylation

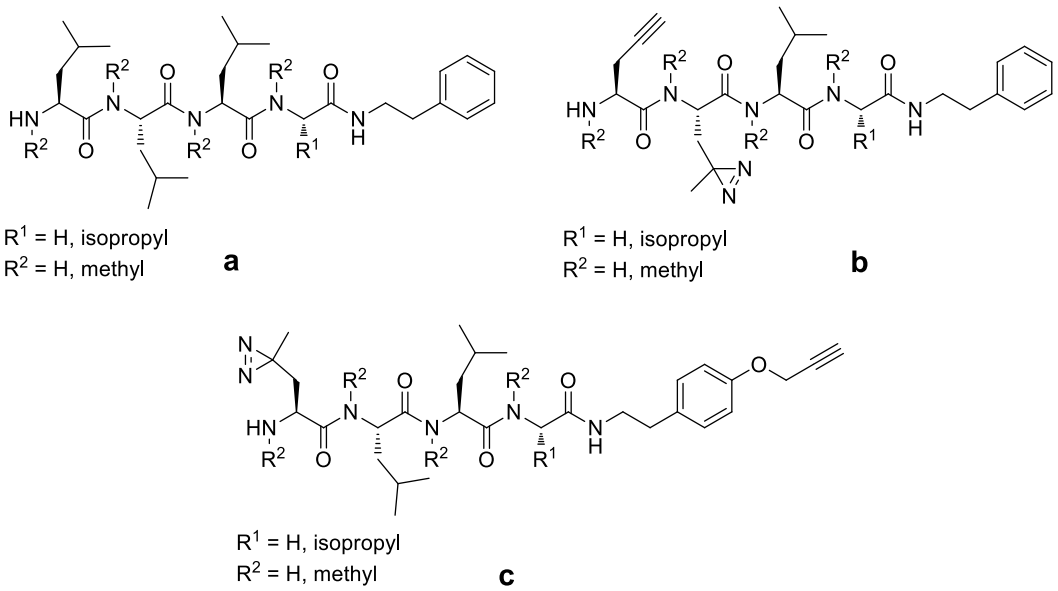

The methylation was prepared in 25 µmol batches. First, a plastic faucet was added to the syringe to exclude air and moisture. Then, the reaction vessel was flushed three times with nitrogen and three times with 5 ml dry THF. In addition, a mixture of LiOtBu (Sigma Aldrich) (20 eq. per amide bond) and 400 µl DMSO (Sigma Aldrich) were added to the resin. After 30 min, the solution was separated from the resin and MeI (Sigma Aldrich) was added (20 eq. per amide bond). After an incubation time of 30 min, the remaining mixture was discarded and the resin was washed five times with DCM, DMF, and NMP. The finished products were cleaved from the resin using the standard protocol (on page 62). The products were purified via semi-preparative HPLC-MS (C18 column; 5-95% ACN/H_2O + 0.1% FA). Products were verified via HR-HLPC-MS analysis (See chapter 3.1 Results for additional information). The reported yield after purification was between 30-40%.

2.10 Synthesis of chiral 3-hydroxyoctanoic acid for phototemtide A

Preparation of chiral 4-benzyl-3-bromoacetyl-2-oxazolidinone

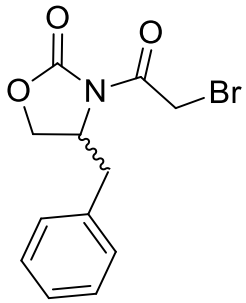

In a Schlenk tube, 1 eq. (*R*)- or (*S*)-4-benzyl-2-oxazolidinone (Sigma Aldrich) (3.0 mmol, 352 mg) was dissolved in 12 ml dry tetrahydrofuran (Sigma Aldrich) under N_2 atmosphere. The tube was cooled at -78°C by using a dry ice/isopropanol bath. Through the septum, 1.1 eq *N*-butyllithium (Sigma Aldrich) (n-BuLi, 1.6 M in n-Hexane, 3.3 mmol, 2.1 ml) was added dropwise under vigorous stirring. 1 eq. bromoacetyl chloride (Sigma Aldrich) (BrAcCl, 3.1 mmol,) was added dropwise after 30 min to the mixture for 20 min. After the addition, the dry ice bath was removed. For an additional 1h, the mixture was allowed to warm to room temperature and stirred. The septum was removed and saturated aqueous potassium hydrogen phosphate (K_2HPO_4 (ACROS Organics), 3 ml) was added to quench the reaction. The organic phase was extracted three times with 3 ml diethyl ether. The extract was dried over magnesium sulfate ($MgSO_4$) and the solvent removed with a rotary evaporator leaving an orange liquid. The crude product was purified by flash silica gel column chromatography to give (351 mg, 39%) (*R*)- or (321 mg, 36%) (*S*)-4-benzyl-3-bromoacetyl-2-oxazolidinone. The structure was verified via NMR. For more information see: Supporting Figure 12: 4-benzyl-3-bromoacetyl-2-oxazolidinone (^{1H} NMR spectra in CDCl3, 250 MHz*)*

Samarium(II) iodide mediated Reformatsky-type reaction

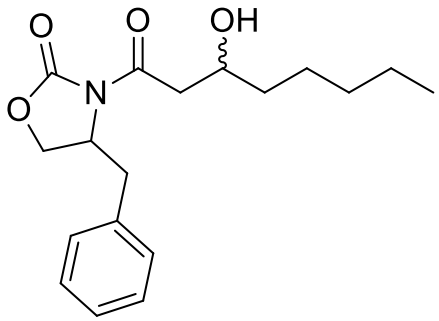

3 eq. Samarium(II) Iodide (Sigma Aldrich) (SmI_2, 0.1 M in THF, 3.0 mmol, 30 ml) was first added into a Schlenk tube and cooled at -78°C. A mixture of 1 eq. n-hexanal (Sigma Aldrich) (1.0 mmol, 124 µl) and 1 eq. *(R)*- or *(S)*-4-benzyl-3-bromoacetyl-2-oxazolidinone (1.0 mmol, 299 mg) in THF (2 ml) was slowly injected dropwise. After stirring for 0.5h, the dry ice bath was removed, and the mixture was allowed to warm to room temperature. After 0.5 h additional stirring, the reaction was quenched with hydrochloric acid (HCl, 0.1 M, 25 ml). Three portions of 20 ml diethyl ether were used to extract the aqueous phase and the organic layer had been washed with saturated aqueous sodium thiosulfate ($Na_2S_2O_3$ (ACROS Organics)). The organic phase was first dried over $MgSO_4$ and the solvent removed under reduced pressure. The crude product was purified by flash silica gel column chromatography to afford (205 mg, 64%) (*R*)-4-Benzyl-3-(*R*)-3-hydroxyoctanoyl-2-oxazolidinone or (210 mg, 65%) (*S*)-4-Benzyl-3-(*S*)-3-hydroxyoctanoyl-2-oxazolidinone as a white solid. The structure was verified via NMR. For more information see: Supporting Figure 12: 4-benzyl-3-bromoacetyl-2-oxazolidinone (^{1H} NMR spectra in CDCl3, 250 MHz).

Hydrolysis of the chiral 4-benzyl-3-3-hydroxyoctanoyl-2-oxazolidinone

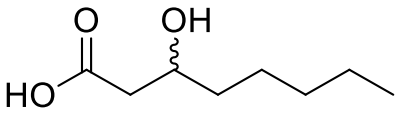

1 eq. (*R*)-4-benzyl-3-(*R*)-3-hydroxyoctanoyl-2-oxazolidinone or (*S*)-4-benzyl-3-(*S*)-3-hydroxyoctanoyl-2-oxazolidinone (0.6 mmol, 192 mg) was added into a round-bottom flask containing a magnetic stirring bar and dissolved in a solution of THF in H_2O (4:1, 3 ml) under a nitrogen atmosphere and cooling at 0°C. A solution of hydrogen peroxide (H_2O_2) (Sigma Aldrich) 4 eq. (30% in H_2O, 2.4 mmol, 273 µl) and a solution of lithium hydroxide 1 eq. (LiOH (ACROS Organics), 1.0 mmol, 24 mg) in H_2O (1.2 ml) were added. After 1h, the septum was removed and a solution of sodium sulfite 4eq. (Na_2SO_3, 2.4 mmol, 300 mg) in H_2O (1.8 ml) was added. By using a rotary evaporator THF was removed and the remaining solution was extracted 3 times with dichloromethane (DCM, 3.6 ml) to remove free oxazolidinone. The carboxylate salt of the desired product was brought to pH 1 with 6 M HCl and cooled at 0°C. Ethyl acetate (2.4 ml) was used 5 times to extract the product from the aqueous solution. The combined organic layer was dried over $MgSO_4$ and the solvent was removed using a rotary evaporator. The product (144 mg, 90% yield) (*R*)- or (122 mg, 76% yield) *(S)*-3-hydroxyoctanoic acid (3-HOA) is a colorless oil. NMR experiments were conducted to verify the molecule structure. (See chapter 3.1 Results). NMR Spectra can be found in Supporting Figure 14.

2.11 Investigation of PAX function and antimicrobial activity

In this project, the mode of action of PAX was elucidated using a microscopy approach together with Dr. Christoph Spahn (Prof. Dr. Mike Heilemann group). Therefore, azido- and alkyne-PAX derivatives were synthesized for the assay. Furthermore, PAX was quantified using HPLC-MS/MS to determine the available amount in the biological context.

PAX synthesis

The following section describes the PAX derivatives that were synthesized during this thesis as well as the synthetic route.

Overview of PAX derivatives with 3'-OH fatty acid

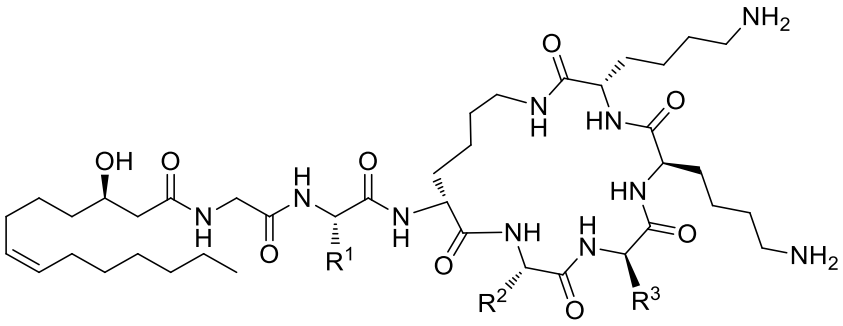

Name	compound	R^1	R^2	R^3
SYN PAX 1	**31**			
SYN PAX 2	**32**			
SYN PAX 3	**33**			
SYN PAX 4	**34**	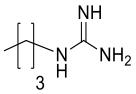		
SYN PAX 5	**35**	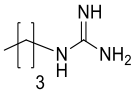		

Overview of PAX derivatives without 3'-OH fatty acid

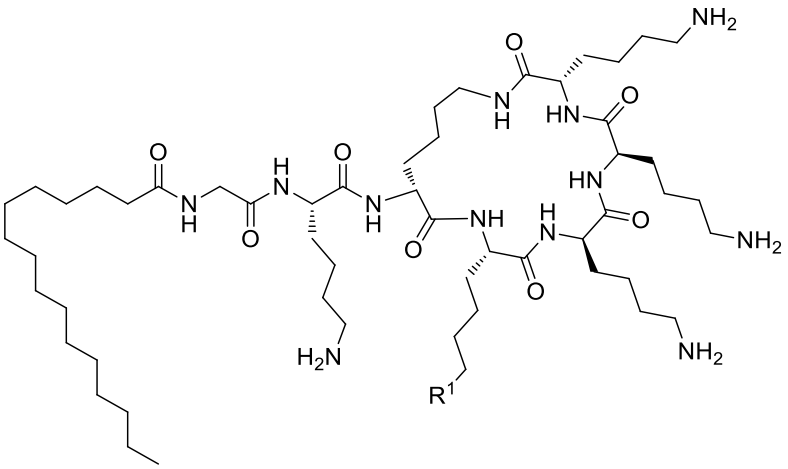

Syn PAX 6

36 R^1 = $-N_3$

Syn PAX 7

37 R^1 = 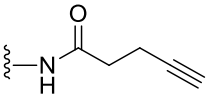

PAX derivatives **32**, **36,** and **37** were used for microscopy and bioactivity experiments and are occasionally referred to as azido-PAX, alkyne-PAX, and new alkyne-PAX respectively throughout this thesis.

Synthesis of PAX derivates

Loading of 2-CTC-resin with Fmoc-L-Lys-OAll*HCl

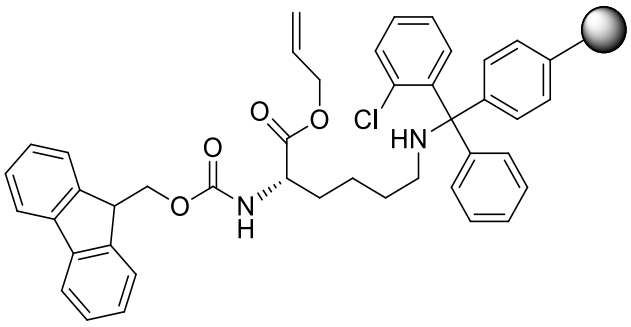

1 eq. 2-CTC resin (100 µmol, 62.5 mg) was added to 1.5 ml dry DCM in a polyethylene syringe under nitrogen and incubated for 30 min at room temperature. In addition, 3.0 eq thionyl chloride (300 µmol, 22 µl) was added and incubated for another 1h. In a separate flask, 1.2 eq Fmoc-L-Lys-OAll*HCl (120 µmol, 45 mg) was dissolved in dry DCM with 4.8 eq DIPEA (30 µmol, 17 µl) and incubated for 1h at room temperature. After 1h thionyl chloride was discarded and the syringe was washed five times with dry DCM. Finally, the mixture with Fmoc-L-Lys-OAll*HCl was uptake into the syringe and incubated overnight at room temperature. The Fmoc group was deprotected by 20% piperidine and the product yield ~80% was elucidated by UV/VIS. The product was confirmed by HPLC-MS. MS (ESI) m/z: $[M + H]^+$ Calcd for $C_{24}H_{29}N_2O_4$ 409.21; Found 409.45.

Peptide elongation

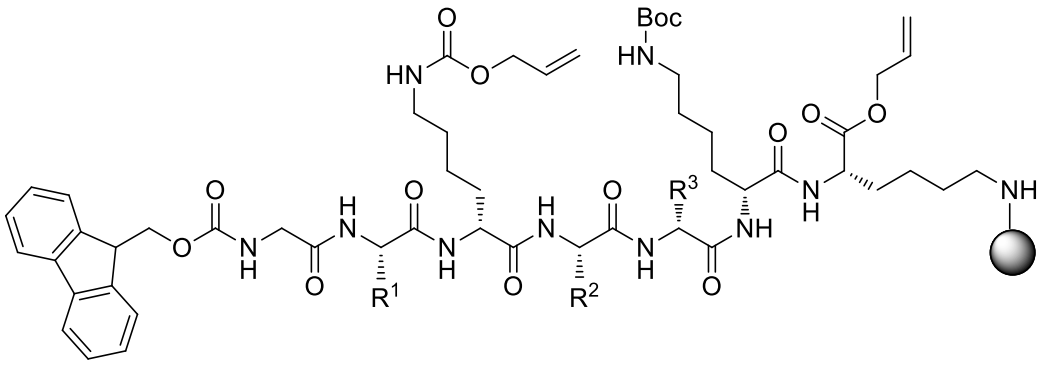

R^1 = 1-azidobutyl, *tert*-butyl butylcarbamate, 1-butylguanidine-Pbf
R^2 = 1-azidobutyl, *tert*-butyl butylcarbamate, *N*-butylpent-4-yanmide
R^3 = 1-azidobutyl, *tert*-butyl butylcarbamate

The peptide was elongated by the peptide synthesizer (Biotage Syro Wave). The common workflow was comprised of the following steps: washing, deprotection with piperidine, washing, amino acid activation, coupling, and washing. The products were confirmed by HPLC-MS.

Alloc deprotection

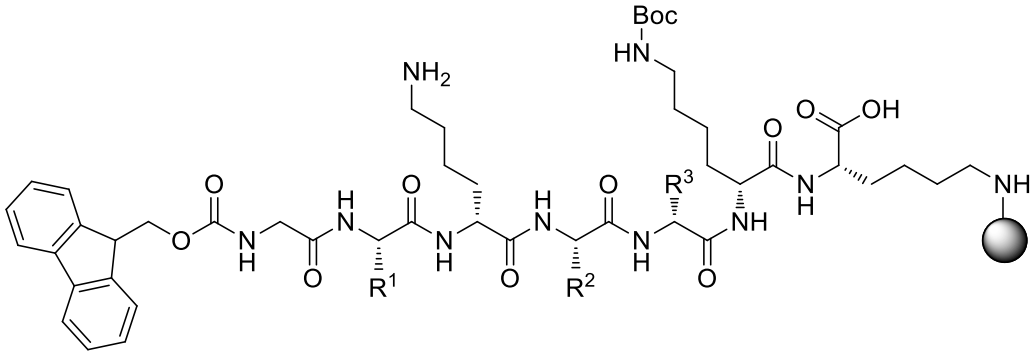

R^1 = 1-azidobutyl, *tert*-butyl butylcarbamate, 1-butylguanidine-Pbf
R^2 = 1-azidobutyl, *tert*-butyl butylcarbamate, *N*-butylpent-4-yanmide
R^3 = 1-azidobutyl, *tert*-butyl butylcarbamate

In a Schlenk tube, 1 eq. (25 µmol, 29.0 mg) TPP palladium(0) (Sigma Aldrich) and 10 eq (250 µmol, 31 µl) phenylsilane (Sigma Aldrich) was added to 2 ml dry DCM under nitrogen atmosphere. The syringe was flushed with nitrogen and the mixture from the Schlenk tube was draw up. The syringe was incubated for 4h at room

temperature. The resin was washed three times with the following solvents: DCM, 1 M pyridine*HCl in MeOH, MeOH, and 25 mM sodium diethyldithiocarbamate (Sigma Aldrich). In addition, the resin was washed excessively with DCM until the resin had a light yellowish color. The products were confirmed by HPLC-MS.

On-resin cyclization

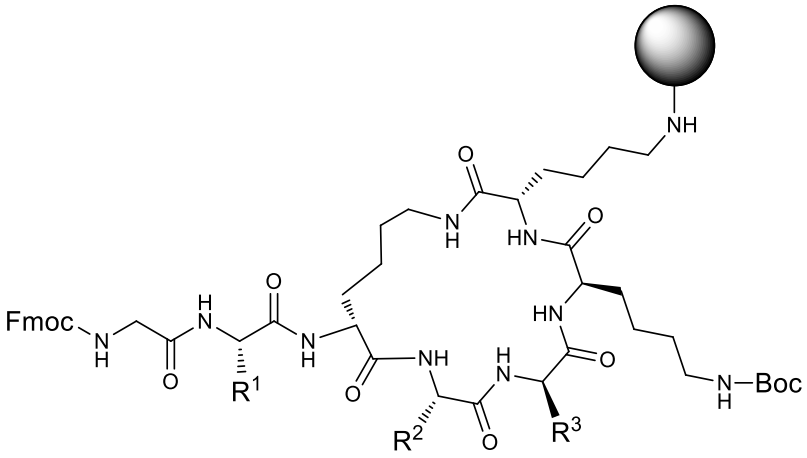

R^1 = 1-azidobutyl, butanyl-1-amine-Boc, 1-butylguanidine-Pbf
R^2 = 1-azidobutyl, *N*-butylpent-4-ynamide, butyl-1-amine-Boc
R^3 = 1-azidobutyl, butyl-1-amine-Boc

10 eq. (250 µmol, 36.0 mg) Oxyma Pure® (Sigma Aldrich) was mixed with 10 eq (250 µmol, 48.0 mg) EDC*HCl (Sigma Aldrich) and dissolved in 1 ml DMF. The reaction mixture had been drawn up into the syringe and was incubated overnight at room temperature. Next, the Fmoc group was removed and the yield was elucidated by UV/VIS. The products were confirmed by HPLC-MS.

Fatty acid coupling

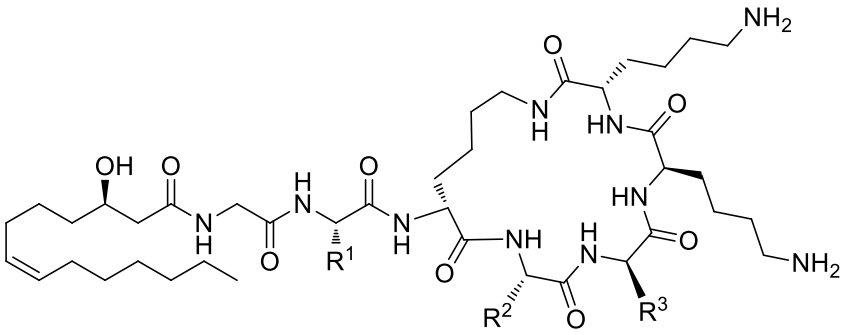

R^1 = 1-azidobutyl, butyl-1-amine, 1-butylguanidine
R^2 = 1-azidobutyl, butyl-1-amine
R^3 = 1-azidobutyl, butyl-1-amine

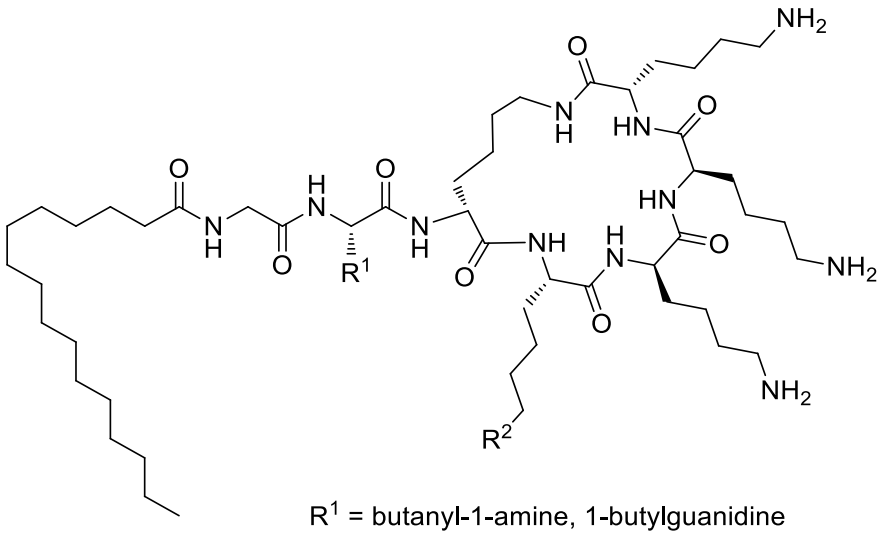

R^1 = butanyl-1-amine, 1-butylguanidine
R^2 = azide, pentyl-4-ynamide

5 eq. (125 µmol, 31.0 mg) *(R, Z)*-3-hydroxytetradec-7-enoic acid or 5 eq. (125 µmol, 32.0 mg) palmitic acid, 5 eq. (125 µmol, 48.0 mg) HATU, 5 eq. (125 µmol, 17.0 mg) HOAT, 10 eq. (250 µmol, 43 µl) DIPEA was dissolved in 1.5 ml DMF. In the next step, the syringe was filled with the reaction mixture and incubated overnight at 37°C. The peptide was cleaved with a TFA, TIS, and H_2O solution (v/v 95:2.5:2.5). The final products were purified by semi-preparative HPLC-MS (C18 column; 20-80% ACN/H_2O + 0.1% FA). The products were confirmed by HR-HPLC-MS (see 3.1 and 3.6 for results).

PAX quantification

To quantify the produced amount of PAX peptides, a PAX mutant strain obtained by Dr. Edna Bode (Goethe University Frankfurt) was used in the experiments. This organism is an arabinose inducible *X. doucetiae* strain with a promotor exchange in front of the NRPS responsible for PAX peptide production. Therefore, it was possible to induce PAX production by adding L-arabinose. Furthermore, a new protocol was established, which facilitated to quantify the produced amount of natural products present in the cell pellet and the supernatant fraction.

Quantification of PAX peptides

Three cell cultures of *X. doucetiae* wild type strain, induced *pax* mutant (*pax*$^+$ culture), and the non-induced *pax*$^-$ mutant were grown for 24 h at 30°C shaking at 220 rpm. 1 ml of each sample was pelleted at 5000 rpm for 4 min at 20°C. The cell pellet and the supernatant fraction were separated. In addition, the pellet was treated for 15 min in a supersonic bath. Both fractions were freeze-dried and resuspended in a 400 µl methanol/H_2O mix (v/v 1:1) and acidified with 1% formic acid. The cell pellet fraction was sonicated for 5 min. Both fractions were pelleted at 5000 rpm for 4 min at 20°C. The soluble fraction was measured by HPLC-MS (Bruker AmaZon X). The peak area from the extracted ion chromatogram from the particular PAX peptide was analyzed. The absolute amount was determined by a standard curve of the natural PAX molecule **38** (also named HB174 in the AG Bode compound collection).

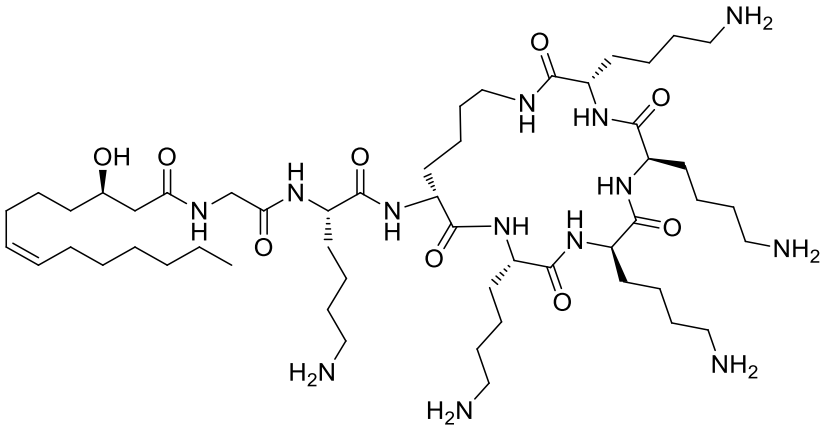

(HB 174)

38

Figure 31: Structure of **38** or (**HB174** AG Bode compound number). This compound was used as a standard for the quantification of PAX peptides.

PAX localization on cells using fluorescence microscopy

This part of the experiments was accomplished in collaboration with Dr. Christoph Spahn (Prof. Dr. Mike Heilemann group).

To localize PAX in a native environment, tests with the *X. doucetiae pax*$^-$ mutant strain and the *E. coli* MG1655 strain were conducted. The PAX peptide derivatives were synthesized with an azide- (**36**) or alkyne-tag (**37**) as described in section 2.11. In the experimental setup, overnight cultures were diluted 1:200 into fresh LB medium. The cells were grown at 30°C at 220 rpm and harvested when the culture reached the exponential growth phase (~0.3 OD) to obtain the optimal cell size for microscopy images. In the next step, **36** and **37** were added to the cell culture for 11–31 minutes. After the indicated incubation time, the cells were chemically fixed and immobilized on poly-L-lysine coated chamber slides (Sarstedt GmbH, Germany). Thereafter, the cells were permeabilized using TX-100 and click-labelled with either Sulfo-Cy5-alkyne (Lumiprobe) or Alexa Fluor 647 (AF647) (Thermo Fischer) azide. Finally, the samples were measured using Confocal Laser Scanning Microscopy (CLSM) or SMLM techniques.

Sample preparation for CLSM experiments

Overnight cultures of *E. coli* cells and *X. doucetiae pax*$^-$ mutant were grown at 37 °C in LB Miller (10 g NaCl) or LB-Lennox (5 g NaCl), respectively. The OD_{600} was monitored every 30 min to determine the culture doubling time. At OD_{600} ~ 0.3, PAX was added at desired concentrations, and cultures were incubated for ~11 min. For PAX treatment, 634 µl of cell suspension was added into 2 ml reaction tubes. Finally, 70 µl of the PAX stock solution was added to the suspension (Table 3).

Table 3: PAX stock dilution for click experiments. *E. coli* and *X. doucetiae* cells were initially incubated with PAX peptides before the microscopy experiment.

desired PAX concentration (in µg/ml)	volume PAX stock solution (1 mg/ml)	Volume ddH_2O	final volume
100	100 µl	-	100 µl
30	30 µl	70 µl	100 µl
10	10 µl	90 µl	100 µl
0 (control)	-	100 µl	100 µl

After 11 min, the cells were fixed using 2% MeOH-free formaldehyde and 0.1% EM-grade glutaraldehyde in sodium phosphate buffer for 15 min at room temperature. 296 µl of the fixation master mix (Table 4) was added to the PAX-treated cell suspension.

Table 4: Composition of fixation master mix. After the PAX treatment, bacteria cells were fixed using formaldehyde and glutaraldehyde.

Chemical/suspension	Stock concentration	Final concentration	Volume (1 ml final volume)	3 ml master mix fix. solution
$NaPO_4$ buffer pH 7.5	200 mM	34 mM	167 µl	1692 µl
formaldehyde	16 %	2%	125 µl	1267 µl
glutaraldehyde	25 %	0.1%	4 µl	40.5 µl
bacterial suspension	-	-	704 µl	-

After the reaction, the cells were pelleted (2 min, 5000 g) and resuspended in freshly prepared quenching solution (0.1-0.2% $NaBH_4$ in PBS). After 2 min incubation (RT), the cells were washed 2-3 times with PBS (depending on the used PAX concentration due to cell destruction). Thereafter, the cells were resuspended in 100-300 µl PBS and immobilized on KOH-cleaned (3 M,1 h, 42 °C) and poly-L-lysine (PLL)-coated (0.01% PLL for 10-20 min) chamber slides. After 20-30 min incubation, cells were removed and chambers were washed thoroughly and permeabilized for 1h at room temperature using 0.5% TX-100 in PBS (950 µl PBS + 50 µl 10% TX-100 per ml permeabilization solution). Finally, the cells were washed twice with PBS buffer.

250 µl click-labeling solution containing 100 mM tris pH 8.0, 1 mM $CuSO_4$, 100 nM Sulfo-Cy5 alkyne or AF647, and 100 mM L-ascorbic acid was added to each chamber and samples were incubated 60 min in the dark. Samples were then rinsed and washed three times (5 min) with PBS to remove unbound fluorophores (Figure 32).

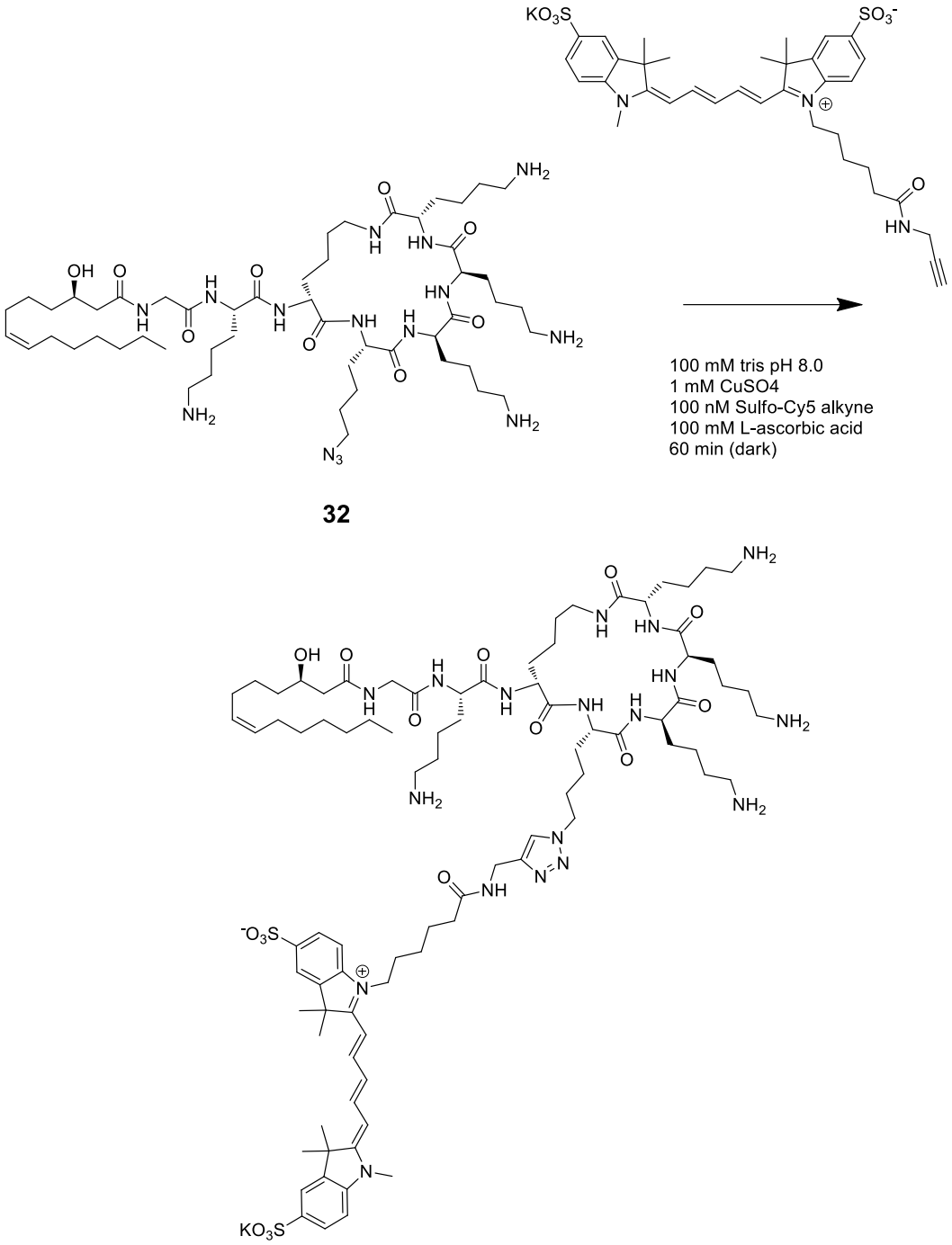

32

Figure 32: Click labeling reaction between PAX derivative **32** and Sulfo-Cy5 alkyne.

Sample preparation for SMLM experiments

E. coli MG1655 WT cells were grown in LB (10 g NaCl) at 37 °C and 220 rpm until mid-exponential phase. At OD ~0.3, synthetic PAX peptides (**36** and **37**, respectively) were added for 11 min at 0, 10, 30 or 100 µg/ml concentration (10% of culture volume, volume adjusted with ddH_2O). Cells were fixed and immobilized as described in the previous section. After permeabilization (1 h, 0.5% TX-100 in PBS), cells were labelled with either Cy5 alkyne or AF647 azide (0.1 µM dye) for 1 h (RT). For multicolor imaging, imaging buffer containing 100 mM tris pH 8.0, 100 mM MEA, 10 mM NaCl, 50% D_2O, 400 - 600 pM Nile Red, and 1-10 nM JF503-Hoechst was added to the samples.

For time-series experiments, *E. coli* MG1655 cells were grown in LB (10 g NaCl) at 37 °C shaking at 220 rpm. At OD600 ~0.3, **37** (10 µg/ml) was added to the culture, while an aliquot of the culture was grown in the absence of PAX peptide as a negative control. Cells were fixed after 11, 21, and 31 min as described before. Imaging buffer (100 mM tris pH 8.0, 100 mM MEA-HCl, 10 mM NaCl, 500 - 800 pM Potomac Gold, 500 pM JF503-Hoechst) was added to the sample before super-resolution imaging.

Multicolor super-resolution imaging and analysis

Triple-color super-resolution images of the cell membrane, AF647/Cy5-labelled PAX peptide, and the nucleoid were recorded on a custom-build setup for single-molecule detection[132]. The cell outlines were determined in the membrane image and overlaid with the nucleoid image and nucleoid/PAX composite.

Bioactivity tests

Plate diffusion assays of PAX derivatives

X. doucetiae WT, *X. doucetiae pax*$^-$, *E. coli*, *M. luteus,* and *B. subtilis* were grown overnight at 30 °C and diluted to OD = 1. A cotton stick (Böttger) was used to inoculate these strains on agar plates. PAX derivatives were first dissolved in H_2O. Then, 10 µl of the mixture was added to a round filter disc (5 mm diameter) and placed on the agar plate. 50 µg/ml kanamycin was used as a positive control, while MeOH was used as a negative control. Similarly, *S. cerevisiae* was first cultivated in liquid YPD medium at 37 °C, adjusted to OD = 1, and then inoculated on a Yeast Extract-Peptone-Dextrose (YPD) plate. Here, G418 (200 µg/ml) was used as a positive control, while MeOH was used as a negative control.

Broth microdilution assays of *X. doucetiae* WT, *pax* mutants, and *E. coli*

X. doucetiae, the *pax*$^-$ mutant, and *E. coli* MG1655 were grown in LB overnight. The cultures were pelleted at 5000 rpm, 4 min at 20 °C. The pellet was dissolved in 1 ml 0.9% NaCl, adjusted to McFarland standard 0.5, and diluted 1:10 (≈1x10^7 CFU/ml). The assays were performed in 96 well plates and triplicates. 100 µl cation-adjusted Mueller Hinton II Broth (Sigma Aldrich) was added in each well. 100 µl of the standard AMP concentration was added in the first row while 100 µl of H_2O was added to the negative control. Polymyxin B was used as positive control and the *pax*$^-$ mutant was induced by 0.2% arabinose. After addition, the liquids were mixed and 100 µl from the top row was mixed with the next row resulting in a dilution series with the factor of two. Finally, 5 µl of the tested cultures were added in each well (~50.000 CFU). The well plate was set in a plate reader (Tecan Spark 100 M) and measured for >20 h.

2.12 Proteome analysis

Sample Preparation

Overnight cultures of *X. nematophila, X. szentirmaii,* and *P. luminescens* were grown in 5 ml LB Lennox at 30 °C for 18 h. In the beginning, these cultures were separated into two different groups with one group induced with 1 ml insect lysate. To prepare this insect lysate, freeze-dried *Galleria mellonella* larva were crushed in a bead mill. Furthermore, negative controls with insect lysate and 5 ml LB media were added.

Lysis and protein digestion

After 18h of growth, the cultures were vortexed at 10000 g for 2 min to obtain the cell pellets, which was then resuspended in ddH_2O. Next, the samples were transferred into a thermo shaker at 95 °C for 5 min and treated in an ultrasonic bath for 15 min. In addition, the protein concentration was adjusted to 20 µg/ml using a Nanodrop machine. For lysis, cells were resuspended in 1 µl lysis buffer per 1-5 µg Protein (Lysis buffer: 6 M guanidine hydrochloride (GdmCl) (Sigma Aldrich), 100 mM Tris/HCl pH 8.5; 10 mM TCEP, 40 mM 2-chloroacetamide). In addition, the samples were diluted 1:10 and guanidine hydrochloride (c = 0.6 M) was added in a 25 mM Tris/HCl pH 8,5 (10 % ACN) buffer. Furthermore, the proteins were digested with 1 µg trypsin/lys-C per 50 µg of protein at 37°C overnight under decent agitation. On the next day, the digestion was stopped by adding TFA (0.1% final concentration).

Prefractionation

The peptides were separated into four different fractions before measurements. Therefore, StageTips were prepared by adding three SCX-disks (strong cation-exchange) and three C18 disks on top into a 100 µl pipette tip.

Hereafter, the StageTips were preconditioned by adding 20 µl methanol, 20 µl **Buffer 2** (0.5 % Acetic acid, 80 % ACN), and 20 µl **Buffer 1** (0.5 % Acetic acid). The StageTips were attached to the lid of a 1.5 ml Eppendorf tube and vortexed after each step at 2500 g for 3 min.

The samples were initially vortexed at 17000 g for 10 min to avoid clogging. Then, the StageTips were loaded at 2500 g. In addition, 20 µl of **Buffer 1** was added and the samples were vortexed at 2500 g for 3 min. The flow-through was discarded. 20 µl of **Buffer 2** was added subsequently and the flow-through was collected as **fraction 1**. **Fraction 2** was collected after adding 20 µl of **Buffer 3** (50 mM ammonium acetate, 20% ACN). **Fraction 3** was collected after adding 20 µl **Buffer 4** (50 mM ammonium bicarbonate, 20% ACN) and **Fraction 4** after adding **Buffer 5** (0,1% ammonium hydroxide, 20% ACN). The four fractions were then dried in the SpeedVac and dissolved in 10 µl (1% ACN, 0,1% formic acid in water).

HPLC-MS/MS

The Samples were measured with the Q Exactive™ Hybrid-Quadrupole-Orbitrap mass spectrometer. The peptides were separated using an in-house packed column (100 µm inner diameter, 30 cm length, 2.4 µm Reprosil-Pur C18 resin) using a gradient from mobile phase A (5% ACN, 0.1% FA) to mobile phase B (95% ACN, 0.1% FA) for 120 min.

Statistical analysis

The data were analyzed by the program MaxQuant Version 1.6.0.1 and Perseus Version 1.6.2.1. The Welch-test was utilized as a statistical method to determine up and down-regulated proteins. The threshold was set to $p \leq 0.05$ and more than two-fold variation.

KEGG visualization

The visualization was performed by loading the fasta file with the up, down, and total proteins of each sample. Pictures of the mapped KEGG protein were saved to the computer. Mapped proteins pathways were recognized utilizing python scripts (Opencv), which ultimately formed overlaid pictures of the measured proteins from the samples.

3. Results

The following section covers the synthesis of various natural products. Furthermore, sections 3.6 and 3.7 covers the microscopy results using clickable PAX derivatives and proteome analysis of *X. szentirmaii*, *X. nematophila,* and *P. luminescens*.

3.1 Compounds collection

Figure 33 shows the structures of all compounds synthesized as part of this thesis.

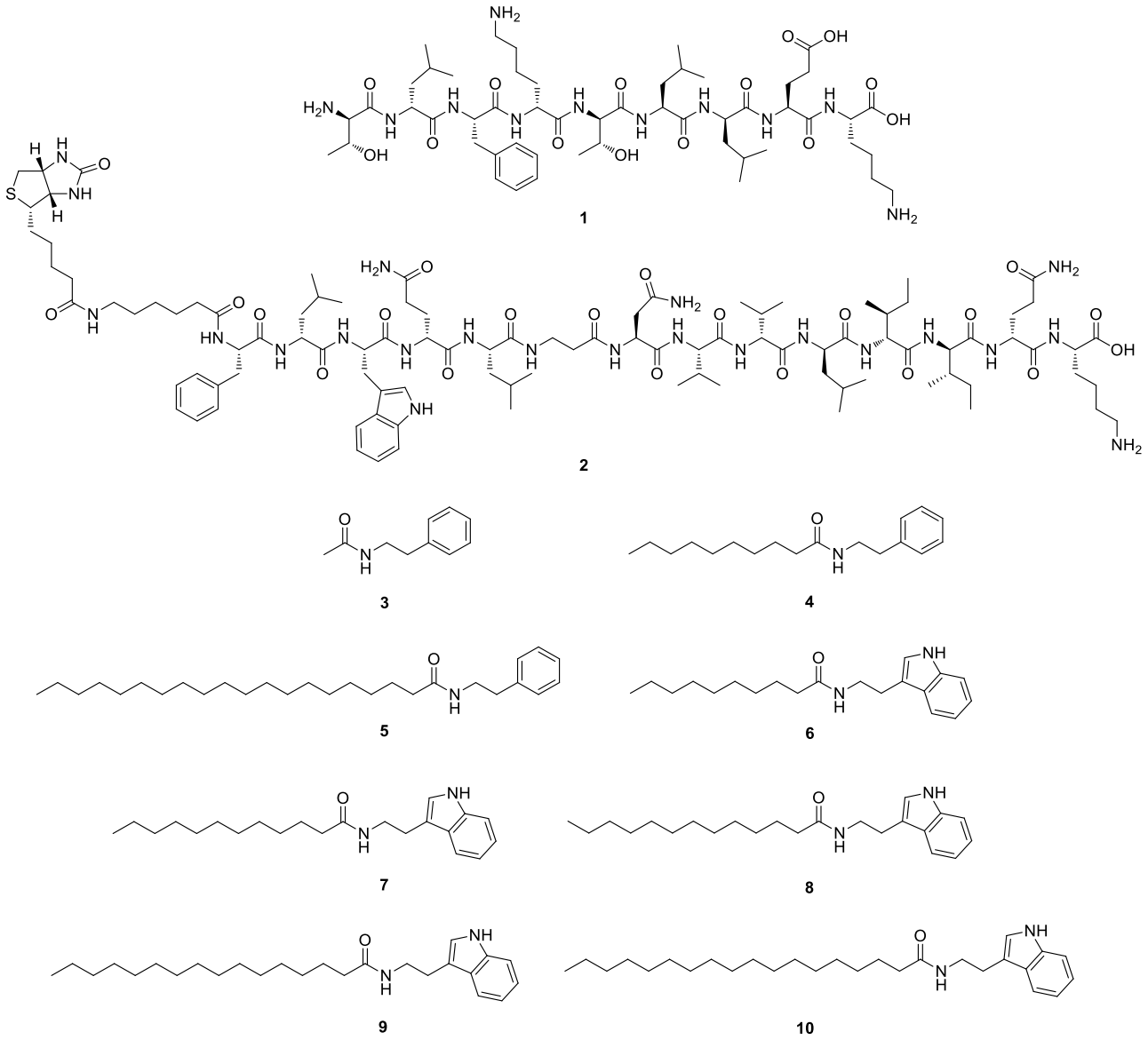

Figure 33: Synthesized compounds during the thesis.

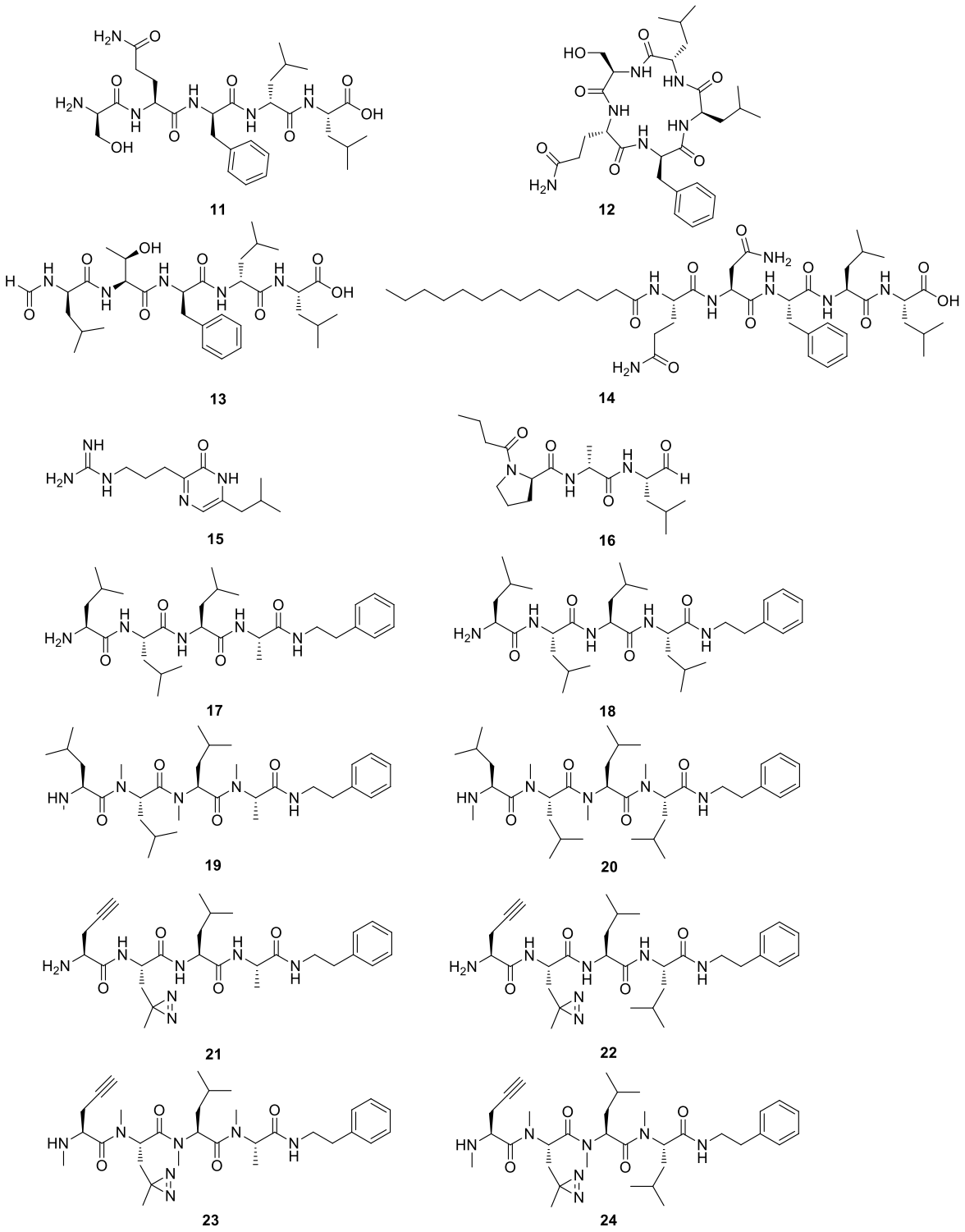

Figure 33: Synthesized compounds (cont.).

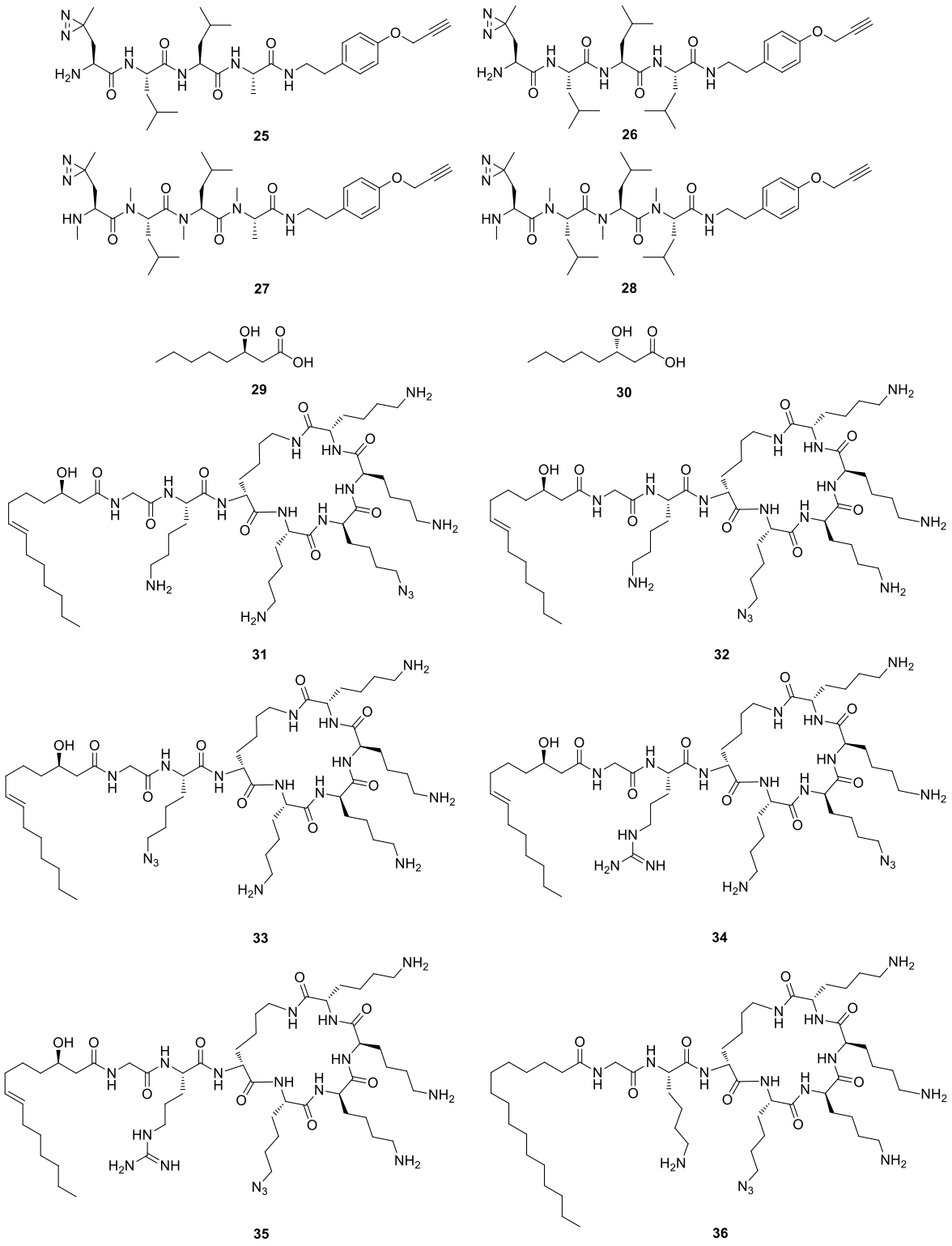

Figure 33: Synthesized compounds (cont.).

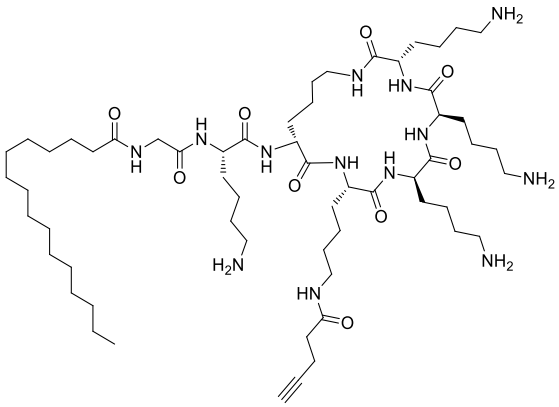

37

Figure 33: Synthesized compounds (cont.).

Table 5: Natural PAX compounds[107] used as standards.

Name	compound number	Chemical formula	m/z $[M+2H]^+$
HB174	**38**	$C_{52}H_{99}N_{13}O_9$	525.891712
PAX 1	**39**	$C_{55}H_{107}N_{13}O_9$	547.923012
PAX 3	**40**	$C_{56}H_{109}N_{13}O_9$	554.930838

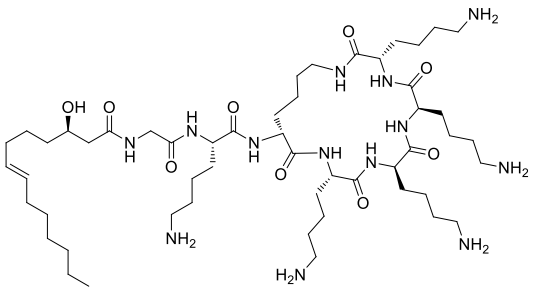

38

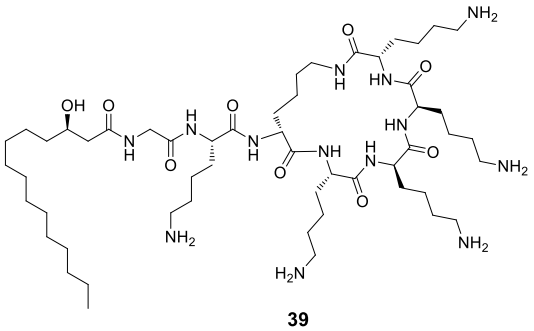

39

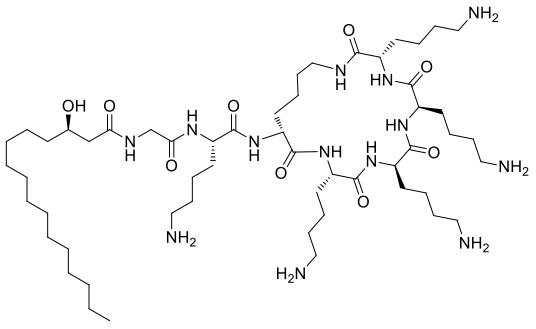

40

Table 6: Mass spectrometry data of all synthesized compounds.

Name	compound number	Chemical formula	Calculated m/z $[M+H]^+$ ($[M+2H]^+$)* ($[M+3H]^+$)**	Measured m/z $[M+H]^+$ ($[M+2H]^+$)* ($[M+3H]^+$)**	Δppm
silathride	**1**	$C_{52}H_{89}N_{11}O_{14}$	1092.6663	1092.6635	2.56
biotinylated xenoautoxin	**2**	$C_{93}H_{147}N_{21}O_{20}S$	637.7023**	637.7013**	1.57
N-phenethylacetamide	**3**	$C_{10}H_{13}NO$	164.1070	164.1067	1.83
N-phenethyldecanamide	**4**	$C_{18}H_{29}NO$	276.2322	276.2316	2.17
N-phenethylicosanamide	**5**	$C_{28}H_{49}NO$	416.3920	416.3911	2.16
N-(2-(1H-indol-3-yl)ethyl) decanamide	**6**	$C_{20}H_{30}N_2O$	315.2431	315.2423	2.54
N-(2-(1H-indol-3-yl)ethyl) dodecanamide	**7**	$C_{22}H_{34}N_2O$	343.2744	343.2736	2.33
N-(2-(1H-indol-3-yl)ethyl)tridecanamide	**8**	$C_{23}H_{36}N_2O$	357.2900	357.2912	3.36
N-(2-(1H-indol-3-yl)ethyl)palmitamide	**9**	$C_{26}H_{42}N_2O$	399.3370	399.3365	1.25
N-(2-(1H-indol-3-yl)ethyl)stearamide	**10**	$C_{28}H_{46}N_2O$	427.3683	427.3679	0.94
SYNZIP peptide 1	**11**	$C_{29}H_{46}N_6O_8$	607.3450	607.3430	-
SYNZIP peptide 2	**12**	$C_{29}H_{44}N_6O_7$	589.3344	589.3326	-
SYNZIP peptide 3	**13**	$C_{32}H_{51}N_5O_8$	634.3810	634.3818	-
SYNZIP peptide 4	**14**	$C_{44}H_{73}N_7O_9$	844.5543	844.5533	-
peptide aldehyde 1	**15**	$C_{12}H_{21}N_5O$	252.1819	252.1815	1.3
peptide aldehyde 2	**16**	$C_{17}H_{29}N_3O_4$	354.2231	354.2387	2.2

rhabdopeptide 1	**17**	$C_{29}H_{49}N_5O_4$	532.3863	532.3848	2.82
rhabdopeptide 2	**18**	$C_{32}H_{55}N_5O_4$	574.4332	574.4314	3.13
rhabdopeptide 3	**19**	$C_{33}H_{57}N_5O_4$	588.4489	588.4500	1.87
rhabdopeptide 4	**20**	$C_{36}H_{63}N_5O_4$	630.4958	630.4962	0.63
rhabdopeptide 5	**21**	$C_{27}H_{39}N_7O_4$	526.3142	526.3133	1.71
rhabdopeptide 6	**22**	$C_{30}H_{45}N_7O_4$	568.3611	568.3600	1.94
rhabdopeptide 7	**23**	$C_{31}H_{47}N_7O_4$	582.3768	582.3749	3.26
rhabdopeptide 8	**24**	$C_{34}H_{53}N_7O_4$	624.4237	624.4216	3.36
rhabdopeptide 9	**25**	$C_{31}H_{47}N_7O_5$	598.3717	598.3725	1.34
rhabdopeptide 10	**26**	$C_{34}H_{53}N_7O_5$	640.4186	640.4204	2.81
rhabdopeptide 11	**27**	$C_{35}H_{55}N_7O_5$	654.4343	654.4323	3.06
rhabdopeptide 12	**28**	$C_{38}H_{61}N_7O_5$	696.4812	696.4790	3.16
(*R*)-3-Hydroxyoctanoic acid	**29**	$C_8H_{16}O_3$	160.1099	-	-
(*S*)-3-Hydroxyoctanoic acid	**30**	$C_8H_{16}O_3$	160.1099	-	-
SYN PAX 1	**31**	$C_{51}H_{95}N_{15}O_9$	531.8791*	531.8776*	2.82
SYN PAX 2	**32**	$C_{52}H_{97}N_{15}O_9$	538.8870*	538.8876*	1.11
SYN PAX 3	**33**	$C_{51}H_{95}N_{15}O_9$	531.8791*	531.8798*	1.32
SYN PAX 4	**34**	$C_{51}H_{95}N_{17}O_9$	545.8822*	545.8834*	2.20
SYN PAX 5	**35**	$C_{52}H_{99}N_{15}O_9$	539.8948*	539.8928*	3.70
SYN PAX 6	**36**	$C_{54}H_{103}N_{15}O_8$	545.9130*	545.9115*	2.74
SYN PAX 7	**37**	$C_{59}H_{109}N_{13}O_9$	572.9308*	572.9300*	1.40

3.2 Synthesis of silathride

The synthesis of silathride was successful using the standard Fmoc SPPS procedure (on page 59 section 2.2). The yield was not determined, as the product was used as a standard for structure verification.

After the synthesis and the purification, the peptide could be verified via comparison with the natural compound by HPLC-MS (Supporting Figure 1).

3.3 Synthesis of xenoautoxin and biotinylated xenoautoxin

Xenoautoxin could be synthesized using the standard procedure (on page 59) with the sequence:

F-l-W-q-L-ß-n-**V-v-l-i-i-**q-K

ß = ß-alanine

i = D-*allo*-isoleucine

The peptide sequence **Vvlii** had to be coupled twice to obtain the desired product. The crude product was purified, verified by HPLC-MS/MS and confirmed by comparison with the natural product (Supporting Figure 3). The product quantity was determined via UV/VIS measurement. 82% (41.15 µmol) of the intermediate product was obtained.

The peptide was subsequently extended using a C6-linker Fmoc-ε-Ahx-OH and then coupled with biotin. The overall yield after purification was ~5%.

Synthetic xenoautoxin and biotinylated xenoautoxin (**3**) were tested against several bacteria strains such as *X. doucetiae* and *E. coli*. Unfortunately, both peptides showed no bioactivity. Therefore, the observed autotoxicity was not verified[73].

3.4 Synthesis of rhabdopeptide derivatives

The rhabdopeptides were synthesized using the standard protocol (on page 71). The reported yield after purification was between 30-40%. The compounds were tested against *Trypanosoma brucei rhodesiense* by collaborators. The results showed that the compounds were active in the µmolar range (Figure 34)[98].

Figure 34: Bioactivity data from rhabdopeptides.

Compounds	**calculated mass**	**IC_{50} (µg/ml) in *T. b. rhodesiense***
17	531.3785	not determined
18	573.4254	13.2 ± 0.9
19	587.4411	31 ± 12
20	629.4880	1.41 ± 0.03
26	639.4108	not determined

In the case of **17** and **26**, the maximum soluble concentration showed no activity towards *T.b. rhodesiense* (above 100 µg/ml).

3.5 Synthesis of chiral 3-Hydroxyoctanoic acid for phototemtide A[105]

(*R*)-3-hydroxyoctanoic acid and (*S*)-3-hydroxyoctanoic acid was obtained following the given protocol (on page 75 section 2.10). The synthesis was accomplished by using the Reformatsky reaction in combination with an oxazolidinone as chiral auxiliaries[137]. The 3-hydroxyoctanoic acid derivatives were purified via flash chromatography and the structure was determined via NMR (Supporting Figure 14).

The chiral fatty acids products were then used in Fmoc SPPS. The most effective synthesis strategy was to esterify the 3'-OH group of the fatty acid and utilize a macrolactamization between threonine and isoleucine. The final synthetic derivatives were compared to the natural compound. The structure was confirmed by HPLC-MS (Supporting Figure 15).

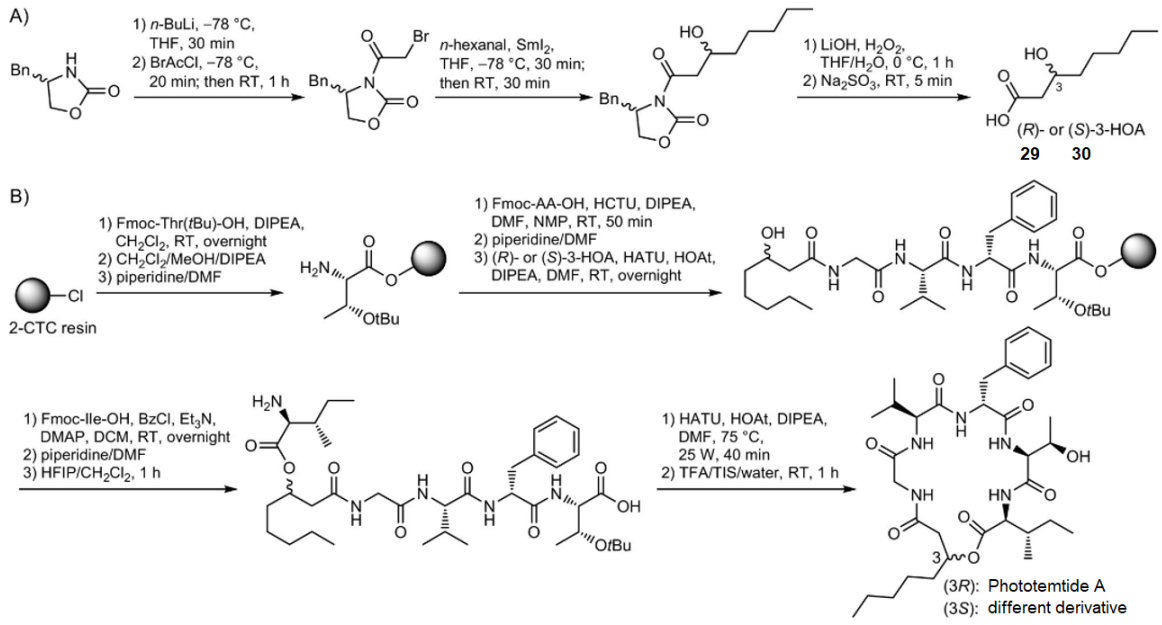

Figure 35: Synthesis of phototemtide A.

In addition, the peptide was tested against *Trypanosoma brucei rhodsiense*, *Trypanosoma cruzi*, *Leishmania donovani*, *Plasmodium falciparum,* and L6 mammalian cells. The results were promising showing activity towards the human pathogenic strains *T.b. rhodsiense*, *T. cruzi,* and *P. falciparum* and no activity towards mammalian L6 cells.

Table 7: Bioactivity of phototemtide A.

Species	**Phototemtide A (IC_{50} in µM)**	**Control* (IC_{50} in µM)**
T.b. rhodesiense	62	0.005
T. cruzi	83	2.1
L. donovani	>100	0.73
P. falciparum	9.8	0.009
mammalian L6 cells	>100	0.007

Different controls were utilized for each target organism: melarsoprol for *T. brucei rhodesiense*, benznidazole for *T. cruzi*, miltefosine for *L. donovani*, chloroquine for *P. falciparum*, and podophyllotoxin for L6 cells[105].

3.6 Investigation of PAX function and antimicrobial activity

PAX Synthesis

Several azido and alkyne-PAX derivatives were first synthesized using the protocol on page 78 (section 2.11 PAX synthesis).

Table 8: Bioactivity results of synthetic PAX molecules vs *X. doucetiae* WT, *pax*$^-$ and *E. coli*.

Name	**MIC (µg/ml) plate diffusion assay (triplicate) in**			
	***X. doucetiae* WT**	***pax*$^-$**	***E. coli***	***B. subtilis***
38 (natural PAX)	>1000	>1000	1000	37.5
31	>1000	>1000	1000	37.5
32	>1000	>1000	1000	37.5
33	>1000	>1000	1000	37.5
34	>1000	>1000	1000	37.5
35	>1000	>1000	1000	37.5
36	>1000	>1000	100	18.7
37	>1000	>1000	100	18.7

The bioactivity of the new PAX derivatives was comparable to the natural compounds. This was verified by plate diffusion and broth microdilution assays in triplicates. The methods were described in section 2.11. New PAX derivatives with palmitic acid residues were more potent towards *M. luteus*, *B. subtillis,* and *E. coli*.

PAX derivatives were also tested against *X. doucetiae* WT and the *pax*$^-$ mutant. In both cases, the measured minimal inhibition concentrations (MICs) were above 125 µg/ml in broth microdilution tests (Supporting Figure 22) and above 250 µg/ml (Supporting Figure 21) in plate diffusion tests. Therefore, the maximum adjusted concentration of PAX in the microscopy experiments was set to 100 µg/ml.

PAX quantification

The quantification of PAX in the native environment is an important aspect of this study. PAX is described as AMP to harm potential competitors. However, the peptide was not quantified until now. Furthermore, in previous works, PAX was only identified in the supernatant after an initial enrichment step using cation exchange material[14,107,108]. Therefore, it is important to elucidate the PAX concentration in the biological context. Here, a new method is presented to quantify PAX in the cell pellet fraction of the cultures.

Using the protocol (on page 84) triplicate samples from *X. doucetiae* WT, induced mutant (*pax*$^{+}$) and non-induced mutant (*pax*$^{-}$) were analyzed. The results showed two dominant peaks of **39** and **40** in the cell pellet fraction (Figure 36). These derivatives have a similar structure to the derivatives **38** and **31-33**.

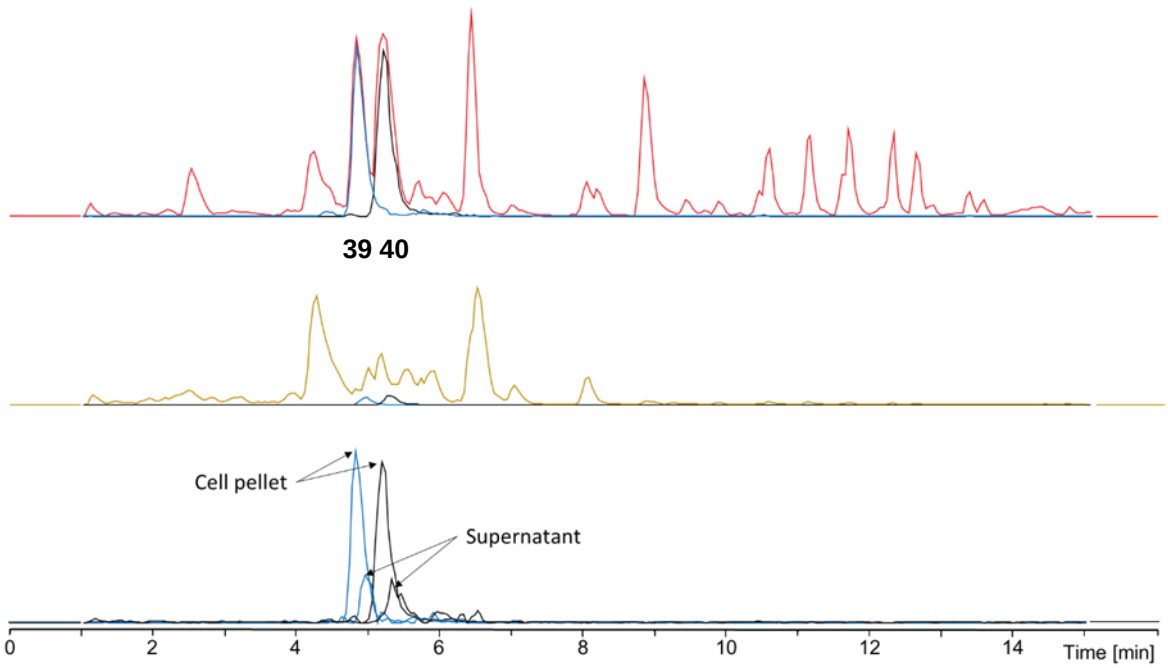

Figure 36: HPLC/MS chromatograms for the quantification of PAX derivatives naturally produced by the *X. doucetiae* WT strain. Base peak chromatograms (BPC) of the cell pellet (top panel) and supernatant fractions (middle panel) are shown including the peaks assigned to derivative **39** and **40**. The bottom panel compares the extracted ion chromatograms (EIC) of both derivatives for the respective fractions.

Signals of **39** and **40** were also identified in the supernatant samples of *X. doucetiae* WT cultures (Figure 36). The extracted ion chromatogram showed a clear PAX signal at a similar retention time and the same fragmentation pattern. However, the overall signals of other classes of natural products in the supernatant samples were higher than in the cell pellet samples (~10x fold difference between the largest peaks in both samples).

The overlaid extracted ion chromatograms showed that the PAX signals were larger in the cell pellet samples than the supernatant samples (Figure 37). The peak area of the signals was plotted to quantify the relative amount of each peptide. 78-89% of the peptides were found in the cell pellet fraction.

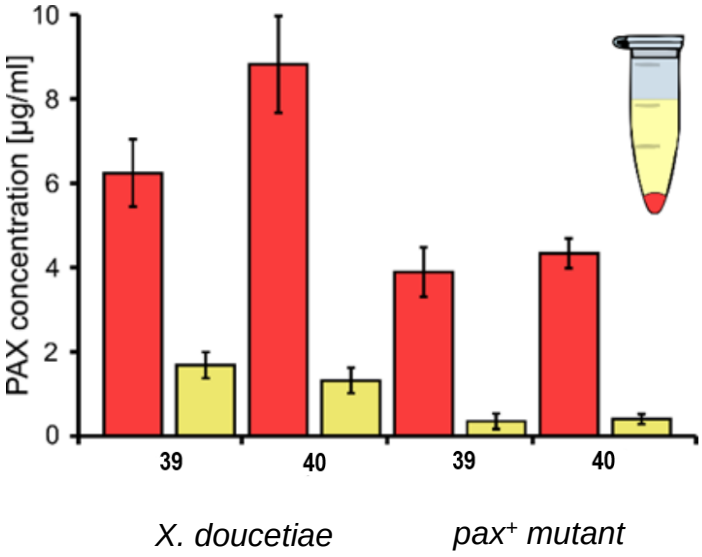

Figure 37: Absolute quantification of natural PAX compounds **39** and **40** in *X. doucetiae* and the induced *pax*$^{+}$ mutant. Red color indicates the cell pellet fraction, while the yellow color indicates the supernatant fraction.

The quantification results were similar for the induced *pax*$^{+}$ mutant. The signals of **39** and **40** were detected in the cell pellet fraction. Also, here **39** and **40** were more difficult to detect due to signals from other secreted natural products (Supporting Figure 17). The overlap of **39** and **40** signals between cell pellet and supernatant

showed similar results to the *X. doucetiae* WT PAX signals. Moreover, 84%-97% of the PAX peptides were found in the cell pellet fraction (Supporting Figure 18). No signals were resulting from PAX molecules in the HPLC-MS analysis in the cell pellet and supernatant fraction from the *pax*$^{-}$ mutant (Supporting Figure 19 and Supporting Figure 20).

In comparison, the *pax*$^{+}$ mutant produced ~55% of **39** and **40** when compared to the *X. doucetiae* WT level (Figure 37). In addition, the reference peptide **38**, a natural occurred PAX peptide was used to produce a fitting curve to obtain the absolute quantity of PAX peptides in the samples. The results showed that the WT produced ~18 mg/l of **39** and **40** derivatives and the *pax*$^{+}$ mutant produced ~9 mg/l of **39** and **40** peptides (Figure 38).

Table 9: PAX amounts in different fractions for different *X. doucetiae* cultures as quantified using HPLC-MS.

PAX derivative	**PAX amount [µg/ml] (WT)**		
	P	**SN**	**P + SN**
39	6.24 ± 0.80	1.68 ± 0.31	7.92 ± 0.86
40	8.82 ± 1.15	1.32 ± 0.30	10.14 ± 1.19
39 + **40**	15.06 ± 1.40	3.00 ± 0.43	**18.07 ± 1.47**
	PAX amount [µg/ml] (*pax*$^{+}$)		
	P	**SN**	**P + SN**
39	3.89 ± 0.59	0.35 ± 0.19	4.24 ± 0.62
40	4.34 ± 0.36	0.40 ± 0.12	4.74 ± 0.38
39 + **40**	8.23 ± 0.69	0.75 ± 0.22	**8.98 ± 0.72**

P = pellet fraction, SN = supernatant fraction. Numbers were obtained from 1 ml culture an adjusted OD600 = 1. Bold numbers indicate the total amount of **39** and **40** produced by the respective strains.

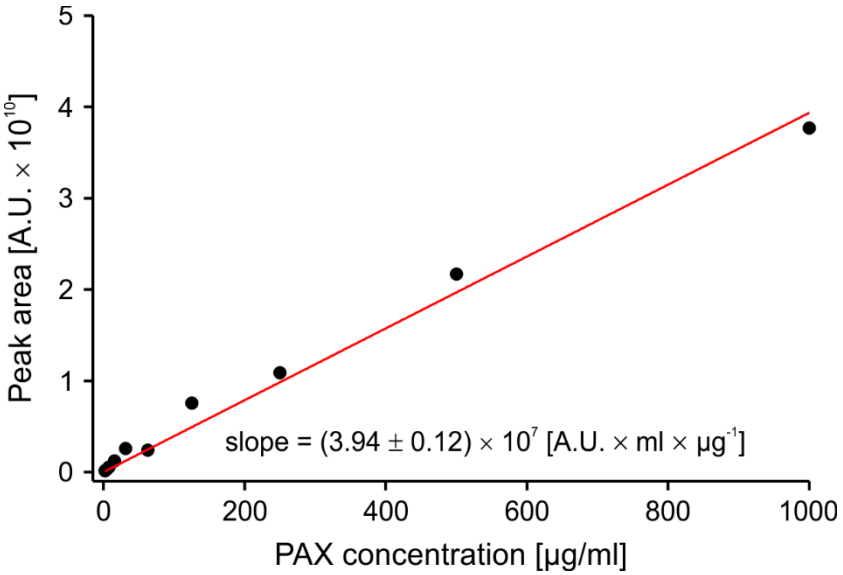

Figure 38: Standard curve and absolute quantification. A standard curve was recorded for the quantification of PAX peptides. Therefore, the natural PAX derivative **38** was diluted in different concentrations. The peak areas of these samples were then plotted against the adjusted concentrations.

A Welch test was performed as a statistical analysis to compare the absolute quantity between cell pellet and supernatant in WT (p = 4E-4) and induced *pax*$^{+}$ mutant (p = 7E-6). The results were statistically significant based on calculated p-values (Figure 39). The produced amount is 15 mg/l in the WT (cell pellet) and in the expected production range of *Xenorhabdus* in comparison with other natural products such as GameXPeptides (49 mg/l)[89]. However, the determined AMP concentration in the supernatant was at 3 mg/l and therefore lower when compared to the bioactive range of natural PAX derivatives[1,14]. In the next step, we conducted microscopy experiments to localize PAX.

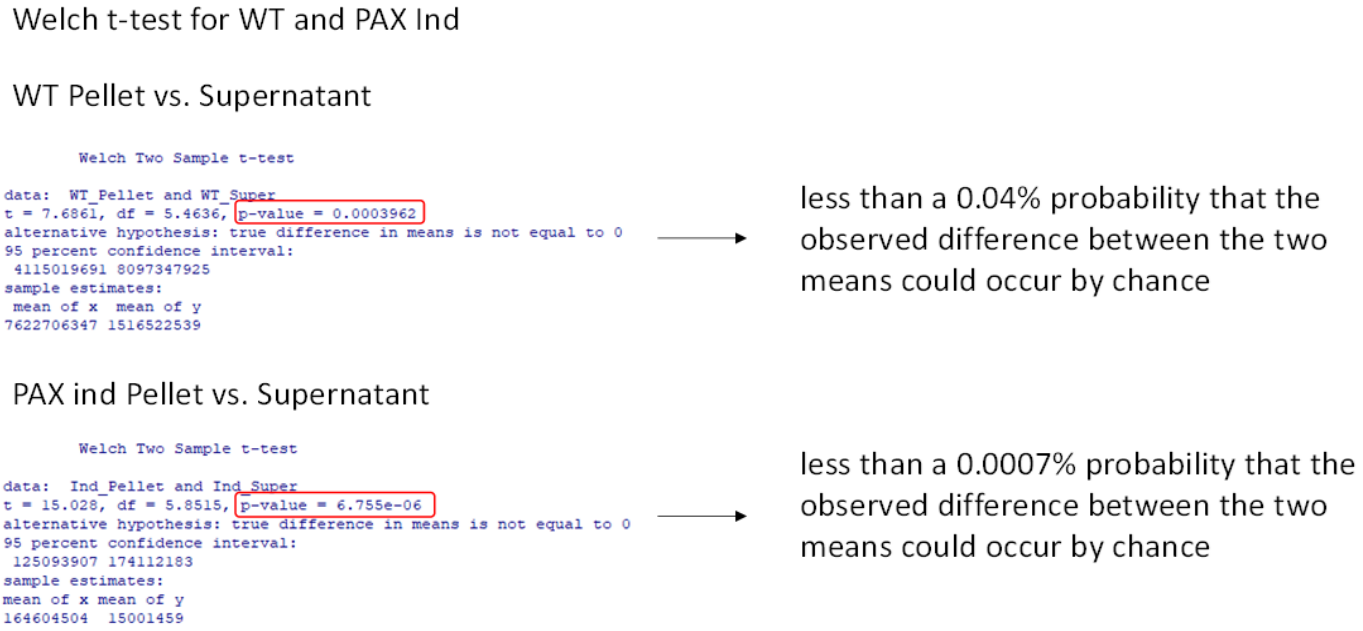

Figure 39: Statistical results for PAX quantification. R version 4.0.2 was used to compute Welch's t-test statistics of triplicate samples from *X. doucetiae* and *pax*$^{+}$ cell pellet and supernatant fractions.

PAX microscopy

This part of the experiments was accomplished in collaboration with Dr. Christoph Spahn (Prof. Dr. Mike Heilemann group).

Based on the microscopy protocol (method section 2.11 PAX localization on cells using fluorescence microscopy on page 85). *E. coli* MG1655, and the *X. doucetiae pax* mutant cultures were grown to the exponential phase and treated with the clickable PAX derivatives **32**, **36**, and **37***.* Treatment, fixation, and fluorescent labeling was performed as described.

While **32** is most similar to **38**, the fatty acid residue was difficult to access. Therefore, **36** and 3**7** had palmitic acid residues and were easier to obtain (Figure 40). **36** had an azide group and was coupled to AF647, while **37** was coupled to an azido sulfo Cy5 dye. Despite the structural differences, the microscopic results were nearly identical. Their bioactivity against strains, such as *M. luteus*, *E. coli,* or *B. subtilis* was conserved. However here, the palmitic derivatives showed increased antibiotic activity (Supporting Figure 21 and Supporting Figure 22).

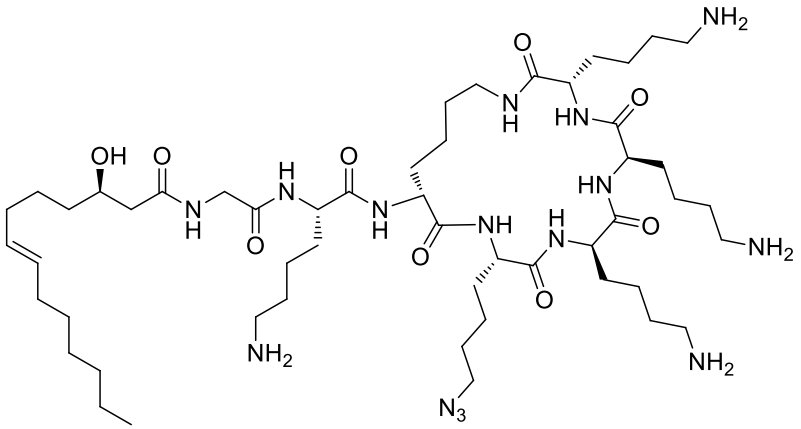

32

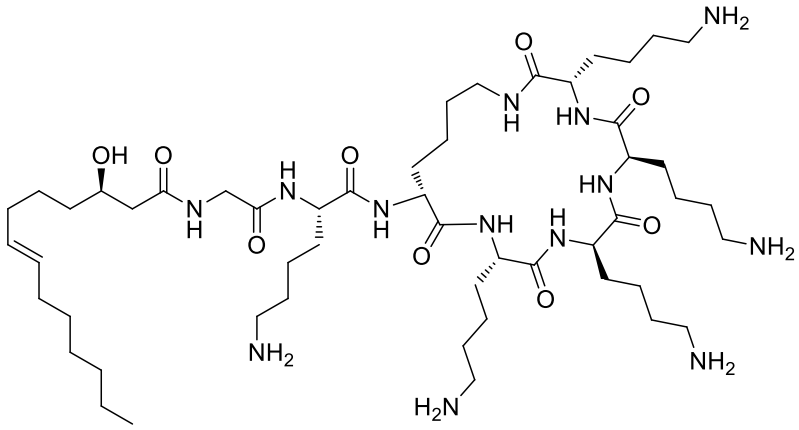

38 (natural PAX derivative)

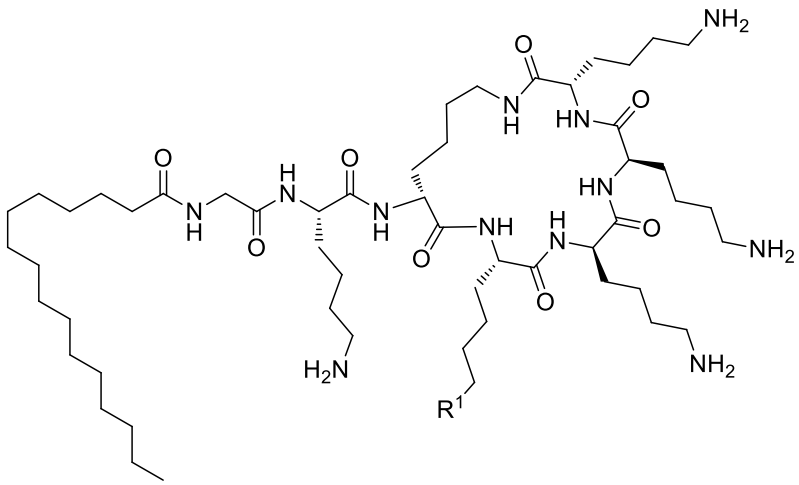

36 R^1 = 

37 R^1 = 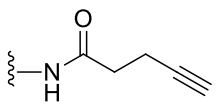

Figure 40: Structure of PAX derivatives used in microscopy experiments.

Confocal microscopy with **32**

Initially, CLSM images of fluorescently labelled *E. coli* and *X. doucetiae* cells, treated with different PAX concentrations, were acquired. The resulting images revealed that the fluorescence signals were located at the cell periphery of *Xenorhabdus* and *E. coli* cells. PAX molecules are presumably bound to the cell surface. However, the exact localization of the peptide cannot be extracted from these measurements due to the diffraction limit of light (200-300 nm spatial resolution).

However, perturbed *E. coli* cells with an intense cytosolic signal showed a 2.3-fold increase in fluorescence. Of note, confocal images of these cells already indicated an inhomogenous intracellular distribution of PAX with low-density regions being present in all perturbed cells. The signal intensity increased with increasing PAX concentration (0-100 µg/ml) for *Xenorhabdus.* But in contrast to the *E. coli* samples, no signals were found in the cytosol (Figure 41 **A**).

To investigate the concentration-dependence of PAX adsorption, the integrated fluorescence signal was quantified. This intensity per area was plotted against the PAX concentration. The results showed that the intensity was correlated with the added PAX concentration, with higher intensity found in the case of *E. coli.* Quantifying the fluorescence signal in titration experiments further revealed that PAX binding to the cell surface saturates at ~100 µg/ml (Figure 41 **C**).

As cell shrinkage was published for other treatments with LL37[138], a human cationic AMP, the average cell size was determined and plotted at different PAX concentration. The results showed that the cell size was unaffected by adding different PAX concentrations (Figure 41 **D**).

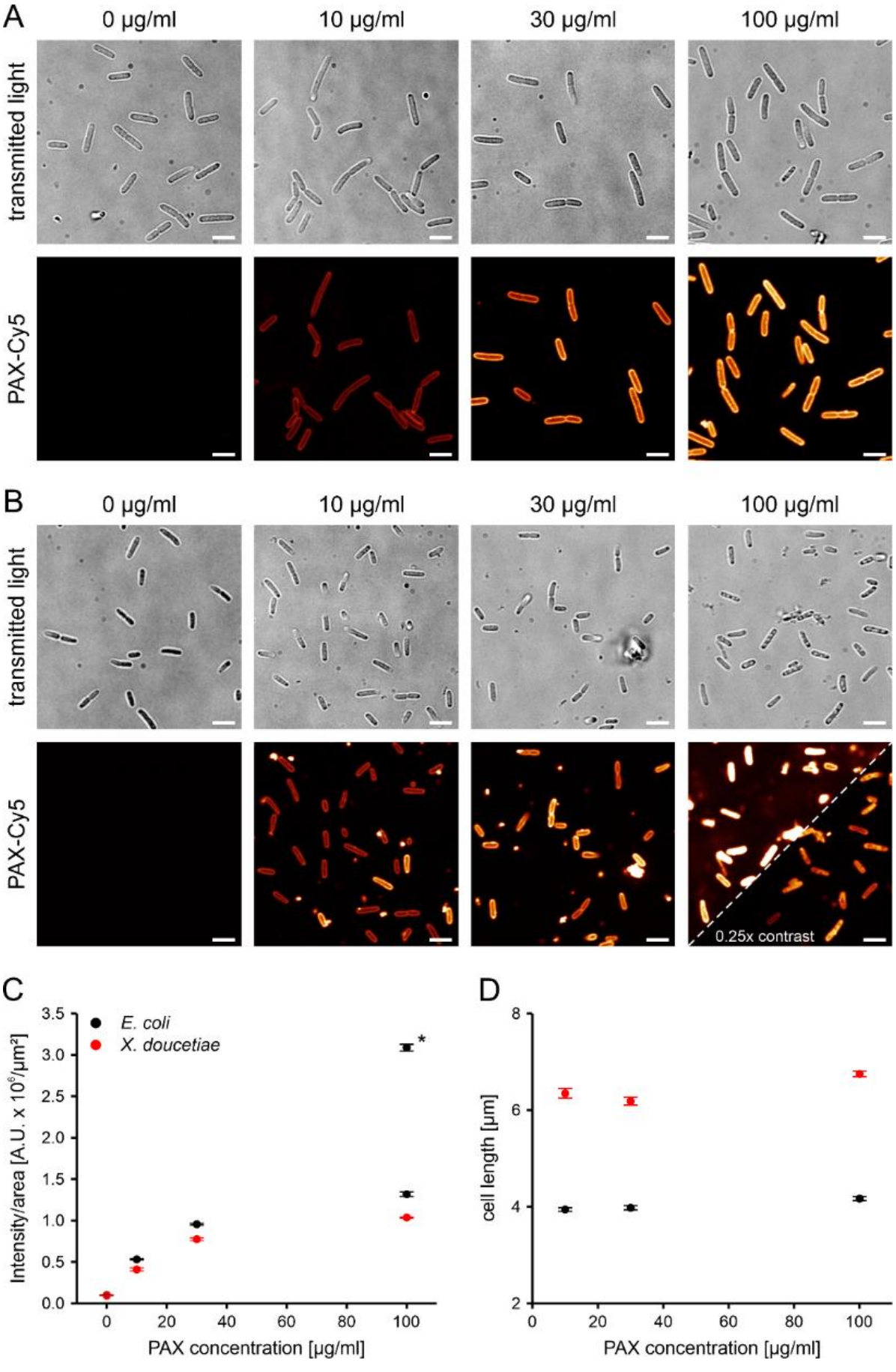
A
0 µg/ml
10 µg/ml
30 µg/ml
100 µg/ml
transmitted light
PAX-Cy5
B
0 µg/ml
10 µg/ml
30 µg/ml
100 µg/ml
transmitted light
PAX-Cy5
0.25x contrast
C
E. coli
X. doucetiae
Intensity/area [A.U. x 10⁶/µm²]
PAX concentration [µg/ml]
D
cell length [µm]
PAX concentration [µg/ml]

Figure 41: Titration of synthetic **36** to *X. doucetiae pax*$^-$ and *E. coli* cultures. **A)** Representative images of *X. doucetiae pax*$^-$ cells treated with various concentrations of **36**. **B)** Representative images *E. coli* cells treated with various concentrations of **36**. Brightness and contrast were kept identical in all PAX-Cy5 images except for *E. coli* cells treated with 100 µg/ml **36** (4-fold reduction, lower right image corner). Scale bars are 5 µm. **C) 36** (azido-PAX) binding analysis. The PAX intensity was measured for single cells and normalized to the cell cross-section area. For *E. coli* cells treated with 100 µg/ml, the dataset was split into cells with membrane-localized signals and cells with cytosolic signals (asterisk). **D)** Average cell length vs. PAX concentration. PAX treatment has no influence on the average cell length both for *E. coli* (filled black circles) and *X. doucetiae* (filled red circles).

Hereafter, control experiments with **37** (alkyne instead of azide functionality) were carried out. This derivate was clicked to AF647. Therefore, the use of different dyes and conditions should prevent the observation of microscopic artefacts[139]. During the sample preparation, the cells were permeabilized after fixation and immobilization to allow the fluorophores to penetrate the cells. As Triton-X100 is known to extract lipids and membrane proteins in non-fixed and chemically fixed specimen[140], a control experiment without permeabilization was conducted to see whether it would influence the samples. The results showed that the images were identical and therefore permeabilization did not affect the outcome (Figure 42).

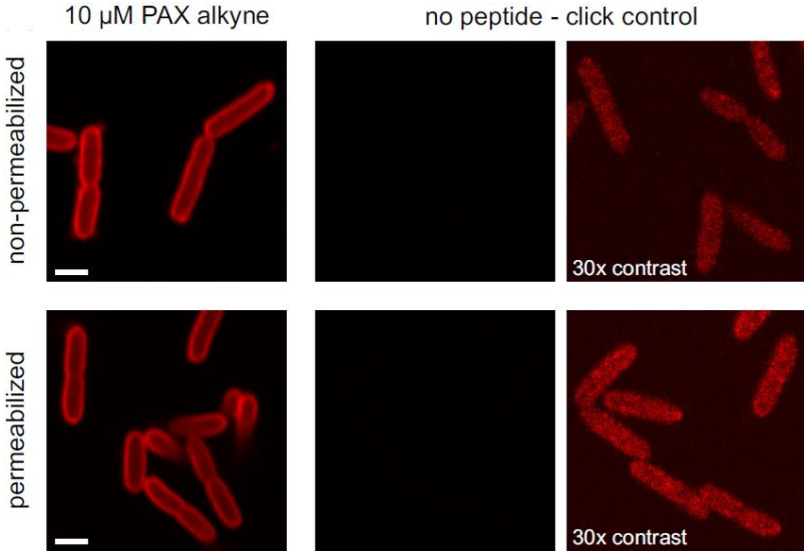

Figure 42: PAX labeling control experiment. 10 µg/ml **37** (alkyne moiety) was clicked with AF647 in permeabilized and non-permeabilized sample sets. A control group with no peptide added showed negligible signals at 30x contrast. Scale bar (2 µm).

Nanoscale localization of **32** on *Xenorhabdus pax*$^-$ cells

Next, we performed super-resolution microscopy to gain additional insights. The resolution of LSM pictures is restricted through the diffraction limit of light, ~ 200-300 nm. Furthermore, the prokaryotes cell size is usually smaller than eukaryotes therefore more difficult to gain detailed information.

The samples were prepared following the instruction (on page 85). In addition to the Cy5 dye (red), Nile red (cyan) was used as a membrane stain and JF_{503}-Hoechst (hot yellow) as a DNA stain. Normally, the nucleoid architecture is highly structured and only a small volume of the cytosol is covered by DNA. These images showed a great resemblance to *E. coli* nucleoid[132,141]. The fluorescence signals showed that the DNA structure of *Xenorhabdus* was intact in all conditions.

Furthermore, **32** signals and the membrane stain signals were at an identical location (Figure 43), indicating that both were bound to the cell surface and membrane of *Xenorhabdus*.

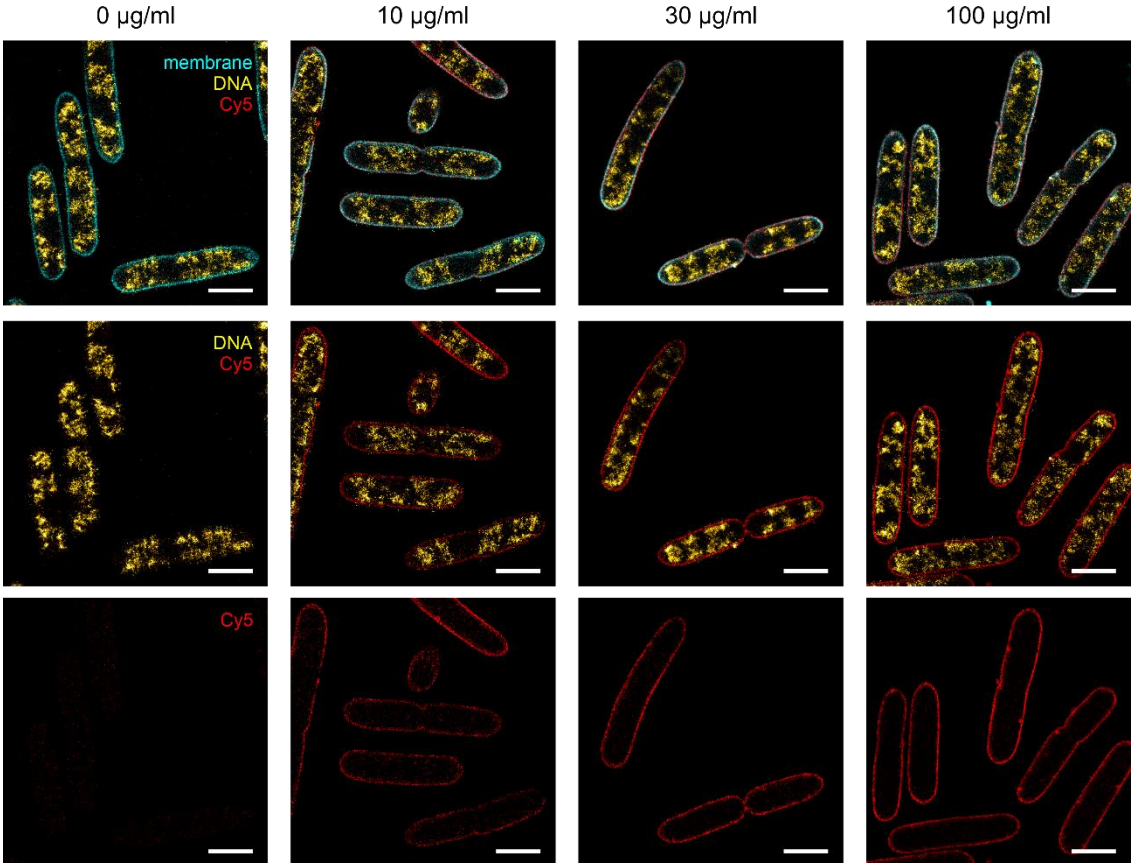

Figure 43: Localization of **32** on *X. doucetiae pax*$^{-}$ cells. **32** (click-labelled with Cy5, red) colocalizes with the bacterial membrane (labelled with Nile Red, cyan) independent on the concentration applied. No change in nucleoid morphology (labelled with JF_{503}-Hoechst, yellow hot) was observed, indicating that *X. doucetiae* cells maintain membrane integrity. Scale bars are 2 µm.

In the subsequent test, the same protocol was applied to *E. coli*. Here, **32** signals were located at the same position as the membrane stain signal. However, a larger number of cells showed cytosolic **32** signals with increasing peptide concentration. In this case, the **32** signal covered the cytosolic area while omitting certain areas. Overlaying the DNA stain with the PAX-Cy5 signal revealed that these areas were covered by deformed DNA. Reorganization of the nucleoid structure was occurring concomitantly when PAX enters the cell (Figure 44). However, as cell fixation does not allow to access the dynamics of PAX action, it remains unclear whether this is a direct effect of PAX or a consequence of the disruption of the cell integrity and will be discussed later.

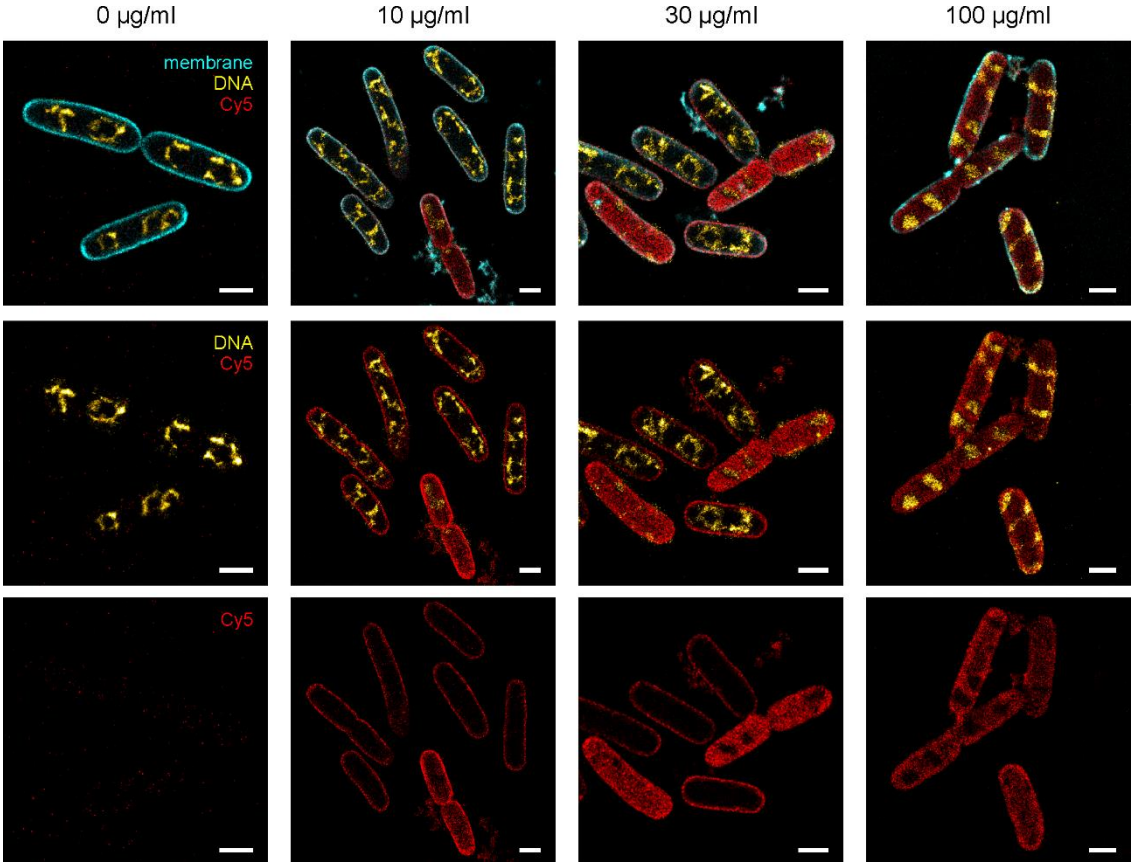

Figure 44: Localization of synthetic azido-PAX on *E. coli* cells. **32** (click-labelled with Cy5, red) mainly colocalises with the bacterial membrane (labelled with Nile Red, cyan) at 10 and 30 µg/ml PAX concentration. A fraction of cells shows the strong PAX signal in the cytosol, only omitting regions where chromosomal DNA (labelled with JF_{503}-Hoechst, yellow hot) is localised. Flooding of the cytosol by PAX is accompanied by a strong reorganisation of the nucleoid. Scale bars are 1 µm.

The results are in line with the previous findings in the LSM pictures showing that PAX molecules were bound to the surface of Gram-negative bacteria. Furthermore, it revealed the mode of action of PAX as AMP. Note here, at 100 µg/ml PAX penetrated most cells. These results are in line with our bioactivity results (MIC over 37.5 µg/ml for **32**).

The influence of the palmitic acid residues on PAX nanoscale localization and antimicrobial activity

Based on the initial results with **32,** two new PAX peptides **36** (azide moiety) and **37** (alkyne moiety) with palmitic acid were synthesized utilizing the standard synthesis protocol (method section 2.11). PAX molecules are expected to bind to the negatively charged cell surface like other AMPs. In the second step, the lipophilic fatty acid of PAX might interact with the membrane and therefore destabilize the structure. Here bioactivity tests have revealed that the two derivatives with palmitic acid residues were more potent. The longer saturated fatty acid might improve lipophilic interaction between PAX and membrane lipids.

High-resolution microscopy experiments were carried out with these new derivatives to elucidate the pathogenic mechanism towards *E. coli*.

The negative control (0 µg/ml PAX) shows negligible unspecific binding and common nucleoid/membrane distributions are observed for both PAX derivatives. At 10 µg/ml PAX, two populations are observed: cells with the only membrane-bound PAX and compromised cells with a strong intracellular PAX signal. Here, the compound **36** shows a higher number of compromised cells, indicating a higher potency as compound **37**. At 100 µg/ml most cells were compromised and additionally show large membrane budding. Higher dye concentrations had to be used for higher PAX concentrations, probably since PAX peptides rigidify the cytosol, thus impairing intracellular diffusion of the used fluorescence labels. For all PAX concentrations and both derivatives, chromosomal DNA is reorganized, appearing less structured and populating PAX-free regions (Figure 45).

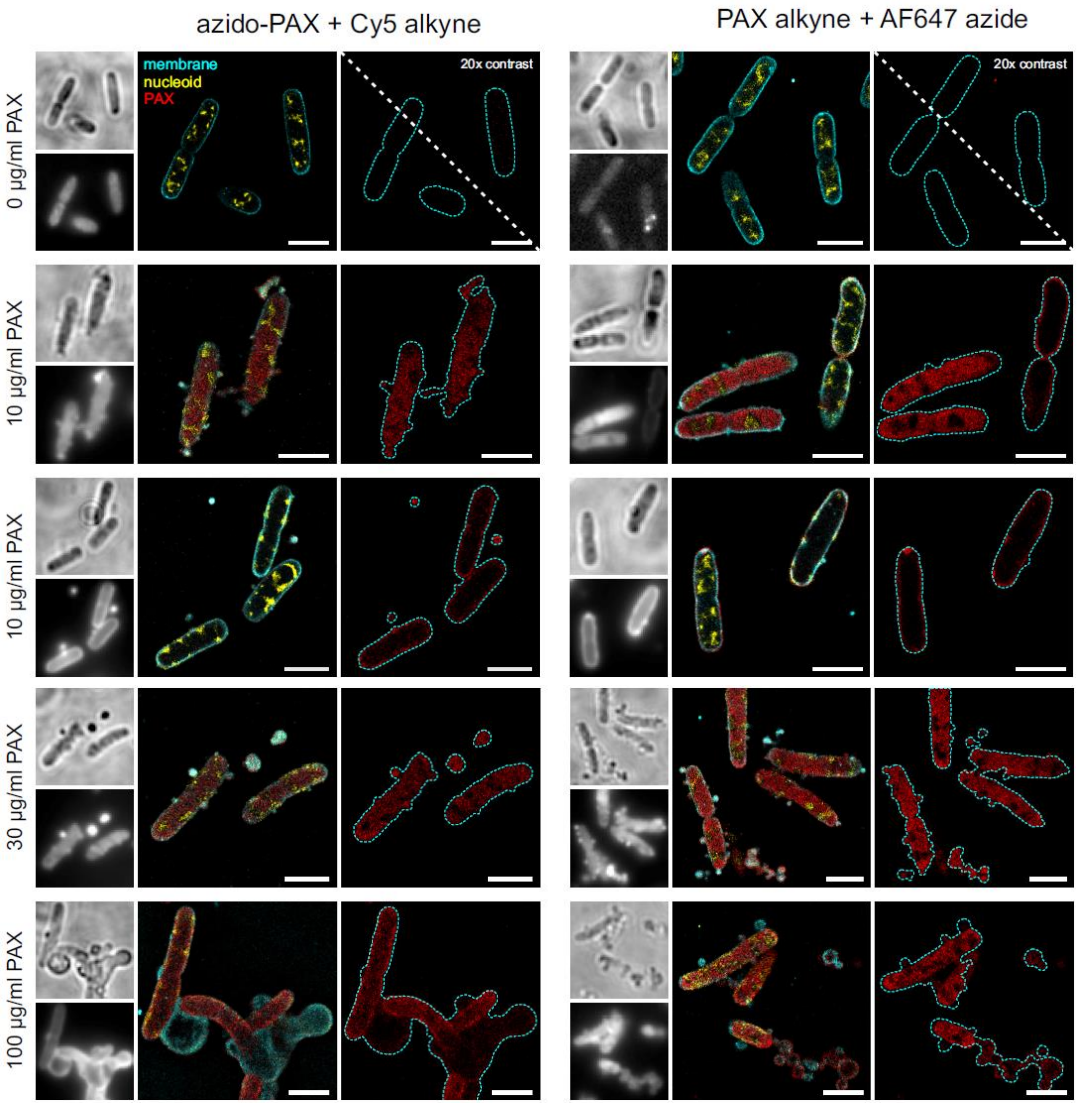

Figure 45: dStorm imaging of new PAX derivatives **36** (azide moiety) and **37** (alkyne moiety) with *E. coli*. Bright light and diffraction-limited Cy5/AF647 wide-field images are shown for comparison. At 100 µg/ml most cells were destroyed by the new PAX derivative. Scale bars are 2 µm.

Influence of PAX exposure time on PAX distribution and cellular organization

Finally, it was important to understand the dynamic of the process. Therefore, experiments were carried out in multiple time frames. The results showed, that **37** was able to penetrate certain *E. coli* cells at 10 µg/ml after 11 min. There were no significant differences between the three selected time points. All conditions were measured via confocal laser scanning microscopy using the same settings for each sample (Figure 46).

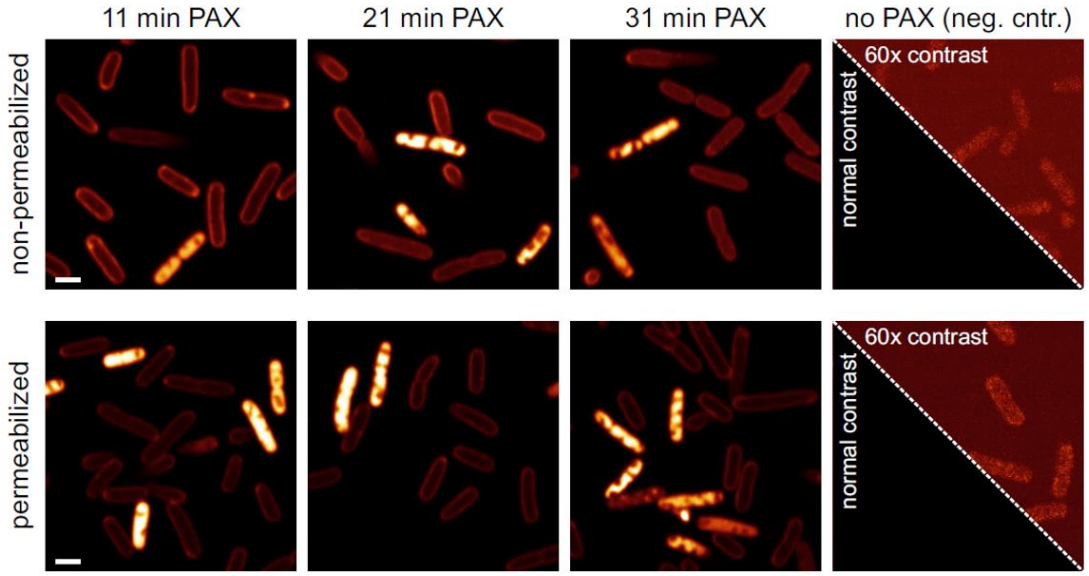

Figure 46: Time series experiment with *E. coli.* Scale bars are 2 µm.

Hereafter, the cells were measured using high-resolution microscopy methods. *E. coli* was incubated with 10 µg/ml of the **37** derivative for 11, 21, or 31 min, respectively (Figure 47). No significant time-dependent differences were observed and the results are in line with the previously shown LSM and high-resolution pictures. The synthetic PAX peptide colocalizes with the cell membrane of intact cells. Note here, Potomac gold was used instead of Nile red as membrane stains for control. Both stains showed consistent colocalization with the labelled PAX peptides signals. **37** enters cells that were permeabilized/killed due to the antimicrobial activity of PAX (red arrows), leading to staining of the entire cytosol. No significant changes were observed with incubation time. The majority of cells

showed continuous labelled PAX peptide signals along the membrane, while killed cells exhibit strong cytosolic signals.

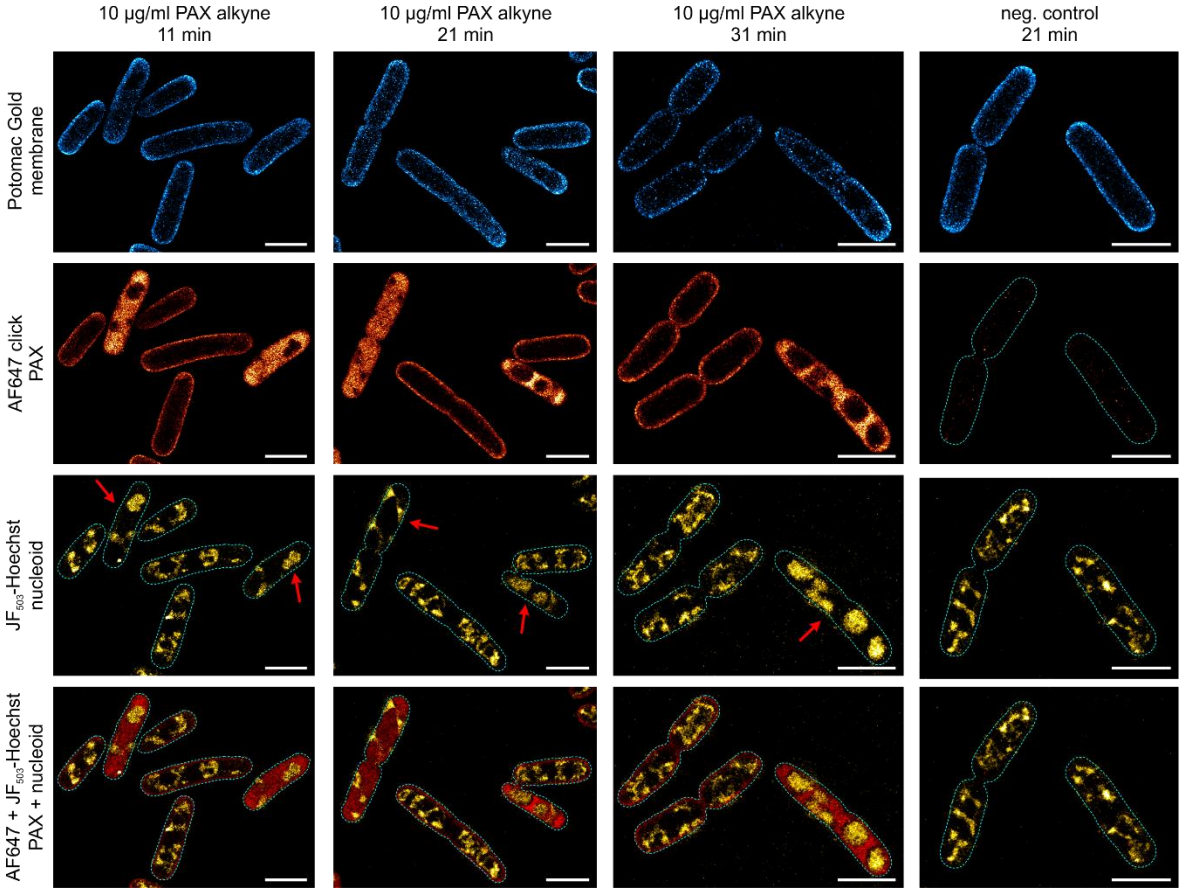

Figure 47: *E. coli* dStorm time series data. 10 µg/ml **37** was clicked with AF647 (red), Potomac gold (blue), and JF-503 Hoechst (yellow). Red arrows indicate the deformed DNA structure, which is surrounded by AF647 signals. Scale bars are 2 µm.

Bioactivity tests

As our findings suggest, PAX peptides are located at the membrane of *X. doucetiae*. We hypothesize that cells with a surface-exposed PAX coat might be able to repulse insect AMPs by modifying the surface charge. If this was the case, the promotor exchange *pax*$^-$ mutant should be more susceptible to AMPs due to lacking PAX production, while the induced *pax*$^+$ mutant produces PAX forming a coat that leads to AMP repulsion and cell survival.

The bioactivity tests were carried out based on the protocol described in section 2.11. *X. doucetiae* WT, *pax*$^+$, and *pax*$^-$ mutant was tested against cecropin, drosocin, and melittin. Cell growth reduction was observed in *X. doucetiae* strains treated with insect AMP in a concentration-dependent manner. Growth of *pax*$^-$ cultures, which do not produce **39** and **40** were delayed or completely abolished compared to the wildtype strain, indicating a higher susceptibility towards cationic insect AMPs (Figure 49). Importantly, this susceptibility could be reversed when inducing PAX expression in the mutant strain using 0.2% arabinose. The growth curves observed for these *pax*$^+$ cultures differed only slightly from *X. doucetiae* wild type cultures.

Growth delay of the cultures was measured by extracting the time points, where cultures entered the exponential growth (OD_{600} = 0.2). The resulting plot confirmed the observations that PAX production protects *X. doucetiae* cells from cationic insect AMPs.

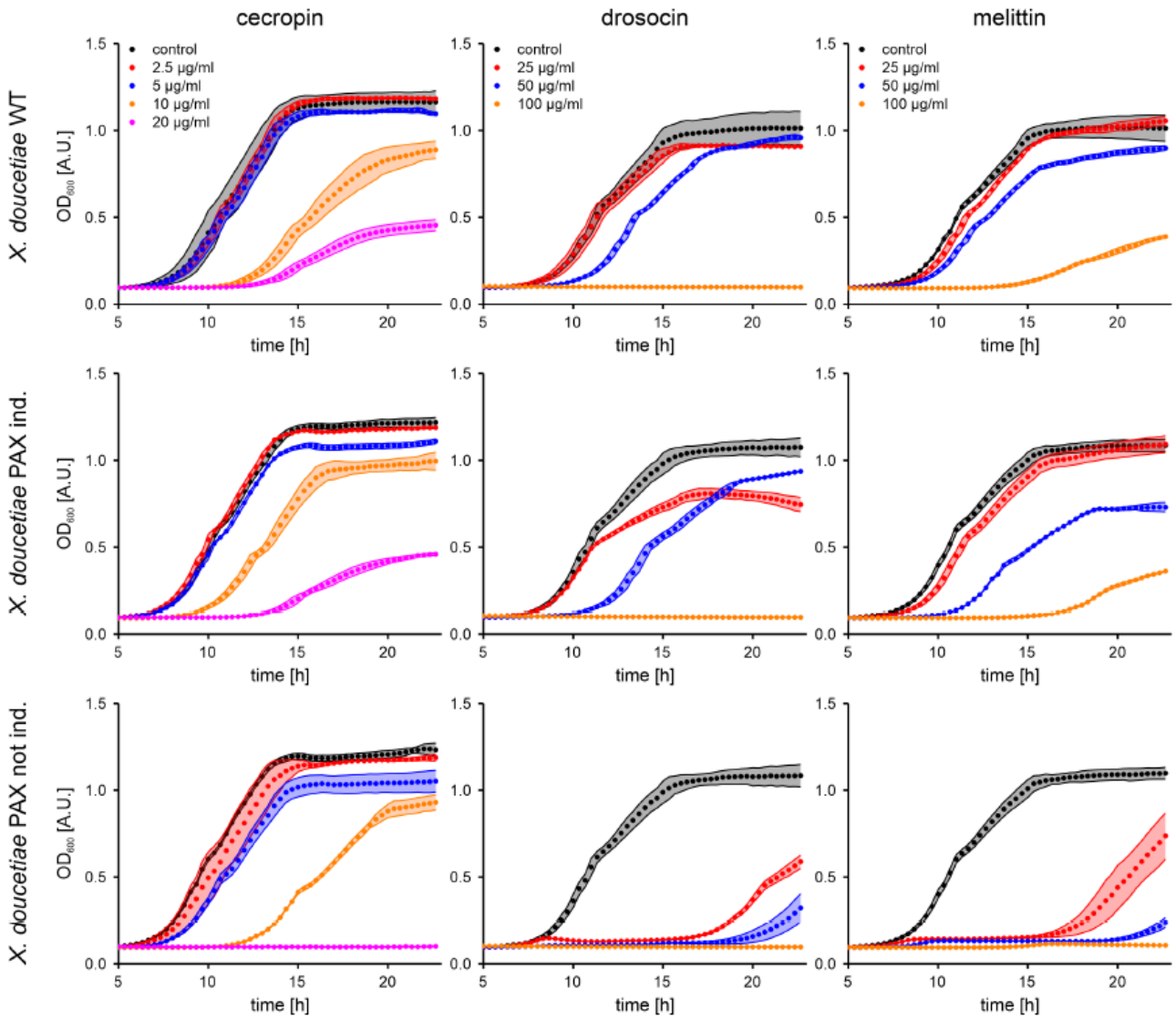

Figure 48: Bioactivity tests of *Xenorhabdus* with cecropin, drosocin, and melittin. *X. doucetiae* WT, *X. doucetiae pax*$^{+}$ and *X. doucetiae pax*$^{-}$ was incubated with cecropin, drosocin, and melittin at different concentrations. Pax^{-} strains were not growing and showed a delayed growth rate in comparison to pax^{+} and WT.

Furthermore, an additional analysis was added. The measured growth time of each strain to reach an optical density (OD) of 0.2 was plotted against the insect AMP concentration. While WT and *pax*$^{+}$ have a similar growth rate. The *pax*$^{-}$ strain is growing at a slower pace and in some case *pax*$^{-}$ does not reach OD 0.2 under higher insect AMP concentration Figure 49.

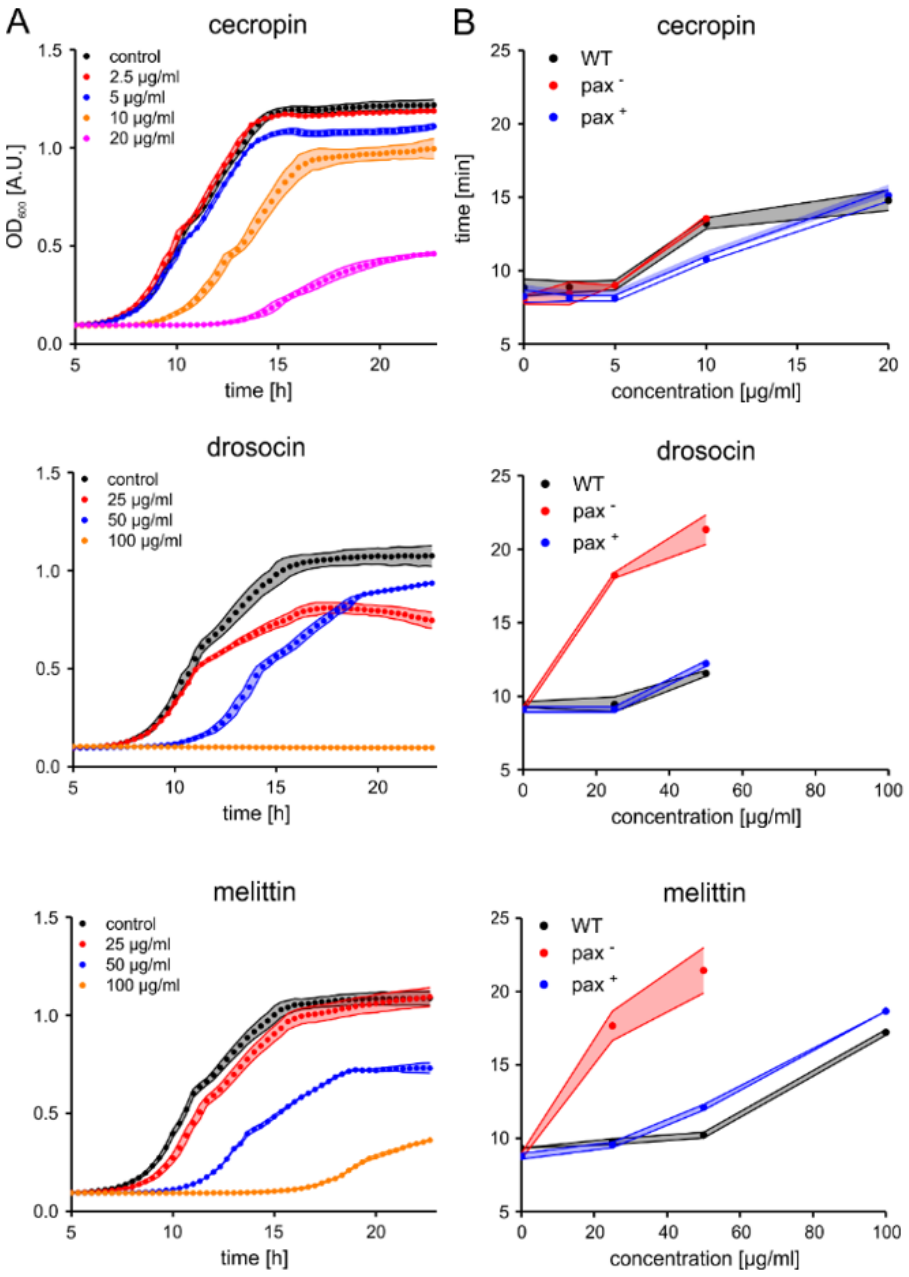

Figure 49: Growth inhibition and growth checkpoint analysis of *Xenorhabdus* with different insect AMPs. **a)** Growth inhibition assay of *X. doucetiae pax*$^{+}$ cultures. **b)** The time to reach OD 0.2 for all three strains was plotted against the inserted insect AMP concentration. Lacking data points (e.g. t = 100 min for drosocin treatment) indicate that cultures did not reach this value over the entire experiment time of 25 h. Data points represent mean values and shaded areas of the respective standard deviation.

E. coli results

To test whether this protective effect of PAX can be transferred to other bacterial species, we treated *E. coli* overnight cultures both with sublethal doses of PAX and insect AMPs at various concentrations. We observed that growth in the absence of PAX was inhibited at lower AMP concentration compared to *X. doucetiae* WT and *pax*$^{+}$ cultures, indicating that *X. doucetiae* indeed has a higher tolerance for cationic AMPs. MICs for cecropin, melittin, and drosocin were reported as 4-32 µg/ml, 4-32 µg/ml, and 25 µg/ml, respectively[142–144], which is in agreement with the inhibitory effects on culture growth observed in our experiments. Intriguingly, we could observe a protective effect of PAX on the growth of *E. coli* cultures in combinatorial treatments with insect AMPs. It is important to note that this effect is not as prominent as for *X. doucetiae* cultures, which can be attributed to the fact that PAX itself acts as an AMP against *E. coli*. Further, we want to stress that the protective effect of PAX can only form as its MIC is lower compared to the insect AMPs used in this study. Under this circumstance, integration of PAX into the membrane presumably leads to the repulsion of the insect AMPs as observed for *X. doucetiae* while at the same time not (or to a smaller extent) compromising the *E. coli* membrane by itself.

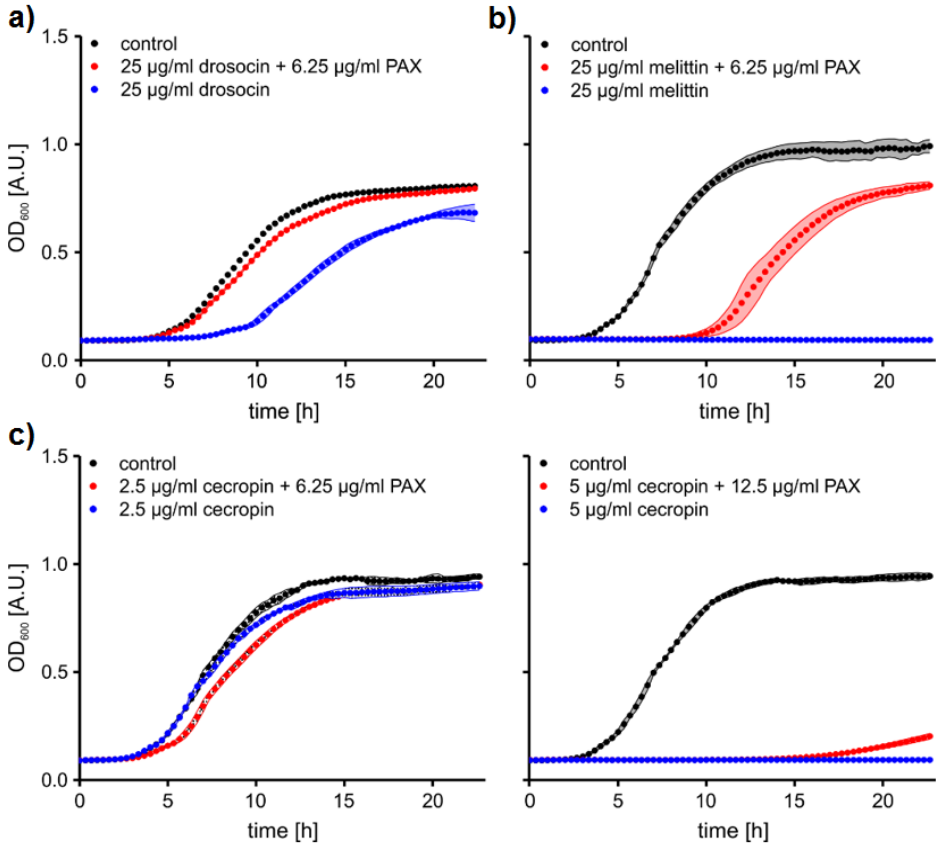

Figure 50: Growth inhibition assay of *E. coli* cultures treated with different insect AMPs (cecropin, melittin, and drosocin). *E. coli* cultures were grown absence (control, black dots, and shaded areas) and presence of **a)** drosocin, **b)** melittin and **c)** cecropin alone (blue dots and shaded areas) or together with natural PAX (**38**, red dots and shaded areas). Since 2.5 µg/ml cecropin showed no antimicrobial effect, the experiment was repeated with a higher cecropin and PAX concentrations. Data points represent mean values and shaded areas of the respective standard deviation.

3.7 Induction and proteome analysis of *X. nematophila*, *X. szentirmaii* and *P. luminescens*

Analysis

The MaxQuant workflow was able to identify 1829 proteins from all samples of in total 4354 theoretical proteins (41.73%) in *X. szentirmaii*.

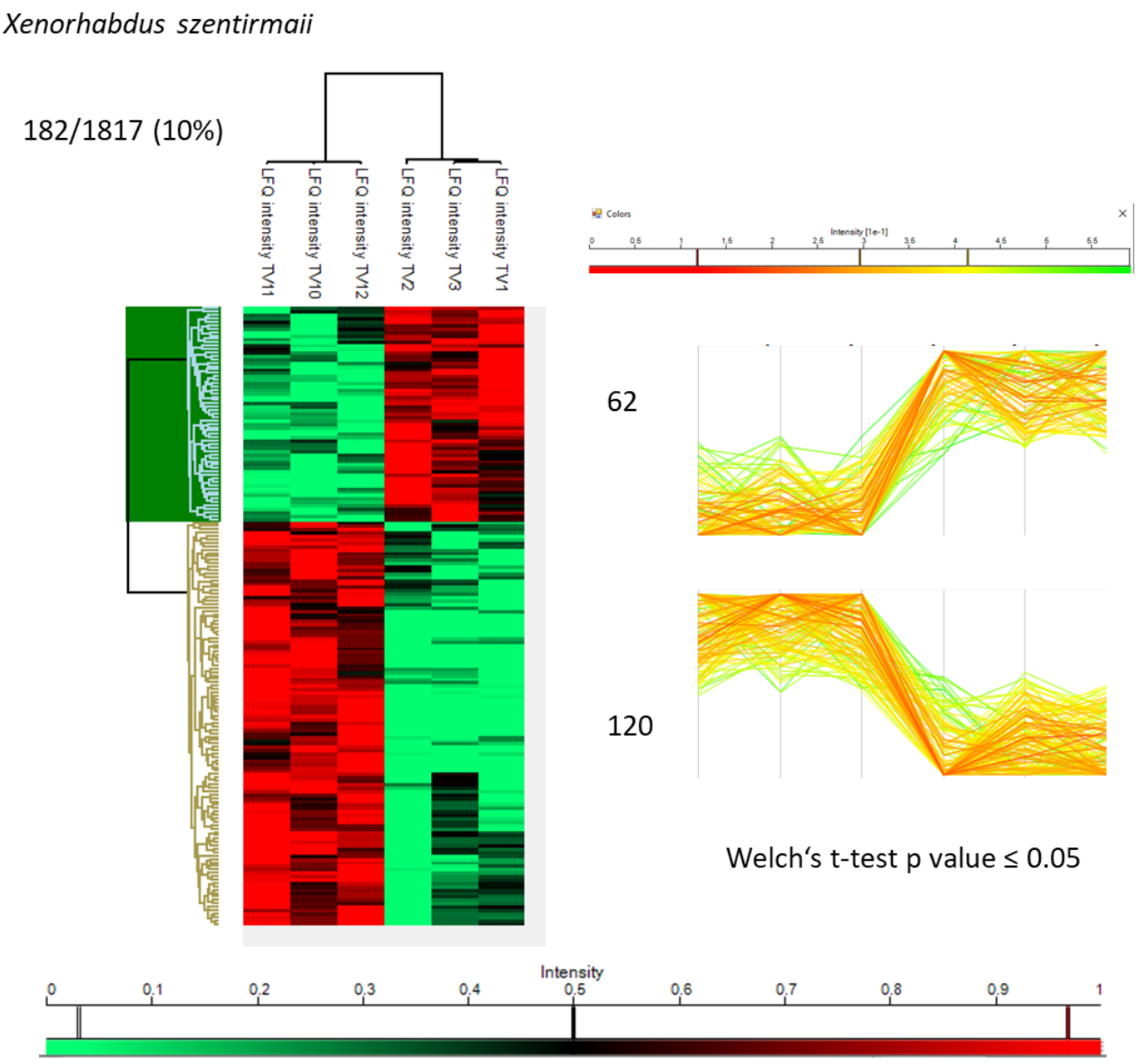

Figure 51: MaxQuant results *for* X. szentirmaii. Visualization of the MaxQuant output using Perseus hierarchical clustering: Samples of triplicates were analyzed, and the protein intensity were plotted using the MaxQuant Label-free quantification algorithm. 182 proteins were selected based on the Welch's t-test p ≤ 0.05.

The number of the theoretical proteins was obtained using a sequenced genome from the three strains generating a hypothetical proteome set (provided by Dr. Nicholas Tobias, Goethe University Frankfurt).

First of all, there are two important observations. The induced and not-induced samples varied significantly from each other. Secondly, the triplicates could be reassigned into the two groups using hierarchal clustering showing the high similarity between the biological triplicates.

To determine the number of up- and downregulated proteins, a Welch's t-test was performed as a statistical analysis with a cutoff at p-value ≤ 0.05. In addition, by using Perseus's hierarchical clustering it was possible to see, that two clusters of induced (left) and not-induced (right) could be obtained (Figure 53). This is in line with our expected results from two sample sets of triplicates with the induced and non-induced experimental setup. Therefore, 182 proteins (10%) were considered to vary significantly between induced and non-induced samples. 62 of them were upregulated, while 120 were downregulated.

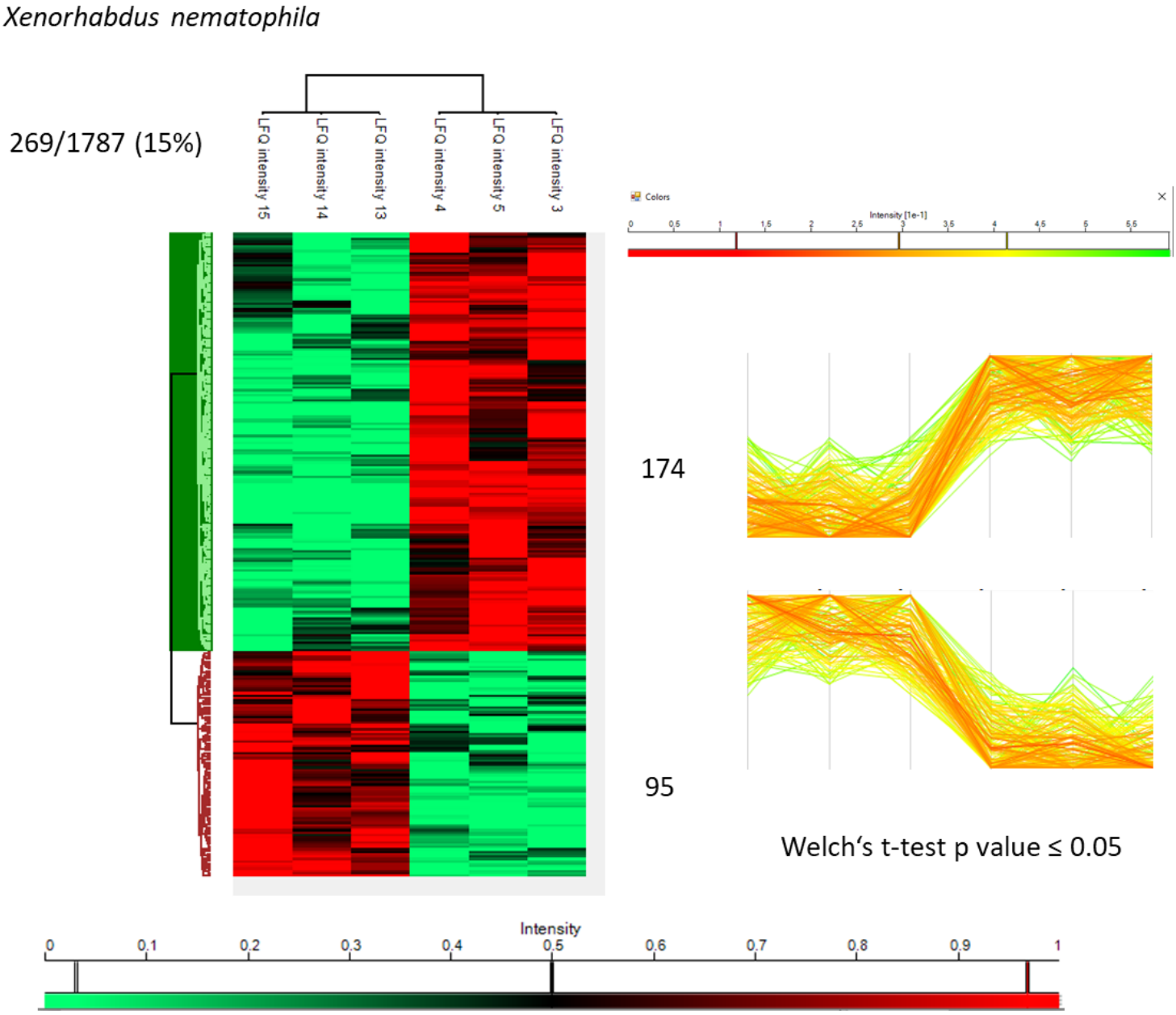

Figure 52: Perseus hierarchical clustering for the data set of *X. nematophila.* (For details see Figure 51).

For *X. nematophila,* 1787/3666 (49%) proteins were identified using the same workflow. Here, 269 proteins (15%) were identified by applying the Welch's t-test (cut-off at $p \leq 0.05$) to differentiate significantly between the not induced and induced samples. 174 proteins were upregulated while 95 proteins were downregulated.

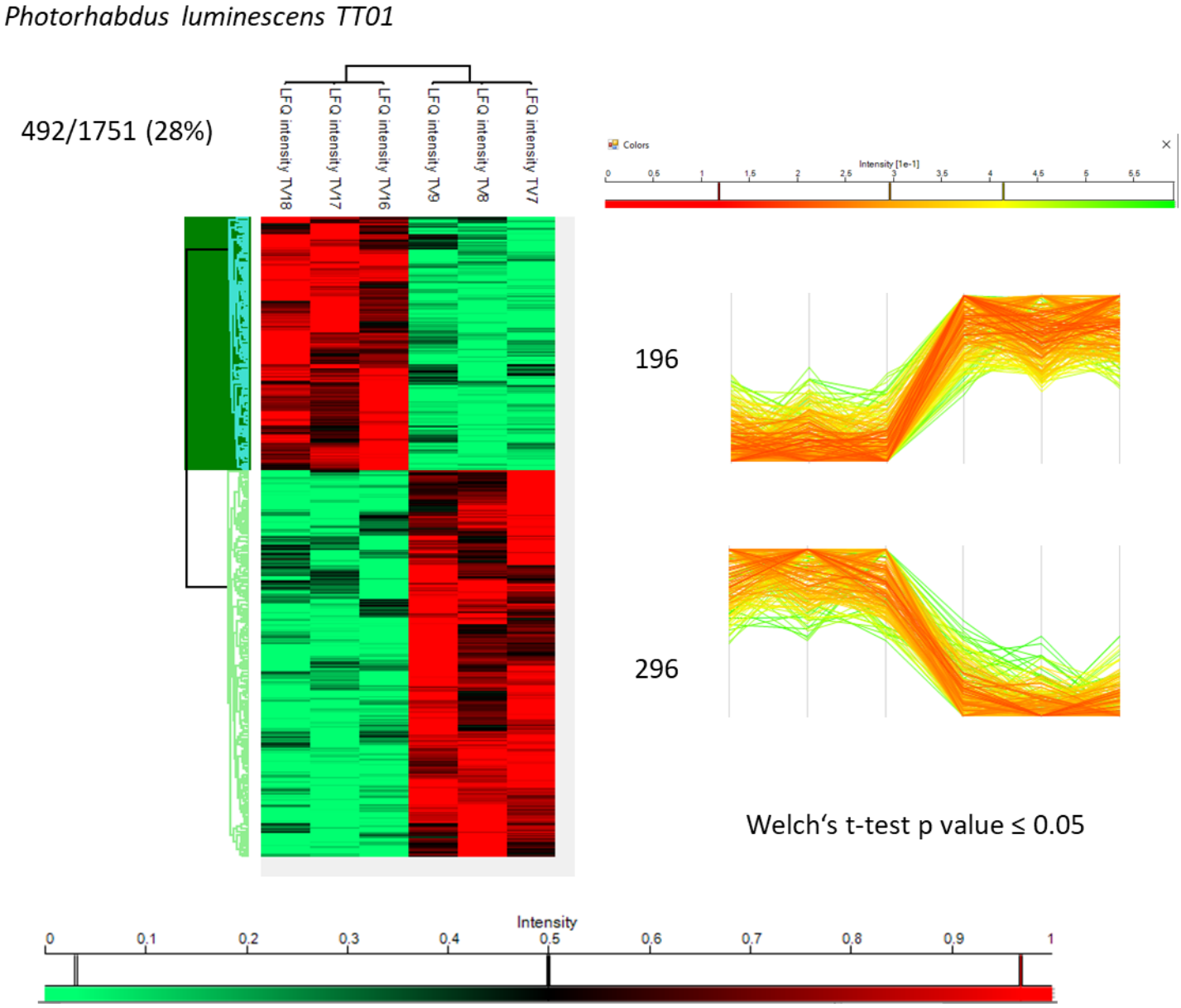

Figure 53: Perseus hierarchical clustering for the data set of *P. luminescens*. (For details see Figure 51).

In *P. luminescens* TT01 1751/4542 (39%) proteins were identified by the algorithm. 492 (26%) of the proteins were affected significantly (Welch's t-test p ≤ 0.05) by the induction with galleria broth. 296 were upregulated and 196 were downregulated.

Using the MaxQuant workflow, it was possible to identify around 39-49% of the overall theoretical proteome of these organisms. Here, in silico peptides were first

generated using fasta files, containing the proteome sets of the organisms *X. szentirmaii*, *P. luminescens,* and *X. nematophila*.

Normally, a student's t-test is used as statistical tools to compare the mean value between sample sets. However, this test assumes, that the error distribution is identical for both sets. This is not observed for MS signal intensity; the variance is different depending on each peptide. Therefore, Welch's t-test ($p \leq 0.05$) was used for statistical analysis. After the applied workflow, around 10-28% of these proteins were found either significantly up- or downregulated after induction with insect lysate.

The results of the quantification of *X. szentirmaii*, *X. nematophila,* and *P. luminescens* can be found in section 5 Supporting information. Supporting table 2, 3, and 4 includes proteins which are either ≥ 2-fold up- or downregulated (Welch's t-test $p \leq 0.05$).

Furthermore, additional results can be found on a CD containing the excel files x_szentirmaii_LFQ.xlsx, x_nematophila_LFQ.xlsx, and p_luminescens_TT01_LFQ.xlsx. Here, quantification results from the three strains are provided excluding proteins with a statistical cut off of $p > 0.05$ (Welch's t-test).

KEGG visualization

The results were mapped to the Kyoto Encyclopedia of Genes and Genomes (KEGG) database to identify the activated pathways. (BlastKOALA) Therefore, fasta files containing identified proteins were uploaded. With the help of these tools, it was possible to annotate around 70% of the entries. Furthermore, the number of selected proteins was reduced by analyzing only entries, which were at least 2-fold up or down-regulated. Finally, the numbers of proteins fitting for the criteria were reduced to 76, 84 and 332 proteins (Figure 54) from the initial 182 proteins for *X. szentirmaii*, 269 proteins for *X. nematophila* and 492 proteins for *P. luminescens*, respectively. Around 70% of the proteins were annotated by the database.

Table 10: KEGG-Annotation from www.kegg.jp using BlastKOALA[145]

p ≤ 0.05 (Welch's t-test)	***X. szentirmaii***	***X. nematophila***	***P. luminescens* TTO1**
>2 fold up	41/64 entries (64.1% annotated)	31/36 entries (86.1% annotated)	60/116 entries (51.7% annotated)
>2 fold down	10/12 entries (83.3% annotated)	32/48 entries (66.7% annotated)	143/216 entries (66.2% annotated)
overall	1299/1829 entries (71% annotated)	1335/1782 entries (71% annotated)	1188/1729 entries (68.7% annotated)

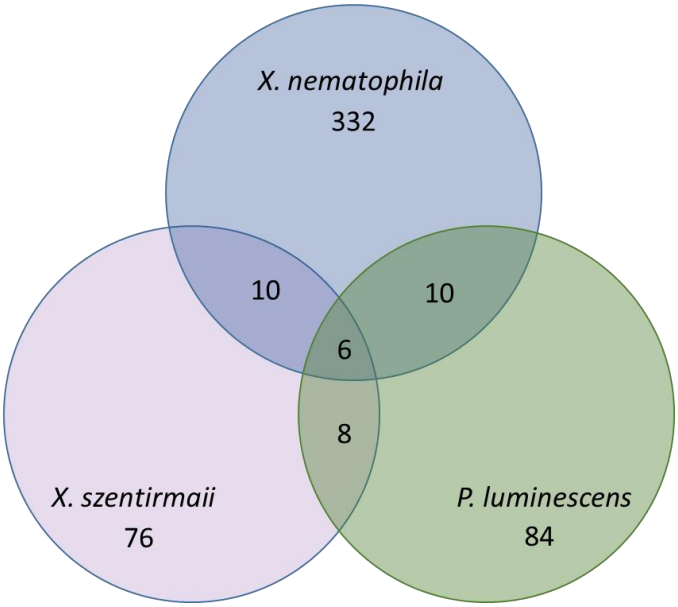

Figure 54: Venn diagram of common proteins in all three strains including two-fold up- and downregulated species (p ≤ 0.05 Welch's t-test).

Table 11: Overlap between the three strains *X. nematophila*, *X. szentirmaii,* and *P. luminescens*. These proteins were at least two-folds upregulated and preselected by applying the Welch's t-test ($p \leq 0.05$).

X. nematophila	**x-fold change**	***X. szentirmaii***	**x-fold change**	***P. luminescens***	**x-fold change**	**KEGG orthology**	**Name**
WP_010846618.1	15	*Xszus_01852*	256	*WP_011145519.1*	74	K06445	FadE; acyl-CoA dehydrogenase [EC:1.3.99.-]
WP_013184888.1	3	*Xszus_00316*	4	*WP_011147407.1*	8	K01782	FadJ; 3-hydroxyacyl-CoA dehydrogenase / enoyl-CoA hydratase / 3-hydroxybutyryl-CoA epimerase [EC:1.1.1.35; 4.2.1.17; 5.1.2.3]
WP_041573727.1	3	*Xszus_03802*	8	*WP_011148493.1*	5	K00632	FadA; acetyl-CoA acyltransferase [EC:2.3.1.16]
		Xszus_00315	4	*WP_011147408.1*	4	K00632	FadA; acetyl-CoA acyltransferase [EC:2.3.1.16]
WP_013185341.1	3	*Xszus_03803*	5	*WP_011148492.1*	5	K01825	FadB; 3-hydroxyacyl-CoA dehydrogenase / enoyl-CoA hydratase / 3-hydroxybutyryl-CoA epimerase / enoyl-CoA isomerase [EC:1.1.1.35; 4.2.1.17; 5.1.2.3; 5.3.3.8]
WP_013183065.1	2	*Xszus_03363*	13E6	*WP_011147977.1*	11	K16087	TC.FEV.OM3; hemoglobin/transferrin /lactoferrin receptor protein
WP_010848783.1	2	*Xszus_03726*	31	*WP_011148485.1*	7	K01637	isocitrate lyase [EC:4.1.3.1]

Table 12: Overlap between the two strains *X. szentirmaii* and *X. nematophila* (excluding the entries from Table 11). These proteins were at least two-folds upregulated and preselected by applying the Welch's t-test ($p \leq 0.05$).

X. szentirmaii	**x-fold change**	***X. nematophila***	**x-fold change**	**KEGG orthology**	**Name**
Xszus_03725	6E7	*WP_038219458.1*	2	K01638	AceB; malate synthase [EC:2.3.3.9]
Xszus_02769	5	*WP_010847478.1*	5	K02892	RP-L23; large subunit ribosomal protein L23

Table 13: Overlap between the two strains *P. luminescens* and *X. szentirmaii* (excluding the entries from Table 11). These proteins were at least two-folds upregulated and preselected by applying the Welch's t-test ($p \leq 0.05$).

P. luminescens	**x-fold change**	***X. szentirmaii***	**x-fold change**	**KEGG orthology**	**Name**
WP_011148122.1	3	*Xszus_03497*	17	K00219	FadH; 2,4-dienoyl-CoA reductase (NADPH2) [EC:1.3.1.34]
WP_011147948.1	3	*Xszus_02143*	5E7	K01588	PurE; 5-(carboxyamino)imidazole ribonucleotide mutase [EC:5.4.99.18]

Table 14: Overlap between the two strains *X. nematophila* and *X. szentirmaii*. These proteins were at least two-folds downregulated and preselected by applying the Welch's t-test ($p \leq 0.05$).

X. szentirmaii	**x-fold change**	***X. nematophila***	**x-fold change**	**KEGG orthology**	**Name**
Xszus_00604	2	*WP_013184257.1*	3	K12686	ApeE; outer membrane lipase/esterase
Xszus_01758	3	*WP_010846889.1*	2	K03704	CspA; cold shock protein
Xszus_01437	1E9			K03704	CspA; cold shock protein

Table 15: Overlap between the two strains *X. nematophila* and *P. luminescens*. These proteins were at least two-folds downregulated and preselected by applying the Welch's t-test ($p \leq 0.05$).

X. nematophila	**x-fold change**	***P. luminescens***	**x-fold change**	**KEGG orthology**	**Name**
WP_013185657.1	3	*WP_011144619.1*	3	K02030	ABC.PA.S; polar amino acid transport system substrate-binding protein
WP_013184782.1	4E7	*WP_049789755.1*	7	K01586	LysA; diaminopimelate decarboxylase [EC:4.1.1.20]
WP_010846688.1	7E7	*WP_011147051.1*	3	K09458	FabF; 3-oxoacyl-[acyl-carrier-protein] synthase II [EC:2.3.1.179]
WP_010848038.1	2E8	*WP_011146572.1*	6E7	K00232	acyl-CoA oxidase [EC:1.3.3.6]

X. szentirmaii

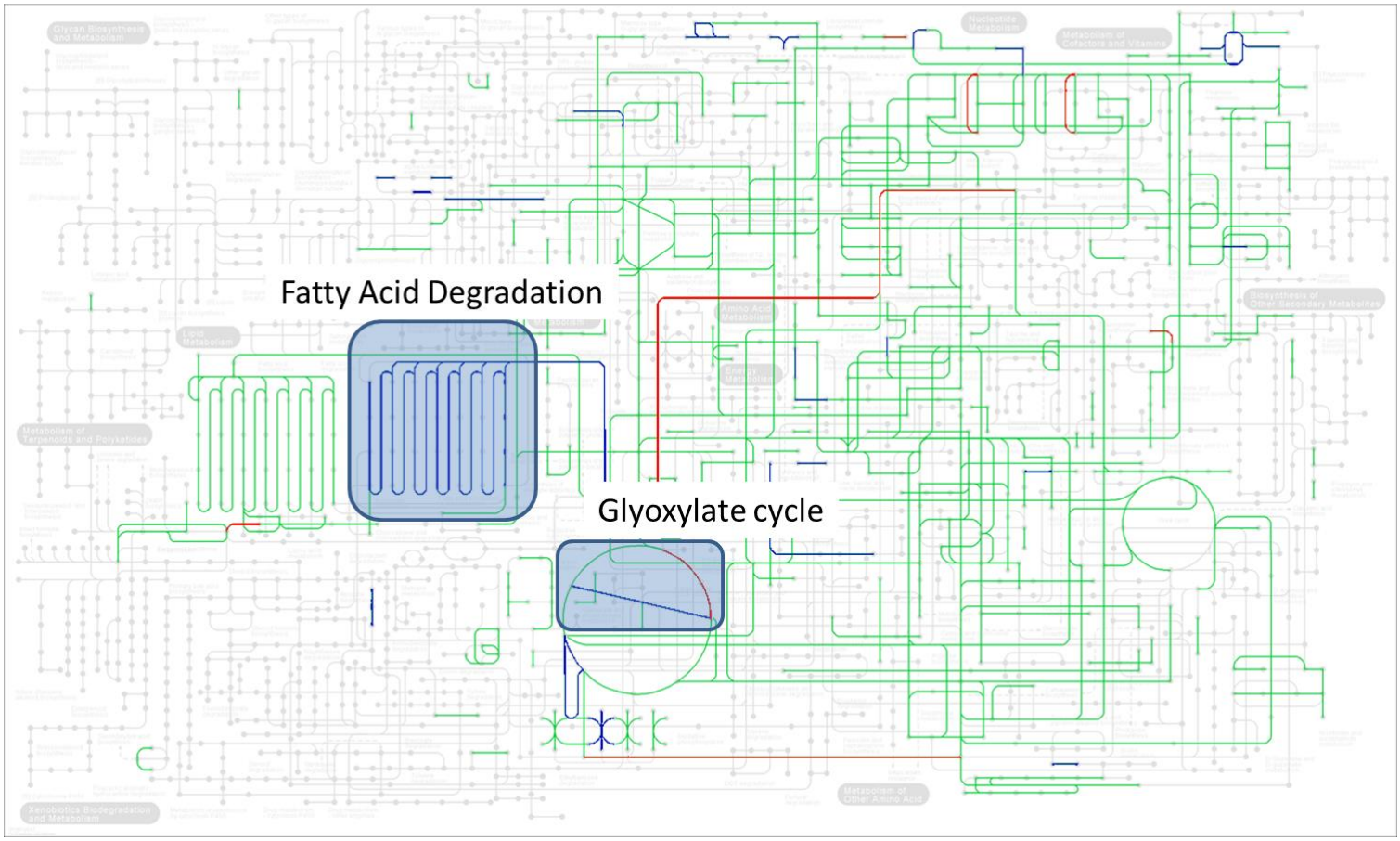

Figure 55: Overview of proteins in *X. szentirmaii*; proteins found (green), upregulated (blue), downregulated (red).

In the next step, these proteins groups were uploaded separately to KEGG. The database was able to map the entries into the reference pathways. The approach produced a map with different metabolic pathways. The identified proteins were mapped in green, while the upregulated proteins were mapped in blue and the downregulated mapped in red. Based on the color, it was immediately possible to identify the upregulation of the fatty acid degradation route. Besides that, several proteins at the glyoxylate cycle were also upregulated. Another difference is the total amount of downregulated and upregulated proteins in *P. luminescens* in comparison to *X. szentirmaii* and *X. nematophila*.

For *X. szentirmaii*, one of the highest upregulated enzymes was acyl-CoA dehydrogenase FadE (*Xszus_01852*), which was responsible for the ß-oxidation of fatty acids. Other enzymes from the fatty acid degradation pathway such as 3-hydroxyacyl-CoA dehydrogenase FadB (*Xszus_03803*), acetyl-CoA acetyltransferase FadA (*Xszus_00315*), isocitrate lyase FadJ (*Xszus_00316*) phospholipase A (*Xszus_00133*), NADPH-dependent 2,4-dienoyl-CoA reductase (*Xszus_03497*) and acetyl-CoA acetyltransferase FadA (*Xszus_03802*) were also identified (Figure 56). Furthermore, proteins from the glyoxylate metabolism such as malate synthase G (*Xszus_03725*) EC:2.3.3.9 and isocitrate lyase (*Xszus_03726*) EC: 4.1.3.1 were upregulated (Figure 57).

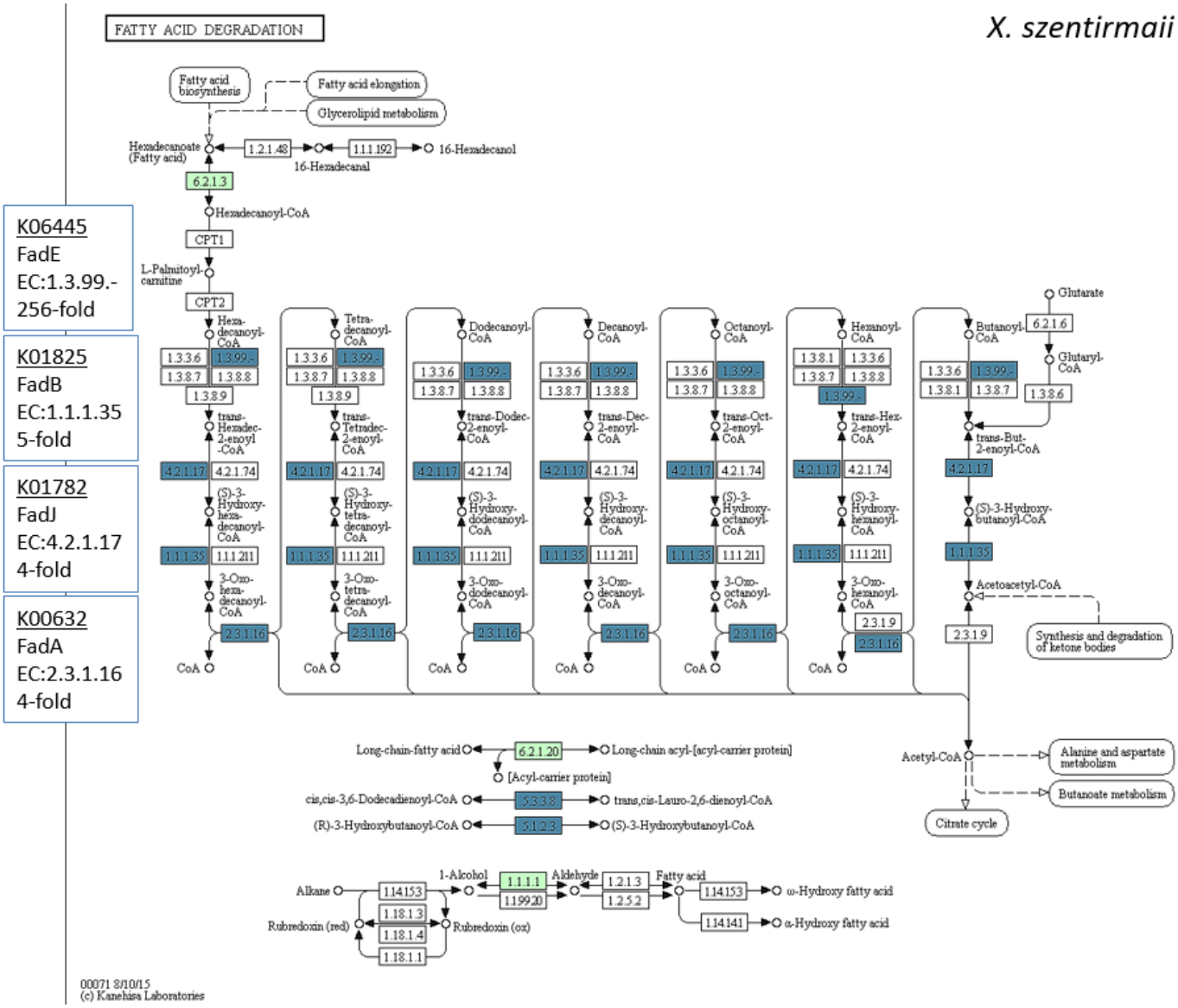

Figure 56: Overview of proteins in the fatty acid degradation cycle in *X. szentirmaii*; proteins found (green), upregulated (blue), downregulated (red).

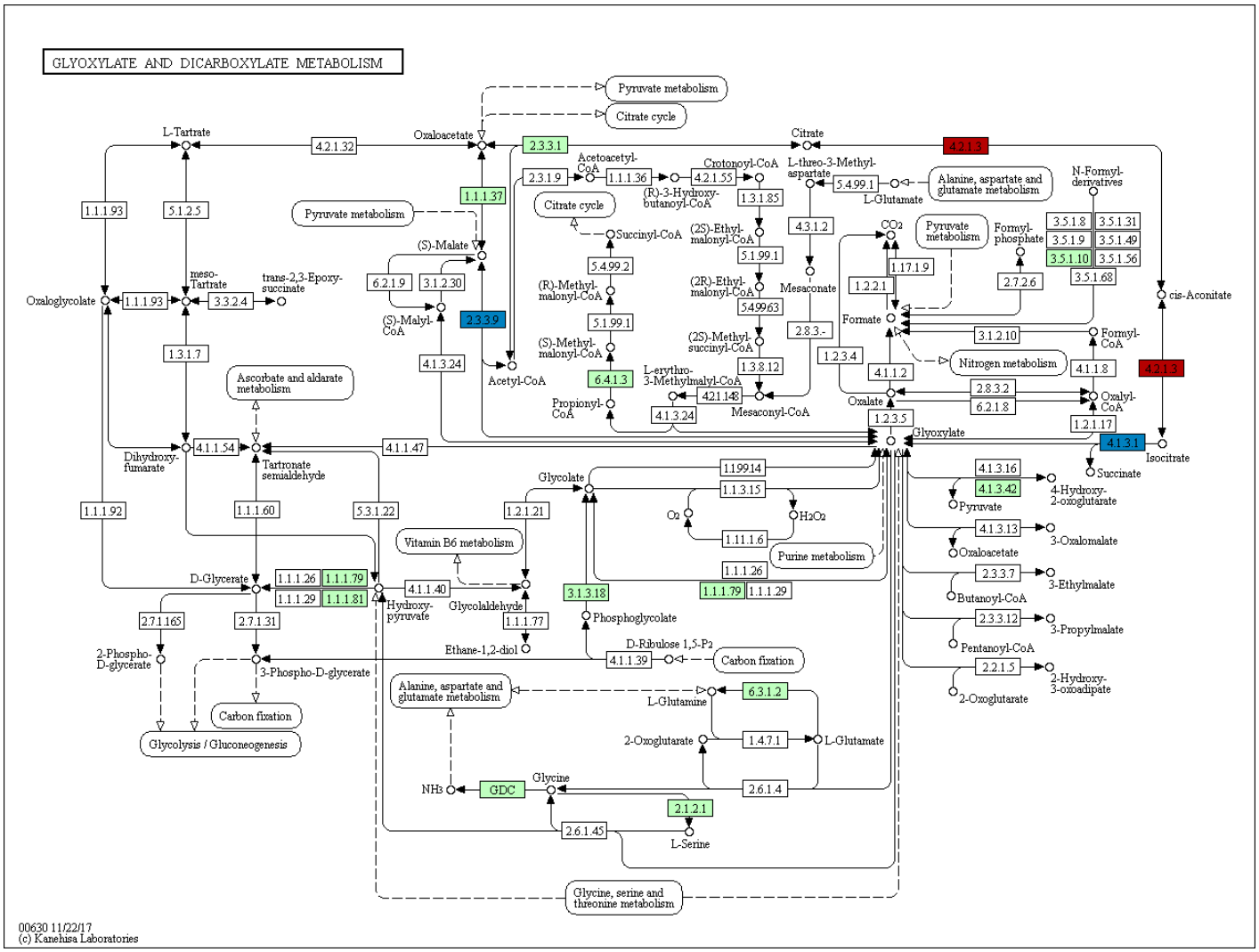

Figure 57: Overview of proteins in the glyoxylate cycle in *X. szentirmaii*; proteins found (green), upregulated (blue), downregulated (red). Malate synthase G (*Xszus_03725*) EC:2.3.3.9 and isocitrate lyase (*Xszus_03726*) EC: 4.1.3.1 are upregulated.

For *X. nematophila,* the fatty acid degradation cycle was upregulated as well. The identified proteins were acyl-CoA dehydrogenase FadE (*WP_010846618.1*), 3-hydroxyacyl-CoA dehydrogenase FadB (*WP_013185341.1*), FadJ (*WP_013184888.1*) and acetyl-CoA C-acyltransferase FadA (*WP_041573727.1*).

X. nematophila

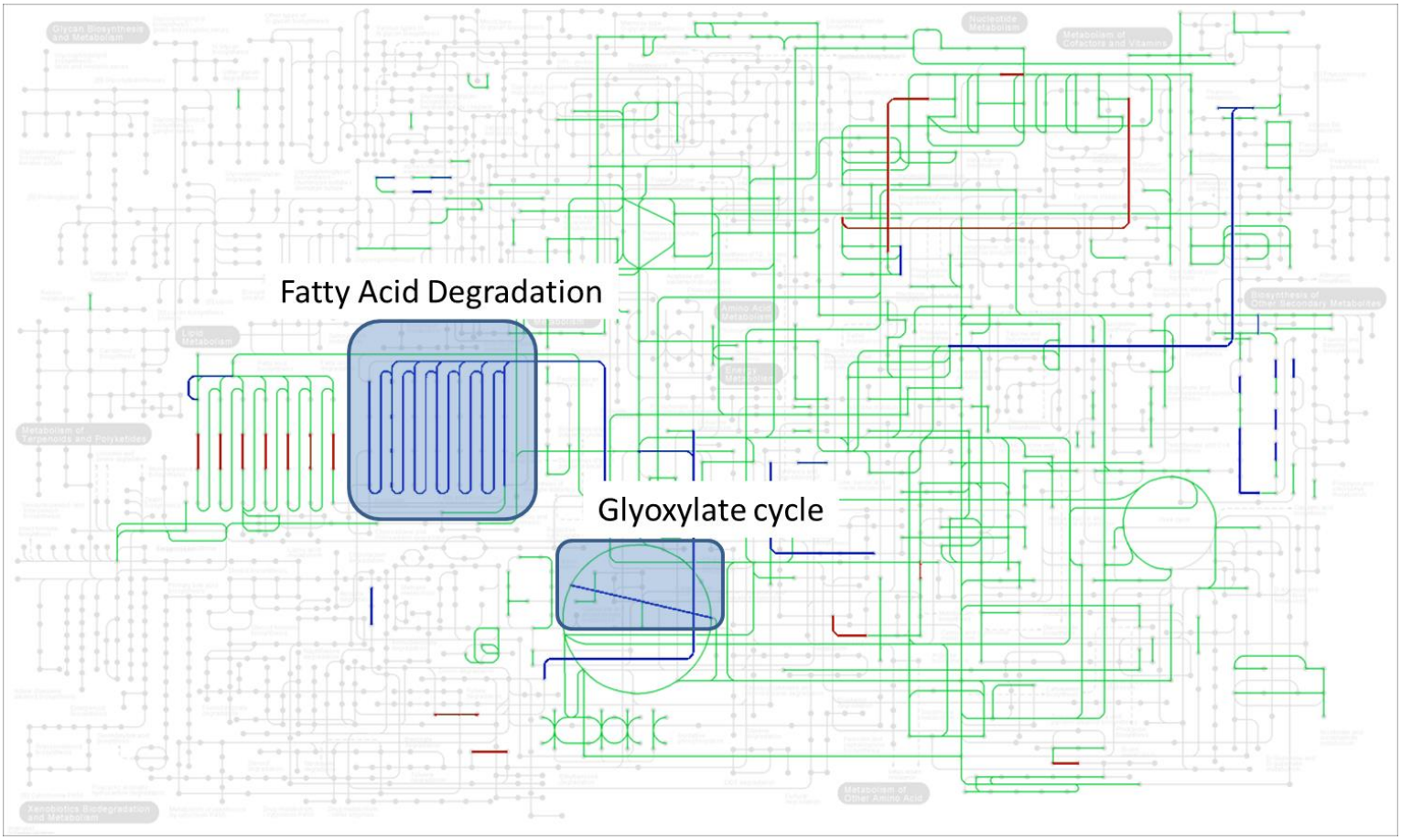

Figure 58 : Overview of proteins in *X. nematophila*; proteins found (green), upregulated (blue), downregulated (red).

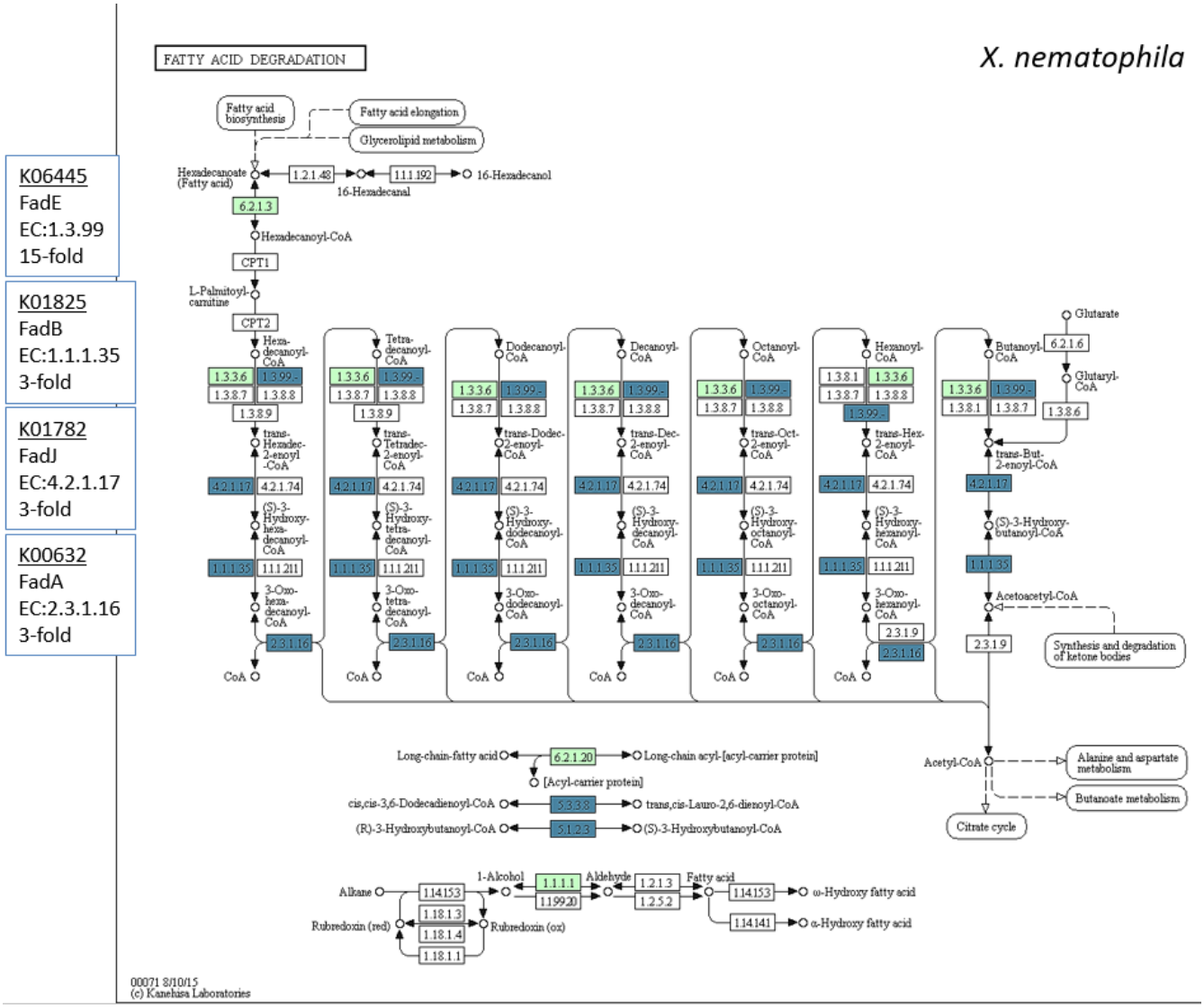

Figure 59: Overview of proteins in the fatty acid degradation cycle in *X. nematophila*; proteins found (green), upregulated (blue), downregulated (red).

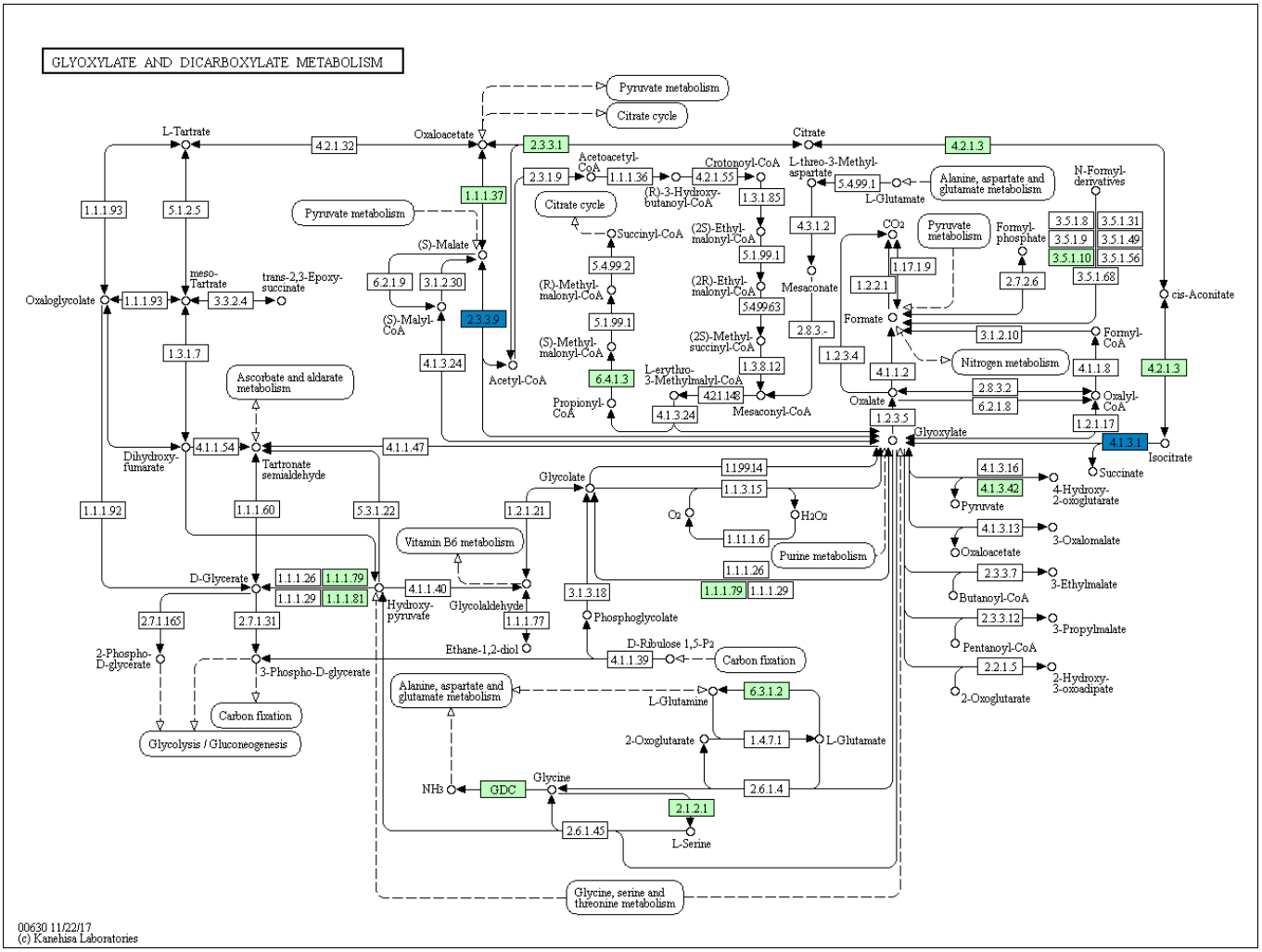

Figure 60: Overview of proteins in the glyoxylate cycle in *X. nematophila*; proteins found (green), upregulated (blue), downregulated (red). Malate synthase G (*WP_038219458.1*) EC:2.3.3.9 and isocitrate lyase (*WP_010848783.1*) EC: 4.1.3.1 are upregulated.

P. luminescens

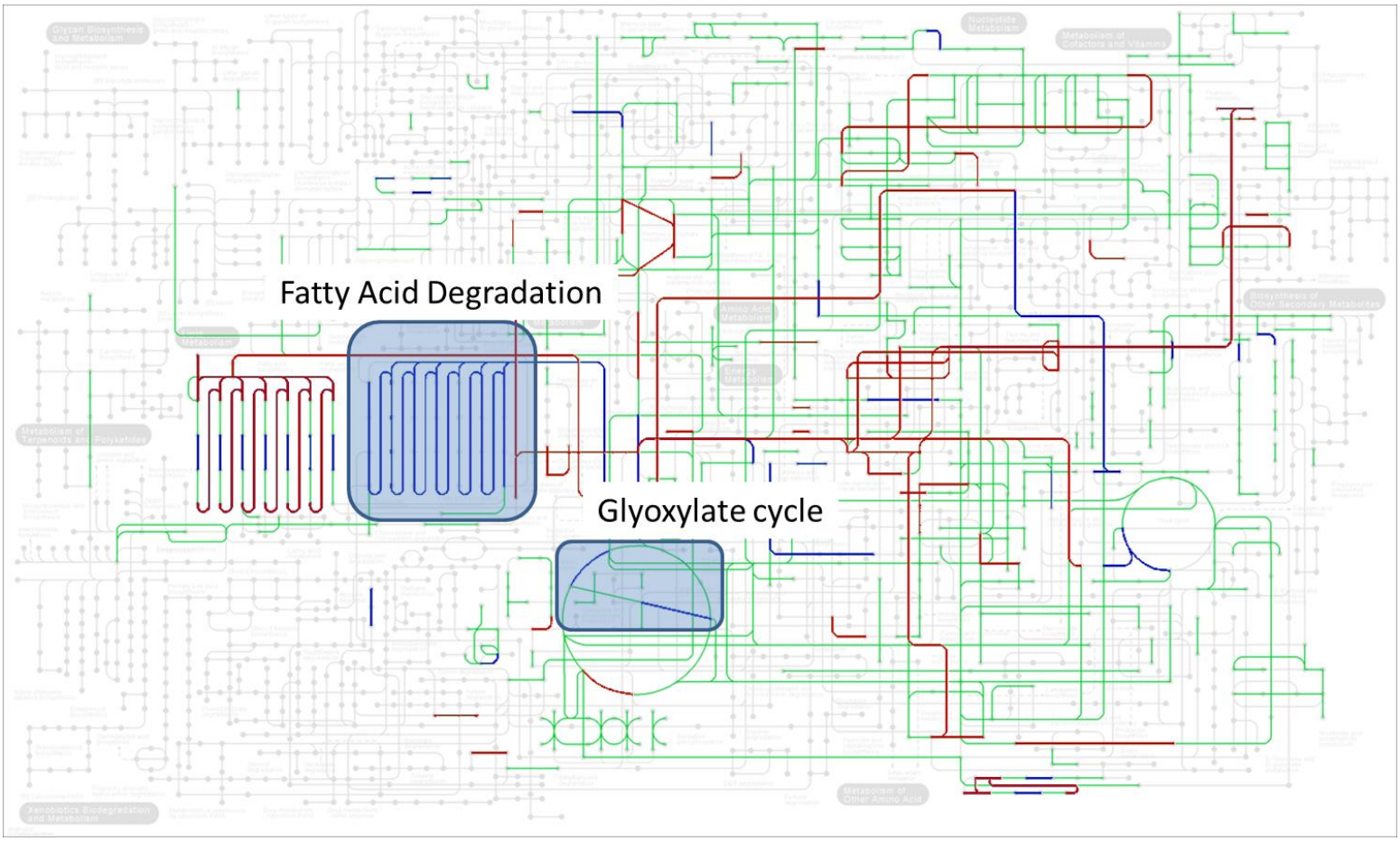

Figure 61: Overview of proteins in *P. luminescens*; proteins found (green), upregulated (blue), downregulated (red)

P. luminescens showed similar results in fatty acid degradation and the glyoxylate pathway. The algorithm identified 58 upregulated proteins and 127 downregulated proteins. The downregulated proteins were identified in the fatty acid biosynthesis, while the fatty acid degradation was upregulated. The involved genes acyl-CoA dehydrogenase FadE (*WP_011145519.1*), FadB (*WP_011148492.1*), FadJ (*WP_011147407.1*), FadI (*WP_011147408.1*) and FadA (*WP_011148493.1*) in the fatty degradation were all more than 2 fold upregulated. Also here FadE was the most upregulated protein (Figure 62).

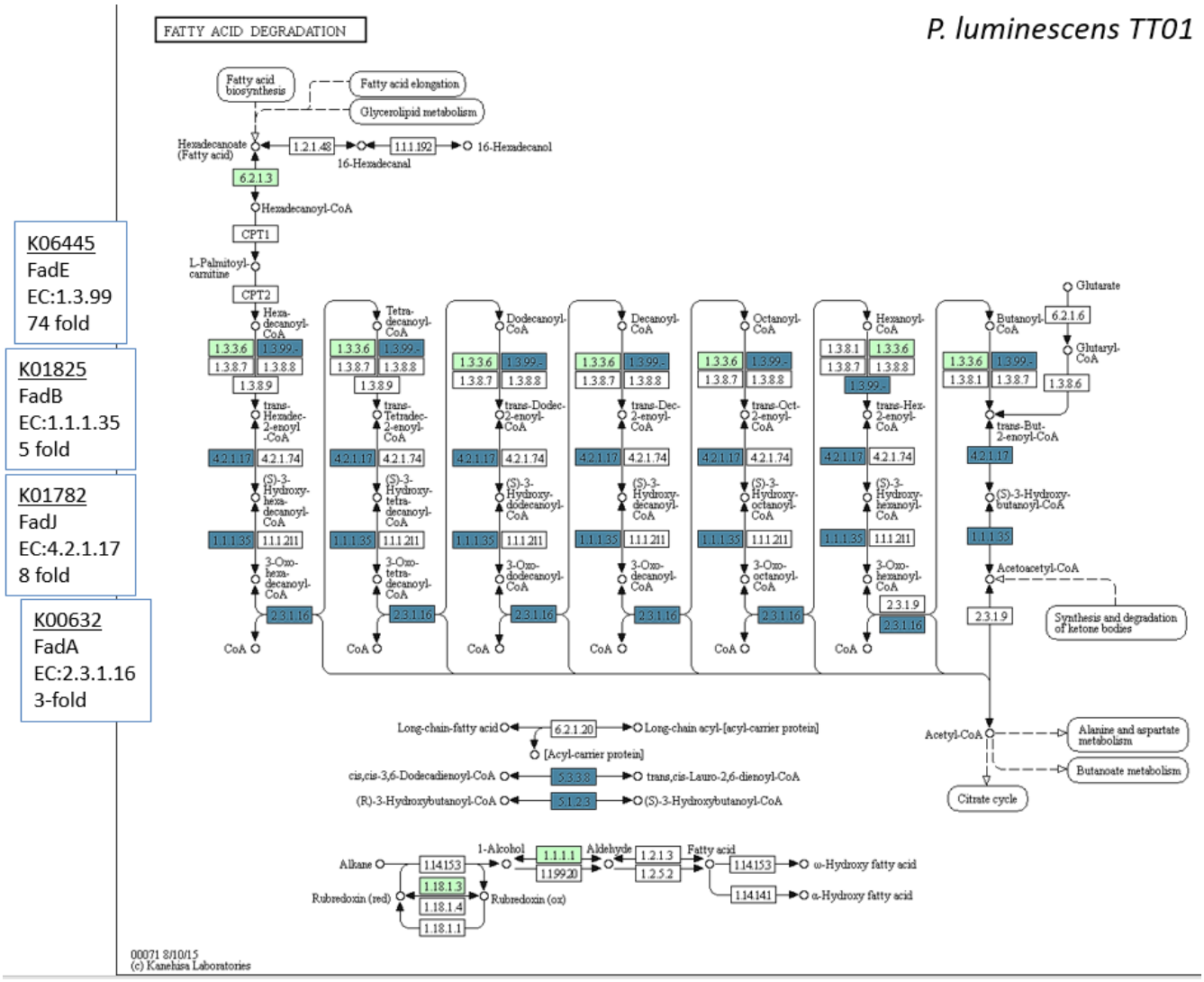

Figure 62: Overview of proteins in the fatty acid degradation cycle in *P. luminescens*; proteins found (green), upregulated (blue), downregulated (red)

Moreover, malate synthase A (WP_011148486.1) and isocitrate lyase (WP_011148485.1) were found to be upregulated (Figure 63).

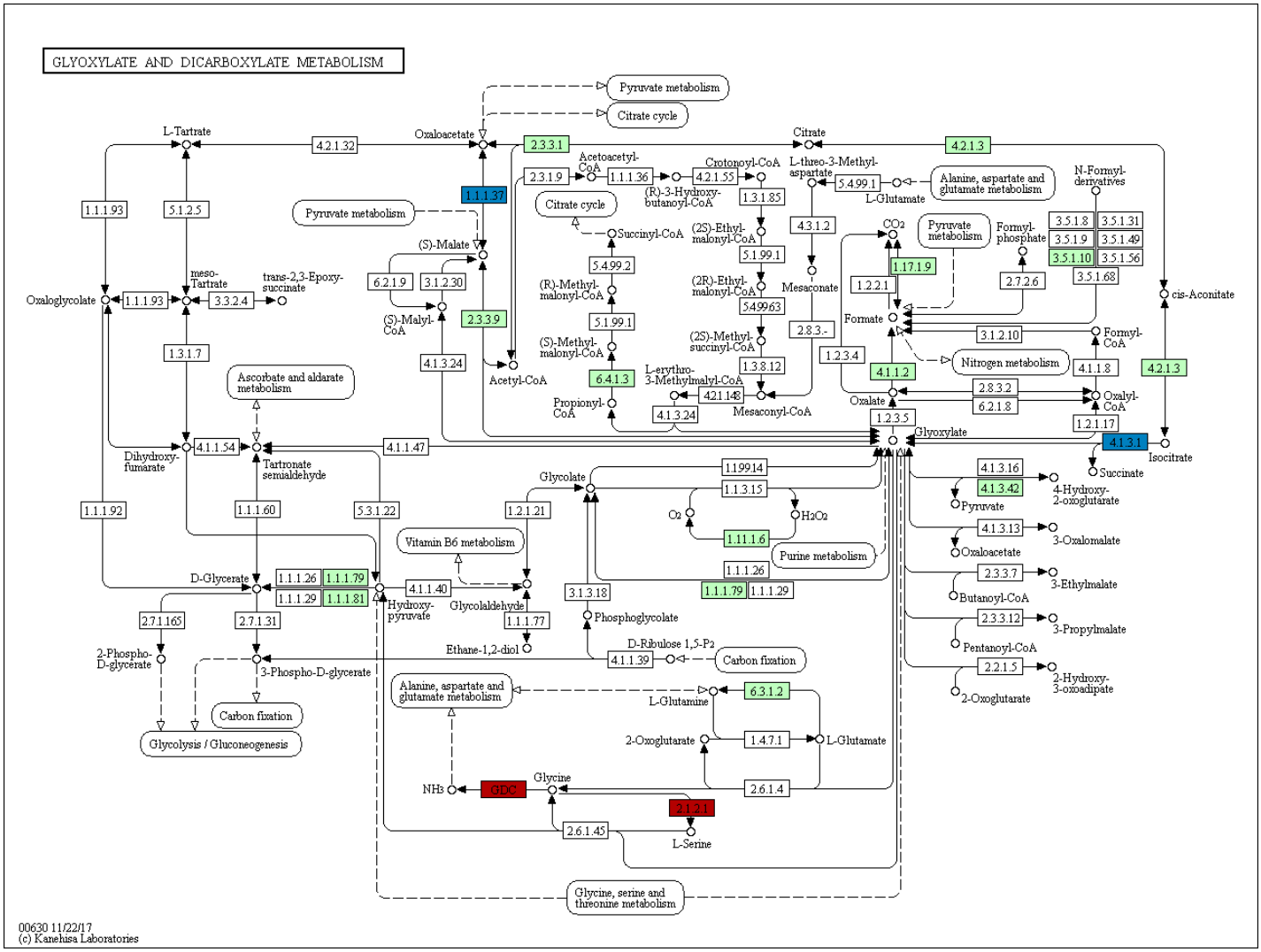

Figure 63: Overview of proteins in the glyoxylate cycle in *P. luminescens* TT01; proteins found (green), upregulated (blue), downregulated (red). Moreover, malate synthase A (*WP_011148486.1*) EC:1.1.1.37 and isocitrate lyase (*WP_011148485.1*) EC:4.1.3.1 were found to be upregulated (Figure 63).

4. Discussion

4.1 Silathride

The synthesis of silathride was unproblematic and was achieved by standard Fmoc SPPS. The peptide showed quorum quenching activity against *Chromobacterium violaceum* similar to other compounds from *P. luminescens* such as ririwpeptide, kolossin, and flesuside. Quorum sensing is a process, where bacteria cells interact with each other via small signal molecules, such as *N*-acyl-homoserine lactones. The disruption of these signal pathways is called quorum quenching and can be induced by enzymes, such as lactonases and acylases[146]. There are several known mechanisms for the quorum quenching mechanism, such as signal degradation, signal competition, and QS gene interference[147]. For *Chromobacterium violaceum* the molecule *N*-hexanoyl-L-homoserine lactone (C6-HSL) has been identified as signal molecule[148]. This small molecule has a different molecular structure than C6-HSL and therefore silathride is unlikely to have a similar mode of action. However, the peptide might disturb the transport process and maybe even bind to C6-HSL resulting in the observed quorum quenching effect. Moreover, Gram-positive bacteria often utilize oligopeptide autoinducers instead of small molecules. Maybe there is some underlying relationship between silathride and these peptide signals[149].

Furthermore, it showed activity against several fungi, such as *Candida parapsilosis*, *Pseudozyma prolifica,* and *Cryophonectria parasitica*. Many peptides have been described with antifungal activities. The described mechanism was cell wall breakage induction, biofilm formation[150], and cell wall synthesis inhibition[151]. Based on silathride's structure the mode of action is not clear yet and needs further experiments.

4.2 Xenoautoxin

The partial xenoautoxin sequence **Vvlii** had to be coupled twice due to steric hindrance. This effect has been previously described in literature[152].

The synthesis of the biotinylated xenoautoxin possessed certain challenges. Initial experiments showed that it was not possible to attach biotin directly at the N-terminus of xenoautoxin. Furthermore, starting the synthesis with biotinylated lysine led to the detachment of the group during the following reaction. The solution was to use the C6-linker Fmoc-ε-Ahx-OH and then add the biotin group at the end.

Xenoautoxin has been previously described as a toxic peptide when expressed in *X. doucetiae*[73] suggesting Gram-negative activity. However, if xenoautoxin was added from the outside of the cell or to *E. coli* cells it showed no toxicity. It is possible, that the peptide was unable to overcome the cell membrane. Therefore, a new biotinylated xenoautoxin peptide was constructed, which might be carried into the cytosol by biotin transporters[153]. However, after adding the new biotinylated xenoautoxin no effect was observed.

It is possible that although the product xenoautoxin was toxic when inside the cell, it was not possible to transport the peptide into the cells resulting in no bioactivity. However, it might be possible to use membrane vesicles as an alternative drug carrier for xenoautoxin[154] and thereby gain the desired toxicity.

4.3 Phenylethylamides and tryptamides

The synthesis of these simple amides was accomplished using the standard protocol. The synthesized products were sent to the Hellmann group in Mainz. Initial data showed that these compounds interact with the membrane or proteins embedded in or positioned on the membrane structure (unpublished results).

In this thesis, a new assay was developed to identify natural products, which are located in the bacterial cell pellet. Here, we could identify PAX and also other natural products, such as phenylethylamide, tryptamide, and GameXPeptides. It is possible, that these peptides adhere to the membrane of *Xenorhabdus*. Bacteria vary their fatty acid composition in the membrane to adapt to different physiological conditions such as temperature-, pH-[155], pressure change[156], and antibiotic stress[157,158]. Therefore, phenylethylamides and tryptamides might play a major role as an alternative mechanism to modify the bacteria cell membrane that has to be studied in more detail in the future.

4.4 Rhabdopeptides

Due to time limitations, the modified rhabdopeptides have not been tested and the PAL assay was not finished. However, many publications have described the successful application of this technique[11,159,160]. Furthermore, it might be possible to build additional rhabdopeptides for a new approach of stable isotope labeling-based quantitative mass spectrometry using deuterated iodomethane. The new method would be similar to isoTOP-ABPP[161]. Here, light and heavy labelled active compounds were first incubated with the cell samples. Later, these active compound protein complexes would be enriched and analyzed by LC-MS/MS. The advantage lies in the usage of different isotopes leading to multiple MS peaks, which yield additional information about the target and specificity.

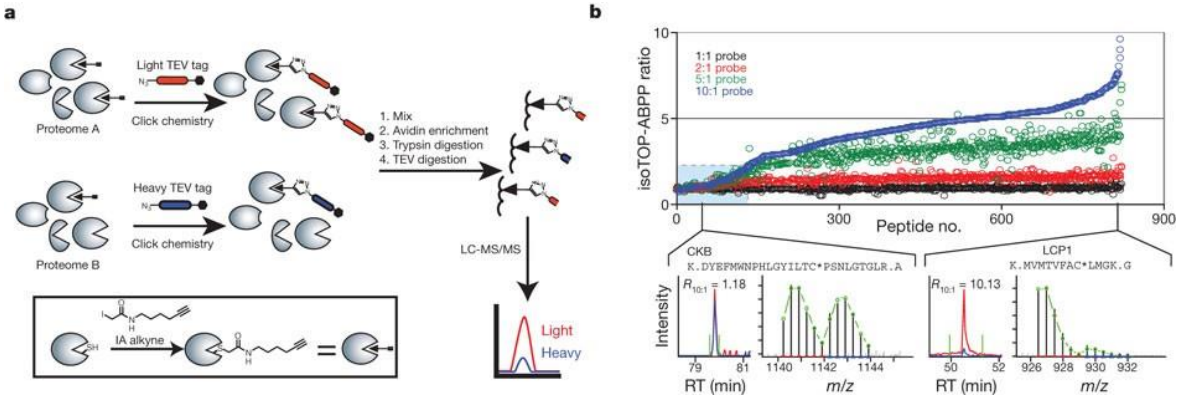

Figure 64: isoTOP-ABPP **a)** The proteins were labelled with a cysteine probe (black box) and subsequently clicked with light (red) and heavy (blue) cleavable TEV tags. These proteins were enriched and digested to provide probe-labelled peptides for MS analysis. **b)** Through the addition of different heavy to light probe concentrations (10:10 µM, 20:10 µM, 50:10 µM, 100:10 µM), it was possible to determine proteins with higher activity isoTOP-ABPP ratios (ratio 100:10 µM (R) < 2.0 in the blue box). At a ratio of R = 1.0, it means that the protein reacted at the same pace independent of 10 µM or 100 µM probe concentration. However, at R = 10, it means that the reaction was 10 times faster at 100 µM indicating that the reaction rate is slower. Two proteins were shown: creatine kinase B (CKB R = 1.18 indicating high activity) and plastin 2 (LCP1 R = 10.13 indicating low activity)[161].

4.5 Phototemtide A

The synthesis of SmI_2 was challenging. The reaction time was around 3-4 h. Furthermore, it was not able to store the product under a protective nitrogen atmosphere overnight without degradation. Therefore, commercially available SmI_2 provided a better alternative.

The synthesis of the final peptide was succeeded with Lei Zhao and the final structure was elucidated with the help of the synthetic products. Phototemtide A's structure contained a 3'-(*R*)-OH fatty acid similar to the hydroxy fatty acid in PAX.

The final peptide product was active against human pathogens *T.b. rhodsiense*, *T. cruzi,* and *P. falciparum*. Furthermore, no activity was determined towards mammalian L6 cells[105].

4.6 Investigation of PAX function and antimicrobial activity

PAX has been previously described as antifungal and antimicrobial peptide[14]. However, the results revealed that PAX was mostly quantified in the cell pellet fraction instead of the supernatant (Figure 37). This was presented in the results section 3.6.

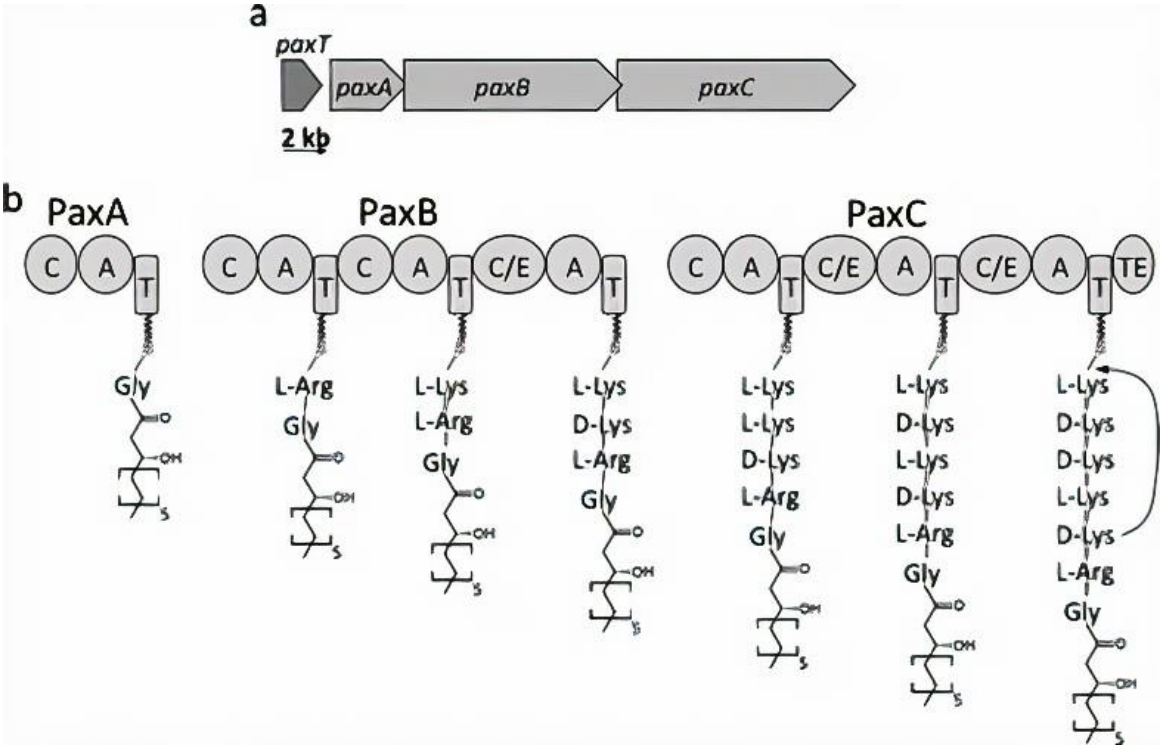

Figure 65: a) Schematic illustration of the PAX biosynthesis gene cluster. **b)** Proposed biosynthesis of PAX[107] (Copyright © Royal Society of Chemistry (Great Britain). Permission/License is granted.).

The biosynthesis of PAX starts in the cytosol and the compound is transferred subsequently into the periplasm by an ABC exporter encoded by PaxT (Figure 65). Here, PAX might be absorbed into the membrane[162] or be able to surpass the periplasm and the outer membrane by diffusion as a biosurfactant.

By using PAX derivatives, which enable click chemistry, it was possible to locate PAX on the surface of the *X. doucetiae* mutant *pax*$^-$ and *E. coli* (Figure 43 and Figure 44). For more information please see section 3.8 Investigation of PAX function and

antimicrobial activity PAX microscopy. Furthermore, the experiments were carried out with both **36** azido- and **37** alkyne-PAX derivatives both leading to identical microscopic results.

Of note, this is the first time that PAX molecules are visualized directly and at the single-cell level. One important aspect here is that instead of using fluorescently labelled derivatives we only added minimal modifications to the molecule. As PAX molecules belong to the smallest members of antimicrobial peptides (size ~ 1 kDa), conjugation with fluorophores before addition to the bacterial cultures leads to a significant increase in size (e.g. ~ 0.7 kDa for Sulfo-Cy5 alkyne used in this study) and change in net charge (-2 for sulfo-Cy5) and both properties can greatly affect PAX binding affinity.

The mode of action of AMPs usually starts with the disruption of the cell membrane[162] (Figure 66). Therefore, the AMP molecules first accumulate on the membrane surface up to a critical concentration. Here, positively charged peptides are attracted by negatively charged LPS. In the next step, the outer membrane structure is permeabilized through electrostatic and hydrophobic interaction between AMP and membrane molecules.

It was shown that PAX peptides with palmitic acid residues showed higher bioactivity towards *E. coli* and *X. doucetiae* than PAX peptides with a 3-OH group and a shorter lipid tail. Here, fatty acids alone such as myristic acid, palmitic acid, or lauric acid are weak antimicrobial agents, and the mechanism is postulated to disrupt the electron transport chain and oxidative phosphorylation through membrane interaction[163].

Similarly to PAX, cecropin[164] and drosocin[165] can lysis *E. coli* cells immediately through a nonpore-forming mode of action. However, peptides such as melittin[166] integrate into the membrane and form pores, which ultimately lead to permeabilization of the membrane correspondingly. After overcoming the outer membrane, AMPs surpass the peptidoglycan barrier and disrupt the cytosolic membrane consequently.

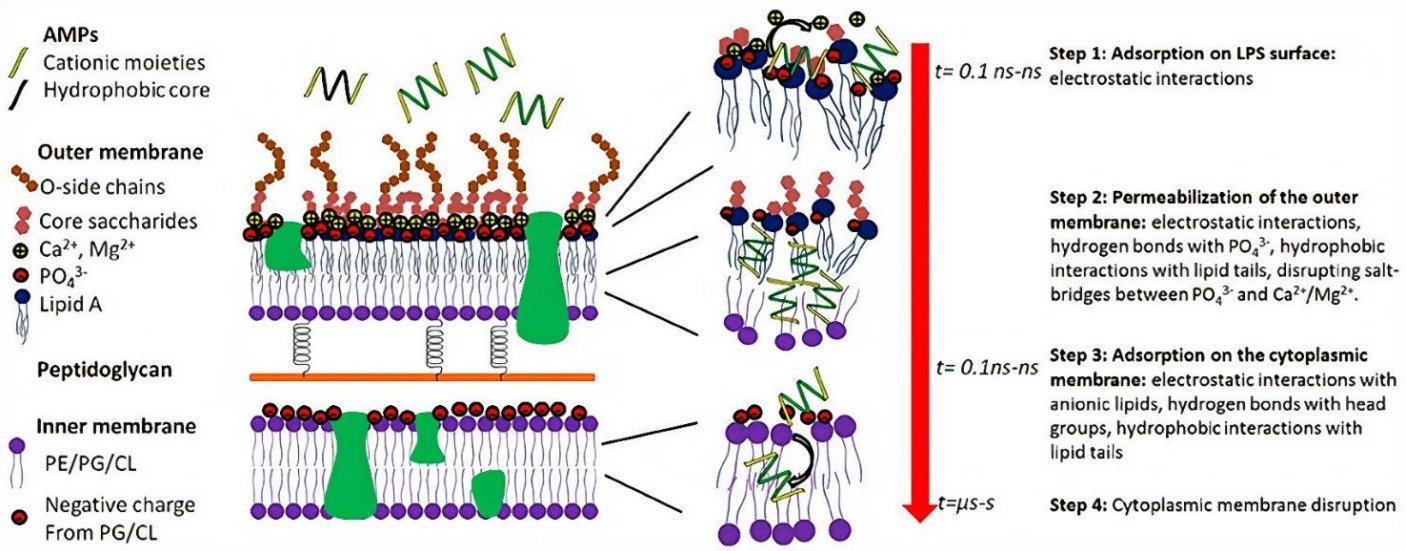

Figure 66: AMP interaction with Gram-negative bacteria membrane[162](Copyright © 2017 Li, Koh, Liu, Lakshminarayanan, Verma, and Beuerman. The figure was distributed under the terms of the Creative Commons Attribution License (CC BY)).

In the case of PAX as AMP versus *E. coli*, similar observations were made at higher PAX concentrations. Initially, PAX peptides were located at the cell surface indicating electrostatic attraction between positively charged PAX and negatively charged bacteria surface. Broth microdilution assay revealed that PAX derivatives could inhibit *E. coli* in 10-100 µg/ml range, which are in line with the microscopy results.

However, certain compromised cells showed cytosolic PAX-signals at lower PAX concentrations (10 and 30 µg/ml) (Figure 44). This indicates, that PAX molecules flood the cytosol once the membrane is disrupted. Intriguingly, we did not observe that PAX interacts with chromosomal DNA as suggested for other cationic AMPs[167], but instead almost exclusively localizes to the remaining cytosolic regions where it might interact with other negatively charged molecules such as mRNA or ribosomes.

Insects produce AMPs such as cecropin[142], melittin[144], or drosocin[143] as a first-line defense system[168]. They typically have a positive net charge and often carry both hydrophilic and hydrophobic parts, which can interact with the bacterial cell membrane[169]. Here, selective toxicity is thought to be a result of varying lipid compositions and transmembrane potentials found for different microbial species[170]. For example, high amounts of cardiolipins and phosphatidylserine (negative net

charge) have been found in bacterial pathogens such as *E. coli*, *S. aureus*, or *B. subtilis*, while mammalian cells, for example, contain phosphatidylcholine and phosphatidylethanolamine (neutral net charge)[171]. Studies have shown that positively charged AMPs are electrostatically attracted to the negatively charged bacteria membrane leading to depolarization and ultimately cause leakage of the cellular contents[171].

Interestingly, *X. doucetiae* cells produce PAX peptides, which are categorized as AMPs and, as our findings suggest, are located at its membrane. We hypothesize that cells with a surface-exposed PAX coat might be able to repulse AMPs by modifying the surface charge. Lysinylation of phospholipids was previously observed for *Enterococcus faecalis*[172] leading to depolarization of the membrane.

If this was the case, the promotor exchange *pax*$^-$ mutant should be more susceptible to AMPs due to lacking PAX production, while the induced *pax*$^+$ mutant produces PAX forming a coat that leads to AMP repulsion and cell survival (Figure 67).

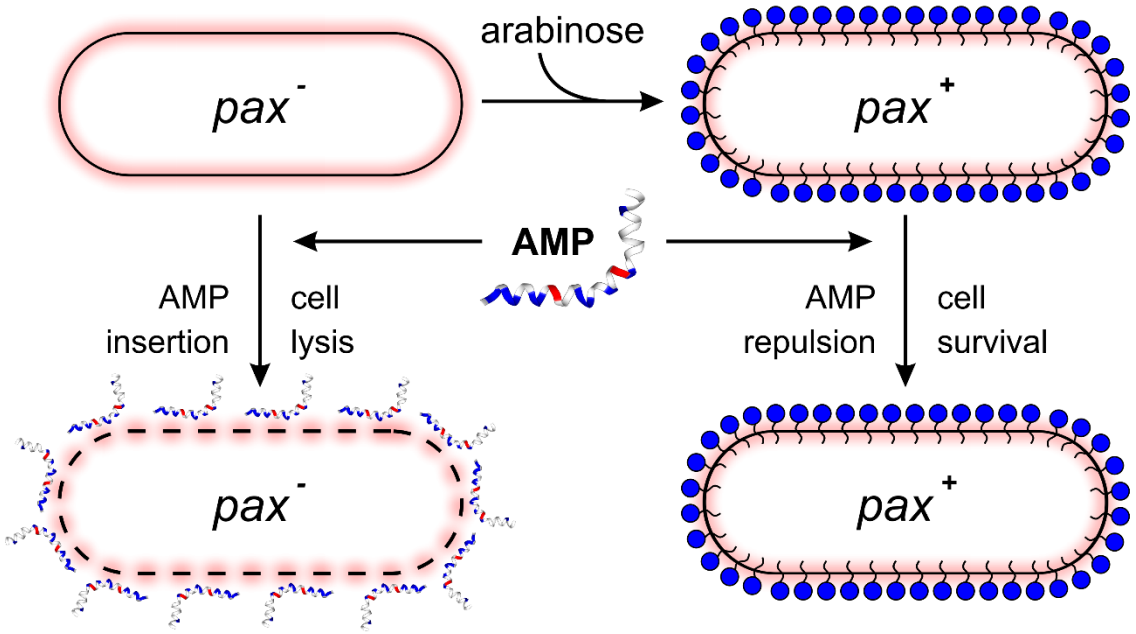

Figure 67: Proposed model of PAX-mediated protection of *X. doucetiae* cells against cationic AMPs. *pax*$^+$ cells produce PAX molecules (blue dots) that are exposed at the cell surface and repulse cationic AMPs, thus promoting cell survival. *pax*$^-$ cells are more susceptible to AMPs that get attracted to the negatively charged surface of cells lacking PAX. Red color indicates a negative charge while positively charged residues/molecules are colored in blue.

To test this hypothesis, we carried out microdilution assays in which we treated *X. doucetiae* WT, *pax*$^{+}$, and *pax*$^{-}$ cultures with different concentrations of cecropin, drosocin, and melittin. Cell growth reduction was observed in all strains. However, in accordance with our expectations, the growth of wild type *X. doucetiae* cultures were less affected by treatment with these insect AMPs compared to the non-induced *pax*$^{-}$ mutant. This mutant does not produce **39**, **40,** and showed delayed or completely abolished growth. However, this process was reversed when the *pax*$^{+}$ mutant was induced with 0.2% arabinose.

This protective effect of PAX also took place in *E. coli.* After adding a sublethal dose of PAX together with insect AMPs, a protective effect of PAX on the growth of *E. coli* cultures was observed. This effect was not as strong as for *X. doucetiae* cultures. A possible explanation would be the integration of PAX into the *E. coli* membrane leading to the repulsion of insect AMPs but at the same time acting as AMP itself.

Another possible function for PAX might be the biogenesis of outer membrane vesicles (OMV). They play a major role as insect pathogenicity factor[173] in *X. nematophila*. There are two known mechanisms where molecules such as lipopolysaccharide (LPS)[174] and quinolone signal[175] interacting with the outer membrane leading to increased OMV production. Therefore, molecules such as PAX, tryptamide, and phenylethylamide which also contain lipid-binding structure might be involved in the regulating process of OMV formation.

4.7 Proteome analysis

The proteome analysis revealed that many proteins are involved in the activation of the three strains *X. szentirmaii*, *X. nematophila,* and *P. luminescens*. However, the data analysis in KEGG showed that two major pathways were activated during this process. First, the fatty degradation processes were heavily increased in all three strains. The involved proteins FadE, FadB, FadJ, and FadA were identified and quantified using the Maxquant workflow.

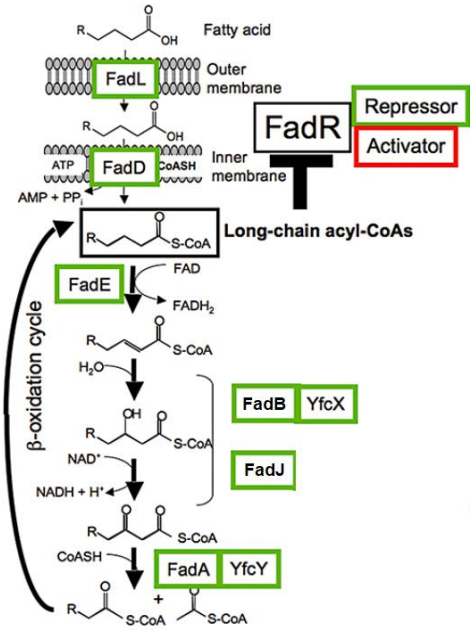

Figure 68: Proteins involved in fatty acid degradation (scheme based on[176]) (Copyright © Fujita Y., Matsuoka H., Hirooka K. Permission granted by Fujita Y.).

This is coherent with the expectation because the major compound in the insect lysate were lipids. To facilitate the resources, the bacteria would produce an increased amount of proteins producing acetyl-CoA at the end of the □-oxidation cycle.

Furthermore, the protein malate synthase and isocitrate lyase were upregulated as well. They play a major role in the glyoxylate cycle[177]. To handle the excess amount of produced acetyl-CoA (C2), the organisms use isocitrate lyase to produce glyoxylate (C2) and succinate (C4) from isocitrate (C6). This reactive glyoxylate (C2) species can be facilitated to produce malate (C4) by a Claisen condensation[178] with

acetyl-CoA (C2). In a subsequent step, the organisms can further process malate (C4) to oxaloacetate (C4). This product can be used for gluconeogenesis, in the urea cycle, amino acid synthesis, or in the citric acid cycle. In comparison to the citric acid cycle[177], which is also able to process acetyl-CoA, this pathway bypasses multiple reaction steps. Therefore, it might be a more efficient pathway to enable lipid absorption in a short period.

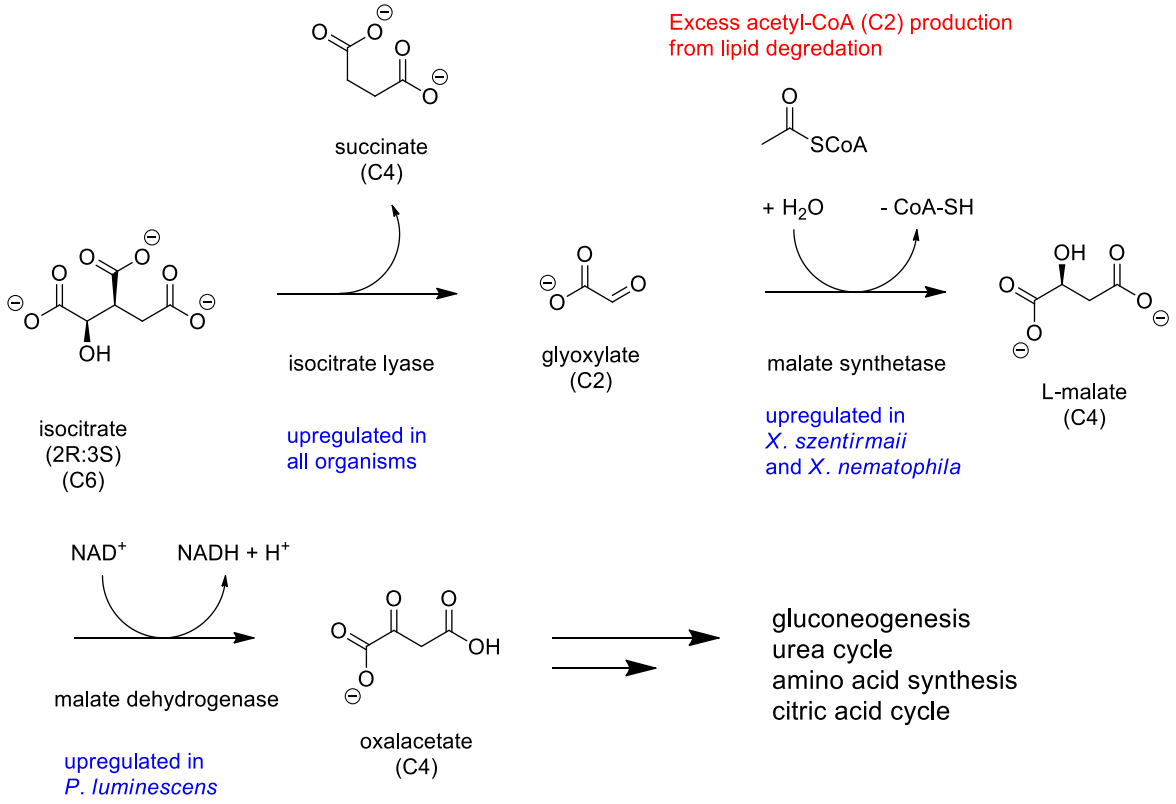

Figure 69: The catalyzed process of the enzyme isocitrate lyase, malate synthase, and malate dehydrogenase. Isocitrate lyase was upregulated in all strains. The reactive product glyoxylate is needed for the conversion of acetyl-CoA to L-malate.

Strikingly, fungal infection has been described as heavily dependent on the glyoxylate cycle as well[179]. In another experiment, *Saccharomyces cerevisiae* was either cultivated alone or with murine macrophage. These two samples were then processed in whole-genome microarray analysis to determine upregulated genes. The results show that isocitrate lyase, malate synthetase, and malate dehydrogenase were highly active in the co-cultivation samples with murine

macrophage. It was then suspected that microbes inside of human lacking of these enzymes are not able to produce glucose and therefore loses their virulence. This was shown by creating *Candida albicans* mutants lacking isocitrate lyase which were markedly less virulent in mice than the wild type. In the case of *X. szentirmaii*, *X. nematophila,* and *P. luminescens*, the virulence might also be highly dependent on these enzymes, as the insect corpse is usually rich in lipid and proteins.

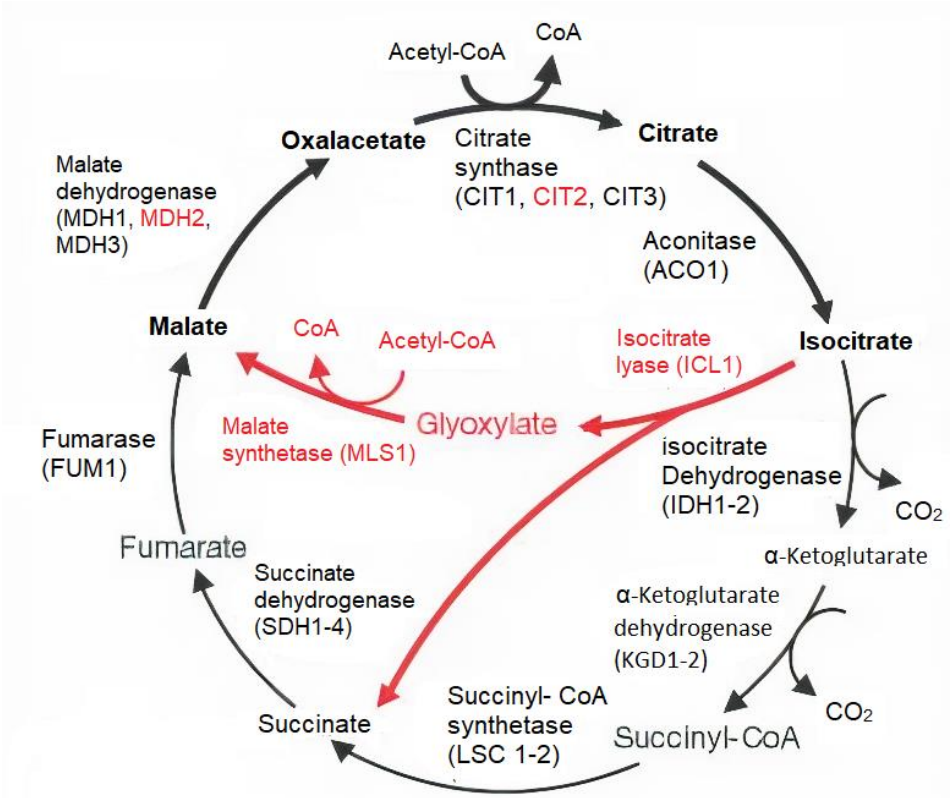

Gene	Induction	Gene	Induction
MLS1	22.7	*SDH3*	1.0
ICL1	22.4	*SDH2*	0.9
MDH2	15.6	*ACO1*	0.8
CIT2	4.9	*MDH3*	0.8
SDH1	1.9	*MDH1*	0.7
SDH4	1.7	*FUM1*	0.6
KGD1	1.4	*IDH1*	0.4
CIT1	1.1		

Figure 70: Citric and glyoxylate cycle in *S. cerevisiae*. By converting isocitrate to glyoxylate and malate, multiple reaction steps were bypassed. Isocitrate lyase and malate synthase were both upregulated in the process of mammalian macrophage ingestion[179] (Copyright © Springer Nature. Permission/License is granted).

In general, the usage of KEGG could bring a more efficient way to look at these processes. In a large number of samples, it is very important to have a framework that can validate and reject the hypothesis. Altogether this work should lay a pipeline for high-throughput proteome analysis. Therefore, protein regulation should be observed in a proteome-wide context, instead of focusing on single proteins.

4.8 Outlook

In this work, various natural products from *Xenorhabdus* and *Photorhabdus* were chemically synthesized to verify their structures and quantify the produced amount in the biological context. Furthermore, several peptide derivatives with click tags were synthesized for various detection methods, such as microscopy and mass spectrometry. Through this method, it was possible to elucidate the mode of action of PAX. Furthermore, the initial work on proteome analysis showed that this method was robust and might be combined with microscopy to deliver extraordinary mechanistic insights of molecules in a biological context.

5 Supporting information

5.1 Supporting Figures

Fragmentation silathride

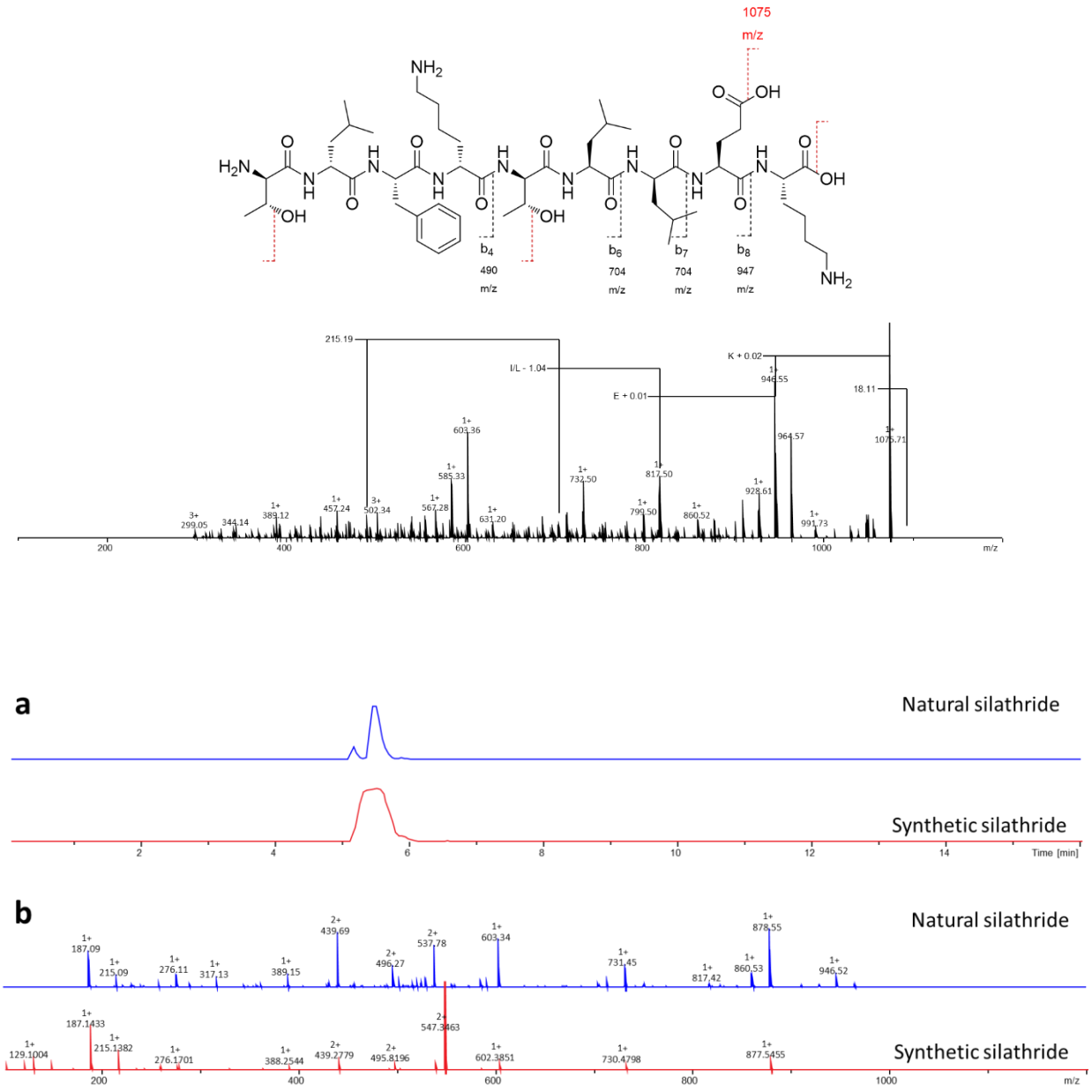

Supporting Figure 1: Structure and fragmentation of silathride. **a)** HPLC runs from natural and synthetic silathride. b) Fragmentation pattern from natural and synthetic silathride.

Fragmentation biotinylated xenoautoxin

Supporting Figure 2: Fragmentation of the biotinylated xenoautoxin derivative **2**.

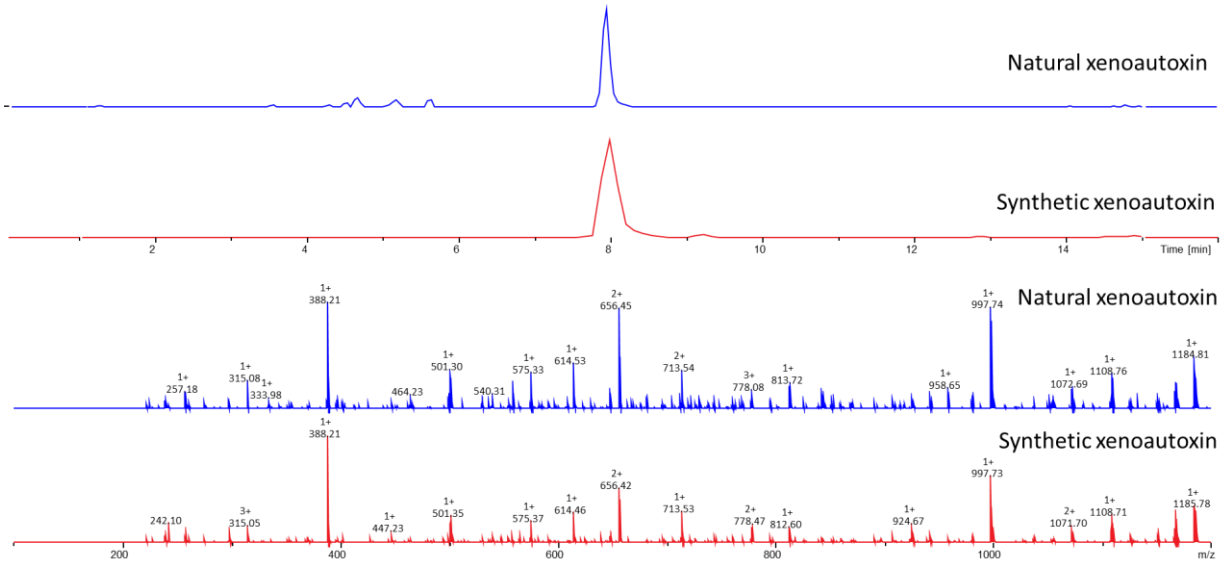

Supporting Figure 3: Retention time and fragmentation pattern of natural and synthetic xenoautoxin.

Phenylethylamide and tryptamide

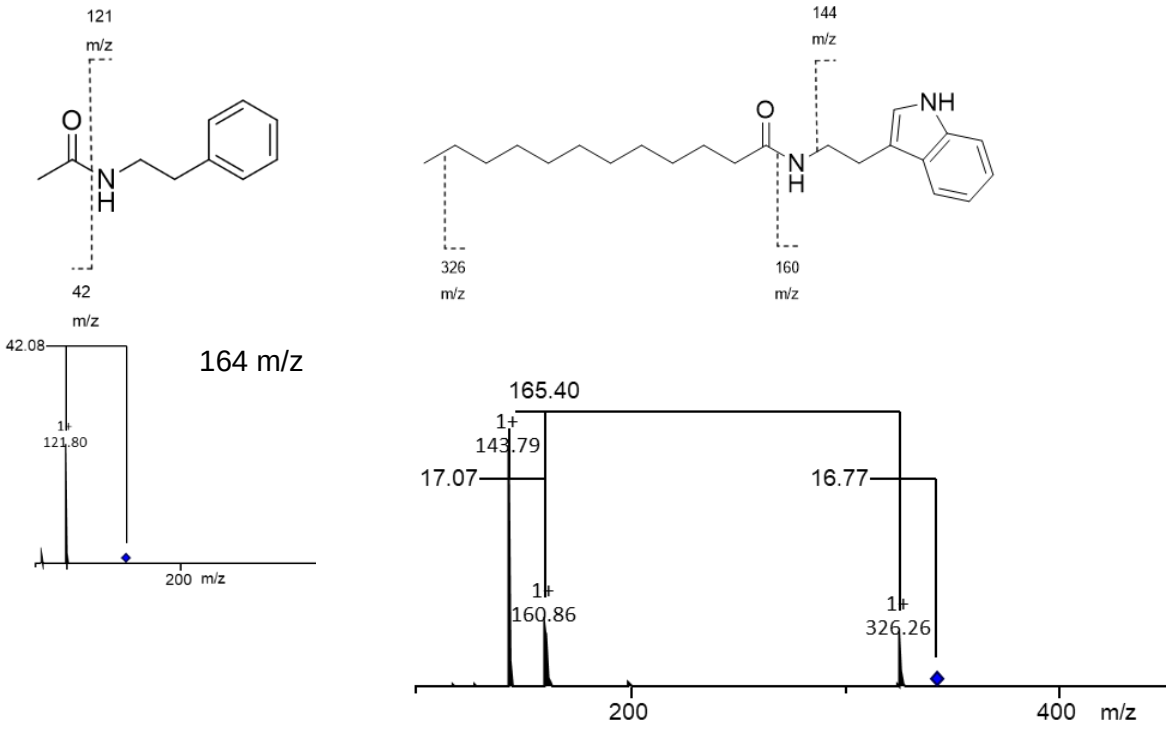

Supporting Figure 4: Fragmentation examples of phenylethyamide and tryptamide.

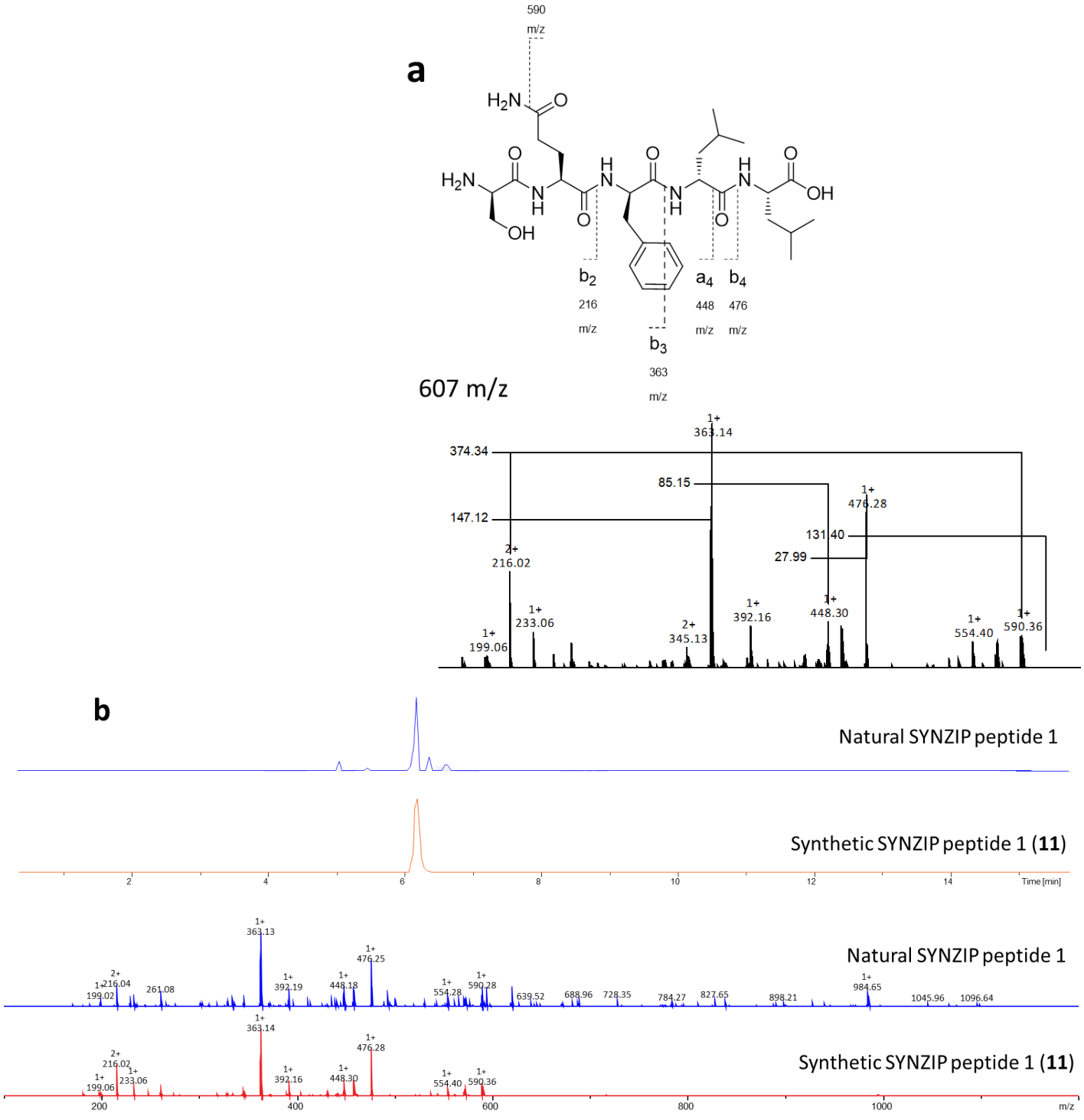

Supporting Figure 5: **a)** Structure and Fragmentation of 11. **b)** HPLC-runs from natural SYNZIP peptide 1 and synthetic SYNZIP peptide **11**.

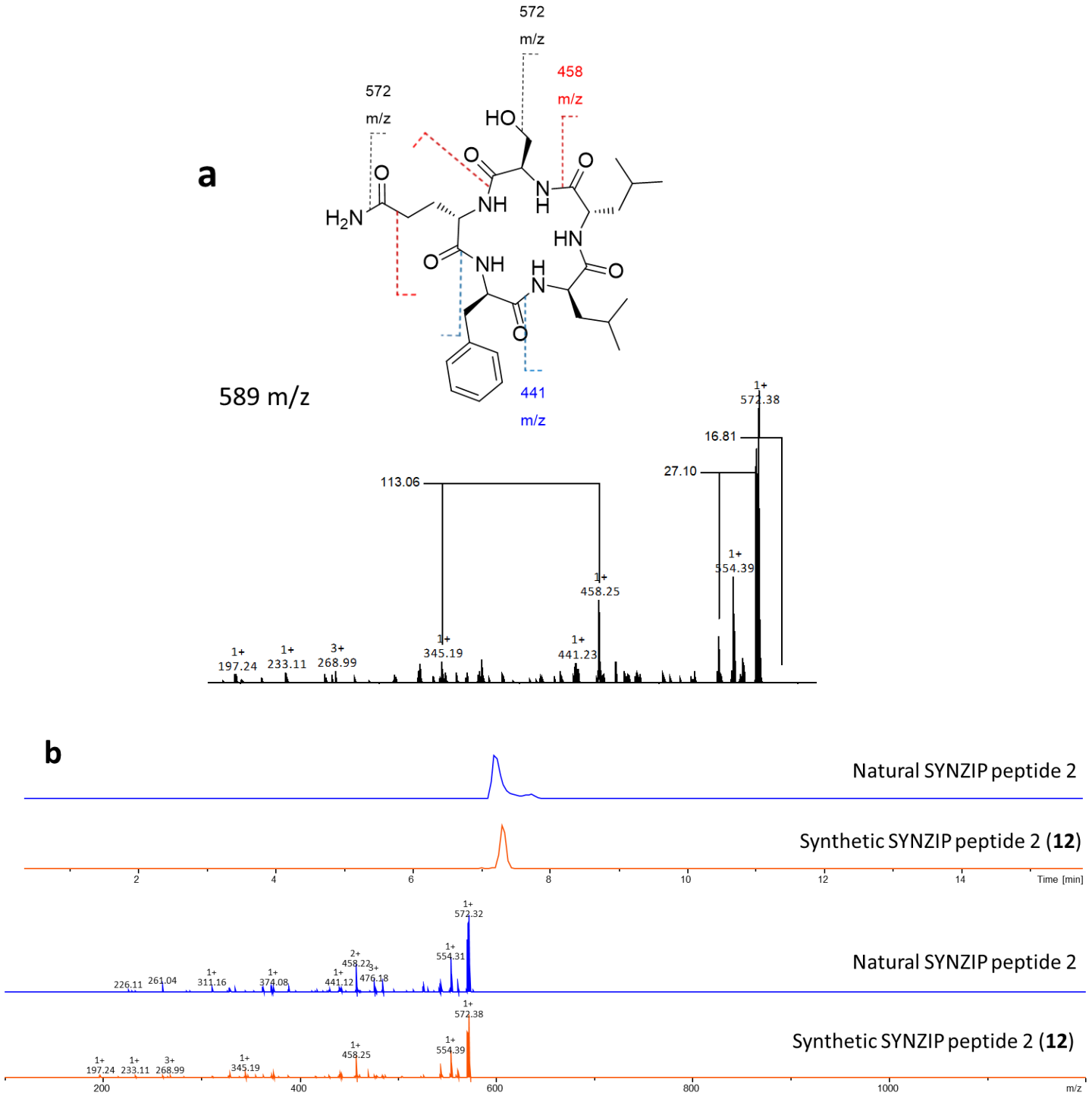

Supporting Figure 6: a) Structure and Fragmentation of **12**. **b)** HPLC-runs from natural SYNZIP peptide 2 and synthetic SYNZIP peptide **12**.

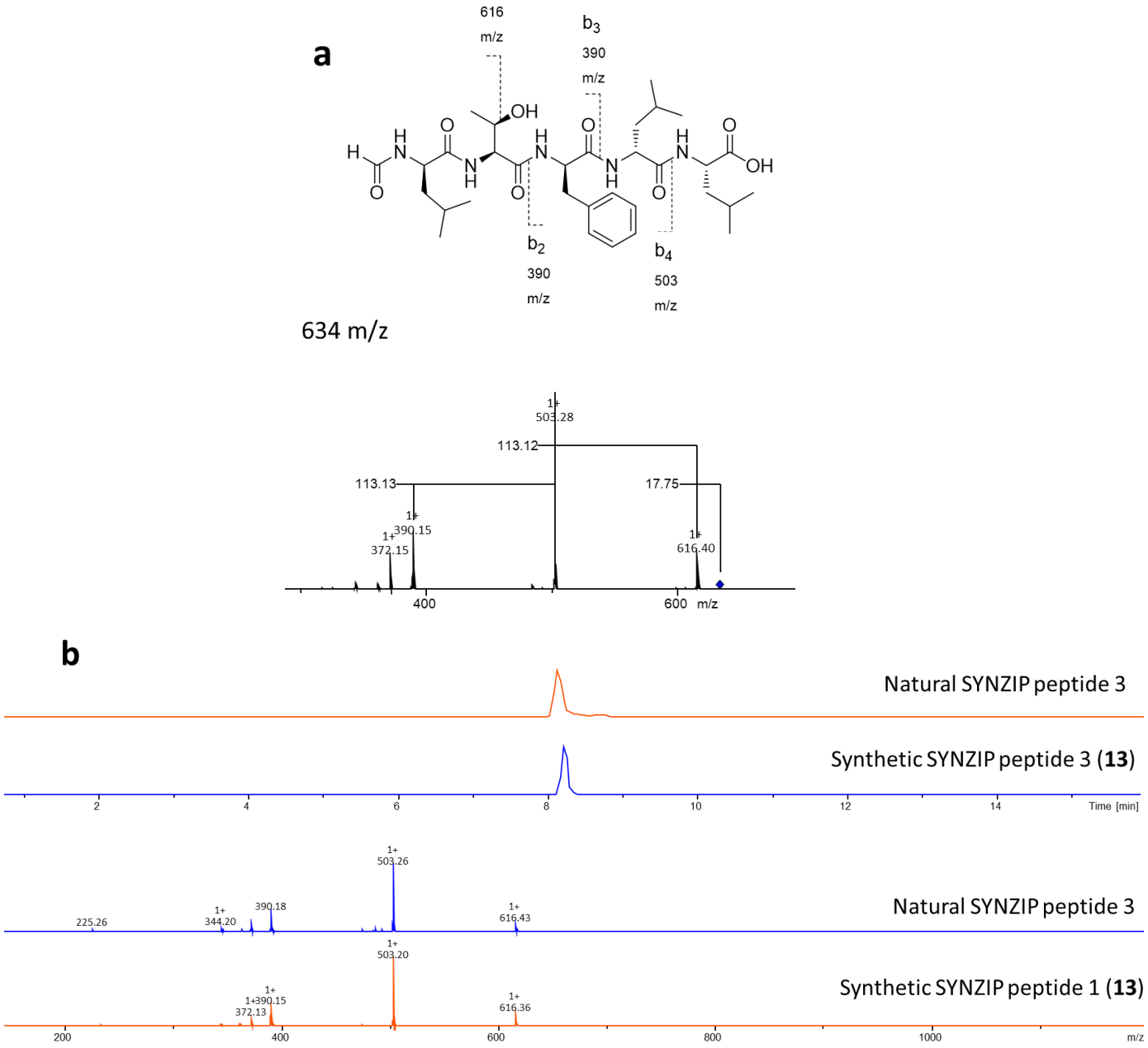

Supporting Figure 7: a) Structure and Fragmentation of 13. **b)** HPLC-runs from natural SYNZIP peptide 13 and synthetic SYNZIP peptide 13.

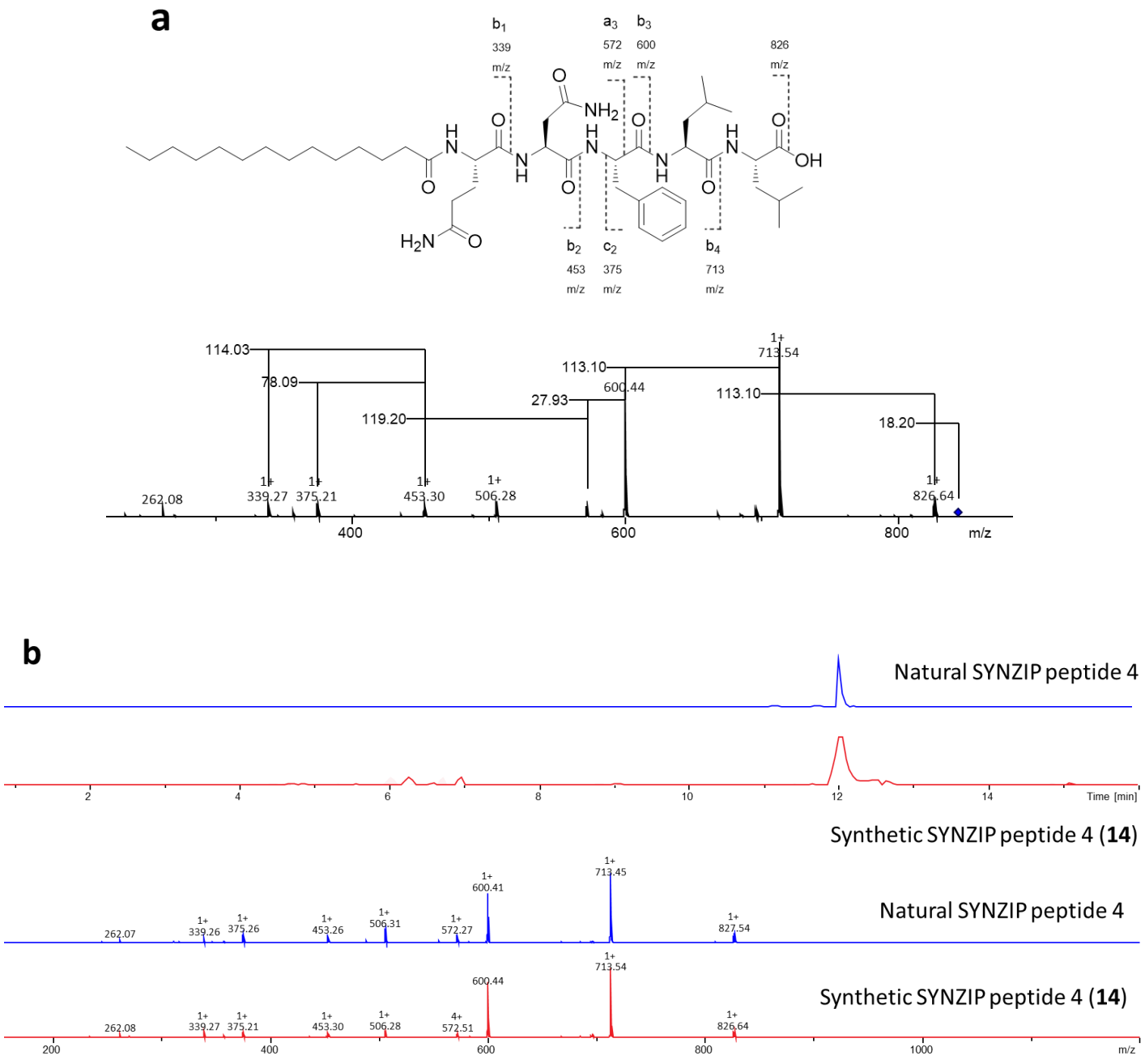

Supporting Figure 8: a) Structure and Fragmentation of 14. **b)** HPLC-runs from natural SYNZIP peptide 14 and synthetic SYNZIP peptide 14.

Fragmentation peptide aldehydes

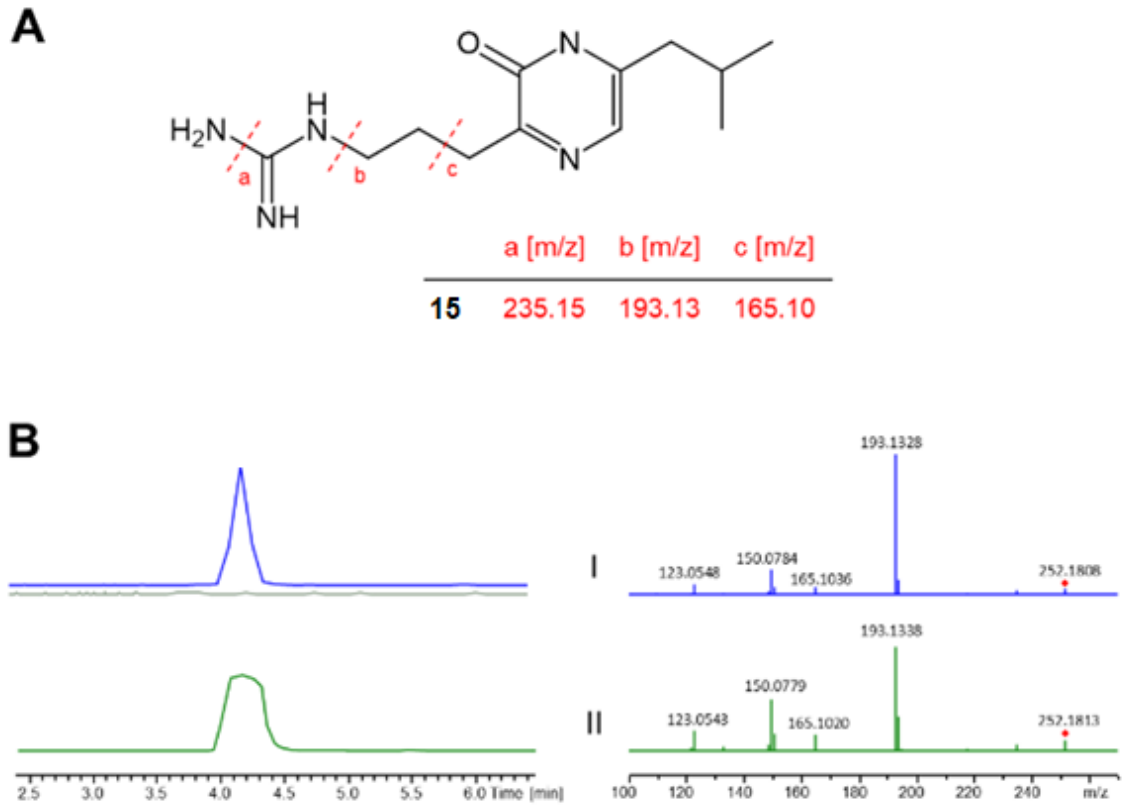

Supporting Figure 9*:* (**A**) Structure of **15** and MS^2 fragments (red). (**B**) Stacked EIC (left) and MS^2 spectra (right) of **15** (**I**, blue, rt = 4.2 min, natural peptide) and chemically synthesized **15** (**II**, green, rt = 4.2 min)[88].

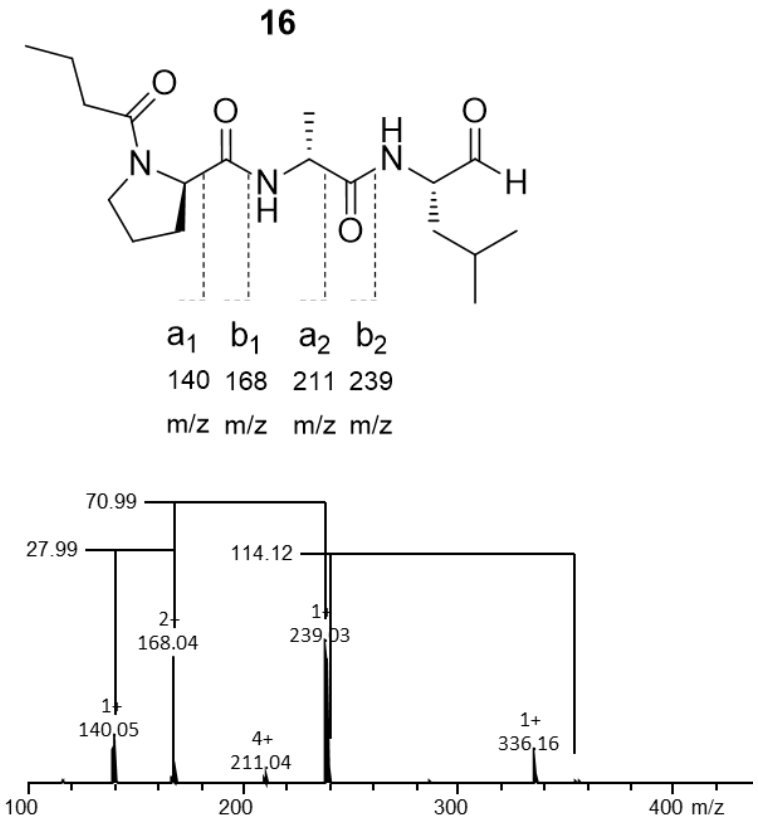

Supporting Figure 10: Structure and fragmentation pattern of **16**.

Fragmentation rhabdopeptide

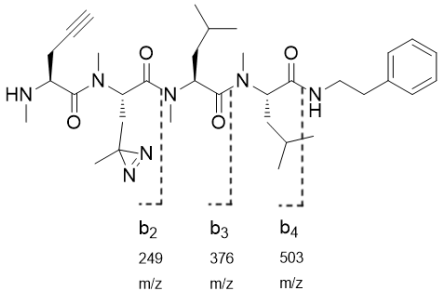

24

624 m/z

21

526 m/z

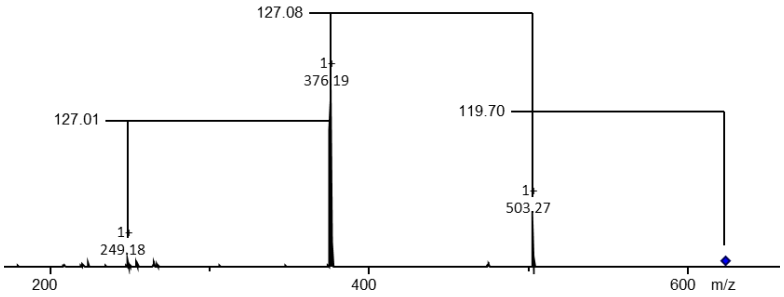

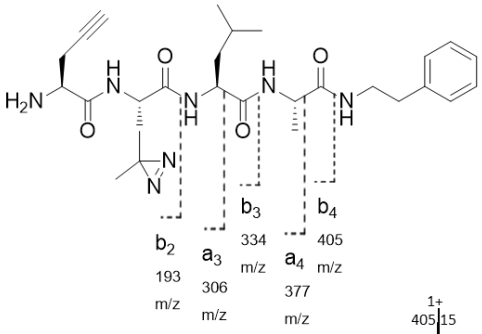

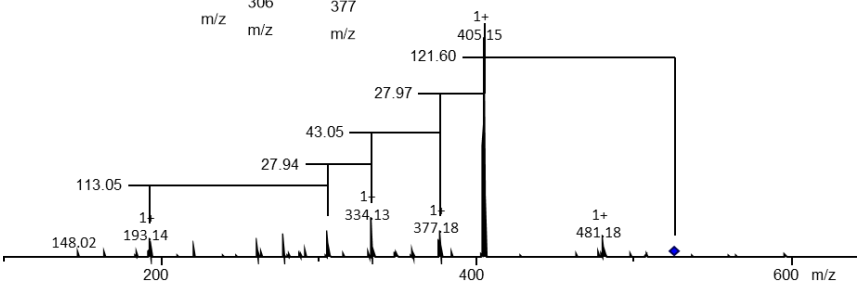

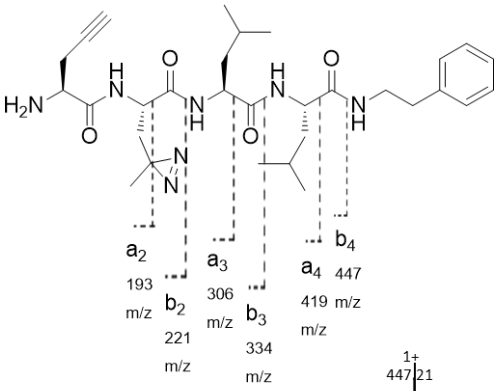

22

568 m/z

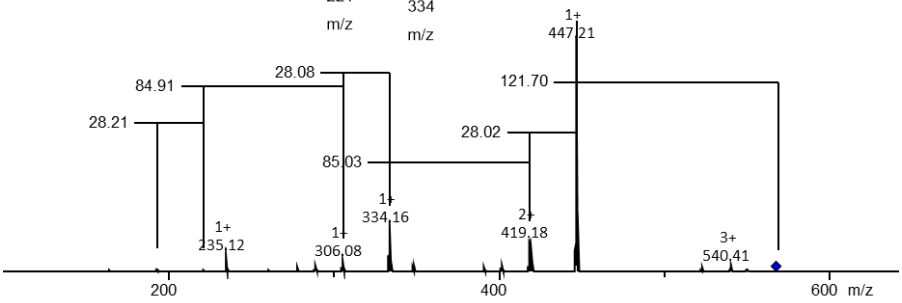

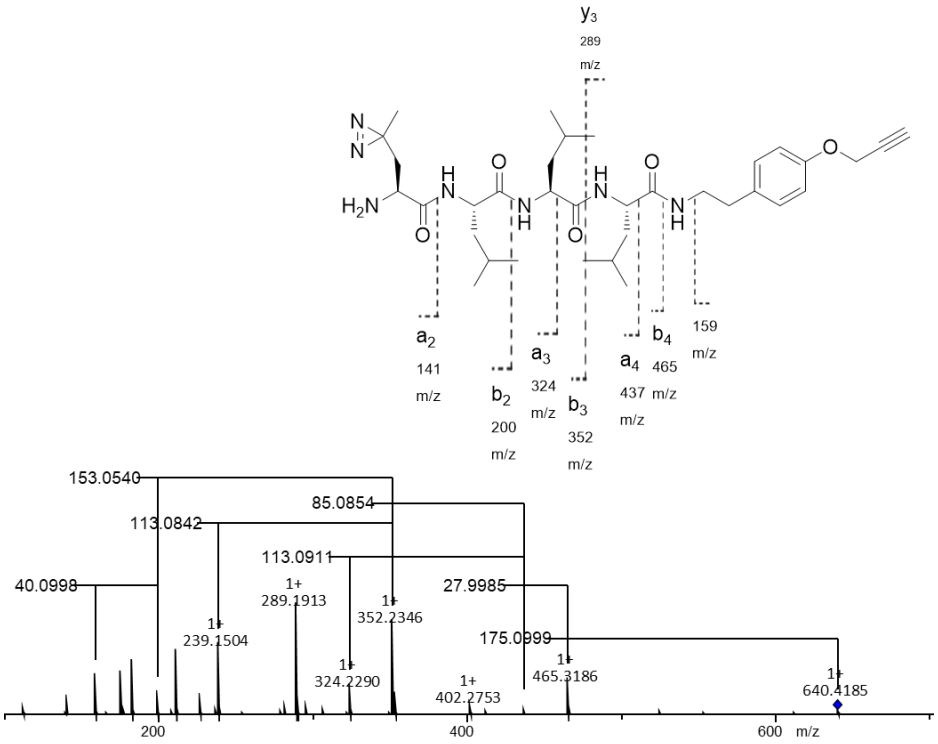

Supporting Figure 11: Fragmentation examples of synthesized rhabdopeptide derivatives.

4-benzyl-3-bromoacetyl-2-oxazolidinone

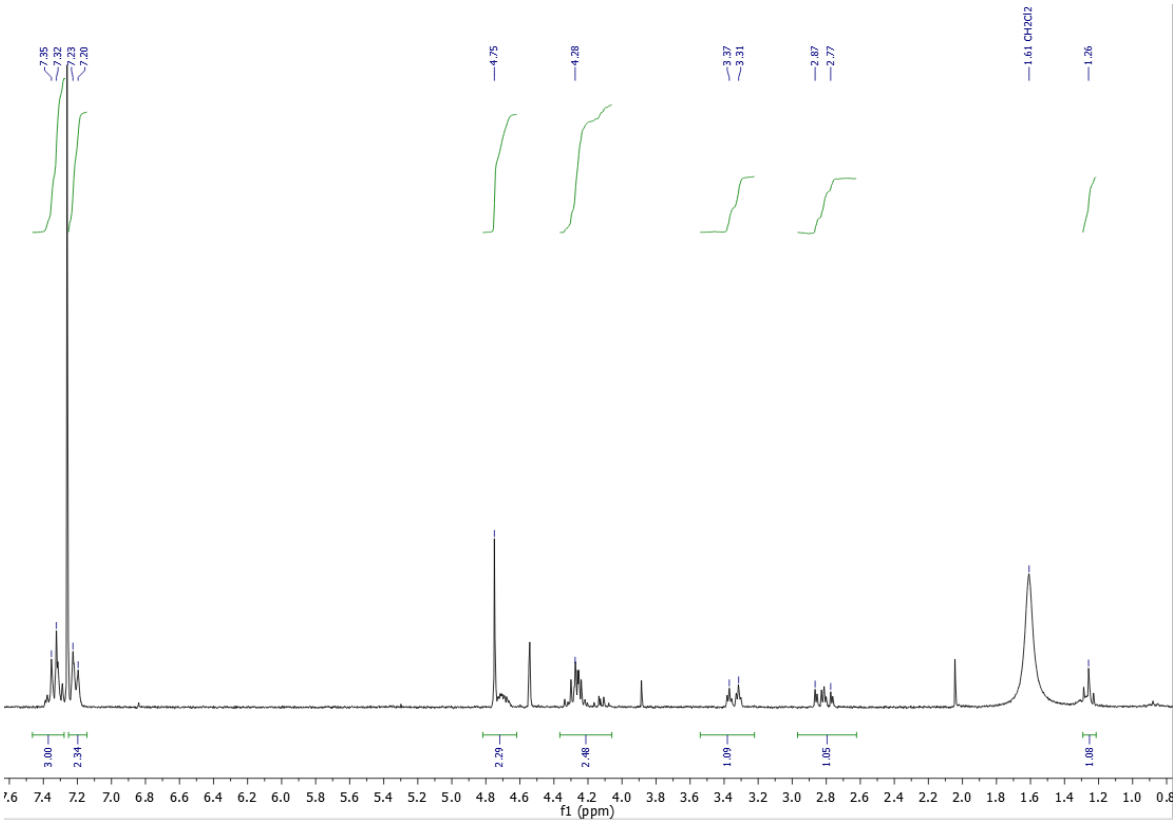

Supporting Figure 12: 4-benzyl-3-bromoacetyl-2-oxazolidinone (^{1}H NMR spectra in $CDCl_3$, 250 MHz)

^{1}H NMR (250 MHz, $CDCl_3$) δ 7.27 (d, *J* = 7.3 Hz, 3H), 7.14 (d, *J* = 7.6 Hz, 2H), 4.68 (s, 2H), 4.21 (s, 2H), 3.47 – 3.15 (m, 1H), 2.75 (d, *J* = 22.9 Hz, 1H), 1.19 (s, 1H).

4-Benzy-3-3-hydroxyoctanoyl-2-oxazolidinone

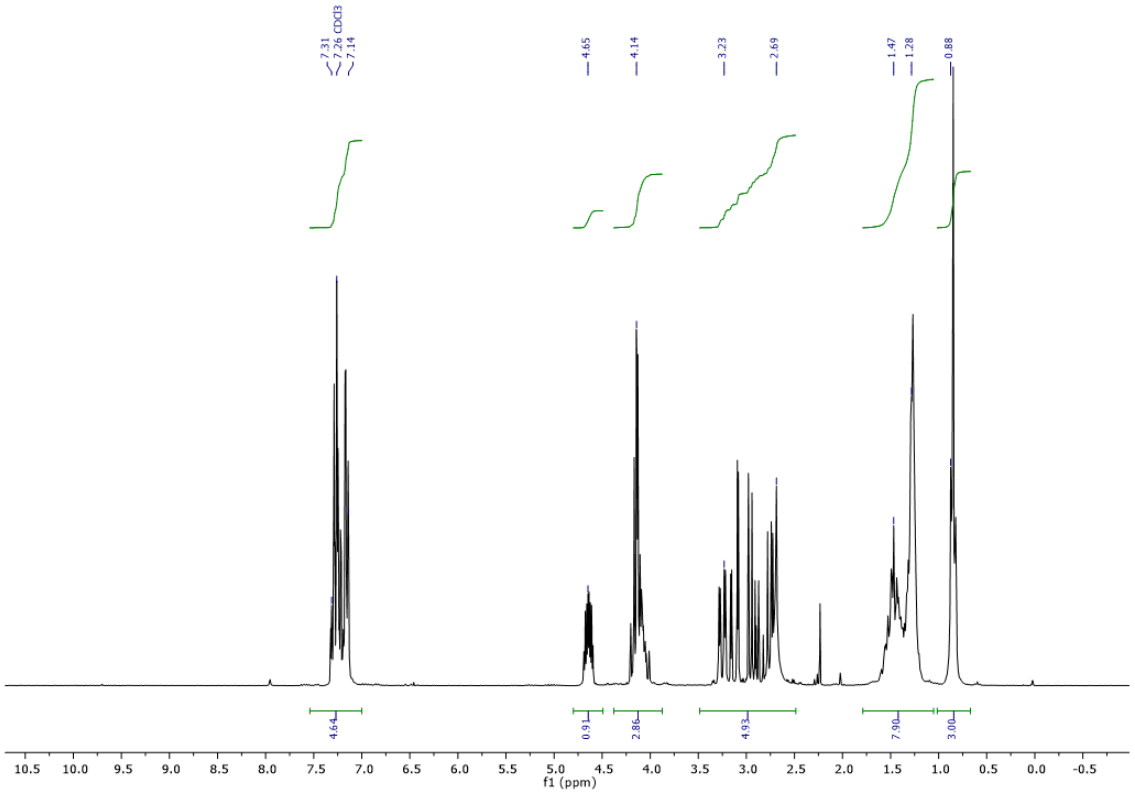

Supporting Figure 13: 4-Benzy-3-3-hydroxyoctanoyl-2-oxazolidinone (^{1}H NMR spectra in $CDCl_3$, 250 MHz)

^{1}H NMR (250 MHz, $CDCl_3$) δ 7.43 – 7.04 (m, 5H), 4.64 (ddt, *J* = 9.4, 6.9, 3.4 Hz, 1H), 4.37 – 3.92 (m, 3H), 3.46 – 2.48 (m, 5H), 1.72 – 1.11 (m, 8H), 0.99 – 0.72 (m, 3H).

(*S*)-3-Hydroxyoctanoic acid

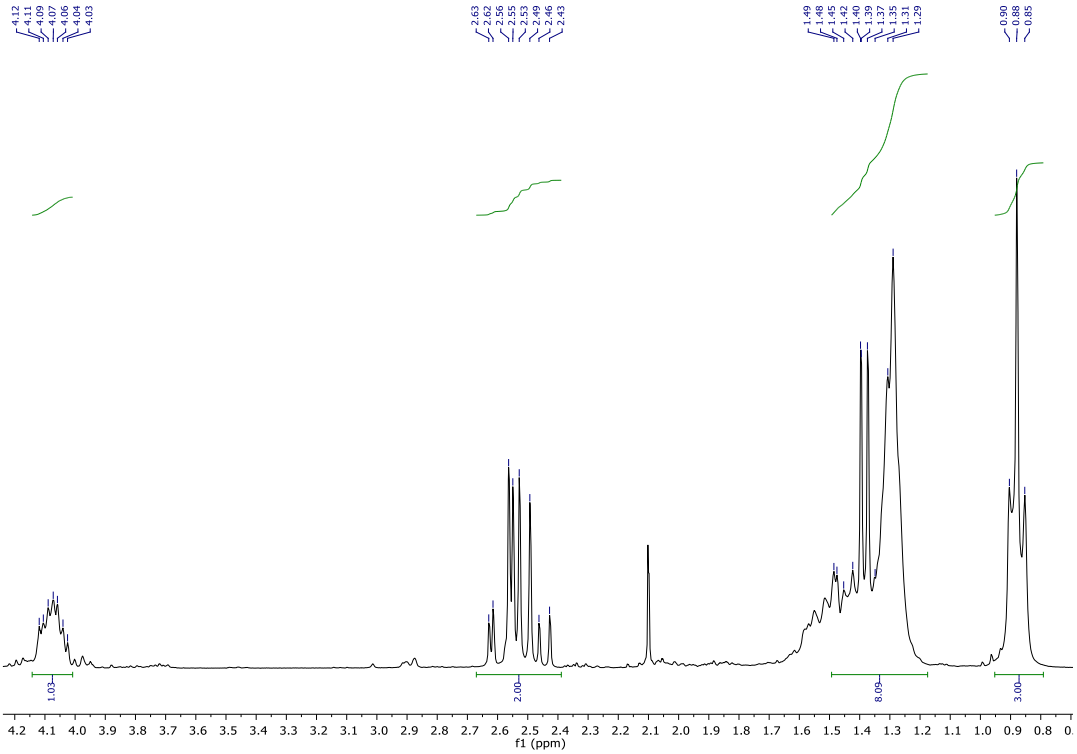

(*R*)-3-Hydroxyoctanoic acid

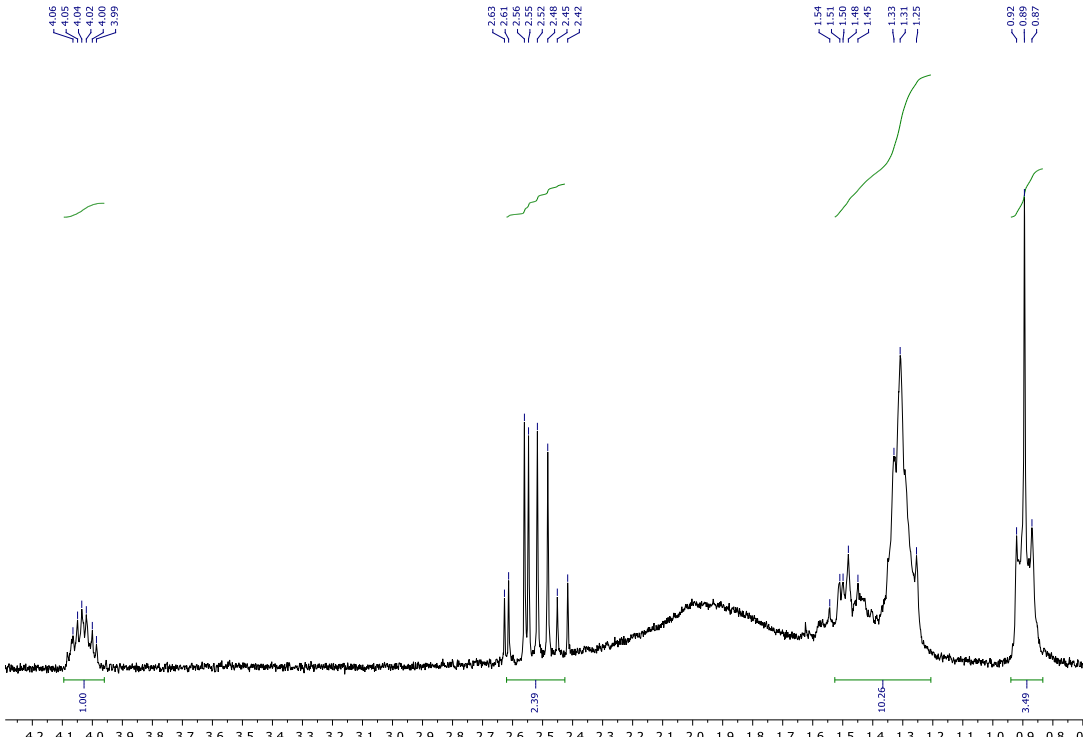

Supporting Figure 14: ^{1}H NMR spectra from chiral 3-hydroxyoctanoic acid. (solvent $CDCl_3$, 250 MHz Bruker)

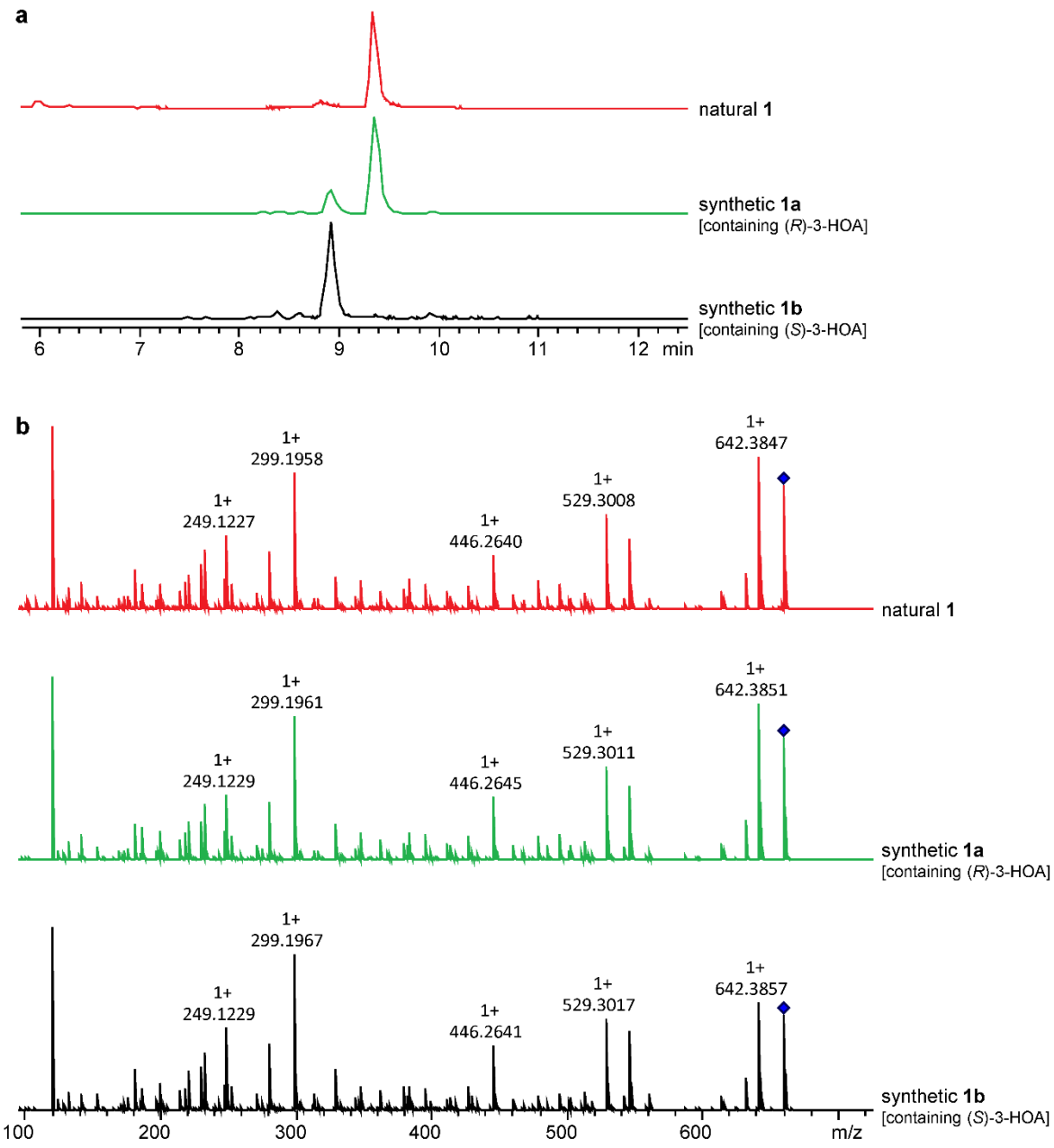

Supporting Figure 15: HPLC-MS runs from phototemtide A with (*R*)- and (*S*)-3-hydroxyoctanoic acid. a) Retention time and b) fragmentation of the natural phototemtide A (1) product vs synthetic products.

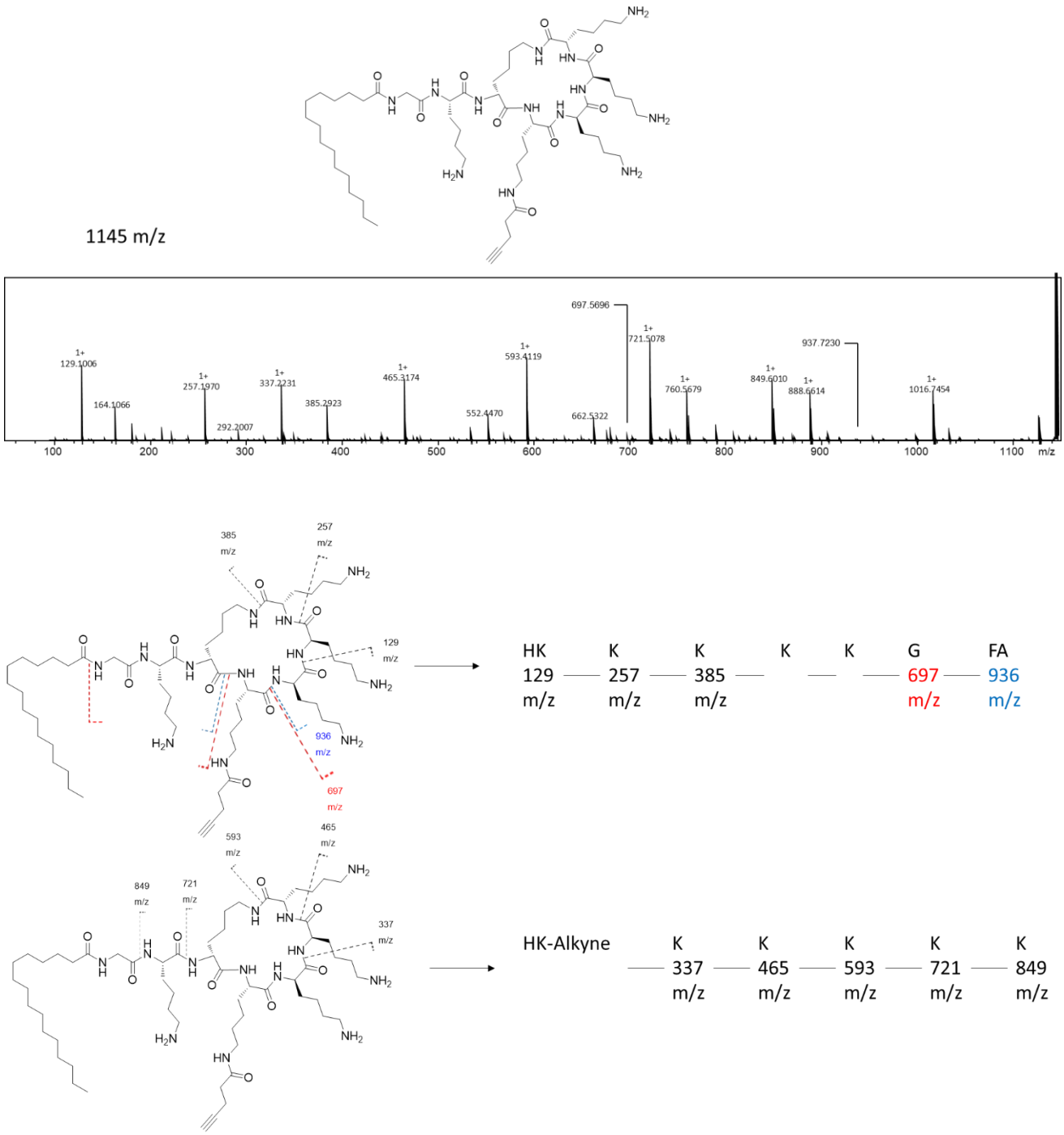

Supporting Figure 16: Fragmentation of a selected alkyne-PAX derivative.

Quantification *pax*⁺ mutant

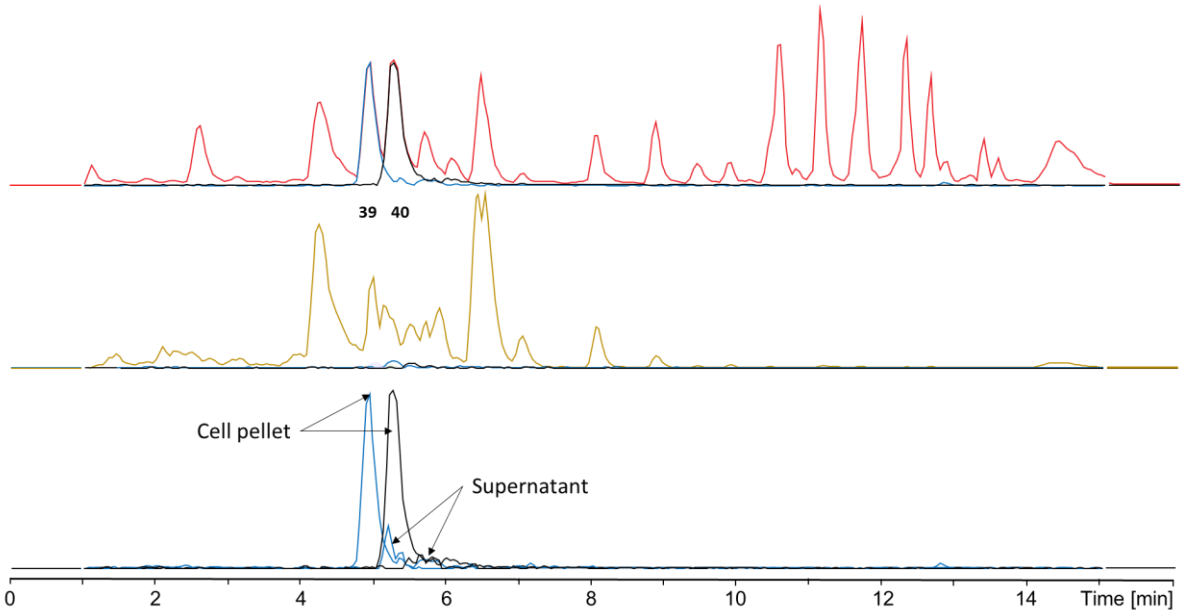

Supporting Figure 17: HPLC/MS chromatograms for the quantification of PAX derivatives produced by the *X. doucetiae* pax⁺ strain after induction with 0.2% arabinose. BPC of the cell pellet (top panel) and supernatant fractions (middle panel) are shown including the peaks assigned to derivative **39** and **40**. The bottom panel compares the extracted ion chromatograms (EIC) of both derivatives for the respective fractions.

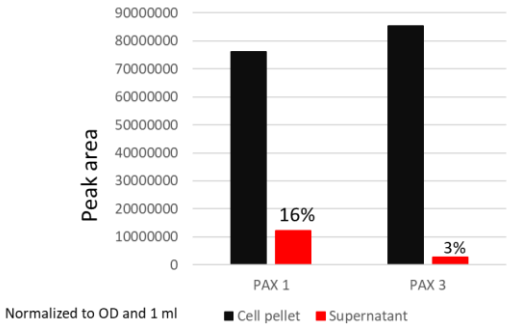

Overlap cell pellet and supernatant

	RT	Chromatogram	Area	S/N
PAX 1	5	EIC 263.87±0.2 +All MS	1713823616	443.8
	5.2	EIC 264.11±0.2 +All MS	274492896	69.9
PAX 3	5.3	EIC 267.38±0.2 +All MS	1918884096	359.5
	5.5	EIC 267.40±0.2 +All MS	60467952	22.03

-> 84-97% of PAX molecules are bound to the cell and not in the supernatant

Supporting Figure 18: Relative quantification of **39** and **40** in cell pellet and supernatant fractions. Most PAX peptides were found at the cell pellet. (PAX 1 = **39**, PAX 3 = **40**)

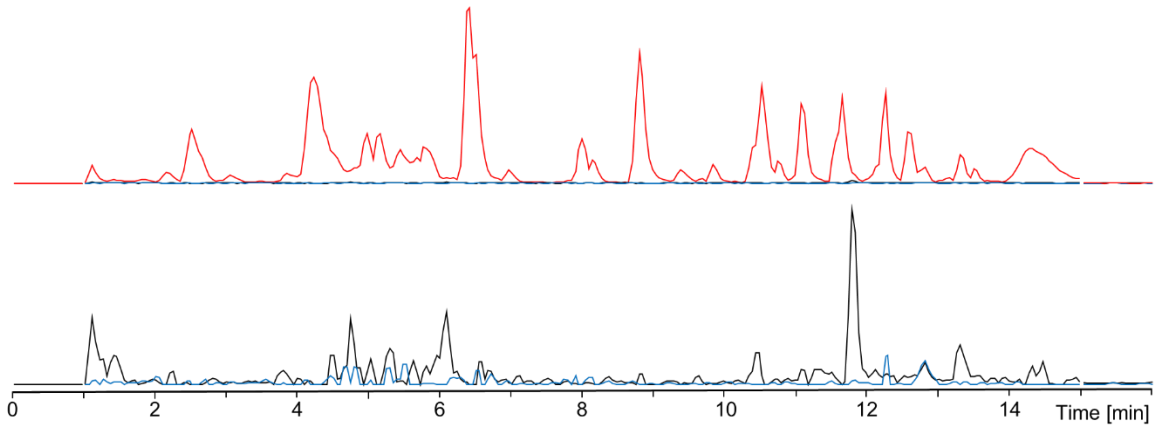

39 (blue) EIC 263.88
40 (black) EIC 356.22

Supporting Figure 19: HPLC/MS chromatograms for the quantification of PAX derivatives produced by the *X. doucetiae* pax$^-$ strain. BPC from pax$^-$ cell pellet (red, top), overlaid with the EICs of **1** (blue) and **2** (black). In the bottom panel, a magnified view of the EICs of **1** and **2** alone is shown (Intensity EIC/BPC ratio = 0.01). Only noise can be detected for both derivatives.

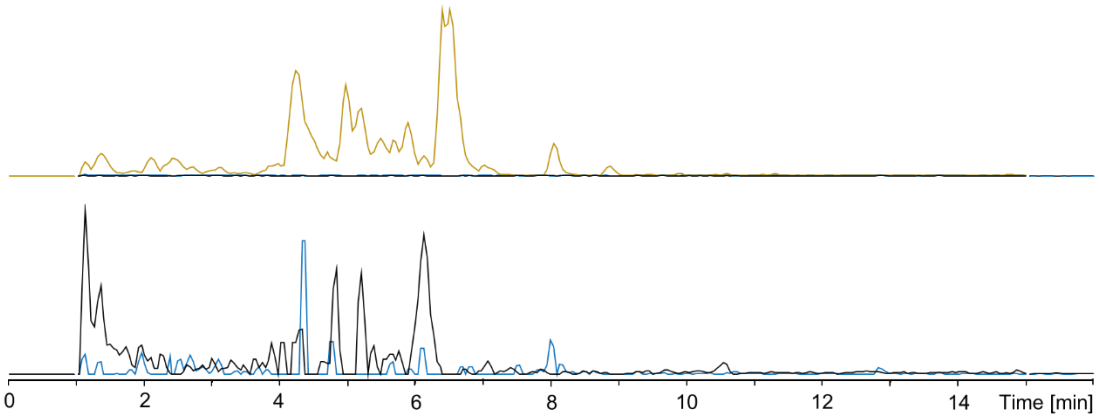

39 (blue) EIC 263.88
40 (black) EIC 356.22

Supporting Figure 20: HPLC/MS chromatograms for the quantification of PAX derivatives produced by the *X. doucetiae* pax$^-$ strain. BPC from pax$^-$ supernatant (golden, top), overlaid with the EICs of **39** (blue) and 40 (black). In the bottom panel, a magnified view of the EICs of **39** and 40 alone is shown (Intensity EIC/BPC ratio = 0.01). Only noise can be detected for both derivatives.

Bioactivity tests

Plate diffusion

Number	1	2	3	4	5	6	7
Compound	36	34	35	37	31	32	33

Supporting table 1: Numbering of PAX peptides used in plate diffusion tests.

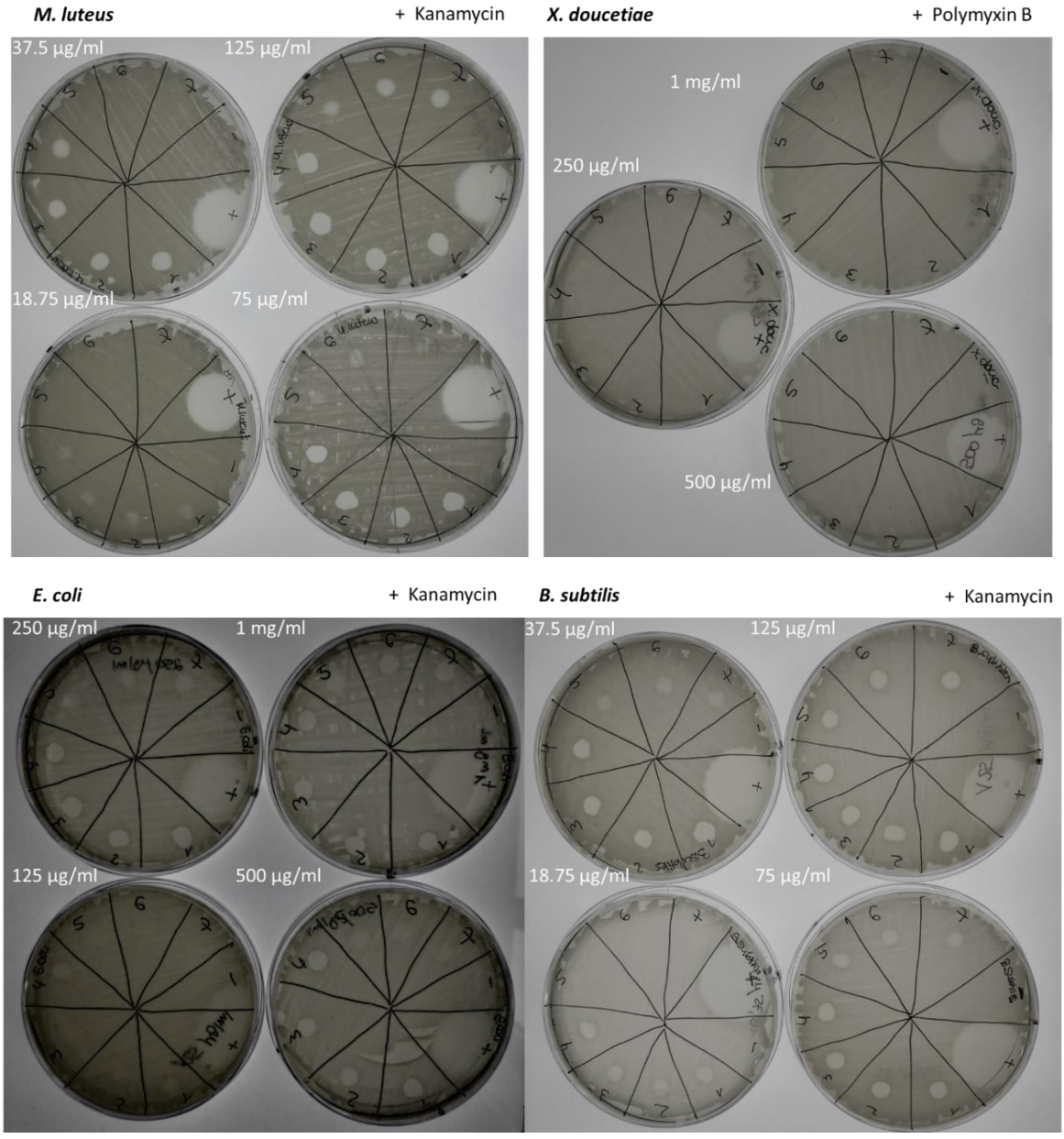

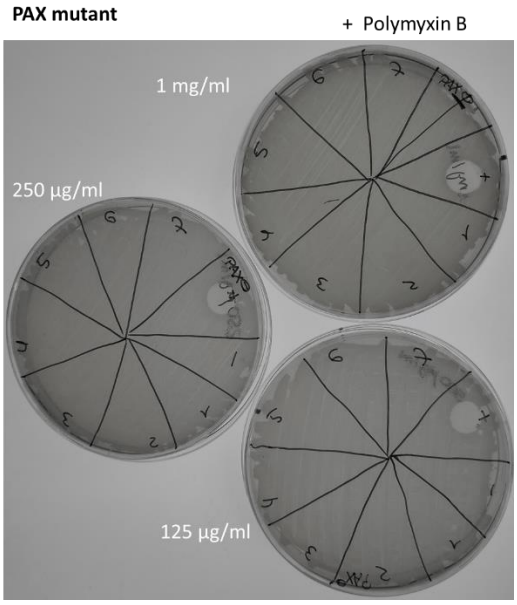

Supporting Figure 21: Plate diffusion assay of different PAX derivatives. The newer PAX derivatives **36** and **37** (with palmitic acid tail) showed higher bioactivity than derivatives with 3-hydroxy-fatty acid. No toxicity was detected towards the *pax*$^{-}$ mutant.

Broth microdilution assays

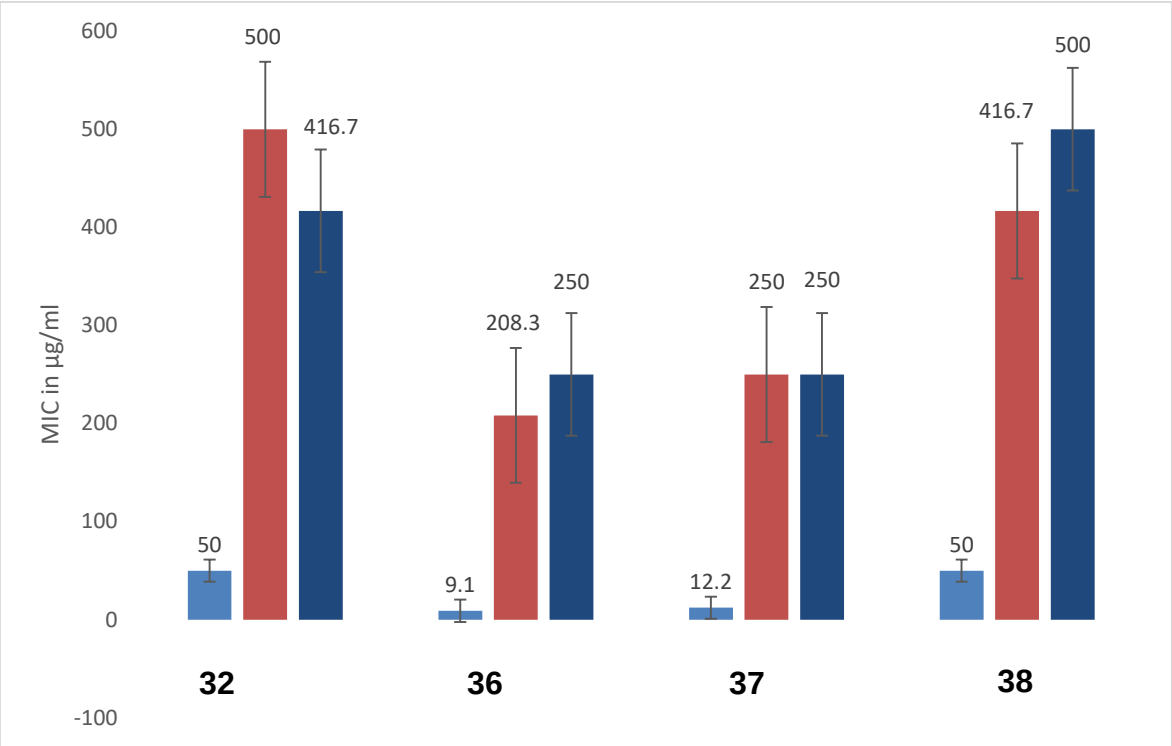

Supporting Figure 22: Broth microdilution bioactivity tests from different PAX derivatives. The new **37**,**36** PAX peptides (azido and alkyne modifications with palmitic residues), WT PAX **38,** and **32** (azido modification) were tested against *E. coli* (light blue), *X. doucetiae* (red) and the *pax*$^{-}$ mutant (dark blue). Here, **37** and **36** showed increased activity when compared with **38** and **32**. Furthermore, activity against *E. coli* was higher than *X. doucetiae* and the *pax*$^{-}$ mutant.

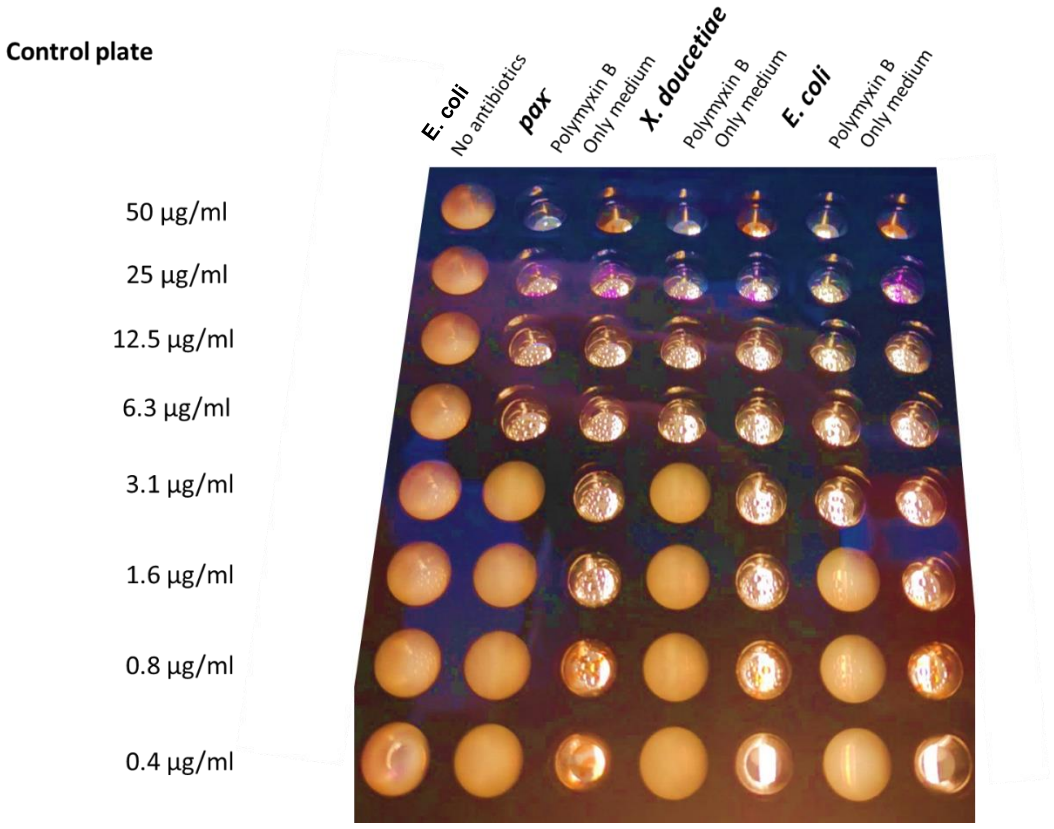

Supporting Figure 23: Control plate with *X. doucetiae*, *E. coli,* and *pax*$^{-}$ mutant. In the control plate, *E. coli*, pax^{-} and *X. doucetiae* were tested against polymyxin B. Here, *E. coli* also showed higher sensitivity towards the antibiotic.

Supporting table 2: Up- and downregulated proteins in *X. szentirmaii* (≥ 2-fold and Welch's t-test p ≤ 0.05).

Fasta headers	x-fold up- or downregulated
Xszus_02891 deoxyuridine 5-triphosphate nucleotidohydrolase [Brucella abortus 2308]	88470001
Xszus_00148 tail component	75696001
Xszus_03725 (Rv1837c) malate synthase G [Fibronectin-binding protein (AI169)] [Mycobacterium tuberculosis H37Rv]	57547001
Xszus_02640 tRNA delta(2)-isopentenyl-pyrophosphate transferase [Shigella sonnei Ss046]	56083001
Xszus_02143 phosphoribosylaminoimidazole carboxylase catalytic subunit [Francisella tularensis subsp. tularensis SCHU S4]	50050001
Xszus_04102 hypothetical protein	47473001
Xszus_04095 hypothetical protein	39311201
Xszus_02890 pantothenate metabolism flavoprotein [Listeria monocytogenes EGD-e]	26693401
Xszus_02343 (mrxG) Fimbrial adaptor, MrxG [Mrx fimbriae (AI077)] [Xenorhabdus nematophila ATCC]	25037101
Xszus_00702 hypothetical protein	19739801
Xszus_00143 hypothetical protein	18401401
Xszus_00133 (yplA) phospholipase A [YplA (CVF053)] [Yersinia enterocolitica subsp. enterocolitica 8081]	17949301
Xszus_00129 NAD(+) kinase	17015201
Xszus_03878 tautomerase	16278101
Xszus_03856 hypothetical protein	15167401
Xszus_02967 restriction endonuclease subunit R	14743801
Xszus_03951 cysteine synthase [Streptococcus pneumoniae TIGR4]	14644101
Xszus_00325 ribosomal protein L3 N(5)-glutamine methyltransferase	13809801
Xszus_03821 sulfite reductase [Mycobacterium tuberculosis H37Rv]	13332001
Xszus_03363 (vctA) putaive Fe-regulated protein B precursor [Enterobactin receptors (CVF277)] [Vibrio parahaemolyticus RIMD]	12762501
Xszus_00432 (cadF) outer membrane fibronectin -binding protein [CadF (CVF389)] [Campylobacter fetus subsp. fetus 82-40]	11745301

Xszus_02871 (cpsF) Glycosyltransferase [Capsular polysaccharide (CVF282)] [Vibrio vulnificus CMCP6]	10887401
Xszus_01826 hypothetical protein	10332101
Xszus_00343 aspartate semialdehyde dehydrogenase [Staphylococcus aureus subsp. aureus N315]	7879101
Xszus_01327 hypothetical protein	5760201
Xszus_00074 major tail tube protein	4681801
Xszus_00224 (fleR/flrC) sigma 54-dependent response regulator [polar flagella (AI149)] [Legionella pneumophila subsp. pneumophila str. Philadelphia 1]	3635301
Xszus_01504 (msbA) fused lipid transporter subunits of ABC superfamily: membrane component/ATP-binding component [LOS (CVF494)] [Haemophilus influenzae PittEE]	2614811
Xszus_01852 (pdtorfO) putative acyl-CoA dehydrogenase [Pyridine-2,6-dithiocarboxylic acid (PDTC) (IA030)] [Pseudomonas stutzeri KC]	255.95
Xszus_03726 (icl) Isocitrate lyase Icl (isocitrase) (isocitratase) [Isocitrate lyase (VF0253)] [Mycobacterium tuberculosis H37Rv]	30.86
Xszus_03497 NADPH-dependent 2,4 -dienoyl-CoA reductase	17.29
Xszus_00316 (icl) isocitrate lyase [Isocitrate lyase (CVF302)] [Mycobacterium tuberculosis RGTB423]	9.89
Xszus_03802 acetyl-CoA acetyltransferase FadA [Mycobacterium tuberculosis H37Rv]	7.95
Xszus_00817 dethiobiotin synthetase [Francisella tularensis subsp. tularensis SCHU S4]	7.54
Xszus_03350 phosphoribosylamine--glycine ligase [Salmonella enterica subsp. enterica serovar Typhimurium str. LT2]	6.87
Xszus_02144 phosphoribosylaminoimidazole carboxylase ATPase subunit [Yersinia pestis biovar Microtus str.]	6.32
Xszus_01230 amino acid transporter [Francisella tularensis subsp. tularensis SCHU S4]	5.69
Xszus_03290 Transcriptional regulator DauR	5.42
Xszus_02530 amino acid ABC transporter ATP-binding protein PEB1 [Campylobacter jejuni subsp. doylei 269.97]	5.20
Xszus_03803 (clbD) putative 3-hydroxyacyl-CoA dehydrogenase [colibactin (TX033)] [Escherichia coli O18:K1:H7 str.]	5.19
Xszus_04097 hypothetical protein	5.11
Xszus_02769 50S ribosomal protein L23 [Francisella tularensis subsp. tularensis SCHU S4]	5.11

Xszus_01159 phosphomethylpyrimidine kinase [Streptococcus pneumoniae TIGR4]	5.02
Xszus_03282 LysR family transcriptional regulator [Streptococcus pneumoniae TIGR4]	4.34
Xszus_00906 (msrA/B(pilB)) peptide methionine sulfoxide reductase MsrA/MsrB [includes: thioredoxin, peptide methionine sulfoxide reductase MsrA (protein-methionine-S-oxide reductase;peptide Met(O) reductase) and peptide methio [Methionine sulphoxide reduc	4.24
Xszus_03763 hypothetical protein	3.69
Xszus_01707 (fur) transcriptional repressor of iron-responsive genes (Fur family) (ferric uptake regulator) [Fur (VF0113)] [Salmonella enterica subsp. enterica serovar Typhimurium str. LT2]	3.64
Xszus_00315 acetyl-CoA acetyltransferase [Mycobacterium tuberculosis H37Rv]	3.63
Xszus_03041 hypothetical protein [Listeria monocytogenes EGD-e]	3.53
Xszus_02760 50S ribosomal protein L24	3.46
Xszus_03107 glycerol-3-phosphate regulon repressor [Brucella melitensis bv. 1 str. 16M]	3.26
Xszus_02342 (mrxH) Fimbrial adhesin, MrxH [Mrx fimbriae (AI077)] [Xenorhabdus nematophila ATCC]	3.15
Xszus_04101 hypothetical protein	2.99
Xszus_00763 hypothetical protein	2.99
Xszus_00556 structural protein	2.84
Xszus_04113 phage tail protein	2.66
Xszus_03351 bifunctional phosphoribosylaminoimidazolecarboxamide formyltransferase/IMP cyclohydrolase [Yersinia pestis biovar Microtus str.]	2.63
Xszus_03195 (AHA_1832) hypothetical protein [T6SS (SS194)] [Aeromonas hydrophila subsp. hydrophila ATCC 7966]	2.38
Xszus_00539 hypothetical protein	2.34
Xszus_00219 phosphoribosylformylglycinamidine synthase [Vibrio cholerae M66-2]	2.31
Xszus_00757 universal stress protein UspE	2.23
Xszus_00394 acetate kinase [Vibrio cholerae O1 biovar El Tor str.]	2.19
Xszus_02828 glycerol kinase [Brucella suis 1330]	2.11
Xszus_04133 CoA-transferase subunit alpha [Mycobacterium tuberculosis H37Rv]	2.00

Xszus_00604 (STM0570) outer membrane esterase [ApeE (SS104)] [Salmonella enterica subsp. enterica serovar Typhimurium str. LT2]	0.49
Xszus_04006 isopropylmalate isomerase large subunit [Brucella melitensis bv. 1 str. 16M]	0.47
Xszus_00726 (ascF) diaminobutyrate--2-oxoglutarate aminotransferase [achromobactin (IA003)] [Pseudomonas syringae pv. syringae B728a]	0.45
Xszus_01758 cold shock-like protein cspE [Salmonella enterica subsp. enterica serovar Typhimurium str.]	0.39
Xszus_02915 (BJAB0715_01028) hypothetical protein [Heme utilization (CVF769)] [Acinetobacter baumannii]	0.34
Xszus_00724 oxidoreductase [Salmonella enterica subsp. enterica serovar Typhimurium str. LT2]	0.33
Xszus_00461 (cblR) two-component regulatory system response regulator protein [cable pilus (AI081)] [Burkholderia cenocepacia]	0.16
Xszus_03312 (sugC) Putative sugar-transport ATP-binding protein ABC transporter SugC [Trehalose-recycling ABC transporter (CVF651)] [Mycobacterium canettii CIPT]	9.59E-08
Xszus_02596 hypothetical protein	9.13E-08
Xszus_01676 (clbK) putative hybrid non-ribosomal peptide-polyketide synthetase [colibactin (TX033)] [Escherichia coli O18:K1:H7 str.]	8.18E-08
Xszus_02332 4-hydroxy-3-methylbut-2-enyl diphosphate reductase	8.12E-08
Xszus_01437 cold shock-like protein CspC [Salmonella enterica subsp. enterica serovar Typhimurium str. LT2]	7.57E-09

Supporting table 3: Up- and downregulated proteins in X. nematophila (≥ 2-fold and Welch's t-test p ≤ 0.05)

Fasta headers	X-fold up- or downregulated
WP_010847402.1 hypothetical protein [Xenorhabdus nematophila]	28512401
WP_010845405.1 methylisocitrate lyase [Xenorhabdus nematophila]	11326401
WP_013183404.1 lipoprotein ABC transporter ATP-binding protein [Xenorhabdus nematophila]	10153601
WP_010847781.1 LysR family transcriptional regulator [Xenorhabdus nematophila]	6266301
WP_012989080.1 MULTISPECIES: hemolysin co-regulated protein (Hcp-like) [Xenorhabdus]	5036601
WP_038219546.1 MULTISPECIES: hypothetical protein [Xenorhabdus]	4879501
WP_013183635.1 16S rRNA (cytosine(1402)-N(4))-methyltransferase [Xenorhabdus nematophila]	2176031
WP_013183538.1 nucleoside triphosphate pyrophosphohydrolase [Xenorhabdus nematophila]	413101
WP_010846618.1 acyl-CoA dehydrogenase [Xenorhabdus nematophila]	15.65
WP_010845205.1 ribosome-binding factor A [Xenorhabdus nematophila]	9.48
WP_013185720.1 hemolysin activation protein [Xenorhabdus nematophila]	6.36
WP_013141541.1 MULTISPECIES: hypothetical protein [Enterobacterales]	4.81
WP_013184888.1 multifunctional fatty acid oxidation complex subunit alpha [Xenorhabdus nematophila]	4.79
WP_010847478.1 MULTISPECIES: 50S ribosomal protein L23 [Xenorhabdus]	4.66
WP_010847629.1 MULTISPECIES: 50S ribosomal protein L33 [Morganellaceae]	4.48
WP_013185584.1 maltose ABC transporter substrate-binding protein MalE [Xenorhabdus nematophila]	4.21
WP_013183683.1 precorrin-8X methylmutase [Xenorhabdus nematophila]	3.27
WP_010847752.1 hypothetical protein [Xenorhabdus nematophila]	3.23
WP_013183679.1 uroporphyrinogen-III C-methyltransferase [Xenorhabdus nematophila]	3.16
WP_013183180.1 homocitrate synthase [Xenorhabdus nematophila]	3.10
WP_013185580.1 maltodextrin phosphorylase [Xenorhabdus nematophila]	2.85

WP_041573727.1 acetyl-CoA C-acyltransferase FadI [Xenorhabdus nematophila]	2.85
WP_010845472.1 cobalt-precorrin-7 (C(5))-methyltransferase [Xenorhabdus nematophila]	2.68
WP_010845467.1 cobalt-precorrin-6A reductase [Xenorhabdus nematophila]	2.48
WP_013184367.1 alkene reductase [Xenorhabdus nematophila]	2.44
WP_013185341.1 multifunctional fatty acid oxidation complex subunit alpha [Xenorhabdus nematophila]	2.40
WP_013185281.1 ketoacyl-ACP synthase III [Xenorhabdus nematophila]	2.31
WP_010848907.1 type VI secretion-associated protein [Xenorhabdus nematophila]	2.27
WP_013183595.1 thioesterase [Xenorhabdus nematophila]	2.25
WP_013183065.1 receptor protein [Xenorhabdus nematophila]	2.22
WP_010847939.1 pyroglutamyl-peptidase I [Xenorhabdus nematophila]	2.20
WP_010846008.1 hypothetical protein [Xenorhabdus nematophila]	2.04
WP_013183724.1 hypothetical protein [Xenorhabdus nematophila]	2.04
WP_013185453.1 thymidylate synthase [Xenorhabdus nematophila]	2.02
WP_038219458.1 malate synthase A [Xenorhabdus nematophila]	2.01
WP_010848783.1 isocitrate lyase [Xenorhabdus nematophila]	2.00
WP_010846889.1 cold shock domain protein CspD [Xenorhabdus nematophila]	0.49
WP_010846945.1 beta-hydroxydecanoyl-ACP dehydratase [Xenorhabdus nematophila]	0.48
WP_013183786.1 lipoyl synthase [Xenorhabdus nematophila]	0.48
WP_013184935.1 Colicin-E6 [Xenorhabdus nematophila]	0.45
WP_010848534.1 N-acetylpuromycin N-acetylhydrolase [Xenorhabdus nematophila]	0.45
WP_013184269.1 hypothetical protein [Xenorhabdus nematophila]	0.44
WP_013184257.1 autotransporter domain-containing esterase [Xenorhabdus nematophila]	0.44

WP_010845455.1 methionine-rich PixA inclusion body protein [Xenorhabdus nematophila]	0.42
WP_013184219.1 hypothetical protein [Xenorhabdus nematophila]	0.41
WP_010847168.1 ferredoxin, 2Fe-2S type, ISC system [Xenorhabdus nematophila]	0.40
WP_013183082.1 sulfate transporter subunit [Xenorhabdus nematophila]	0.37
WP_013184445.1 hypothetical protein [Xenorhabdus nematophila]	0.35
WP_013185657.1 cysteine ABC transporter substrate-binding protein [Xenorhabdus nematophila]	0.31
WP_013184956.1 Fe-S assembly protein IscX [Xenorhabdus nematophila]	0.25
WP_013184984.1 hypothetical protein [Xenorhabdus nematophila]	0.15
WP_010848009.1 phosphoglycerate mutase [Xenorhabdus nematophila]	0.14
WP_013184302.1 adenylosuccinate synthetase [Xenorhabdus nematophila]	1.91E-06
WP_010845068.1 prephenate dehydrogenase [Xenorhabdus nematophila]	7.50E-07
WP_038219718.1 cell division protein FtsQ [Xenorhabdus nematophila]	5.56E-07
WP_013184815.1 phage capsid protein [Xenorhabdus nematophila]	5.10E-07
WP_010847620.1 3-deoxy-D-manno-octulosonic acid transferase [Xenorhabdus nematophila]	4.67E-07
WP_038220023.1 hypothetical protein [Xenorhabdus nematophila]	3.37E-07
WP_010848681.1 hypothetical protein [Xenorhabdus nematophila]	3.28E-07
WP_013183567.1 short-chain dehydrogenase/reductase [Xenorhabdus nematophila]	3.20E-07
WP_013183127.1 glycosyl transferase family 1 [Xenorhabdus nematophila]	3.03E-07
WP_038218921.1 protein TolA [Xenorhabdus nematophila]	2.84E-07
WP_013185300.1 bifunctional riboflavin kinase/FMN adenylyltransferase [Xenorhabdus nematophila]	2.60E-07
WP_010845323.1 UDP-N-acetylglucosamine 2-epimerase (non-hydrolyzing) [Xenorhabdus nematophila]	2.56E-07
WP_010848454.1 DNA helicase RecG [Xenorhabdus nematophila]	2.45E-07

WP_013184782.1 diaminopimelate decarboxylase [Xenorhabdus nematophila]	2.41E-07
WP_013183561.1 cysteine--tRNA ligase [Xenorhabdus nematophila]	2.15E-07
WP_013183888.1 hypothetical protein [Xenorhabdus nematophila]	1.95E-07
WP_013184544.1 envelope stress response membrane protein PspC [Xenorhabdus nematophila]	1.95E-07
WP_010848131.1 CoA-binding protein [Xenorhabdus nematophila]	1.72E-07
WP_010846312.1 patatin family protein [Xenorhabdus nematophila]	1.51E-07
WP_010846688.1 beta-ketoacyl-[acyl-carrier-protein] synthase II [Xenorhabdus nematophila]	1.45E-07
WP_013184327.1 hypothetical protein [Xenorhabdus nematophila]	1.35E-07
WP_010847798.1 UDP-N-acetylenolpyruvoylglucosamine reductase [Xenorhabdus nematophila]	1.30E-07
WP_010847351.1 fructosamine kinase family protein [Xenorhabdus nematophila]	1.29E-07
WP_013184663.1 bifunctional 3-demethylubiquinone 3-O-methyltransferase/2-octaprenyl-6-hydroxy phenol methylase [Xenorhabdus nematophila]	1.27E-07
WP_010845615.1 sulfate adenylyltransferase subunit 2 [Xenorhabdus nematophila]	1.26E-07
WP_010846023.1 peptide ABC transporter permease [Xenorhabdus nematophila]	1.16E-07
WP_071827907.1 ribonuclease P protein component [Xenorhabdus nematophila]	1.08E-07
WP_010845581.1 cystathionine beta-lyase [Xenorhabdus nematophila]	9.91E-08
WP_010848270.1 hypothetical protein [Xenorhabdus nematophila]	7.69E-08
WP_013185535.1 hypothetical protein [Xenorhabdus nematophila]	5.73E-08
WP_010847392.1 helix-turn-helix transcriptional regulator [Xenorhabdus nematophila]	5.08E-08
WP_010848038.1 cytochrome-c oxidase [Xenorhabdus nematophila]	4.44E-08

Supporting table 4: Up- and downregulated proteins in *P. luminescens* (≥ 2-fold and Welch's t-test p ≤ 0.05)

Fasta headers	X-fold up- or downregulated
WP_011144748.1 type VI secretion system membrane subunit TssM [Photorhabdus luminescens];WP_011144729.1 type VI secretion system membrane subunit TssM [Photorhabdus luminescens]	29028201
WP_011147742.1 aminodeoxychorismate synthase, component I [Photorhabdus luminescens]	10947901
WP_011146954.1 hypothetical protein [Photorhabdus luminescens]	9482001
WP_011144439.1 tail protein X [Photorhabdus luminescens]	4444301
WP_011145942.1 hypothetical protein [Photorhabdus luminescens]	1192061
WP_011145519.1 acyl-CoA dehydrogenase [Photorhabdus luminescens]	73.70
WP_011146180.1 flagellar hook protein FlgE [Photorhabdus luminescens]	21.21
WP_011147977.1 TonB-dependent receptor [Photorhabdus luminescens]	11.34
WP_011148069.1 glycoside hydrolase family 39 [Photorhabdus luminescens]	11.08
WP_011146008.1 phage tail protein [Photorhabdus luminescens]	8.89
WP_011147407.1 fatty acid oxidation complex subunit alpha FadJ [Photorhabdus luminescens]	8.40
WP_011148485.1 isocitrate lyase [Photorhabdus luminescens]	7.14
WP_011144998.1 prolipoprotein diacylglyceryl transferase [Photorhabdus luminescens]	7.07
WP_011145280.1 cysteine desulfurase [Photorhabdus luminescens]	6.18
WP_011147308.1 pyridoxal phosphate-dependent aminotransferase [Photorhabdus luminescens]	6.08
WP_011148476.1 hypothetical protein [Photorhabdus luminescens]	5.59
WP_011147982.1 prephenate dehydrogenase [Photorhabdus luminescens]	5.56
WP_011148492.1 fatty acid oxidation complex subunit alpha FadB [Photorhabdus luminescens]	5.48
WP_011146216.1 flagellin FliC [Photorhabdus luminescens]	5.19
WP_011144567.1 hypothetical protein [Photorhabdus luminescens]	5.18
WP_041380011.1 lipase [Photorhabdus luminescens]	5.01
WP_011148493.1 acetyl-CoA C-acyltransferase FadA [Photorhabdus luminescens]	4.97

WP_011147746.1 FAD-dependent oxidoreductase [Photorhabdus luminescens]	4.88
WP_011146012.1 phage tail protein [Photorhabdus luminescens];WP_011145973.1 phage tail protein [Photorhabdus luminescens]	4.80
WP_011144856.1 maltodextrin phosphorylase [Photorhabdus luminescens]	4.70
WP_011148093.1 type II toxin-antitoxin system RelE/ParE family toxin [Photorhabdus luminescens]	4.58
WP_011147519.1 hypothetical protein [Photorhabdus luminescens]	4.32
WP_041380111.1 2,3-dihydro-2,3-dihydroxybenzoate dehydrogenase [Photorhabdus luminescens]	4.31
WP_011145997.1 DUF4255 domain-containing protein [Photorhabdus luminescens]	4.30
WP_041380178.1 aminotransferase class V-fold PLP-dependent enzyme [Photorhabdus luminescens]	4.30
WP_011146351.1 hypothetical protein [Photorhabdus luminescens]	4.15
WP_011145995.1 hypothetical protein [Photorhabdus luminescens]	4.15
WP_011147408.1 acetyl-CoA C-acyltransferase FadI [Photorhabdus luminescens]	4.14
WP_011147070.1 ligand-gated channel protein [Photorhabdus luminescens]	4.14
WP_011146067.1 hypothetical protein [Photorhabdus luminescens]	4.12
WP_049789826.1 phage baseplate protein [Photorhabdus luminescens]	4.10
WP_041380029.1 phage tail sheath family protein [Photorhabdus luminescens]	4.05
WP_011145059.1 beta-hydroxyacyl-ACP dehydratase [Photorhabdus luminescens]	4.05
WP_011148870.1 DegT/DnrJ/EryC1/StrS family aminotransferase [Photorhabdus luminescens]	4.03
WP_011146001.1 hypothetical protein [Photorhabdus luminescens]	3.99
WP_041381227.1 TonB-dependent siderophore receptor [Photorhabdus luminescens]	3.94
WP_011144435.1 phage tail protein I [Photorhabdus luminescens]	3.91
WP_011144511.1 DUF3372 domain-containing protein [Photorhabdus luminescens]	3.87

WP_011144992.1 RNA polymerase-associated protein RapA [Photorhabdus luminescens]	3.84
WP_011145905.1 formate C-acetyltransferase [Photorhabdus luminescens]	3.83
WP_011144564.1 hypothetical protein [Photorhabdus luminescens]	3.70
WP_011148339.1 hypothetical protein [Photorhabdus luminescens]	3.59
WP_011147182.1 hypothetical protein [Photorhabdus luminescens]	3.46
WP_041381054.1 TonB-dependent copper receptor [Photorhabdus luminescens]	3.33
WP_011147178.1 hypothetical protein [Photorhabdus luminescens]	3.30
WP_011146005.1 hypothetical protein [Photorhabdus luminescens]	3.28
WP_011146002.1 hypothetical protein [Photorhabdus luminescens]	3.27
WP_011145138.1 hypothetical protein [Photorhabdus luminescens]	3.21
WP_011146003.1 hypothetical protein [Photorhabdus luminescens]	3.20
WP_011146212.1 DUF2829 domain-containing protein [Photorhabdus luminescens]	3.20
WP_011146802.1 transcriptional regulator TyrR [Photorhabdus luminescens]	3.20
WP_011146030.1 porin OmpC [Photorhabdus luminescens]	3.06
WP_011144434.1 phage tail protein [Photorhabdus luminescens]	3.03
WP_011146000.1 hypothetical protein [Photorhabdus luminescens]	3.01
WP_011145779.1 molybdate ABC transporter substrate-binding protein [Photorhabdus luminescens]	3.01
WP_011147180.1 phage tail protein [Photorhabdus luminescens]	2.95
WP_011146413.1 fimbrial protein [Photorhabdus luminescens]	2.93
WP_011146484.1 histidine ammonia-lyase [Photorhabdus luminescens]	2.92
WP_011148478.1 hypothetical protein [Photorhabdus luminescens]	2.92
WP_011148294.1 hypothetical protein [Photorhabdus luminescens]	2.92
WP_011146272.1 helix-turn-helix transcriptional regulator [Photorhabdus luminescens]	2.91

WP_011148068.1 glycoside hydrolase family 39 [Photorhabdus luminescens]	2.85
WP_011145313.1 MarR family transcriptional regulator [Photorhabdus luminescens]	2.82
WP_011144436.1 phage baseplate protein [Photorhabdus luminescens]	2.81
WP_011145035.1 peptidase [Photorhabdus luminescens]	2.77
WP_011148480.1 hypothetical protein [Photorhabdus luminescens]	2.74
WP_041380240.1 hypothetical protein [Photorhabdus luminescens]	2.73
WP_011146013.1 hypothetical protein [Photorhabdus luminescens]	2.70
WP_011144422.1 late control protein D [Photorhabdus luminescens]	2.67
WP_011145523.1 NADH:ubiquinone reductase (Na(+)-transporting) subunit A [Photorhabdus luminescens]	2.62
WP_011146423.1 type II toxin-antitoxin system RelE/ParE family toxin [Photorhabdus luminescens]	2.61
WP_011148292.1 long-chain fatty acid--CoA ligase [Photorhabdus luminescens]	2.61
WP_011148122.1 NADPH-dependent 2,4-dienoyl-CoA reductase [Photorhabdus luminescens]	2.59
WP_011148867.1 UDP-N-acetylglucosamine 2-epimerase (non-hydrolyzing) [Photorhabdus luminescens]	2.57
WP_011146473.1 hypothetical protein [Photorhabdus luminescens]	2.56
WP_011146836.1 enoyl-CoA hydratase [Photorhabdus luminescens]	2.56
WP_011147948.1 5-(carboxyamino)imidazole ribonucleotide mutase [Photorhabdus luminescens]	2.54
WP_011145031.1 serralysin [Photorhabdus luminescens]	2.53
WP_011146664.1 alpha/beta hydrolase [Photorhabdus luminescens]	2.53
WP_011148336.1 hypothetical protein [Photorhabdus luminescens]	2.51
WP_011147944.1 hypothetical protein [Photorhabdus luminescens]	2.47
WP_011144776.1 hypothetical protein [Photorhabdus luminescens]	2.46
WP_011144844.1 maltose/maltodextrin ABC transporter substrate-binding protein MalE [Photorhabdus luminescens]	2.45
WP_011145160.1 fimbrial protein [Photorhabdus luminescens]	2.43

WP_011145759.1 hypothetical protein [Photorhabdus luminescens]	2.43
WP_011145239.1 pantoate--beta-alanine ligase [Photorhabdus luminescens]	2.43
WP_011148765.1 peptide deformylase [Photorhabdus luminescens]	2.42
WP_011147181.1 phage tail protein [Photorhabdus luminescens]	2.36
WP_011146892.1 non-ribosomal peptide synthetase [Photorhabdus luminescens]	2.35
WP_011148623.1 malate dehydrogenase [Photorhabdus luminescens]	2.34
WP_011147707.1 acylase [Photorhabdus luminescens]	2.33
WP_011148296.1 hypothetical protein [Photorhabdus luminescens]	2.32
WP_011146010.1 phage tail sheath family protein [Photorhabdus luminescens]	2.32
WP_011146558.1 TonB-dependent receptor [Photorhabdus luminescens]	2.31
WP_011146096.1 dihydroorotase [Photorhabdus luminescens]	2.30
WP_011147336.1 non-ribosomal peptide synthetase [Photorhabdus luminescens]	2.28
WP_011146937.1 oligopeptidase B [Photorhabdus luminescens]	2.24
WP_011144530.1 oligopeptidase A [Photorhabdus luminescens]	2.24
WP_011147219.1 trypsin [Photorhabdus luminescens]	2.22
WP_011148571.1 ornithine carbamoyltransferase [Photorhabdus luminescens]	2.20
WP_041380546.1 hypothetical protein [Photorhabdus luminescens]	2.19
WP_011146551.1 hypothetical protein [Photorhabdus luminescens]	2.17
WP_011147207.1 cobalt-factor II C(20)-methyltransferase [Photorhabdus luminescens]	2.15
WP_049789807.1 phosphoenolpyruvate synthase [Photorhabdus luminescens]	2.10
WP_011146398.1 heat-inducible protein [Photorhabdus luminescens]	2.09
WP_011148293.1 hypothetical protein [Photorhabdus luminescens]	2.09
WP_011148272.1 hypothetical protein [Photorhabdus luminescens]	2.09
WP_011148161.1 outer membrane lipid asymmetry maintenance protein MlaD [Photorhabdus luminescens]	2.09

WP_011147766.1 FAD-dependent 2-octaprenylphenol hydroxylase [Photorhabdus luminescens]	2.08
WP_011146776.1 signal peptide peptidase SppA [Photorhabdus luminescens]	2.05
WP_011145700.1 PTS glucose transporter subunit IIA [Photorhabdus luminescens]	2.03
WP_011146684.1 toxin [Photorhabdus luminescens]	2.03
WP_011146323.1 outer membrane lipoprotein LolB [Photorhabdus luminescens]	2.01
WP_011146848.1 FAD-binding oxidoreductase [Photorhabdus luminescens]	2.00
WP_011144454.1 ATP synthase subunit gamma [Photorhabdus luminescens]	0.50
WP_011148037.1 protein translocase subunit SecD [Photorhabdus luminescens]	0.50
WP_011145736.1 dihydrolipoyllysine-residue succinyltransferase [Photorhabdus luminescens]	0.50
WP_011148646.1 30S ribosomal protein S6 [Photorhabdus luminescens]	0.50
WP_011144818.1 elongation factor Tu [Photorhabdus luminescens]	0.50
WP_011148603.1 tRNA pseudouridine(55) synthase TruB [Photorhabdus luminescens]	0.50
WP_011145064.1 acetyl-CoA carboxylase carboxyl transferase subunit alpha [Photorhabdus luminescens]	0.49
WP_011148150.1 serine endoprotease DegQ [Photorhabdus luminescens]	0.49
WP_011144950.1 transaldolase [Photorhabdus luminescens]	0.49
WP_011146775.1 NAD(P)H nitroreductase [Photorhabdus luminescens]	0.49
WP_011148215.1 high-affinity branched-chain amino acid ABC transporter ATP-binding protein LivF [Photorhabdus luminescens]	0.48
WP_011146391.1 septum site-determining protein MinD [Photorhabdus luminescens]	0.48
WP_011144461.1 tRNA uridine-5-carboxymethylaminomethyl(34) synthesis enzyme MnmG [Photorhabdus luminescens]	0.48
WP_011144879.1 phosphoribosylamine--glycine ligase [Photorhabdus luminescens]	0.48
WP_011146669.1 hypothetical protein [Photorhabdus luminescens]	0.48
WP_011146690.1 tryptophan synthase subunit beta [Photorhabdus luminescens]	0.48
WP_011148733.1 transcription termination factor Rho [Photorhabdus luminescens]	0.48
WP_011146640.1 hypothetical protein [Photorhabdus luminescens]	0.47

WP_011148792.1 50S ribosomal protein L2 [Photorhabdus luminescens]	0.47
WP_011146586.1 ABC transporter substrate-binding protein [Photorhabdus luminescens]	0.47
WP_011146390.1 cell division topological specificity factor [Photorhabdus luminescens]	0.47
WP_011146073.1 type I-F CRISPR-associated endoribonuclease Cas6/Csy4 [Photorhabdus luminescens]	0.47
WP_011146510.1 hypothetical protein [Photorhabdus luminescens]	0.47
WP_011145338.1 4-hydroxyphenylacetate 3-monooxygenase, oxygenase component [Photorhabdus luminescens]	0.47
WP_011144821.1 MULTISPECIES: 50S ribosomal protein L11 [Photorhabdus]	0.47
WP_011145911.1 3-phosphoserine/phosphohydroxythreonine aminotransferase [Photorhabdus luminescens]	0.46
WP_011147324.1 N-succinylglutamate 5-semialdehyde dehydrogenase [Photorhabdus luminescens]	0.46
WP_011145738.1 succinate--CoA ligase subunit alpha [Photorhabdus luminescens]	0.46
WP_011148229.1 zinc/cadmium/mercury/lead-transporting ATPase [Photorhabdus luminescens]	0.46
WP_011145703.1 cysteine synthase A [Photorhabdus luminescens]	0.46
WP_011148772.1 MULTISPECIES: DNA-directed RNA polymerase subunit alpha [Photorhabdus]	0.46
WP_011147423.1 LuxR family transcriptional regulator [Photorhabdus luminescens]	0.46
WP_011146671.1 hypothetical protein [Photorhabdus luminescens]	0.46
WP_011146855.1 hemin-degrading factor [Photorhabdus luminescens]	0.46
WP_011147332.1 hypothetical protein [Photorhabdus luminescens]	0.46
WP_011148618.1 MULTISPECIES: 50S ribosomal protein L21 [Photorhabdus]	0.45
WP_011146479.1 hypothetical protein [Photorhabdus luminescens]	0.45
WP_011145319.1 phosphoglycerate kinase [Photorhabdus luminescens]	0.45
WP_011148025.1 1-deoxy-D-xylulose-5-phosphate synthase [Photorhabdus luminescens]	0.45
WP_011144414.1 chromosomal replication initiator protein DnaA [Photorhabdus luminescens]	0.44
WP_011145549.1 MULTISPECIES: XRE family transcriptional regulator [Photorhabdus]	0.44

WP_011147812.1 cell division protein FtsZ [Photorhabdus luminescens]	0.44
WP_011145914.1 30S ribosomal protein S1 [Photorhabdus luminescens]	0.44
WP_041380064.1 hypothetical protein [Photorhabdus luminescens]	0.44
WP_011148147.1 MULTISPECIES: 50S ribosomal protein L13 [Morganellaceae]	0.43
WP_011148647.1 23S rRNA (guanosine(2251)-2-O)-methyltransferase RlmB [Photorhabdus luminescens]	0.43
WP_011148776.1 50S ribosomal protein L15 [Photorhabdus luminescens]	0.43
WP_041380326.1 molecular chaperone HtpG [Photorhabdus luminescens]	0.43
WP_011146337.1 alkanal monooxygenase subunit beta [Photorhabdus luminescens]	0.43
WP_011148781.1 MULTISPECIES: 30S ribosomal protein S8 [Photorhabdus]	0.42
WP_011144619.1 cysteine ABC transporter substrate-binding protein [Photorhabdus luminescens]	0.42
WP_011148604.1 ribosome-binding factor A [Photorhabdus luminescens]	0.42
WP_011148281.1 hypothetical protein [Photorhabdus luminescens]	0.42
WP_011146762.1 DUF2829 domain-containing protein [Photorhabdus luminescens]	0.42
WP_011146222.1 NAD(P)-dependent alcohol dehydrogenase [Photorhabdus luminescens]	0.41
WP_011148278.1 hypothetical protein [Photorhabdus luminescens]	0.41
WP_011144823.1 50S ribosomal protein L10 [Photorhabdus luminescens]	0.41
WP_011148225.1 signal recognition particle-docking protein FtsY [Photorhabdus luminescens]	0.41
WP_011145617.1 MULTISPECIES: hypothetical protein [Photorhabdus]	0.41
WP_011144947.1 threonine synthase [Photorhabdus luminescens]	0.40
WP_011148145.1 stringent starvation protein A [Photorhabdus luminescens]	0.40
WP_011145871.1 hypothetical protein [Photorhabdus luminescens]	0.40
WP_011145251.1 hypothetical protein [Photorhabdus luminescens]	0.39

WP_011146816.1 glutathione transferase GstA [Photorhabdus luminescens]	0.39
WP_011144822.1 50S ribosomal protein L1 [Photorhabdus luminescens]	0.39
WP_011145774.1 2,3-bisphosphoglycerate-dependent phosphoglycerate mutase [Photorhabdus luminescens]	0.39
WP_011148198.1 acetyl-CoA carboxylase biotin carboxylase subunit [Photorhabdus luminescens]	0.39
WP_011147478.1 IscS subfamily cysteine desulfurase [Photorhabdus luminescens]	0.38
WP_011148823.1 50S ribosomal protein L31 [Photorhabdus luminescens]	0.38
WP_011146285.1 DUF2594 domain-containing protein [Photorhabdus luminescens]	0.38
WP_011147051.1 beta-ketoacyl-[acyl-carrier-protein] synthase II [Photorhabdus luminescens]	0.37
WP_011144645.1 Pyoverdin chromophore biosynthetic protein pvcC [Photorhabdus luminescens]	0.37
WP_011148779.1 MULTISPECIES: 50S ribosomal protein L18 [Photorhabdus]	0.37
WP_011147358.1 3-hydroxy-5-phosphonooxypentane-2,4-dione thiolase LsrF [Photorhabdus luminescens]	0.36
WP_011148275.1 hypothetical protein [Photorhabdus luminescens]	0.36
WP_011146584.1 polyketide cyclase [Photorhabdus luminescens]	0.35
WP_011148195.1 oxidoreductase [Photorhabdus luminescens]	0.35
WP_011145044.1 hypothetical protein [Photorhabdus luminescens]	0.35
WP_011145511.1 glutathione synthetase [Photorhabdus luminescens]	0.35
WP_011148061.1 bifunctional 2,3-cyclic-nucleotide 2-phosphodiesterase/3-nucleotidase [Photorhabdus luminescens]	0.35
WP_011145502.1 hypothetical protein [Photorhabdus luminescens]	0.35
WP_011148839.1 6-phosphofructokinase [Photorhabdus luminescens]	0.35
WP_011147061.1 ribonuclease E [Photorhabdus luminescens]	0.34
WP_041380511.1 hypothetical protein [Photorhabdus luminescens]	0.34
WP_011144628.1 GTPase-activating protein [Photorhabdus luminescens]	0.34

WP_011146920.1 PTS mannose/fructose/sorbose transporter subunit IIC [Photorhabdus luminescens]	0.33
WP_011148784.1 50S ribosomal protein L24 [Photorhabdus luminescens]	0.33
WP_011148312.1 type VI secretion system tube protein Hcp [Photorhabdus luminescens]	0.33
WP_011146312.1 inverse autotransporter beta-barrel domain-containing protein [Photorhabdus luminescens]	0.33
WP_011148616.1 GTPase ObgE [Photorhabdus luminescens]	0.32
WP_011144958.1 molecular chaperone DnaK [Photorhabdus luminescens]	0.32
WP_011146520.1 PhzF family phenazine biosynthesis protein [Photorhabdus luminescens]	0.32
WP_011148787.1 50S ribosomal protein L29 [Photorhabdus luminescens]	0.32
WP_011144968.1 30S ribosomal protein S20 [Photorhabdus luminescens]	0.32
WP_011147486.1 serine hydroxymethyltransferase [Photorhabdus luminescens]	0.31
WP_011145037.1 LOG family protein [Photorhabdus luminescens]	0.31
WP_011147040.1 peptidase [Photorhabdus luminescens]	0.31
WP_011148080.1 2,5-didehydrogluconate reductase DkgA [Photorhabdus luminescens]	0.31
WP_011147031.1 NAD-dependent protein deacylase [Photorhabdus luminescens]	0.31
WP_011147474.1 molecular chaperone HscA [Photorhabdus luminescens]	0.30
WP_011145860.1 L-threonine dehydrogenase [Photorhabdus luminescens]	0.30
WP_001144069.1 MULTISPECIES: 30S ribosomal protein S21 [Bacteria]	0.30
WP_011148009.1 trigger factor [Photorhabdus luminescens]	0.29
WP_011148606.1 transcription termination/antitermination protein NusA [Photorhabdus luminescens]	0.29
WP_011146232.1 phospholipase D [Photorhabdus luminescens]	0.28
WP_011148605.1 translation initiation factor IF-2 [Photorhabdus luminescens]	0.28
WP_011148091.1 glutathionylspermidine synthase family protein [Photorhabdus luminescens]	0.28
WP_011144946.1 homoserine kinase [Photorhabdus luminescens]	0.27
WP_011146330.1 SDR family oxidoreductase [Photorhabdus luminescens]	0.27
WP_011146336.1 alkanal monooxygenase alpha chain [Photorhabdus luminescens]	0.27

WP_011145650.1 ferric iron uptake transcriptional regulator [Photorhabdus luminescens]	0.27
WP_011145873.1 hypothetical protein [Photorhabdus luminescens]	0.27
WP_071824118.1 translation initiation factor IF-3 [Photorhabdus luminescens]	0.27
WP_011146365.1 Holliday junction branch migration protein RuvA [Photorhabdus luminescens]	0.26
WP_011147477.1 Fe-S cluster assembly scaffold IscU [Photorhabdus luminescens]	0.26
WP_011146331.1 hypothetical protein [Photorhabdus luminescens]	0.26
WP_011144877.1 DNA-binding protein HU-alpha [Photorhabdus luminescens]	0.26
WP_011145577.1 S-ribosylhomocysteine lyase [Photorhabdus luminescens]	0.25
WP_002209449.1 MULTISPECIES: carbon storage regulator [Enterobacterales]	0.25
WP_011147765.1 aminomethyltransferase [Photorhabdus luminescens]	0.25
WP_011146190.1 hypothetical protein [Photorhabdus luminescens]	0.24
WP_011145585.1 2-succinyl-6-hydroxy-2,4-cyclohexadiene-1-carboxylate synthase [Photorhabdus luminescens]	0.24
WP_011146149.1 branched-chain alpha-keto acid dehydrogenase subunit E2 [Photorhabdus luminescens]	0.24
WP_011147954.1 LLM class flavin-dependent oxidoreductase [Photorhabdus luminescens]	0.24
WP_011147391.1 beta-ketoacyl-[acyl-carrier-protein] synthase I [Photorhabdus luminescens]	0.23
WP_011146822.1 SlyA family transcriptional regulator [Photorhabdus luminescens]	0.23
WP_011145550.1 hypothetical protein [Photorhabdus luminescens]	0.22
WP_041379927.1 hypothetical protein [Photorhabdus luminescens]	0.22
WP_011148751.1 threonine ammonia-lyase, biosynthetic [Photorhabdus luminescens]	0.22
WP_011148238.1 glycerophosphodiester phosphodiesterase [Photorhabdus luminescens]	0.21
WP_011146164.1 hypothetical protein [Photorhabdus luminescens]	0.21
WP_011148935.1 hypothetical protein [Photorhabdus luminescens]	0.21
WP_011147045.1 histidine triad nucleotide-binding protein [Photorhabdus luminescens]	0.21

WP_011145558.1 signal transduction histidine kinase [Photorhabdus luminescens]	0.19
WP_011146225.1 NAD(P)H:quinone oxidoreductase [Photorhabdus luminescens]	0.19
WP_041379889.1 DUF3396 domain-containing protein [Photorhabdus luminescens]	0.18
WP_011145821.1 3-mercaptopyruvate sulfurtransferase [Photorhabdus luminescens]	0.17
WP_010847629.1 MULTISPECIES: 50S ribosomal protein L33 [Morganellaceae]	0.17
WP_011146880.1 bifunctional UDP-glucuronic acid oxidase/UDP-4-amino-4-deoxy-L-arabinose formyltransferase [Photorhabdus luminescens]	0.17
WP_011148644.1 50S ribosomal protein L9 [Photorhabdus luminescens]	0.16
WP_041380730.1 serine-type D-Ala-D-Ala carboxypeptidase [Photorhabdus luminescens]	0.16
WP_041380457.1 DNA repair protein [Photorhabdus luminescens]	0.16
WP_011148236.1 DUF29 domain-containing protein [Photorhabdus luminescens]	0.16
WP_011145878.1 MULTISPECIES: GrxA family glutaredoxin [Photorhabdus]	0.15
WP_011144948.1 peroxide stress protein YaaA [Photorhabdus luminescens]	0.15
WP_011147054.1 [acyl-carrier-protein] S-malonyltransferase [Photorhabdus luminescens]	0.15
WP_011146691.1 tryptophan synthase subunit alpha [Photorhabdus luminescens]	0.15
WP_011146532.1 virulence sensor protein BvgS precursor [Photorhabdus luminescens]	0.15
WP_011148076.1 cystathionine beta-lyase [Photorhabdus luminescens]	0.15
WP_011146151.1 cupin domain-containing protein [Photorhabdus luminescens]	0.15
WP_049789755.1 diaminopimelate decarboxylase [Photorhabdus luminescens]	0.14
WP_011146575.1 DUF29 domain-containing protein [Photorhabdus luminescens]	0.14
WP_011146509.1 aspartate aminotransferase family protein [Photorhabdus luminescens]	0.14
WP_011146193.1 XRE family transcriptional regulator [Photorhabdus luminescens]	0.13
WP_041380017.1 D-alanyl-D-alanine carboxypeptidase [Photorhabdus luminescens]	0.13

WP_011146487.1 class I SAM-dependent methyltransferase [Photorhabdus luminescens]	0.13
WP_011145038.1 NADPH-dependent 7-cyano-7-deazaguanine reductase QueF [Photorhabdus luminescens]	0.12
WP_011147377.1 SPOR domain-containing protein [Photorhabdus luminescens]	0.12
WP_011148032.1 N utilization substance protein B [Photorhabdus luminescens]	0.12
WP_011146482.1 hypothetical protein [Photorhabdus luminescens]	0.12
WP_011145794.1 type VI secretion system tip protein VgrG [Photorhabdus luminescens];WP_049789726.1 type VI secretion system tip protein VgrG [Photorhabdus luminescens]	0.12
WP_011146801.1 thiol peroxidase [Photorhabdus luminescens]	0.12
WP_011148901.1 divergent polysaccharide deacetylase family protein [Photorhabdus luminescens]	0.11
WP_011147482.1 alpha,alpha-phosphotrehalase [Photorhabdus luminescens]	0.11
WP_011146379.1 hypothetical protein [Photorhabdus luminescens]	0.10
WP_011147252.1 DUF3277 domain-containing protein [Photorhabdus luminescens]	0.10
WP_011148324.1 type VI secretion system ATPase TssH [Photorhabdus luminescens]	0.09
WP_011146432.1 universal stress protein E [Photorhabdus luminescens]	0.09
WP_011145796.1 DUF3396 domain-containing protein [Photorhabdus luminescens]	0.09
WP_011145826.1 2,5-didehydrogluconate reductase DkgB [Photorhabdus luminescens]	0.09
WP_011148345.1 BON domain-containing protein [Photorhabdus luminescens]	0.09
WP_011144704.1 MULTISPECIES: tautomerase [Photorhabdus]	0.07
WP_011148020.1 nucleotide-binding protein [Photorhabdus luminescens]	0.07
WP_011146163.1 hypothetical protein [Photorhabdus luminescens]	0.07
WP_011148948.1 hypothetical protein [Photorhabdus luminescens]	0.07
WP_011146454.1 alpha/beta hydrolase [Photorhabdus luminescens]	0.06
WP_011144713.1 hypothetical protein [Photorhabdus luminescens]	0.06
WP_011144527.1 universal stress protein A [Photorhabdus luminescens]	0.05

WP_011145034.1 HlyD family type I secretion periplasmic adaptor subunit [Photorhabdus luminescens]	0.04
WP_011148713.1 iron donor protein CyaY [Photorhabdus luminescens]	0.04
WP_011148640.1 hypothetical protein [Photorhabdus luminescens]	0.02
WP_011146363.1 YebC/PmpR family DNA-binding transcriptional regulator [Photorhabdus luminescens]	0.02
WP_011146460.1 2,3-dihydroxyphenylpropionate/2,3-dihydroxicinnamic acid 1,2-dioxygenase [Photorhabdus luminescens]	0.02
WP_011146459.1 3-phenylpropionate-dihydrodiol/cinnamic acid-dihydrodiol dehydrogenase [Photorhabdus luminescens]	0.01
WP_011146456.1 3-phenylpropionate/cinnamic acid dioxygenase subunit alpha [Photorhabdus luminescens]	0.00
WP_011144416.1 DNA replication and repair protein RecF [Photorhabdus luminescens]	8.47E-07
WP_011148558.1 integrase [Photorhabdus luminescens]	7.36E-07
WP_011148643.1 cysteine synthase family protein [Photorhabdus luminescens]	7.09E-07
WP_011148596.1 hypothetical protein [Photorhabdus luminescens]	6.70E-07
WP_041381184.1 GntR family transcriptional regulator [Photorhabdus luminescens]	5.75E-07
WP_011148749.1 multidrug export protein EmrA [Photorhabdus luminescens]	5.44E-07
WP_011147819.1 UDP-N-acetylmuramoyl-L-alanine--D-glutamate ligase [Photorhabdus luminescens]	5.27E-07
WP_011144632.1 hypothetical protein [Photorhabdus luminescens]	4.71E-07
WP_011147033.1 lipoprotein-releasing system ATP-binding protein LolD [Photorhabdus luminescens]	4.57E-07
WP_011146169.1 hypothetical protein [Photorhabdus luminescens]	4.14E-07
WP_011148852.1 hypothetical protein [Photorhabdus luminescens]	3.95E-07
WP_011148511.1 HTH-type transcriptional regulator MetR [Photorhabdus luminescens]	3.88E-07
WP_011147719.1 propionate--CoA ligase [Photorhabdus luminescens]	3.86E-07
WP_011147274.1 PIN domain-containing protein [Photorhabdus luminescens]	3.07E-07
WP_041380819.1 tail fiber assembly protein [Photorhabdus luminescens]	2.88E-07
WP_011147557.1 NAD(+) kinase [Photorhabdus luminescens]	2.87E-07

WP_011146835.1 pyruvate kinase PykF [Photorhabdus luminescens]	2.59E-07
WP_011148081.1 cell division protein FtsP [Photorhabdus luminescens]	2.38E-07
WP_011145899.1 replication-associated recombination protein A [Photorhabdus luminescens]	2.12E-07
WP_011148472.1 D-alanyl-lipoteichoic acid biosynthesis protein DltD [Photorhabdus luminescens]	2.07E-07
WP_011146189.1 DUF4123 domain-containing protein [Photorhabdus luminescens]	1.81E-07
WP_082302960.1 N-acetyltransferase [Photorhabdus luminescens]	1.67E-07
WP_011146572.1 cytochrome-c oxidase [Photorhabdus luminescens]	1.67E-07
WP_011147726.1 ISNCY family transposase ISPlu15 [Photorhabdus luminescens]	1.46E-07
WP_011148958.1 tRNA uridine-5-carboxymethylaminomethyl(34) synthesis GTPase MnmE [Photorhabdus luminescens]	1.45E-07
WP_011148130.1 LysR family transcriptional regulator [Photorhabdus luminescens]	9.77E-08
WP_011148499.1 twin-arginine translocase subunit TatB [Photorhabdus luminescens]	8.32E-08
WP_011146268.1 helix-turn-helix transcriptional regulator [Photorhabdus luminescens]	3.78E-08
WP_011146461.1 3-phenylpropionate/cinnamic acid dioxygenase ferredoxin--NAD+ reductase component [Photorhabdus luminescens]	1.71E-08
WP_011146457.1 3-phenylpropionate/cinnamic acid dioxygenase subunit beta [Photorhabdus luminescens]	1.39E-08

References

1. Bode, E. *et al.* Promoter Activation in *Δ hfq* Mutants as an Efficient Tool for Specialized Metabolite Production Enabling Direct Bioactivity Testing. *Angew. Chem.* **131,** 19133–19139; 10.1002/ange.201910563 (2019).
2. Forst, S., Dowds, B., Boemare, N. & Stackebrandt, E. *Xenorhabdus* and *Photorhabdus* spp.: bugs that kill bugs. *Annu. Rev. Microbiol.* **51,** 47–72; 10.1146/annurev.micro.51.1.47 (1997).
3. Renn N. Routes of penetration of the entomopathogenic nematode *steinernema feltiae* attacking larval and adult houseflies (*Musca domestica*). *J. Invertebr. Pathol.* **72,** 281–287; 10.1006/jipa.1998.4811 (1998).
4. Georgis, R. & Hague, N. G. M. A Neoaplectanid nematode in the larch sawfly *Cephalcia lariciphila* (Hymenoptera: Pamphiliidae). *Ann. Appl. Biol.* **99,** 171–177; 10.1111/j.1744-7348.1981.tb05144.x (1981).
5. Sicard, M. *et al.* Stages of infection during the tripartite interaction between *Xenorhabdus nematophila*, its nematode vector, and insect hosts. *Appl. Environ. Microbiol.* **70,** 6473–6480; 10.1128/AEM.70.11.6473-6480.2004 (2004).
6. Gaugler, R. *Entomopathogenic nematology* (CABI, Wallingford, 2002).
7. Hu, K. & Webster, J. M. Antibiotic production in relation to bacterial growth and nematode development in *Photorhabdus-Heterorhabditis* infected *Galleria mellonella* larvae. *FEMS Microbiol. Lett.* **189,** 219–223; 10.1111/j.1574-6968.2000.tb09234.x (2000).
8. Williams, J. S., Thomas, M. & Clarke, D. J. The gene stlA encodes a phenylalanine ammonia-lyase that is involved in the production of a stilbene antibiotic in *Photorhabdus luminescens* TT01. *Microbiol. (Reading, England)* **151,** 2543–2550; 10.1099/mic.0.28136-0 (2005).
9. Bozhüyük, K. A. J. *et al.* De novo design and engineering of non-ribosomal peptide synthetases. *Nat. Chem.* **10,** 275–281; 10.1038/nchem.2890 (2018).

10. Klaus, M., D'Souza, A. D., Nivina, A., Khosla, C. & Grininger, M. Engineering of Chimeric Polyketide Synthases Using SYNZIP Docking Domains. *ACS Chem. Biol.* **14,** 426–433; 10.1021/acschembio.8b01060 (2019).

11. Mathur, S., Fletcher, A. J., Branigan, E., Hay, R. T. & Virdee, S. Photocrosslinking Activity-Based Probes for Ubiquitin RING E3 Ligases. *Cell Chem. Biol.* **27,** 74-82.e6; 10.1016/j.chembiol.2019.11.013 (2020).

12. Hecker, M. *et al.* (eds.). *Proteomics of Microorganisms. Fundamental Aspects and Application* (Springer, Berlin, Heidelberg, 2003).

13. Sickmann, A., Mreyen, M. & Meyer, H. E. in *Proteomics of Microorganisms,* edited by M. Hecker*, et al.* (Springer, Berlin, Heidelberg, 2003), pp. 141–176.

14. Gualtieri, M., Aumelas, A. & Thaler, J.-O. Identification of a new antimicrobial lysine-rich cyclolipopeptide family from *Xenorhabdus nematophila*. *J. Antibiot* **62,** 295–302; 10.1038/ja.2009.31 (2009).

15. Sauer, M. & Heilemann, M. Single-Molecule Localization Microscopy in Eukaryotes. *Chem. Rev.* **117,** 7478–7509; 10.1021/acs.chemrev.6b00667 (2017).

16. Forst, S. & Nealson, K. Molecular biology of the symbiotic-pathogenic bacteria *Xenorhabdus* spp. and *Photorhabdus* spp. *Microbiol. Rev.* **60,** 21–43 (1996).

17. Götze, S. *et al.* Structure, Biosynthesis, and Biological Activity of the Cyclic Lipopeptide Anikasin. *ACS Chem. Biol.* **12,** 2498–2502; 10.1021/acschembio.7b00589 (2017).

18. Wyche, T. P., Hou, Y., Vazquez-Rivera, E., Braun, D. & Bugni, T. S. Peptidolipins B-F, antibacterial lipopeptides from an ascidian-derived *Nocardia* sp. *J. Nat. Prod.* **75,** 735–740; 10.1021/np300016r (2012).

19. Neuhof, T. *et al.* Hassallidin A, a glycosylated lipopeptide with antifungal activity from the cyanobacterium *Hassallia* sp. *J. Nat. Prod.* **68,** 695–700; 10.1021/np049671r (2005).

20. Tan, K. C., Wakimoto, T. & Abe, I. Lipodiscamides A-C, new cytotoxic lipopeptides from *Discodermia kiiensis*. *Org. Lett.* **16,** 3256–3259; 10.1021/ol501271v (2014).

21. Hein, C. D., Liu, X.-M. & Wang, D. Click chemistry, a powerful tool for pharmaceutical sciences. *Pharm. Res.* **25,** 2216–2230; 10.1007/s11095-008-9616-1 (2008).

22. Adam, G. C., Sorensen, E. J. & Cravatt, B. F. Chemical strategies for functional proteomics. *Mol. Cell. Proteom.* **1,** 781–790; 10.1074/mcp.r200006-mcp200 (2002).

23. Virant, D. *et al.* A peptide tag-specific nanobody enables high-quality labeling for dSTORM imaging. *Nat. Commun.* **9,** 1–14; 10.1038/s41467-018-03191-2.

24. Allen, D. R. & McWhinney, B. C. Quadrupole Time-of-Flight Mass Spectrometry: A Paradigm Shift in Toxicology Screening Applications. *Clin. Biochem Rev.* **40,** 135–146; 10.33176/AACB-19-00023 (2019).

25. Hu, Q. *et al.* The Orbitrap: a new mass spectrometer. *J. Mass Spectrom.* **40,** 430–443; 10.1002/jms.856 (2005).

26. Thomas, M. G. & Poinar, G. O. *Xenorhabdus* gen. nov., a Genus of Entomopathogenic, Nematophilic Bacteria of the Family Enterobacteriaceae. *Int. J. Syst. Bacteriol.* **29,** 352–360; 10.1099/00207713-29-4-352 (1979).

27. Akhurst, R. J. & Boemare, N. E. A numerical taxonomic study of the genus *Xenorhabdus* (Enterobacteriaceae) and proposed elevation of the subspecies of *X. nematophilus* to species. *J. Gen. Microbiol.* **134,** 1835–1845; 10.1099/00221287-134-7-1835 (1988).

28. Akhurst, R. J. *Xenorhabdus nematophilus subsp. beddingii* (*Enterobacteriaceae*): A New Subspecies of Bacteria Mutualistically Associated with Entomopathogenic Nematodes. *Int. J. Syst. Bacteriol.* **36,** 454–457; 10.1099/00207713-36-3-454 (1986).

29. Poinar, G. O. & Grewal, P. S. History of Entomopathogenic Nematology. *J. Nematol.* **44,** 153–161 (2012).

30. Shi, Y.-M. & Bode, H. B. Chemical language and warfare of bacterial natural products in bacteria-nematode-insect interactions. *Nat. Prod. Rep.* **35,** 309–335; 10.1039/c7np00054e (2018).

31. Hughes, A. B. (ed.). *Amino acids, peptides, and proteins in organic chemistry* (Wiley-VCH, Weinheim, 2009-2012).

32. Peters, B. M., Shirtliff, M. E. & Jabra-Rizk, M. A. Antimicrobial peptides: primeval molecules or future drugs? *PLoS Pathog.* **6,** e1001067; 10.1371/journal.ppat.1001067 (2010).

33. Cheng, S., Tu, M., Liu, H., Zhao, G. & Du, M. Food-derived antithrombotic peptides: Preparation, identification, and interactions with thrombin. *Crit. Rev. Food Sci. Nutr.* **59,** S81-S95; 10.1080/10408398.2018.1524363 (2019).

34. Norris, R. & J., R. in *Whey Proteins as Source of Bioactive Peptides Against Hypertension,* edited by B. Hernndez-Ledesma (INTECH Open Access Publisher2013).

35. Remesic, M., Lee, Y. S. & Hruby, V. J. Cyclic opioid peptides. *Curr. Med. Chem.* **23,** 1288–1303 (2016).

36. He, X. *et al.* A Frog-Derived Immunomodulatory Peptide Promotes Cutaneous Wound Healing by Regulating Cellular Response. *Front. Immunol.* **10,** 2421; 10.3389/fimmu.2019.02421 (2019).

37. Vegarud, G. E., Langsrud, T. & Svenning, C. Mineral-binding milk proteins and peptides; occurrence, biochemical and technological characteristics. *Br. J. Nutr.* **84 Suppl 1,** S91-8; 10.1017/s0007114500002300 (2000).

38. Sarmadi, B. H. & Ismail, A. Antioxidative peptides from food proteins: a review. *Peptides* **31,** 1949–1956; 10.1016/j.peptides.2010.06.020 (2010).

39. Laupacis, A., Keown, P. A., Ulan, R. A., McKenzie, N. & Stiller, C. R. Cyclosporin A: a powerful immunosuppressant. *Can. Med. Assoc. J.* **126,** 1041–1046 (1982).

40. Matsuda, S. & Koyasu, S. Mechanisms of action of cyclosporine. *Immunopharmacology* **47,** 119–125; 10.1016/S0162-3109(00)00192-2 (2000).

41. Rhee, M. K. & Mah, F. S. Clinical utility of cyclosporine (CsA) ophthalmic emulsion 0.05% for symptomatic relief in people with chronic dry eye: a review of the literature. *Clin. Ophthalmol. (Auckland, N.Z.)* **11,** 1157–1166; 10.2147/OPTH.S113437 (2017).

42. McGrath, N. A., Brichacek, M. & Njardarson, J. T. A Graphical Journey of Innovative Organic Architectures That Have Improved Our Lives. *J. Chem. Educ.* **87,** 1348–1349; 10.1021/ed1003806 (2010).

43. Strieker, M., Tanović, A. & Marahiel, M. A. Nonribosomal peptide synthetases: structures and dynamics. *Curr. Opin. Struct. Biol.* **20,** 234–240; 10.1016/j.sbi.2010.01.009 (2010).

44. Felnagle, E. A. *et al.* Nonribosomal peptide synthetases involved in the production of medically relevant natural products. *Mol. Pharm.* **5,** 191–211; 10.1021/mp700137g (2008).

45. Wang, H., Fewer, D. P., Holm, L., Rouhiainen, L. & Sivonen, K. Atlas of nonribosomal peptide and polyketide biosynthetic pathways reveals common occurrence of nonmodular enzymes. *Proc. Natl. Acad. Sci. U.S.A* **111,** 9259–9264; 10.1073/pnas.1401734111 (2014).

46. Kirkpatrick, P., Raja, A., LaBonte, J. & Lebbos, J. Daptomycin. *Nat. Rev. Drug Discov.* **2,** 943–944; 10.1038/nrd1258 (2003).

47. Baldeweg, F., Warncke, P., Fischer, D. & Gressler, M. Fungal Biosurfactants from *Mortierella alpina*. *Org. Lett.* **21,** 1444–1448; 10.1021/acs.orglett.9b00193 (2019).

48. Carroll, C. S. & Moore, M. M. Ironing out siderophore biosynthesis: a review of non-ribosomal peptide synthetase (NRPS)-independent siderophore synthetases. *Crit. Rev. Biochem. Mol. Biol.* **53,** 356–381; 10.1080/10409238.2018.1476449 (2018).

49. Schellenberg, B., Bigler, L. & Dudler, R. Identification of genes involved in the biosynthesis of the cytotoxic compound glidobactin from a soil bacterium. *Environ. Microbiol.* **9,** 1640–1650; 10.1111/j.1462-2920.2007.01278.x (2007).

50. Lipmann, F., Gevers, W., Kleinkauf, H. & Roskoski, R. Polypeptide synthesis on protein templates: the enzymatic synthesis of gramicidin S and tyrocidine. *Adv. Enzymol. Relat. Areas Mol. Biol.* **35,** 1–34; 10.1002/9780470122808.ch1 (1971).

51. Marahiel, M. A. Protein templates for the biosynthesis of peptide antibiotics. *Chem. Biol.* **4,** 561–567; 10.1016/S1074-5521(97)90242-8 (1997).

52. Jursic, B. S. & Zdravkovski, Z. A Simple Preparation of Amides from Acids and Amines by Heating of Their Mixture. *Synth. Commun.* **23,** 2761–2770; 10.1080/00397919308013807 (1993).

53. Perreux, L., Loupy, A. & Volatron, F. Solvent-free preparation of amides from acids and primary amines under microwave irradiation. *Tetrahedron* **58,** 2155–2162; 10.1016/S0040-4020(02)00085-6 (2002).

54. El-Faham, A. & Albericio, E.-F. Peptide coupling reagents, more than a letter soup. *Chem. Rev.* **111,** 6557–6602; 10.1021/cr100048w (2011).

55. Hood, C. A. *et al.* Fast conventional Fmoc solid-phase peptide synthesis with HCTU. *J. Pept. Sci.* **14,** 97–101; 10.1002/psc.921 (2008).

56. Carpino, L. A. *et al.* The Uronium/Guanidinium Peptide Coupling Reagents: Finally the True Uronium Salts. *Angew. Chem. Int. Ed.* **41,** 441–445; 10.1002/1521-3773(20020201)41:3<441::AID-ANIE441>3.0.CO;2-N (2002).

57. Hruby, V. J., Barstow, L. E. & Linhart, T. A new machine for automated solid phase peptide synthesis. *Anal. Chem.* **44,** 343–350; 10.1021/ac60310a004 (1972).

58. Merrifield, R. B., Stewart, J. M. & Jernberg, N. Instrument for automated synthesis of peptides. *Anal. Chem.* **38,** 1905–1914; 10.1021/ac50155a057 (1966).

59. Al-Warhi, T. I., Al-Hazimi, H. M.A. & El-Faham, A. Recent development in peptide coupling reagents. *J. Saudi Chem. Soc.* **16,** 97–116; 10.1016/j.jscs.2010.12.006 (2012).

60. Albericio, E.-F. & El-Faham, A. Choosing the Right Coupling Reagent for Peptides: A Twenty-Five-Year Journey. *Org. Process Res. Dev.* **22,** 760–772; 10.1021/acs.oprd.8b00159 (2018).

61. Subirós-Funosas, R., Prohens, R., Barbas, R., El-Faham, A. & Albericio, E.-F. Oxyma: an efficient additive for peptide synthesis to replace the benzotriazole-based HOBt and HOAt with a lower risk of explosion. *Chemistry* **15,** 9394–9403; 10.1002/chem.200900614 (2009).

62. Sureshbabu, V. V., Lalithamba, H. S., Narendra, N. & Hemantha, H. P. New and simple synthesis of acid azides, ureas and carbamates from carboxylic acids: application of peptide coupling agents EDC and HBTU. *Org. Biomol. Chem.* **8,** 835–840; 10.1039/b920290k (2010).

63. Gu, L., Yang, B. & Liu, F. Synthesis and biological activity of novel statine derivatives containing ferrocenyl moiety. *J. Braz. Chem. Soc.* **21,** 58–62; 10.1590/S0103-50532010000100010 (2010).

64. Vrettos, E. I. *et al.* Unveiling and tackling guanidinium peptide coupling reagent side reactions towards the development of peptide-drug conjugates. *RSC Adv.* **7,** 50519–50526; 10.1039/C7RA06655D (2017).

65. Ágoston, K., Streicher, H. & Fügedi, P. Orthogonal protecting group strategies in carbohydrate chemistry. *Tetrahedron: Asymmetry* **27,** 707–728; 10.1016/j.tetasy.2016.06.010 (2016).

66. Carganico, S. & Papini, A. M. Orthogonal Protecting Groups and Side-Reactions in Fmoc/tBu Solid-Phase Peptide Synthesis. *Amino acids* **25,** 313–348; 10.1002/9783527631803.ch9.

67. Friedman, M. Applications of the ninhydrin reaction for analysis of amino acids, peptides, and proteins to agricultural and biomedical sciences. *J. Agric. Food Chem.* **52,** 385–406; 10.1021/jf030490p (2004).

68. Amblard, M., Fehrentz, J.-A., Martinez, J. & Subra, G. Methods and Protocols of Modern Solid Phase Peptide Synthesis. *Mol. Biotechnol.* **33,** 239–254; 10.1385/MB:33:3:239 (2006).

69. Tobias, N. J. *et al.* Natural product diversity associated with the nematode symbionts *Photorhabdus* and *Xenorhabdus*. *Nat. Microbiol.* **2,** 1676–1685; 10.1038/s41564-017-0039-9 (2017).

70. Shtatland, T., Guettler, D., Kossodo, M., Pivovarov, M. & Weissleder, R. PepBank--a database of peptides based on sequence text mining and public peptide data sources. *BMC Bioinform.* **8,** 280; 10.1186/1471-2105-8-280 (2007).

71. Deutsch, E. W., Lam, H. & Aebersold, R. PeptideAtlas: a resource for target selection for emerging targeted proteomics workflows. *EMBO Rep.* **9,** 429–434; 10.1038/embor.2008.56 (2008).

72. Apweiler, R. *et al.* UniProt: the Universal Protein knowledgebase. *Nucleic Acids Res.* **32,** D115-9; 10.1093/nar/gkh131 (2004).

73. Bode E. Structure, function and biosynthesis of natural products from *Xenorhabdus doucetiae*. Dissertation. Johann Wolfgang Goethe-Universität, 2017.

74. Bode, E. *et al.* Biosynthesis and function of simple amides in *Xenorhabdus doucetiae*. *Environ. Microbiol.* **19,** 4564–4575; 10.1111/1462-2920.13919 (2017).

75. Chen, Y. *et al.* New phenethylamine derivatives from *Arenibacter nanhaiticus sp. nov. NH36A T* and their antimicrobial activity. *J. Antibiot.* **66,** 655–661; 10.1038/ja.2013.65 (2013).

76. Malloy, K. L. *et al.* Credneramides A and B: neuromodulatory phenethylamine and isopentylamine derivatives of a vinyl chloride-containing fatty acid from cf. *Trichodesmium* sp. nov. *J. Nat. Prod.* **75,** 60–66; 10.1021/np200611f (2012).

77. Tan, L. T., Okino, T. & Gerwick, W. H. Hermitamides A and B, toxic malyngamide-type natural products from the marine cyanobacterium *Lyngbya majuscula*. *J. Nat. Prod.* **63,** 952–955; 10.1021/np000037x (2000).

78. Teasdale, M. E., Liu, J., Wallace, J., Akhlaghi, F. & Rowley, D. C. Secondary metabolites produced by the marine bacterium *Halobacillus salinus* that inhibit

quorum sensing-controlled phenotypes in gram-negative bacteria. *Appl. Environ. Microbiol.* **75,** 567–572; 10.1128/AEM.00632-08 (2009).

79. Mehmood, R., Imran, M., Safder, M., Anjum, S. & Malik, A. Structural determination of crotamides A and B, the new amides from *Croton sparsiflorus*. *J. Asian Nat. Prod. Res.* **12,** 662–665; 10.1080/10286020.2010.489896 (2010).

80. Das, L. K. L., Verma, M. & Sahai, M. Three new acyltyramines from *Anisodus luridus* Link et Otto (Solanaceae). *Nat. prod. res.* **30,** 2434–2441; 10.1080/14786419.2016.1198346 (2016).

81. Rupčić, J. & Marić, V. Isolation and chemical composition of the ceramide of the *Candida lipolytica* yeast. *Chem. Phys. Lipids* **91,** 153–161; 10.1016/S0009-3084(97)00106-0 (1998).

82. Zhao, G., Yang, C., Li, B. & Xia, W. A new phenylethyl alkyl amide from the *Ambrostoma quadriimpressum* Motschulsky. *Beilstein J. Org. Chem.* **7,** 1342–1346; 10.3762/bjoc.7.158 (2011).

83. Liyanage, G. K. & Schmitz, F. J. Cytotoxic amides from the octocoral *telesto riisei*. *J. Nat. Prod.* **61,** 1180; 10.1021/np980264n (1998).

84. Gutiérrez, M. *et al.* Antiplasmodial metabolites isolated from the marine octocoral *Muricea austera*. *J. Nat. Prod.* **69,** 1379–1383; 10.1021/np060007f (2006).

85. Teasdale, M. E., Donovan, K. A., Forschner-Dancause, S. R. & Rowley, D. C. Gram-Positive Marine Bacteria as a Potential Resource for the Discovery of Quorum Sensing Inhibitors. *Mar. Biotechnol.* **13,** 722–732; 10.1007/s10126-010-9334-7 (2011).

86. Bozhueyuek, K. A. J., Watzel, J., Abbood, N. & Bode, H. B. *Synthetic Zippers as an Enabling Tool for Engineering of Non-Ribosomal Peptide Synthetases* (2020).

87. Schimming, O., Fleischhacker, F., Nollmann, F. I. & Bode, H. B. Yeast Homologous Recombination Cloning Leading to the Novel Peptides Ambactin and Xenolindicin. *ChemBioChem* **15,** 1290–1294; 10.1002/cbic.201402065 (2014).

88. Tietze, A., Shi, Y.-N., Kronenwerth, M. & Bode, H. B. Nonribosomal Peptides Produced by Minimal and Engineered Synthetases with Terminal Reductase Domains. *ChemBioChem*; 10.1002/cbic.202000176 (2020).

89. Bozhüyük, K. A. J. *et al.* Modification and de novo design of non-ribosomal peptide synthetases using specific assembly points within condensation domains. *Nat. Chem.* **11,** 653–661; 10.1038/s41557-019-0276-z (2019).

90. Manavalan, B., Murugapiran, S. K., Lee, G. & Choi, S. Molecular modeling of the reductase domain to elucidate the reaction mechanism of reduction of peptidyl thioester into its corresponding alcohol in non-ribosomal peptide synthetases. *BMC Struct. Biol.* **10,** 1; 10.1186/1472-6807-10-1 (2010).

91. Field-Smith, A., Morgan, G. J. & Davies, F. E. Bortezomib (Velcade™) in the Treatment of Multiple Myeloma. *Ther. Clin. Risk. Manag.* **2,** 271–279 (2006).

92. *Bortezomib (Millennium Pharmaceuticals) ,*

93. Adams, J. The Development of Proteasome Inhibitors as Anticancer Drugs. *Cancer cell* **5**; 10.1016/s1535-6108(04)00120-5 (2004).

94. Cai, X. *et al.* Entomopathogenic bacteria use multiple mechanisms for bioactive peptide library design. *Nat. Chem.* **9,** 379–386; 10.1038/nchem.2671 (2017).

95. Reimer, D. *et al.* Rhabdopeptides as insect-specific virulence factors from entomopathogenic bacteria. *ChemBioChem* **14,** 1991–1997; 10.1002/cbic.201300205 (2013).

96. Bode, H. B. *et al.* Determination of the absolute configuration of peptide natural products by using stable isotope labeling and mass spectrometry. *Chemistry* **18,** 2342–2348; 10.1002/chem.201103479 (2012).

97. Tobias, N. J. *et al. Photorhabdus*-nematode symbiosis is dependent on *hfq*-mediated regulation of secondary metabolites. *Environ. Microbiol.* **19,** 119–129; 10.1111/1462-2920.13502 (2017).

98. Wesche, F. *et al.* Combined Approach of Backbone Amide Linking and On-Resin N-Methylation for the Synthesis of Bioactive and Metabolically Stable

Peptides. *J. Med. Chem.* **61,** 3930–3938; 10.1021/acs.jmedchem.7b01809 (2018).

99. Szponar, B., Kraśnik, L., Hryniewiecki, T., Gamian, A. & Larsson, L. Distribution of 3-hydroxy fatty acids in tissues after intraperitoneal injection of endotoxin. *Clin. Chem.* **49,** 1149–1153; 10.1373/49.7.1149 (2003).

100. Lee, A. K.Y., Chan, C. K., Fang, M. & Lau, A. P.S. The 3-hydroxy fatty acids as biomarkers for quantification and characterization of endotoxins and Gram-negative bacteria in atmospheric aerosols in Hong Kong. *Atmos. Environ.* **38,** 6307–6317; 10.1016/j.atmosenv.2004.08.013 (2004).

101. Thorn, J., Beijer, L. & Rylander, R. Airways inflammation and glucan exposure among household waste collectors. *Am. J. Ind. Med.* **33,** 463–470; 10.1002/(SICI)1097-0274(199805)33:5<463::AID-AJIM5>3.0.CO;2-T (1998).

102. Kline, J. N. *et al.* Variable airway responsiveness to inhaled lipopolysaccharide. *Am. J. Respir. Crit. Care Med.* **160,** 297–303; 10.1164/ajrccm.160.1.9808144 (1999).

103. Wan, G. H. & Li, C. S. Indoor endotoxin and glucan in association with airway inflammation and systemic symptoms. *Arch. Environ. Health* **54,** 172–179; 10.1080/00039899909602256 (1999).

104. Douwes, J., Thorne, P., Pearce, N. & Heederik, D. Bioaerosol health effects and exposure assessment: progress and prospects. *Ann. Occup. Hyg.* **47,** 187–200; 10.1093/annhyg/meg032 (2003).

105. Zhao, L., Vo, T. D., Kaiser, M. & Bode, H. B. Phototemtide A, a Cyclic Lipopeptide Heterologously Expressed from Photorhabdus temperata Meg1, Shows Selective Antiprotozoal Activity. *ChemBioChem*; 10.1002/cbic.201900665.

106. Grundmann, F. *et al.* Antiparasitic chaiyaphumines from entomopathogenic *Xenorhabdus* sp. PB61.4. *J. Nat. Prod.* **77,** 779–783; 10.1021/np4007525 (2014).

107. Fuchs, S. W., Proschak, A., J., T. W., Karas, M. & Bode, H. B. Structure elucidation and biosynthesis of lysine-rich cyclic peptides in *Xenorhabdus nematophila*. *Org. Biomol. Chem.* **9,** 3130–3132; 10.1039/c1ob05097d (2011).

108. Dreyer, J. *et al. Xenorhabdus khoisanae SB10* produces Lys-rich PAX lipopeptides and a Xenocoumacin in its antimicrobial complex. *BMC Microbiol.* **19,** 1–11; 10.1186/s12866-019-1503-x (2019).

109. Tressaud, A. Fluorine, a key-element for the XXIst century: Uses of fluoride materials in modern technologies. *J. Material. Sci. Eng.*; 10.4172/2169-0022-C5-104.

110. Nakashima, S. *et al.* A novel tag-free probe for targeting molecules interacting with a flavonoid catabolite. *Biochem. Biophys. Rep.* **7,** 240–245; 10.1016/j.bbrep.2016.06.020 (2016).

111. McKay, C. S. & Finn, M. G. Click Chemistry in Complex Mixtures: Bioorthogonal Bioconjugation. *Chem. Biol.* **21,** 1075–1101; 10.1016/j.chembiol.2014.09.002 (2014).

112. Li, S. *et al.* Copper-Catalyzed Click Reaction on/in Live Cells. *Chem. Sci.* **8,** 2107–2114; 10.1039/C6SC02297A (2017).

113. Tornøe, C. W., Christensen, C. & Meldal, M. Peptidotriazoles on solid phase: 1,2,3-triazoles by regiospecific copper(i)-catalyzed 1,3-dipolar cycloadditions of terminal alkynes to azides. *J. Org. Chem.* **67,** 3057–3064; 10.1021/jo011148j (2002).

114. Dennehy, M. K., Richards, K. A. M., Wernke, G. R., Shyr, Y. & Liebler, D. C. Cytosolic and nuclear protein targets of thiol-reactive electrophiles. *Chem. Res. Toxicol.* **19,** 20–29; 10.1021/tx050312l (2006).

115. Miranda, J. J. Highly Reactive Cysteine Residues in Rodent Hemoglobins. *Biochem. Biophys. Res. Commun.* **275,** 517–523; 10.1006/bbrc.2000.3326 (2000).

116. Arora, B., Tandon, R., Attri, P. & Bhatia, R. Chemical Crosslinking: Role in Protein and Peptide Science. *Curr. Protein Pept. Sc.* **18,** 946–955; 10.2174/1389203717666160724202806 (2017).

117. Smith, E. & Collins, I. Photoaffinity labeling in target- and binding-site identification. *Future Med. Chem.* **7,** 159–183; 10.4155/fmc.14.152 (2015).

118. Mackinnon, A. L. & Taunton, J. Target Identification by Diazirine Photo-Cross-linking and Click Chemistry. *Curr. Protoc. Mol. Biol.* **1,** 55–73; 10.1002/9780470559277.ch090167 (2009).

119. Sadaghiani, A. M., Verhelst, S. H. & Bogyo, M. Tagging and detection strategies for activity-based proteomics. *Curr. Opin. Chem. Biol.* **11,** 20–28; 10.1016/j.cbpa.2006.11.030 (2007).

120. Berkers, C. R. *et al.* Activity probe for in vivo profiling of the specificity of proteasome inhibitor bortezomib. *Nat. methods* **2,** 357–362; 10.1038/nmeth759 (2005).

121. Speers, A. E., Adam, G. C. & Cravatt, B. F. Activity-based protein profiling in vivo using a copper(i)-catalyzed azide-alkyne 3 + 2 cycloaddition. *J. Am. Chem. Soc* **125,** 4686–4687; 10.1021/ja034490h (2003).

122. Mann, M., Hendrickson, R. C. & Pandey, A. Analysis of proteins and proteomes by mass spectrometry. *Annu. Rev. Biochem.* **70,** 437–473; 10.1146/annurev.biochem.70.1.437 (2001).

123. Rappsilber, J., Mann M. & Ishihama, Y. Protocol for micro-purification, enrichment, pre-fractionation and storage of peptides for proteomics using StageTips. *Nat. Protoc.* **2,** 1896–1906; 10.1038/nprot.2007.261 (2007).

124. Jessani, N. *et al.* A streamlined platform for high-content functional proteomics of primary human specimens. *Nat. methods* **2,** 691–697; 10.1038/nmeth778 (2005).

125. Cox, J. *et al.* Andromeda: a peptide search engine integrated into the MaxQuant environment. *J. Proteome Res.* **10,** 1794–1805; 10.1021/pr101065j (2011).

126. Cox, J. *et al.* Accurate Proteome-wide Label-free Quantification by Delayed Normalization and Maximal Peptide Ratio Extraction, Termed MaxLFQ. *Mol. Cell. Proteom.* **13,** 2513–2526; 10.1074/mcp.M113.031591 (2014).

127. Ong, S.-E. *et al.* Stable isotope labeling by amino acids in cell culture, SILAC, as a simple and accurate approach to expression proteomics. *Mol. Cell. Proteom.* **1,** 376–386; 10.1074/mcp.m200025-mcp200 (2002).

128. Boersema, P. J., Raijmakers, R., Lemeer, S., Mohammed, S. & Heck, A. J. R. Multiplex peptide stable isotope dimethyl labeling for quantitative proteomics. *Nat. Protoc.* **4,** 484–494; 10.1038/nprot.2009.21 (2009).

129. Thompson, A. *et al.* Tandem mass tags: a novel quantification strategy for comparative analysis of complex protein mixtures by MS/MS. *Anal. Chem.* **75,** 1895–1904; 10.1021/ac0262560 (2003).

130. Ross, P. L. *et al.* Multiplexed protein quantitation in *Saccharomyces cerevisiae* using amine-reactive isobaric tagging reagents. *Mol. Cell. Proteomics* **3,** 1154–1169; 10.1074/mcp.M400129-MCP200 (2004).

131. Press, W. H. *Numerical recipes. The art of scientific computing.* 3rd ed. (Cambridge Univ. Press, Cambridge, 2007).

132. Spahn, C. K. *et al.* A toolbox for multiplexed super-resolution imaging of the *E. coli* nucleoid and membrane using novel PAINT labels. *Sci. Rep.* **8,** 14768; 10.1038/s41598-018-33052-3 (2018).

133. Tailliez, P., Pagès, S., Ginibre, N. & Boemare, N. New insight into diversity in the genus *Xenorhabdus*, including the description of ten novel species. *Int. J. Syst. Evol. Microbiol.* **56,** 2805–2818; 10.1099/ijs.0.64287-0 (2006).

134. Lengyel, K. *et al.* Description of four novel species of *Xenorhabdus*, family Enterobacteriaceae: *Xenorhabdus budapestensis* sp. nov., *Xenorhabdus ehlersii* sp. nov., *Xenorhabdus innexi* sp. nov., and *Xenorhabdus szentirmaii* sp. nov. *Syst. Appl. Microbiol.* **28,** 115–122; 10.1016/j.syapm.2004.10.004 (2005).

135. Tsutsumi, L. S., Tan, G. T. & Sun, D. Solid-phase synthesis of cyclic hexapeptides wollamides A, B and desotamide B. *Tetrahedron letters* **58,** 2675–2680; 10.1016/j.tetlet.2017.05.084 (2017).

136. Wanka, L., Cabrele, C., Vanejews, M. & Schreiner, P. R. γ-Aminoadamantanecarboxylic Acids Through Direct C–H Bond Amidations. *Eur. J. Org. Chem.* **2007,** 1474–1490; 10.1002/ejoc.200600975 (2007).

137. Fukuzawa S., Matsuzawa H. & Yoshimitsu S. Asymmetric Samarium-Reformatsky Reaction of Chiral alpha-Bromoacetyl-2-oxazolidinones with Aldehydes. *J. Org. Chem.* **65,** 1702–1706; 10.1021/jo9914317 (2000).

138. Yang, Z. & Weisshaar, J. C. HaloTag Assay Suggests Common Mechanism of *E. coli* Membrane Permeabilization Induced by Cationic Peptides. *ACS Chem. Biol.* **13,** 2161–2169; 10.1021/acschembio.8b00336 (2018).

139. Letschert, S. Quantitative Analysis of Membrane Components using Super-Resolution Microscopy. Universität Würzburg, 2019.

140. Jamur, M. C. & Oliver, C. Permeabilization of cell membranes. *Methods Mol. Biol.* **588,** 63–66; 10.1007/978-1-59745-324-0_9 (2010).

141. Spahn, C., Endesfelder, U. & Heilemann, M. Super-resolution imaging of *Escherichia coli* nucleoids reveals highly structured and asymmetric segregation during fast growth. *J. Struct. Biol.* **185,** 243–249; 10.1016/j.jsb.2014.01.007 (2014).

142. Silvestro, L., Weiser, J. N. & Axelsen, P. H. Antibacterial and antimembrane activities of cecropin A in *Escherichia coli*. *Antimicrob. Agents Chemother.* **44,** 602–607; 10.1128/aac.44.3.602-607.2000 (2000).

143. Bulet, P., Urge, L., Ohresser, S., Hetru, C. & Otvos, L. Enlarged scale chemical synthesis and range of activity of drosocin, an O-glycosylated antibacterial peptide of *Drosophila*. *Eur. J. Biochem* **238,** 64–69; 10.1111/j.1432-1033.1996.0064q.x (1996).

144. Kreil, G. Biosynthesis of melittin, a toxic peptide from bee venom. Amino-acid sequence of the precursor. *Eur. J. Biochem* **33,** 558–566; 10.1111/j.1432-1033.1973.tb02716.x (1973).

145. Kanehisa, M., Sato, Y. & Morishima, K. BlastKOALA and GhostKOALA: KEGG Tools for Functional Characterization of Genome and Metagenome Sequences. *J. Mol. Biol.* **428,** 726–731; 10.1016/j.jmb.2015.11.006 (2016).

146. Rehman, Z. U. & Leiknes, T. Quorum-Quenching Bacteria Isolated From Red Sea Sediments Reduce Biofilm Formation by *Pseudomonas aeruginosa*. *Front. Microbiol.* **9,** 1354; 10.3389/fmicb.2018.01354 (2018).

147. Dobretsov, S., Teplitski, M. & Paul, V. Mini-review: quorum sensing in the marine environment and its relationship to biofouling. *Biofouling* **25,** 413–427; 10.1080/08927010902853516 (2009).

148. Cha, C., Gao, P., Chen, Y. C., Shaw, P. D. & Farrand, S. K. Production of acyl-homoserine lactone quorum-sensing signals by gram-negative plant-associated bacteria. *Mol. Plant Microbe Interact.* **11,** 1119–1129; 10.1094/MPMI.1998.11.11.1119 (1998).

149. Verbeke, F. *et al.* Peptides as Quorum Sensing Molecules: Measurement Techniques and Obtained Levels In vitro and In vivo. *Front. Neurosci.* **11,** 183; 10.3389/fnins.2017.00183 (2017).

150. Oshiro, K. G. N., Rodrigues, G., Monges, B. E. D., Cardoso, M. H. & Franco, O. L. Bioactive Peptides Against Fungal Biofilms. *Front. Microbiol.* **10,** 2169; 10.3389/fmicb.2019.02169 (2019).

151. Matejuk, A. *et al.* Peptide-based Antifungal Therapies against Emerging Infections. *Drugs Future* **35,** 197 (2010).

152. Hyde, C., Johson, T., Owen, D., Quibell, M. & Sheppard, R. C. Some ‘difficult sequences’ made easy. *Int. J. Pept. Protein Res.* **43,** 431–440; 10.1111/j.1399-3011.1994.tb00541.x (1994).

153. Walker, J. R. & Altman, E. Biotinylation facilitates the uptake of large peptides by *Escherichia coli* and other gram-negative bacteria. *Appl. Environ. Microbiol.* **71,** 1850–1855; 10.1128/AEM.71.4.1850-1855.2005 (2005).

154. Jain, S. & Pillai, J. Bacterial membrane vesicles as novel nanosystems for drug delivery. *Int. J. Nanomed.* **12,** 6329–6341; 10.2147/IJN.S137368 (2017).

155. Bajerski, F., Wagner, D. & Mangelsdorf, K. Cell Membrane Fatty Acid Composition of *Chryseobacterium frigidisoli* PB4T, Isolated from Antarctic Glacier Forefield Soils, in Response to Changing Temperature and pH Conditions. *Front. Microbiol.* **8,** 677; 10.3389/fmicb.2017.00677 (2017).

156. Siliakus, M. F., van der Oost, J. & Kengen, S. W. M. Adaptations of archaeal and bacterial membranes to variations in temperature, pH and pressure. *Extremophiles* **21,** 651–670; 10.1007/s00792-017-0939-x (2017).

157. Limonet, M., Revol-Junelles, A.-M. & Millière, J.-B. Variations in the membrane fatty acid composition of resistant or susceptible *Leuconostoc* or *Weissella* strains in the presence or absence of Mesenterocin 52A and Mesenterocin 52B produced by *Leuconostoc mesenteroides* subsp. *mesenteroides* FR52. *Appl. Environ. Microbiol.* **68,** 2910–2916; 10.1128/aem.68.6.2910-2916.2002 (2002).

158. Boudjemaa, R. *et al.* Impact of Bacterial Membrane Fatty Acid Composition on the Failure of Daptomycin To Kill *Staphylococcus aureus*. *Antimicrob. Agents Chemother.* **62**; 10.1128/AAC.00023-18 (2018).

159. Baek, M. *et al.* Photo Cross-linking Probes Containing ε-N-Thioacyllysine and ε-N-Acyl-(δ-aza)lysine Residues. *Chemistry*; 10.1002/chem.201905338 (2020).

160. Wang, J., Chen, Q., Shan, Y., Pan, X. & Zhang, J. Activity-based proteomic profiling. The application of photoaffinity probes in the target identification of bioactive molecules. *Trends Anal. Chem.* **115,** 110–120; 10.1016/j.trac.2019.03.028 (2019).

161. Weerapana, E. *et al.* Quantitative reactivity profiling predicts functional cysteines in proteomes. *Nature* **468,** 790–795; 10.1038/nature09472 (2010).

162. Li, J. *et al.* Membrane Active Antimicrobial Peptides: Translating Mechanistic Insights to Design. *Front. Neurosci.* **11,** 73; 10.3389/fnins.2017.00073 (2017).

163. Desbois, A. P. & Smith, V. J. Antibacterial free fatty acids: activities, mechanisms of action and biotechnological potential. *Appl. Environ. Microbiol.* **85,** 1629–1642; 10.1007/s00253-009-2355-3 (2010).

164. Boman, H. G., Agerberth, B. & Boman, A. Mechanisms of action on *Escherichia coli* of cecropin P1 and PR-39, two antibacterial peptides from pig intestine. *Infect. Immun.* **61,** 2978–2984 (1993).

165. Gobbo, M. *et al.* Antimicrobial peptides: synthesis and antibacterial activity of linear and cyclic drosocin and apidaecin 1b analogues. *J. Med. Chem.* **45,** 4494–4504; 10.1021/jm020861d (2002).

166. van den Bogaart, G., Guzmán, J. V., Mika, J. T. & Poolman, B. On the mechanism of pore formation by melittin. *J. Biol. Chem.* **283,** 33854–33857; 10.1074/jbc.M805171200 (2008).

167. Zhu, Y., Mohapatra, S. & Weisshaar, J. C. Rigidification of the Escherichia coli cytoplasm by the human antimicrobial peptide LL-37 revealed by superresolution fluorescence microscopy. *Proc. Natl. Acad. Sci. U.S.A.* **116,** 1017–1026; 10.1073/pnas.1814924116 (2019).

168. Wu, Q., Patočka, J. & Kuča, K. Insect Antimicrobial Peptides, a Mini Review. *Toxins* **10**; 10.3390/toxins10110461 (2018).

169. Yeaman, M. R. & Yount, N. Y. Mechanisms of antimicrobial peptide action and resistance. *Pharmacol. Rev.* **55,** 27–55; 10.1124/pr.55.1.2 (2003).

170. Hancock, R. E. W. Peptide antibiotics. *Lancet* **349,** 418–422; 10.1016/S0140-6736(97)80051-7 (1997).

171. Aoki, W. & Ueda, M. Characterization of Antimicrobial Peptides toward the Development of Novel Antibiotics. *Pharmaceuticals* **6,** 1055–1081; 10.3390/ph6081055 (2013).

172. Kumariya, R., Sood, S. K., Rajput, Y. S., Saini, N. & Garsa, A. K. Increased membrane surface positive charge and altered membrane fluidity leads to cationic antimicrobial peptide resistance in *Enterococcus faecalis*. *Biochim. Biophys. Acta* **1848,** 1367–1375; 10.1016/j.bbamem.2015.03.007 (2015).

173. Khandelwal, P. & Banerjee-Bhatnagar, N. Insecticidal activity associated with the outer membrane vesicles of *Xenorhabdus nematophilus*. *Appl. Environ. Microbiol.* **69,** 2032–2037; 10.1128/aem.69.4.2032-2037.2003 (2003).

174. Li, Z., Clarke, A. J. & Beveridge, T. J. A major autolysin of *Pseudomonas aeruginosa*: subcellular distribution, potential role in cell growth and division and secretion in surface membrane vesicles. *J. Bacteriol.* **178,** 2479–2488; 10.1128/jb.178.9.2479-2488.1996 (1996).

175. Mashburn-Warren, L. *et al.* Interaction of quorum signals with outer membrane lipids: insights into prokaryotic membrane vesicle formation. *Mol. Microbiol.* **69,** 491–502; 10.1111/j.1365-2958.2008.06302.x (2008).

176. Fujita, Y., Matsuoka, H. & Hirooka, K. Regulation of fatty acid metabolism in bacteria. *Mol. Microbiol.* **66,** 829–839; 10.1111/j.1365-2958.2007.05947.x (2007).

177. Berg, J. M., Tymoczko, J. L. & Stryer, L. (eds.). *Biochemistry. 5th edition* (W H Freeman, 2002).

178. Howard, B. R., Endrizzi, J. A. & Remington, S. J. Crystal structure of *Escherichia coli* malate synthase G complexed with magnesium and glyoxylate at 2.0 A resolution: mechanistic implications. *Biochemistry* **39,** 3156–3168; 10.1021/bi992519h (2000).

179. Lorenz, M. C. & Fink, G. R. The glyoxylate cycle is required for fungal virulence. *Nature* **412,** 83–86; 10.1038/35083594 (2001).

List of publications and record of conferences

Publications

Bode, E., Heinrich, A. K., Hirschmann, M., Abebew, D., Shi, Y. N., Vo, T. D., Wesche, F., Shi, Y. M., Grün, P., Simonyi, S., Keller, N., Engel, Y., Wenski, S., Bennet, R., Beyer, S., Bischoff, I., Buaya, A., Brandt, S., Cakmak, I., Çimen, H., Eckstein, S., Frank, D., Fürst, R., Gand, M., Geisslinger, G., Hazir, S., Henke, M., Heermann, R., Lecaudey, V., Schäfer, W., Schiffmann, S., Schüffler, A., Schwenk, R., Skaljac, M., Thines, E., Thines, M., Ulshöfer, T., Vilcinskas, A., Wichelhaus, T. A. & Bode, H. B. Promoter Activation in Δhfq Mutants as an Efficient Tool for Specialized Metabolite Production Enabling Direct Bioactivity Testing. Angew. Chem. 131, 19133–19139; 10.1002/ange.201910563 (2019).

Zhao, L., Vo, T. D., Kaiser, M. & Bode, H. B. Phototemtide A, a Cyclic Lipopeptide Heterologously Expressed from *Photorhabdus temperata* Meg1, Shows Selective Antiprotozoal Activity. *ChemBioChem*; 10.1002/cbic.201900665 (2019).

Bode, E., He Y., Vo, T. D., Schultz R., Kaiser M. & Bode, H. B. Biosynthesis and function of simple amides in *Xenorhabdus doucetiae*. *Environmental Microbiology* **19,** 4564–4575; 10.1111/1462-2920.13919 (2017).

Conference

10th Maxquant summer school (Computational Proteomics)

July 8th- 13th 2018 Barcelona

Erklärung

Ich erkläre hiermit, dass ich mich bisher keiner Doktorprüfung im Mathematisch-Naturwissenschaftlichen Bereich unterzogen habe.

Frankfurt am Main, den 03.08.2020 Tien Duy Vo

Versicherung

Ich erkläre hiermit, dass ich die vorgelegte Dissertation selbstständig angefertigt und mich anderer Hilfsmittel als der in ihr angegebenen nicht bedient habe, insbesondere, dass alle Entlehnungen aus anderen Schriften mit Angabe der betreffenden Schrift gekennzeichnet sind.

Ich versichere, die Grundsätze der guten wissenschaftlichen Praxis beachtet, und nicht die Hilfe einer kommerziellen Promotionsvermittlung in Anspruch genommen zu haben.

Frankfurt am Main, den 03.08.2020 Tien Duy Vo